



THE HONG KONG
POLYTECHNIC UNIVERSITY

香港理工大學

Pao Yue-kong Library

包玉剛圖書館

Copyright Undertaking

This thesis is protected by copyright, with all rights reserved.

By reading and using the thesis, the reader understands and agrees to the following terms:

1. The reader will abide by the rules and legal ordinances governing copyright regarding the use of the thesis.
2. The reader will use the thesis for the purpose of research or private study only and not for distribution or further reproduction or any other purpose.
3. The reader agrees to indemnify and hold the University harmless from and against any loss, damage, cost, liability or expenses arising from copyright infringement or unauthorized usage.

IMPORTANT

If you have reasons to believe that any materials in this thesis are deemed not suitable to be distributed in this form, or a copyright owner having difficulty with the material being included in our database, please contact lbsys@polyu.edu.hk providing details. The Library will look into your claim and consider taking remedial action upon receipt of the written requests.

**1,3-PROPANEDIOL AND CAPROATE
CO-PRODUCTION THROUGH GLYCEROL
FERMENTATION AND CARBOXYLATE CHAIN
ELONGATION IN MIXED CULTURE**

LENG LING

Ph.D

The Hong Kong Polytechnic University

2018

The Hong Kong Polytechnic University
Department of Civil and Environmental Engineering

**1,3-PROPANEDIOL AND CAPROATE
CO-PRODUCTION THROUGH GLYCEROL
FERMENTATION AND CARBOXYLATE CHAIN
ELONGATION IN MIXED CULTURE**



LENG Ling

A Thesis Submitted in Partial Fulfillment of the
Requirements for the Degree of Doctor of Philosophy

August 2017

CERTIFICATE OF ORIGINALITY

I hereby declare that this thesis is my own work and that, to the best of my knowledge and belief, it reproduces no material previously published or written, nor material that has been accepted for the award of any other degree or diploma, except where due acknowledgement has been made in the text.

_____ (Signed)

LENG Ling (Name of Student)

DEDICATION

To my family and friends who love and trust me

*To my supervisor who inspires me and has supported me
every step of the way*

To the fellows who devote to this research field

To the microorganisms that complete the pathways

Also to the endless nights accompanying my growth

ABSTRACT

Mixed culture chain elongation of short chain fatty acids (SCFAs) for a medium chain fatty acid (MCFA), caproate, formation is an attractive option for resource recovery in anaerobic wastewater treatment. Caproate, a value-added chemical, is slightly soluble in water and can be used by various industries. Biological production of caproate with ethanol as electron donor has been successfully achieved in anaerobic mixed culture. However, the underlying metabolic pathways of microorganisms except *Clostridium kluyveri* are not well understood. Another potential electron donor is glycerol which is presently being generated in surplus with the rapid growth of the biodiesel industry. In the current approach, an industrial chemical, 1,3-propanediol (1,3-PDO) is produced from crude glycerol along with a formation of other soluble byproducts including ethanol and SCFAs, which necessitates a significant amount of energy input for separation and purification. To circumvent the energy sink requirement and upcycle both the wastewater treatment process and the biodiesel industry, it is highly beneficial to co-produce caproate from the byproducts of glycerol dissimilation along with 1,3-PDO.

At first, thermodynamic and physiological insights gained into the co-production of 1,3-PDO and caproate from glycerol are investigated. Thermodynamics analysis demonstrated that a higher pH range is more favorable when either glycerol or ethanol acting as an electron donor, whereas a high partial pressure (27% at 1 atm) and a low pH (≤ 5.5) are advantageous for caproate formation with hydrogen. With

the glycerol-to-acetate molar ratio of 4 and pH of 7, the physiological experiments achieved a co-production of 1,3-PDO and caproate. However, the caproate yield was low and found to be kinetic-limited. Caproate formation was significantly increased by the intermediate ethanol addition with the optimal mono-caproate formation obtained at the ethanol-to-acetate molar ratio of 3. A synergistic relationship was evinced through microbial characterization, resulting in *C. kluyveri* and some bacteria with function of converting glycerol to SCFAs.

Whilst the metabolic pathway of *C. kluyveri* in carboxylates chain elongation has been discovered, the role of other co-existing microbiomes which promote the elongation remained unclear in mixed culture. Thus, we conducted a fermentation experiment at optimal conditions which is inoculated with fresh anaerobic digestion (AD) sludge and fed with ethanol and acetate. Both 16S rRNA gene-based amplicon and shotgun metagenomics sequencing were employed to elucidate the mixed culture chain elongation by uncovering the microbes and functional pathways. Results revealed a synergistic relationship between *C. kluyveri* and three co-dominant species *Desulfovibrio vulgaris*, *Fusobacterium varium* and *Acetoanaerobium sticklandii*. The co-existence of these three species were able to boost the carboxylates chain elongation by *C. kluyveri*. Draft genomes of *C. kluyveri*, *D. vulgaris* and *A. sticklandii* were successfully recovered, revealing that butyrate and caproate can be directly produced from ethanol and acetate by *C. kluyveri* and indirectly produced through a syntrophic partnership between *D. vulgaris* and *A. sticklandii* with

hydrogen serving as a reducing equivalent messenger. This study presents evidences of a syntrophic partnership between bacterial species and unveils an intricate and synergistic microbial network in mixed culture carboxylates chain elongation.

Moreover, this study enriched a microbial community capable of efficiently co-producing 1,3-PDO and caproate via glycerol fermentation and carboxylate chain elongation. A co-production of 6.38 mM C 1,3-PDO d⁻¹ and 2.95 mM C caproate d⁻¹ was achieved in a 2-L semi-continuous fermenter with a glycerol-ethanol-acetate stoichiometric ratio of 4:3:1. Microbimes, *E. limosum*, *C. kluyveri* and *M. senegalense*, utilize a unique combination of metabolic pathways to facilitate the above conversion. Based on metagenomics, *E. limosum* is capable of converting glycerol to 1,3-PDO, ethanol and H₂, and also redirecting the electron potential of H₂ into acetate via the Wood–Ljungdahl pathway for chain elongation. *C. kluyveri* worked synergistically with *E. limosum* by consuming ethanol and acetate for caproate production. *M. senegalense* encodes for ethanol oxidation to acetate and butyrate, facilitating the caproate production by *C. kluyveri*. During the transition between fermentation and elongation, an unexpected phenomenon of poly-β-hydroxybutyrate (PHB) formation and reutilization by *M. senegalense* was observed, which may be associated with butyrate formation for further caproate generation. Significant ethanol production as an intermediate of glycerol dissimilation and the non-inhibiting level of 1,3-PDO production, which allows the dominance of *C. kluyveri*, are key to increasing caproate production.

Finally, a batch test of glycerol fermentation for the co-production with ethanol self-sufficiency inoculated by the fermenter-enriched microbial community was conducted. This study answers whether the enriched versatile glycerol degrader, *E. limosum*, could convert glycerol-derived energy to ethanol and H₂ in a balance with 1,3-PDO and acetate and whether the ethanol could be further utilized by caproate producer within the cultivation matrix. In addition, this study also investigated the electron flux of glycerol fermentation and chain elongation. The co-production of 1,3-PDO and caproate was achieved with a favorable glycerol/acetate stoichiometric ratio. Significant ethanol production from glycerol oxidation is the main reason for the caproate production enhancement. A dynamic balance of three dominant microbiomes, *E. limosum*, *M. senegalense*, and *C. kluyveri*, could complete the multiple stages co-production process. *E. limosum* dominated in the glycerol fermentation phase, while *M. senegalense* and *C. kluyveri* worked together for caproate production with ethanol and acetate in the carboxylates chain elongation phase. Redirection of the electron potential of H₂ back into acetate for chain elongation by *E. limosum* and PHB formation and reutilization by *M. senegalense* were proved by electron flux calculation. The physiological performance and dynamic microbial community disclosed a unique combination of metabolic pathways successfully facilitated the co-production. The knowledge gleaned paves new avenues for both the wastewater treatment process and the biodiesel industry by upcycling their resources recovery.

PUBLICATIONS ARISING FROM THE THESIS

Journal Papers:

1. **LENG, L.**, Yang, P., Mao, Y., Wu, Z., Zhang, T., & Lee P.-H. (2017). Thermodynamic and physiological study of caproate and 1,3-propanediol co-production through glycerol fermentation and fatty acids chain elongation. *Water Res. 114*, 200-209.
2. **LENG, L.**, Yang, P., Singh, S., Zhuang, H., Xu L., Chen W.-H., Dolfing, J., Li, D., Zhang, Y., Zeng, H., Chu W., & Lee P.-H. (2017). A review on the bioenergetics of anaerobic microbial metabolism close to the thermodynamic limits and its implications for digestion applications. *Bioresour Technol. 247*, 1095-1106.
3. **LENG, L.**, Nobu, M. K., Narihiro, T., Yang, P., Tan, G.-Y., & Lee P.-H. (2017). Biological co-production of 1,3-propanediol and caproate through glycerol fermentation and carboxylate chain elongation by shaping microbial consortia: Pathways and Mechanisms. (Under review in *Environ Sci Technol*)

Conference Presentations:

1. **LENG, L.**, Yang, P., & Lee P.-H. Synergistic network in carboxylates chain elongation with ethanol. The 9th Asia-Pacific Landfill Symposium, The University of Hong Kong, Hong Kong, Nov., 2016
2. **LENG, L.**, Yang, P., & Lee P.-H. Fatty acids chain elongation with glycerol in mixed culture. Second International Conference on Sustainable Urbanization (ICSU 2015), The Hong Kong Polytechnic University, Hong Kong, Jan., 2015

ACKNOWLEDGEMENTS

Foremost, I would like to express my deepest gratitude to my supervisor, Dr. Henry Lee, for his consistent trust and support. Without his inspiration, I could not finish this thesis. Without his invaluable guidance, I could not grow up to a devoted researcher from the one like a white paper. His ideas and morals build up a role model of the way I pursue. I really appreciate being one of the kids in his research family. I also want to deliver my sincere gratitude to my supervisor, Dr. Takashi Narihiro, in National Institute of Advanced Industrial Science and Technology (AIST), Japan for his generous instruction and help in academics and life during the research attachment. Besides, my sincere appreciation goes to our lab technicians, especially Mr. Lam Wai-Shung, for their technical support and patient assistance in the past four years. I am also grateful for the valuable guidance and constructive suggestions of Dr. Masaru K Nobu.

I sincerely thank my excellent colleagues and great friends, Ms. Yang Peixian, Dr. Giin-Yu Amy Tan, Mr. Dong Chengyu, Ms. Xu Linji, Mr. Zhuang Huichuan, Dr. Wu Zhuoying and Mr. Lin Yu-Ping. Without their kind help and genuine care, I could not get through the tough times of difficulty and solitude.

Last but not the least, I would like to express my sincere gratitude to my beloved parents who support and trust me all the time. Looking forward to a bright future.

TABLE OF CONTENTS

CERTIFICATE OF ORIGINALITY	I
DEDICATION.....	II
ABSTRACT.....	III
PUBLICATIONS ARISING FROM THE THESIS	VII
ACKNOWLEDGEMENTS	VIII
TABLE OF CONTENTS.....	IX
LIST OF FIGURES	XII
LIST OF TABLES.....	XX
LIST OF ABBREVIATIONS	XXII
CHAPTER 1. INTRODUCTION	1
1.1 BACKGROUND.....	1
1.2 OBJECTIVES	2
1.3 THESIS ORGANIZATION.....	3
CHAPTER 2. LITERATURE REVIEW	6
2.1 DEMAND OF WASTE TO BIOPRODUCTS CONVERSION WITH MIXED CULTURE MICROBIOMES.....	6
2.1.1 <i>Environmental threats, economics and sustainability.....</i>	6
2.1.2 <i>Sustainable production of biofuels and chemicals.....</i>	8
2.1.3 <i>Undefined mixed culture fermentation.....</i>	11
2.2 CARBOXYLATES CHAIN ELONGATION FOR CAPROATE PRODUCTION	11
2.2.1 <i>Applications and manufacture technologies of caproate.....</i>	11
2.2.2 <i>Carboxylates chain elongation and caproate production in undefined mixed culture</i>	13
2.2.3 <i>Caproate formation microbiomes and biological pathways.....</i>	17
2.3 WASTE-DERIVED REDUCED COMPOUNDS FOR CARBOXYLATE CHAIN ELONGATION	21
2.4 GLYCEROL FERMENTATION	22
2.4.1 <i>Crude glycerol produced in biodiesel process.....</i>	22
2.4.2 <i>Glycerol fermentation pathways and microbiomes.....</i>	23
2.4.3 <i>Glycerol fermentation with undefined mixed culture.....</i>	27
2.5 CHALLENGES ON 1,3-PDO AND CAPROATE CO-PRODUCTION	30
2.6 BIOENERGETICS OF ANAEROBIC MICROBIAL METABOLISM	30
2.6.1 <i>Thermodynamics in metabolism</i>	32
2.6.2 <i>Energy conservation in anaerobic syntrophy.....</i>	33
2.7 ECONOMIC ANALYSIS OF THE PROCESSES FOR TWO VALUE-ADDED CHEMICALS CO-PRODUCTION FROM GLYCEROL.....	35
CHAPTER 3. MATERIALS AND METHODOLOGY	37
3.1 THERMODYNAMICS CALCULATION OF BIOCHEMICAL REACTIONS	37

3.2	INOCULUM AND MEDIUM FOR FERMENTATION	41
3.3	BATCH TEST EXPERIMENT	43
3.3.1	<i>Batch tests design for the study in chapter four.....</i>	43
3.3.2	<i>Batch test design for the study in chapter five</i>	44
3.3.3	<i>Batch tests design for the study in chapter six and seven</i>	44
3.4	SEMI-CONTINUOUS FERMENTATION	45
3.5	ANALYTICAL PROCEDURES	46
3.6	DNA EXTRACTION AND HIGH-THROUGHPUT SEQUENCING	48
3.7	BIOINFORMATICS ANALYSIS	49
CHAPTER 4. THERMODYNAMIC AND PHYSIOLOGICAL STUDY OF CAPROATE AND 1,3-PDO CO-PRODUCTION THROUGH GLYCEROL FERMENTATION AND FATTY ACIDS CHAIN ELONGATION		52
4.1	OVERVIEW.....	52
4.2	RESULTS AND DISCUSSION	53
4.2.1	<i>Thermodynamic analysis of chain elongation with different electron donors</i>	53
4.2.2	<i>MCFA production with ethanol.....</i>	63
4.2.3	<i>1,3-PDO and MCFA production with glycerol</i>	66
4.2.4	<i>1,3-PDO and MCFA production with ethanol and glycerol</i>	69
4.2.5	<i>Microbial characterization</i>	70
4.3	CHAPTER SUMMARY	76
CHAPTER 5. UNVEILING A NEW SYNERGISTIC AND SYNTROPHIC MICROBIAL NETWORK FOR CARBOXYLATES CHAIN ELONGATION WITH ETHANOL		78
5.1	OVERVIEW.....	78
5.2	RESULTS AND DISCUSSION	79
5.2.1	<i>Microbial community structures under different physiological stages of carboxylate chain elongation with ethanol</i>	79
5.2.2	<i>Metagenomics-based metabolic pathways characterization</i>	89
5.3	CHAPTER SUMMARY	100
CHAPTER 6. 1,3-PDO AND CAPROATE CO-PRODUCTION THROUGH GLYCEROL FERMENTATION AND CARBOXYLATE CHAIN ELONGATION BY SHAPING MICROBIAL CONSORTIA		102
6.1	OVERVIEW.....	102
6.2	RESULTS AND DISCUSSION	104
6.2.1	<i>Glycerol fermentation in a semi-continuous reactor</i>	104
6.2.2	<i>Effect of substrates on caproate and 1,3-PDO formation.....</i>	106
6.2.3	<i>Fermenter microbiome enrichment and physiological performance with an ethanol addition.....</i>	114
6.2.4	<i>Microbial community structure analysis.....</i>	119
6.2.5	<i>Genome reconstruction and metabolic pathways characterization.....</i>	127
6.3	CHAPTER SUMMARY	145
CHAPTER 7. CO-PRODUCTION OF 1,3-PDO AND CAPROATE FROM GLYCEROL WITH ENRICHED MICROBIAL COMMUNITY		149

7.1	OVERVIEW.....	149
7.2	RESULTS AND DISCUSSION	150
7.2.1	<i>Physiological performance of batch tests</i>	<i>150</i>
7.2.2	<i>Microbial community of glycerol fermentation for two value-added chemicals co-production</i>	<i>152</i>
7.2.3	<i>Electron flow of glycerol fermentation.....</i>	<i>154</i>
7.3	CHAPTER SUMMARY	157
CHAPTER 8. CONCLUSIONS AND RECOMMENDATIONS.....		159
8.1	CONCLUSIONS	159
8.2	RECOMMENDATIONS FOR FUTURE WORK	163
APPENDIX I TABLE.....		164
APPENDIX II TABLE.....		171
APPENDIX III TABLE.....		180
APPENDIX IV TABLE.....		184
APPENDIX V TABLE.....		187
APPENDIX VI TABLE.....		243
REFERENCES.....		244

LIST OF FIGURES

Figure 1.1. Co-production of caproate and 1,3-PDO from glycerol with mixed culture.	2
Figure 2.1. Waste(water) treatment and recycling to bioproducts as alternatives to methane in anaerobic undefined mixed culture to tackle with global issues.	6
Figure 2.2. The schematic of process of biofuels production from biomass.	10
Figure 2.3. Chain elongation pathways in anaerobic mixed culture adopted from Spirito et al. (2014).	14
Figure 2.4. Chain elongation of acetate with ethanol as electron donor in <i>C. kluyveri</i> adopted from Seedorf et al. (2008).	18
Figure 2.5. Biological pathways of caproate production in different anaerobes (partial).....	21
Figure 2.6. Glycerol production as a byproduct in biodiesel process from fats and oils (a); Biodiesel production and its impact on crude glycerol prices in US (b) adopted from Yazdani and Gonzalez (2007).....	23
Figure 2.7. Metabolic pathways for glycerol metabolism in <i>clostridia</i> adopted from Johnson and Taconi (2007).	26
Figure 2.8. Utilization of electron donor for energy production and cell synthesis adopted from Rittmann and McCarty (2012).....	32
Figure 3.1. Inoculum source for fermentation (Drainage Services Department, Hong Kong).	41
Figure 3.2. Semi-continuous fermentation system.....	46

Figure 3.3. The HPLC system (SHIMADZU) used for quantification of the target compounds and GC system (Agilent) used for quantification of the target gases.	47
Figure 3.4. Flowchart of 16S rRNA gene-based amplicon sequencing for microbial analysis.....	48
Figure 3.5. Metagenomic analysis flowchart.....	51
Figure 4.1. Standard transformed Gibbs free energy values in KJ mol^{-1} as a function of pH and ionic strength (I) for (a) caproate formation with ethanol (Eq. R1 to R6), (b) caproate formation with H_2 (Eq. R7 and R8), (c) different product formation with glycerol fermentation (Eq. R9 to R12), and (d) caproate formation with glycerol (Eq. R13 and R14).	55
Figure 4.2. Standard transformed Gibbs free energy values per electron transfer in KJ mol^{-1} as a function of pH and ionic strength (I) for caproate formation with ethanol as electron donor (Eq. R1 to R6).....	58
Figure 4.3. Transformed Gibbs free energy values in KJ mol^{-1} at a pH of 7, an ionic strength (I) of 0.1 M, a temperature of 310 K and pressure of 1 atm for (a) Eq. R1 and R2 as a function of the dissolved H_2 and acetate; (b) Eq. R3 to R6 as a function of the dissolved H_2 and butyrate, acetate of 50 mM; (c) Eq. R7 and R8 as a function of the dissolved H_2 and acetate; (d) Eq. R13 and R14 as a function of the dissolved H_2 and butyrate, acetate of 50 mM, CO_2 formation of twice of butyrate.	59
Figure 4.4. Transformed Gibbs free energy values per electron transfer in KJ mol^{-1} at	

pH 7 and ionic strength (<i>I</i>) of 0.1 M for Eq. R4/R5/R6 as a function of the dissolved H ₂ and butyrate, [Acetate] = 50 mM.	60
Figure 4.5. Standard transformed Gibbs free energy of reaction in KJ mol ⁻¹ as a function of pH and ionic strength (<i>I</i>) for Eq. R15 to R20.....	62
Figure 4.6. (a) Chain elongation of 150 mM ethanol and 50 mM acetate with AD sludge at a pH 7 and 37°C, (b) Product generation of glycerol fermentation in mmol electron with AD sludge at pH 7 and 37°C.	65
Figure 4.7. Kinetics of butyric acid, caproic acid, and H ₂ production with 150 mM alcohol-contained lignocellulose solution and 50 mM acetate at pH 7 and 37°C.	66
Figure 4.8. Glycerol fermentation with and without acetate.....	66
Figure 4.9. 1,3-PDO and caproate co-production with both ethanol and glycerol in the substrate, and the relationship with H ₂ level at a pH 7 and 37°C, (a) Ethanol and glycerol addition on Day 0, (b) Ethanol addition on Day 20.....	70
Figure 4.10. Composition of relative abundances of OTUs at Genus level in different sludge samples. Hierarchical clustering of five sludge samples was performed based on all OTUs from the microbial communities with a UPGMA algorithm to generate a newick-formatted tree.....	72
Figure 4.11. Microbial pathways occurred in mixed culture glycerol-acetate fermentation.	76
Figure 5.1. Microbial pathways occurred in mixed culture glycerol-acetate fermentation.	79

Figure 5.2. Mixed culture carboxylates chain elongation from ethanol with acetate inoculated with fresh AD sludge. The batch fermentation kinetics conducted at 37 °C, pH of 7 and 150 rpm in an incubator with methanogenesis inhibition. Corresponding representative OTUs, collected at three time points, collectively formed 28.25%-37.04% of the bacterial community. 80

Figure 5.3. Composition of relative abundance of OTUs at the Genus level in different samples. The different OTUs in the same genus level were combined to show in the columns. Hierarchical clustering of the total 8 samples was performed based on all OTUs from the microbial communities with a UPGMA algorithm to generate a newick-formatted tree. D0_1 and D0_2, D6_1 and D6_2, D15_1 and D15_2, D23_1 and D23_2 represent samples collected at Day 0, Day 6, Day 15 and Day 23 from duplicated bottles, respectively. 81

Figure 5.4. UniFrac emperor principal coordinate analysis (PCoA) (a. unweighted, b. weighted) of total 8 samples based on all OTUs from the microbial communities. D0_1 and D0_2, D6_1 and D6_2, D15_1 and D15_2, D23_1 and D23_2 represent samples collected at Day 0, Day 6, Day 15 and Day 23 from duplicated bottles, respectively. 82

Figure 5.5. Neighbor-joining tree based on 16S rRNA gene sequences and related reference lineages. 20 most abundant OTUs of 8 samples were selected for analysis and shown with average abundance and taxonomy information. The phylogenetic tree (bootstrap 1000: > 90% black node, > 70% gray node with black outline and > 50% gray node) were performed in ARB with SILVA

database SSU NR99 as reference.....	84
Figure 5.6. Association network among top 10 abundant microbes. Each node represents an OTU and each edge represents a negative (blue) or positive (red) interaction between the two connect nodes. Arrow demonstrates the direction of the influence and the width of edges indicates the strength of the interaction. .	88
Figure 5.7. The proposed synergistic and syntrophic network during the active phase of mixed culture carboxylates chain elongation with ethanol.	90
Figure 5.8. Phylogenetic tree based on whole-genome sequence using PhyloPhlAn.	91
Figure 5.9. The carboxylates chain elongation pathways of <i>C. kluyveri</i> or a syntrophic partnership of <i>D. vulgaris</i> and <i>A. sticklandii</i> . (a) Ethanol-acetate fermentation to butyrate along with H ₂ formation; (b) Ethanol oxidation to acetate and H ₂ ; (c) Amino-acids-acetate-H ₂ fermentation to butyrate.....	92
Figure 5.10. The carboxylates chain elongation pathways of <i>C. kluyveri</i> or a syntrophic partnership of <i>D. vulgaris</i> and <i>A. sticklandii</i> . (a) Ethanol-butyrates fermentation to caproate along with H ₂ formation; (b) Ethanol oxidation to acetate and H ₂ ; (c) Amino-acids-butyrates-H ₂ fermentation to caproate.....	94
Figure 6.1. Two value-added chemicals, 1,3-PDO and caproate, co-production through glycerol fermentation and carboxylate chain elongation.....	103
Figure 6.2. Physiologic performance and microbial characterization of semi-continuous mixed culture fermentation at 37 °C, pH of 7, stirring rate of 150 rpm and HRT of 30 days with methanogenesis inhibition. Substrates in influent (a)	

and products in effluent (b) of the six stages differ from substrate compositions. Corresponding representative OTUs are covered 63.04%–73.56%, 63.54%–86.63%, 65.32%–79.73%, 73.99%–82.40%, 79.21%–86.62%, and 70.44%–77.43% of the whole sequence at each stage, respectively (c). 105

Figure 6.3. Mixed culture fermentation from different substrates inoculated with fresh AD sludge: glycerol with acetate (a), ethanol and glycerol with acetate (b), ethanol with acetate (c). Corresponding representative OTUs collected at three time points are covered 63.23%–76.59%, 59.31%–67.21%, and 28.25%–37.04% of the sequences from each culture, respectively (d–f)..... 107

Figure 6.4. Venn diagrams (Oliveros, 2007-2015) of OTUs from three different substrate-enriched cultures in batch fermentation conducted at 37 °C, pH of 7, and 150 rpm with methanogenesis inhibition. Each culture includes 6 samples taken at three time points in duplicate. All OTUs involved (a), OTUs with reads higher than 100 of each culture involved (b), and OTUs with reads higher than 1000 of each culture involved (c). 112

Figure 6.5. Neighbor-joining tree based on 16S rRNA gene sequences determined in stage 6 of semi-continuous fermenter and related reference lineages. 15 most abundant OTUs were selected for analysis and shown with abundance and taxonomy information. The phylogenetic tree (bootstrap 1000: > 90% black node, > 70% gray node with black outline and > 50% gray node) were performed in ARB with SILVA database SSU NR99 as reference..... 118

Figure 6.6. Composition of relative abundance of OTUs at genus level in different

sludge samples. Hierarchical clustering of a total of 39 samples was performed based on all OTUs from the microbial communities with a UPGMA algorithm to generate a newick-formatted tree. For sample labels, F represents fresh AD sludge; E is batch test with ethanol as electron donor; G is batch test with glycerol as electron donor; M is batch test with both ethanol and glycerol as electron donors; S stands for semi-continuous fermentation. The numbers represent stage and order (E1_1: stage 1, parallel number 1; S1_1: stage 1, phase 1)..... 120

Figure 6.7. UniFrac emperor PCoA (a. weighted, b. unweighted) of a total of 39 samples based on all OTUs from the microbial communities. For sample labels, F represents fresh AD sludge; E is batch test with ethanol as electron donor; G is batch test with glycerol as electron donor; M is batch test with both ethanol and glycerol as electron donors; S stands for semi-continuous fermentation. The numbers represent stage and order (E1_1: stage 1, parallel number 1; S1_1: stage 1, phase 1). 123

Figure 6.8. CCA of microbial community structure with fermentation operational conditions. Arrows represent the three substrate-based environmental variables, glycerol, ethanol, and acetate, and indicate the direction and magnitude of variables associated with the microbial community structure. The 39 samples, including both batch and semi-continuous fermentation, are demonstrated by circles. Triangles with numbers stand for the 35 most-abundant OTUs of all 39 samples. Axes 1 and 2 account for 36.07% and 6.03% of the variation, respectively. 124

Figure 6.9. Phylogenetic tree of genome bins in stage 3 using PhyloPhlAn.	129
Figure 6.10. Phylogenetic tree of genome bins in stage 6 using PhyloPhlAn.....	130
Figure 6.11. Phylogenetic tree of genome bins closely related to <i>Bacteroidia</i> bacteria using PhyloPhlAn.	131
Figure 6.12. Annotated metabolic pathways of glycerol fermentation and carboxylate chain elongation in the system.	131
Figure 7.1. Glycerol fermentation with fermenter-enriched culture.	151
Figure 7.2. Neighbor-joining tree based on 16S rRNA gene sequences and related reference lineages. 20 most abundant OTUs were selected for analysis and shown with average abundance and taxonomy information. The phylogenetic tree was performed in ARB with SILVA database SSU NR99 as reference.	153
Figure 7.3. Physiologic performance of enriched culture from stage 6 with glycerol in batch. Corresponding representative OTUs at four time points are covered 72.04%–89.14% of the total sequences.	154
Figure 7.4. Metabolic pathway of caproate and 1,3-PDO co-production from glycerol with enriched mixed culture.....	157

LIST OF TABLES

Table 2.1. Energy density and market price of selected biomass, liquid fuels and gas.	10
Table 2.2. Applications of caproate in industrial market.	12
Table 2.3. Manufacture technologies of caproate.	13
Table 2.4. A summary of caproate producers.....	19
Table 2.5. A summary of glycerol-fermenting bacteria.	25
Table 3.1. Medium composition for fermentation.	42
Table 4.1. Potential stoichiometry of chain elongation to caproate and glycerol fermentation to 1,3-PDO, ethanol, butanol and caproate.....	54
Table 4.2. Electrons transfer of chain elongation with ethanol and acetate at different ethanol/acetate ratio.	57
Table 4.3. Potential electron production with various electron donors for the NAD ⁺ /NADH electron carrier pair.	61
Table 4.4. Butyric acid and caproic acid production with different substrate molar ratios at a fixed theoretical acetate concentration of 50 mM.	63
Table 4.5. Product distribution in carbon from glycerol fermentation with acetate (50 mM) at different substrate molar ratios.	67
Table 4.6. Products formation distribution of glycerol fermentation with acetate inoculated with fresh anaerobic digestion sludge and ethanol screened culture.	69
Table 4.7. Abundance of most abundant and functional OTUs of each sample.	72

Table 4.8. Abundance and taxonomy of top 20 most abundant OTUs in fresh AD sludge sample.....	75
Table 5.1. Summary of processed sequences and results from alpha diversity analysis.	80
Table 5.2. Abundance and taxonomy of top 20 most abundant OTUs in fresh AD sludge samples.	83
Table 5.3. Comparison of abundant OTUs of previous observation with this study.	89
Table 5.4. A summary of genomes recovered from shotgun <i>de-novo</i> assembly.	90
Table 5.5. Standard transformed Gibbs free energy of ethanol oxidation to acetate and H ₂ by <i>D. vulgaris</i> , and butyrate formation from acetate and H ₂ by <i>A. sticklandii</i>	97
Table 6.1. Average concentrations of substrates and products in stage 6 of semi-continuous fermenter. Standard deviation is given in parentheses.	117
Table 6.2. Label and taxonomic information of 35 most-abundant OTUs in Figure 6.7.	125
Table 6.3. High-quality recovered genome bins.	128
Table 6.4. Glycerol fermentation and carboxylate chain elongation pathways in some high-quality recovered genome bins.	135
Table 6.5. Energy conservation modes (excluding substrate-level phosphorylation) of recovered genome bins.	142
Table 7.1. Electron flow calculation of glycerol fermentation with enriched culture.	156

LIST OF ABBREVIATIONS

SCFAs	Short chain fatty acids
1,3-PDO	1,3-Propanediol
VFAs	Volatile fatty acids
MCFAs	Medium chain fatty acids
MSW	Municipal solid waste
CCS	Carbon capture and storage
DGGE	Denaturing gradient gel electrophoresis
UASB	Upflow anaerobic sludge blanket
MEC	Microbial electrolysis cell
<i>T</i>	Temperature
<i>I</i>	Ionic strength
AD	Anaerobic digestion
SWH	Shek Wu Hui
BESA	2-Bromoethanosulfonic acid
PBS	Phosphate Buffer Saline
HRT	Hydraulic retention time
HPLC	High-performance liquid chromatography
RID	Refractive index detector
GC	Gas chromatography
TCD	Thermal conductivity detector
PE	Paired-end
bp	Base pairs

OTU	Operational taxonomic unit
UPGMA	Unweighted-pair group mean average
CCEP	Carboxylates chain elongation process
PCoA	Principal coordinate analysis
SRB	Sulfate-reducing bacteria
G+C content	Guanine-cytosine content
CDS	Coding DNA sequences
Rnf	<i>Rhodobacter</i> nitrogen fixation
IMG	Integrated Microbial Genomes
DOE JGI	Department of Energy Joint Genome Institute
CCA	Canonical correspondence analysis
SLP	Substrate-level phosphorylation
ETP	Electron transport phosphorylation
FBEB	Flavin-based electron bifurcation
PHB	Poly- β -hydroxybutyrate

Chapter 1. Introduction

1.1 Background

An alternative process for anaerobic wastewater treatment with methane recovery is to elongate the carbon chain of short chain fatty acids (SCFAs) with a formation of medium chain fatty acids (MCFAs), e.g. *n*-caproic acid with higher monetary value. Mixed culture carboxylates chain elongation for renewable caproate production with ethanol as an electron donor has been developed, and several liter-scale studies have been conducted and a first pilot-scale study is underway (Angenent et al., 2016). However, the underlying microbial pathways in anaerobic mixed culture are not well understood. In addition to the chain elongating bacterium, *Clostridium kluyveri*, the roles and metabolism of other dominant bacteria in chain elongation process still need further investigation (Agler et al., 2012).

A recent study of environmental life cycle on production of caproate from mixed organic wastes recommended that future associated research focus on the reduction of ethanol use in chain elongation and improve the recovery efficiency of the extraction solvent (Chen et al., 2017). Another potential electron donor is glycerol as a surplus byproduct from the rapid growth of waste-derived biodiesel industry. Biological reduction of glycerol to 1,3-propanediol (1,3-PDO) concurrently produces oxidative byproducts (SCFAs and ethanol) which limit its purity and cause the cost for separation and distillation (Leng et al., 2017). To circumvent the energy sink requirement and upcycle both the wastewater treatment process and the biodiesel

industry, it is highly beneficial to produce a valuable secondary product from the byproducts along with 1,3-PDO. The upgrade of byproducts for the production of caproate could make the 1,3-PDO recovery more cost-efficient. The key point is how to cultivate a consortium of function bacteria who are able to reduce glycerol to 1,3-PDO and transfer the electrons into acetate and butyrate for caproate production via carboxylate chain elongation. The hypothesized biological pathways are shown in Figure 1.1.

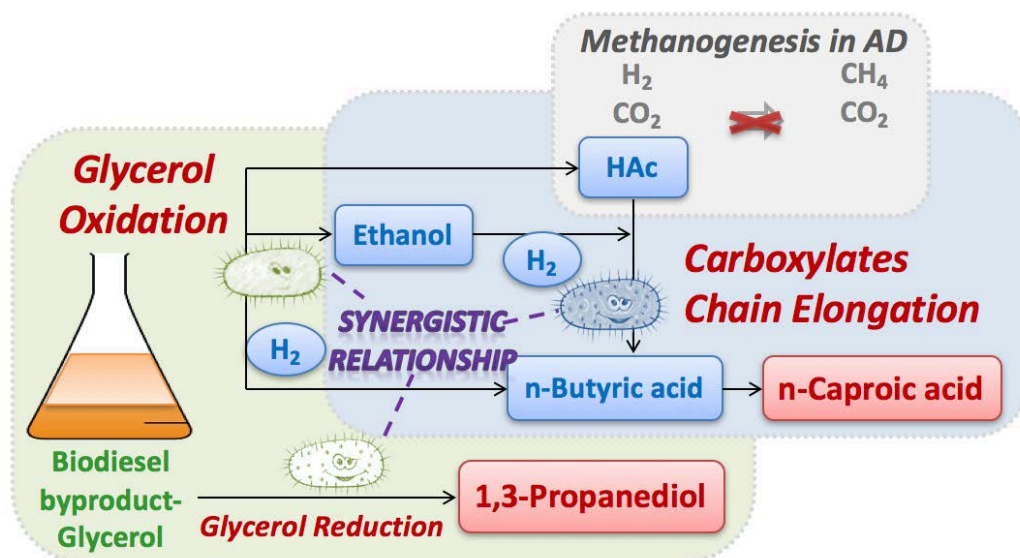


Figure 1.1. Co-production of caproate and 1,3-PDO from glycerol with mixed culture.

1.2 Objectives

The broad aim of this study is to evaluate two value-added chemicals, caproate and 1,3-PDO, co-production from glycerol and disclose the microbial networks and biological pathways of glycerol fermentation and carboxylate chain elongation. The specific objectives of this study are shown as follows:

- (1) To evaluate the thermodynamic feasibility of different electron donors for carboxylate chain elongation and determine optimized environmental conditions of biochemical reactions for caproate production.
- (2) To determine the optimized substrate-level stoichiometric ratios of ethanol to acetate for caproate production and glycerol to acetate for caproate and 1,3-PDO co-production.
- (3) To investigate the physiological performance of ethanol-acetate, glycerol-acetate, and glycerol-ethanol-acetate fermentation with optimized substrates stoichiometric ratios in batch and semi-continuous fermentation.
- (4) To explore the microbial community associated with carboxylate chain elongation and glycerol fermentation, and reconstruct metabolic pathways of the enriched mixed culture.
- (5) To examine the co-production of caproate and 1,3-PDO from glycerol with ethanol self-sufficiency inoculated by enriched mixed culture.

1.3 Thesis Organization

This thesis is composed of eight chapters. The first chapter includes the background information, motivation, objectives and the structure of this thesis.

Chapter Two provides a comprehensive literature review of related study. Chain elongation for caproate production and glycerol fermentation with different products formation are introduced, in particular in mixed culture.

In Chapter Three, the experimental materials and specific experiment design are described.

In Chapter Four, thermodynamic and physiological insights gained into the caproate production from ethanol and acetate, co-production of 1,3-PDO and caproate from glycerol are reported. The optimized substrate-level stoichiometric ratios of ethanol to acetate for caproate production and glycerol to acetate for caproate and 1,3-PDO co-production are also discussed.

In Chapter Five, 16S rRNA gene-based amplicon and shotgun metagenomics sequencing were employed to elucidate the mixed culture chain elongation with ethanol by uncovering the microbes and functional pathways involved. An intricate and synergistic microbial network in mixed culture carboxylates chain elongation is unveiled.

Chapter Six discusses the physiological performance of ethanol-acetate, glycerol-acetate, and glycerol-ethanol-acetate fermentation with optimized substrates stoichiometric ratios in both batch and semi-continuous fermentation. The microbial community associated with carboxylate chain elongation and glycerol fermentation are disclosed and the reconstructed metabolic pathways in enriched mixed culture are described.

Chapter Seven demonstrates the co-production of caproate and 1,3-PDO from glycerol with ethanol self-sufficiency inoculated by enriched mixed culture, and discusses a unique combination of metabolic pathways successfully facilitating the hypothesized conversion.

In the last chapter, conclusions of the work present in this thesis are summarized. Moreover, the limitations of the present study and recommendations for the future work are proposed.

Chapter 2. Literature review

2.1 Demand of waste to bioproducts conversion with mixed culture microbiomes



Figure 2.1. Waste(water) treatment and recycling to bioproducts as alternatives to methane in anaerobic undefined mixed culture to tackle with global issues.

2.1.1 Environmental threats, economics and sustainability

The global generation of municipal solid waste (MSW) is estimated at 1.7 to 1.9 billion metric tons per year (Balasubramanian & Tyagi, 2017b; Chen et al., 2016), and the global generation of wastewater of municipal origin is estimated at 330 km³ (Balasubramanian & Tyagi, 2017a). This huge quantity of waste(water) includes a large proportion of recyclable matters, which could be efficiently used for bioproduct conversion, and the disposal of the large quantity of biodegradable food waste brings heavy loading to landfills and squanders the recyclable organic contents. Therefore,

sustainable strategies and technologies must be implemented to treat and reuse the large amount of organic wastes.

Accessible fossil fuel with limited amount as energy resource is a global economic constraint. According to the International Energy Outlook 2016, total world consumption of marketed energy increases 48% from 2012 to 2040 (U.S. Energy Information Administration, 2016). Although the large resources of fossil fuel are still available recently and the global average fossil fuel conversion efficiency has been improved, they will be depleted very quickly in the near future, and only 1% of the worldwide power plants using fossil fuel will be equipped with carbon capture and storage (CCS) technology by 2035 (Patel, 2014). Therefore, in order to tackle with energy scarcity problem, sustainable alternative fuels, such as biofuels, must be combined with fossil fuel as energy resources in the near future.

Global climate change, one of the most critical environmental threats in 21st century, leads to the extreme weather, affects water supply, food security and ecological diversity. Greenhouse gas emission from rapid fossil fuel burning is one of the major reasons. The carbon storage in fossil fuel of thousands years is released from deep earth layer into atmosphere in carbon dioxide and methane, breaking the carbon cycle. Methane is a stronger greenhouse gas with 25 times of global warming potential per unit mass than carbon dioxide (Parry & Intergovernmental Panel on Climate Change. Working Group II., 2007). Methane generation from natural

decomposition of organic waste accounts for the main methane emission source. Anaerobic digestion of waste(water) with methane production needs to be technically upgraded for an efficient utilization of the methane. A challenge but also an opportunity, therefore, exists to change the view of organic wastes (biomass) to versatile renewable resources which can be used by various industries. With the strategy of waste(water) recycling for bioproducts production as an alternative to methane, the wastes can be reused, the fossil fuel consumption can be reduced, and the net greenhouse gas emission decrease (Figure 2.1).

2.1.2 Sustainable production of biofuels and chemicals

The sustainability of biofuels and chemicals are highly depending on the biomass feedstock (Groom et al., 2008). For example, corn-based ethanol manufacturing uses large quantities of fossil fuel and brings about food competition to the society (Granda et al., 2007). According to the viewpoint of a previous study (Tilman et al., 2009), sustainable biofuels should be derived from feedstock generated with much lower life-cycle greenhouse gas emissions than fossil fuels and with little or no competition with food production. In addition, energy input for the recovery of biofuels and chemicals from waste biomass should be minimized. Municipal and industrial organic waste with a large biodegradable proportion is one of the best biofuel feedstocks.

The first generation biofuels are made from sugar, starch and vegetable oil, such as

ethanol, butanol and biodiesel (Ho et al., 2014). Among them, ethanol is the most common biofuel, which is successfully applied in ethanol–gasoline blend spark-ignition engines (Yuksel & Yuksel, 2004). The disadvantages of bioethanol fuel are the low energy density and the high energy input for its distillation. The second generation biofuels are made from various types of biomass, such as lignocellulose biomass (Ho et al., 2014). It solves the problem of food competition from feedstock, however, makes the biofuels extraction even harder (Hendriks & Zeeman, 2009). In addition to the traditional biofuels, there are other biofuels or bio-chemicals, such as biogas, syngas, caproate. Table 2.1 summarizes the energy density and market prices for some of them.

Regarding to conversion technologies, biofuels production has two main pathways, namely thermos-chemical pathway and biological pathway (Mandegari et al., 2016). The schematic process of biofuels production is shown in Figure 2.2 (Liu et al., 2010; McKendry, 2002). In contrast to thermo-chemical pathway which requires external heat, chemical additions and is unfavorable for biofuel production from high water content biomass, biological pathway is preferable with advantages of less energy, chemical input, and capacity to use high water content sources including organic fraction of municipal solid waste.

Table 2.1. Energy density and market price of selected biomass, liquid fuels and gas.

Product	Specific density (MJ/kg)	Energy density (MJ/L)	Market price* (US\$/Ton)
Ethanol	23.4 - 26.8	18.4 - 21.2	400 - 600
Butanol	36	29.2	1,450 - 2,450
Biodiesel	37.8	33.3 - 35.7	400 - 1,500
Methane	55 - 55.7	(Liquefied) 23.0 - 23.3	3500 - 5600
Methane	55.5	0.0364	-
Hydrogen	120 - 142	(Liquefied) 8.5 - 10.1	-
Acetate	14 - 15	14 - 15	600 - 700
Caproate	30 - 31	27.5 - 28.5	3,600 - 5,800

* Market price in China enquiry online

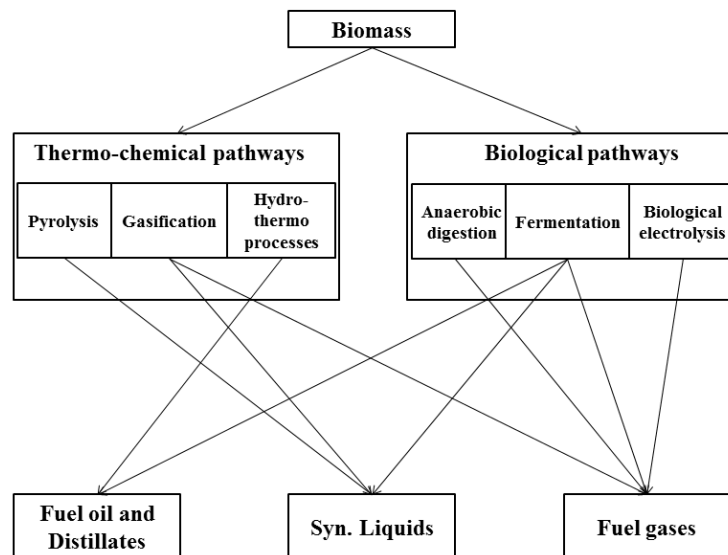


Figure 2.2. The schematic of process of biofuels production from biomass.

2.1.3 Undefined mixed culture fermentation

Mixed culture biotechnology contains the traditional elements of environmental biotechnology in the fields of waste streams treatment with industrial biotechnology that aims at specific nutrients, organics products recovery and product maximization (Kleerebezem & van Loosdrecht, 2007). Using undefined mixed culture, microbial population with expected metabolic capacities can be enriched from a natural seed inoculum by the selection of substrate and operational conditions. In contrast to pure culture, undefined mixed culture for waste treatment and recycling is vital, because it's an open and anaerobic system that has adaptive capacity, the tolerance to the complexity and variability of substrates, and no need for energetically unfavorable sterilization and aeration (Agler et al., 2011).

In conclusion, production of high energy density biofuels and chemicals from organic waste under undefined mixed culture is a sustainable way to tackle with waste disposal, global climate change and energy scarcity problems.

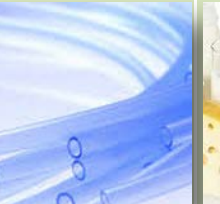
2.2 Carboxylates chain elongation for caproate production

2.2.1 Applications and manufacture technologies of caproate

Caproate (*n*-caproic acid), a 6-carbon saturated MCFA, is capable of serving as a fuel precursor or industrial commodity, and can be easily separated from the fermentation

media to reduce the energy input for distillation (Agler et al., 2012). It has higher energy value per carbon atom than methane, ethanol or acetate, and the low solubility property (1.082 g/100 mL at 20 °C) in water. Caproate is a basic industrial chemical and widely applied to artificial flavor, pharmaceuticals, lubricant, and plasticizer manufacturing processes (Cheon et al., 2014; Kenealy et al., 1995; Panke et al., 2004; Pommet et al., 2003). Ethyl caproate made from caproate is a valuable artificial flavor with pineapple fragrance for wine manufacture (Li et al., 2008). Caproin made from caproate is used for dairy industry (Harper, 1957). The market demand of caproate rapidly increase recently due to the versatile applications (Table 2.2).

Table 2.2. Applications of caproate in industrial market.

Industrial applications of caproate				
				
Artificial flavor	Medicine	Lubricant	Plasticizer	Dairy

The technology for caproate production varies. With coconut oil hydrolysis, caproate can be refined via distillation (Hoover et al., 1973). This process highly depends on the coconut oil and is not suitable for Hong Kong and Mainland China which lacks of coconut oil. Caproate can also be produced with paraffin oxidation and refined via distillation (Boss et al., 1973), and with octanol oxidation which is a byproduct of the

process from castor oil to sebacic acid. However, these processes require high cost but keep low efficiency. Another major process for caproate production is octanol oxidation with nitric acid (Xu et al., 1990). The selectivity of this process is poor with more than 10% byproduct heptylic acid generation. And a large amount of NO, NO₂ will be generated in this process, which brings threat to environment (Table 2.3). In contrast, caproate production from organic wastes has been reported through mixed culture chain elongation in carboxylate platform (Agler et al., 2011).

Table 2.3. Manufacture technologies of caproate.

Coconut oil hydrolysis	Paraffin, Castor oil	Octanol oxidation with nitric acid	Mixed culture fermentation
Highly depending on the coconut oil resource; Not suitable for Hong Kong and Mainland China	High cost but low efficiency	Poor selectivity with more than 10% byproduct; A large amount of NO, NO ₂ generation bringing threat to environment	Low cost, high efficiency, sustainability

2.2.2 Carboxylates chain elongation and caproate production in undefined mixed culture

The carbon chains of molecules can be elongated by different microbial pathway in undefined mixed culture under anaerobic conditions. Three major pathways have been summarized including homoacetogenesis, succinate production and reverse β -oxidation, shown in Figure 2.3 (Spirito et al., 2014). Through these pathways,

complex substrates from organic waste can be treated and recovered into renewable chemicals and fuels. In homoacetogenesis which is well known as Wood-Ljungdahl pathway, the inorganic carbon dioxide can be reduced to formate and carbon monoxide (Ragsdale & Pierce, 2008). The formyl group from formate is reduced to a methyl group and then combined with carbon monoxide and Coenzyme A to produce acetyl-CoA for further 2-carbon acetate formation. In succinate formation, 3-carbon glycerol, serving as a carbon source and electron donor, combines with carbon dioxide to produce 4-carbon succinate. With reverse β -oxidation pathway, the SCFAs, such as 2-carbon acetate and 4-carbon butyrate, are elongated into a 6-carbon MCFA, caproate, with ethanol or lactate as electron donor (Spirito et al., 2014).

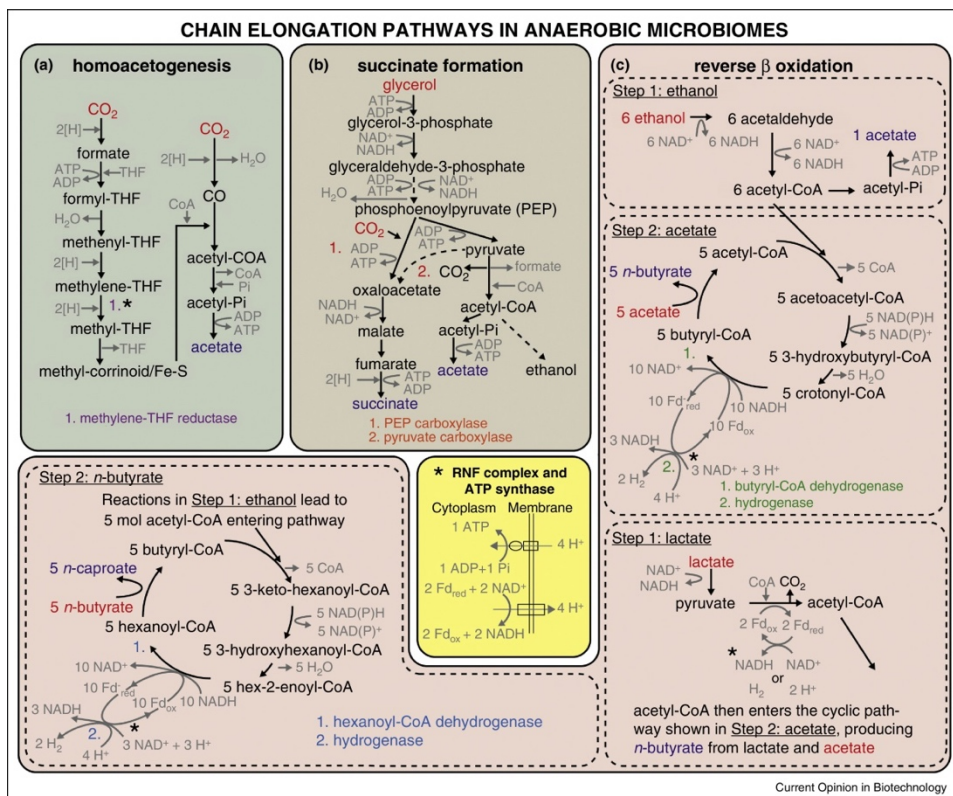


Figure 2.3. Chain elongation pathways in anaerobic mixed culture adopted from Spirito et al.

(2014).

In undefined mixed culture, the persistent methanogens compete for substrates, acetate and ethanol, with chain elongation bacteria. In order to achieve the caproate production through reverse β -oxidation pathway, the methanogenesis barrier must be overcome. There are several methods to inhibit methanogens, such as chemical inhibition (Steinbusch et al., 2011), periodic heat shock (Oh et al., 2003), low pH inhibition (Agler et al., 2011), or combined low pH with thermal pre-treatment of inoculum (Steinbusch et al., 2009). The first method which has been commonly used is expensive, especially in large scale. Schlegel found that methanogens are killed when they are exposed to temperature over 80 °C while ethanol and butyrate production microorganisms are not heat-sensitive (Schlegel, 1993). The second one with demand of heat input is only suitable for waste-heat-rich biorefinery process. In terms of effect of pH, the methanogenesis rate was 33 times smaller at pH 6 than at pH 7, while the reduction rate of acetate to ethanol was optimal at pH 6 along with butyrate production with ethanol consumption (Steinbusch et al., 2009). However, the low pH inhibition might affect the thermodynamic feasibility of biochemical reactions of caproate production communities (Alberty, 2005).

Caproate production with chain elongation of SCFAs using ethanol as electron donor has been successfully achieved. For example, Steinbusch conducted a fed batch in a UASB reactor with 1 L working volume. The reactor was inoculated with non-sterilized granular sludge and operated at pH 7 and Temperature 30 °C. The substrate was 50 mM ethanol (continuous-maintained) and 50 mM acetate. Hydrogen

with flowrate of 200 mL h⁻¹ was fed. The highest *n*-caproic acid production rate of 25.6 mM C d⁻¹ was achieved, equivalent to 0.6 mol C per mol C of acetate. The dominant strains were *C. kluyveri* & *Azospira oryzae* from Denaturing Gradient Gel Electrophoresis (DGGE) profile (Steinbusch et al., 2011). Agler conducted a semi-continuous (47h fermentation+1h biomass settling period) reactor with 5 L working volume and HRT of 12 days. The reactor was inoculated with non-sterilized natural microbiomes and ran at pH 5.5, Temperature 30 °C. Diluted yeast fermentation beer of 5.7 g COD L⁻¹d⁻¹ (ethanol loading rate 83.3 mM C d⁻¹) was fed as substrate. He got the highest *n*-caproic acid production rate of 76.5 mM C d⁻¹ and identified the dominant species of *C. kluyveri* and *Clostridium acetobutylicum* (Agler et al., 2012). An in-line membrane based liquid/liquid continuous extraction system of the unionized *n*-caproic acid was utilized in the research of Agler to avoid the toxicity of it towards microbial community at low pH (Agler et al., 2012). The driving force of *n*-caproic acid was a hydrophobic selective solvent with a pH gradient. However, energy-intensive in-line membrane based liquid/liquid *n*-caproic acid extraction system is not necessary if the fermentation is running at neutral pH. Because the density of *n*-caproic acid is 0.929 g/cm³, and the solubility of it in water is 1.082 g/100 mL, supernatant extraction in the fermenter is enough for semi-continuous system.

2.2.3 Caproate formation microbiomes and biological pathways

C. kluyveri is a strict anaerobe first enriched from the mud of a canal by H. A. Barker, 1937 in Delft, The Netherlands (Barker, 1937). It's a motile, rod shaped, endospore forming and gram-positive bacterium. The main substrates of *C. kluyveri* are ethanol, acetate for metabolism and bicarbonates only for cell synthesis (Barker et al., 1945; Bornstein & Barker, 1948; Jungermann et al., 1968). The bacterium is able to grow in a range of pH from 5.2 to 8.0 and a range of temperature from 25 to 43 °C (optimized from 35 to 37 °C) (Kenealy & Waselefsky, 1985). The chain elongation of acetate with ethanol for butyrate and caproate production through reverse β -oxidation pathway has been annotated in *C. kluyveri*, as shown in Figure 2.4. The enzymes list in Figure 2.4 could also have a function in caproyl-CoA (hexanoyl-CoA) formation (Seedorf et al., 2008). The butyryl-CoA: acetate CoA transferase (Cat3) has a broad substrate specificity, which could work on butyrate and caproate formation with butyryl- and caproyl-CoA reacting with acetate (Seedorf et al., 2008).

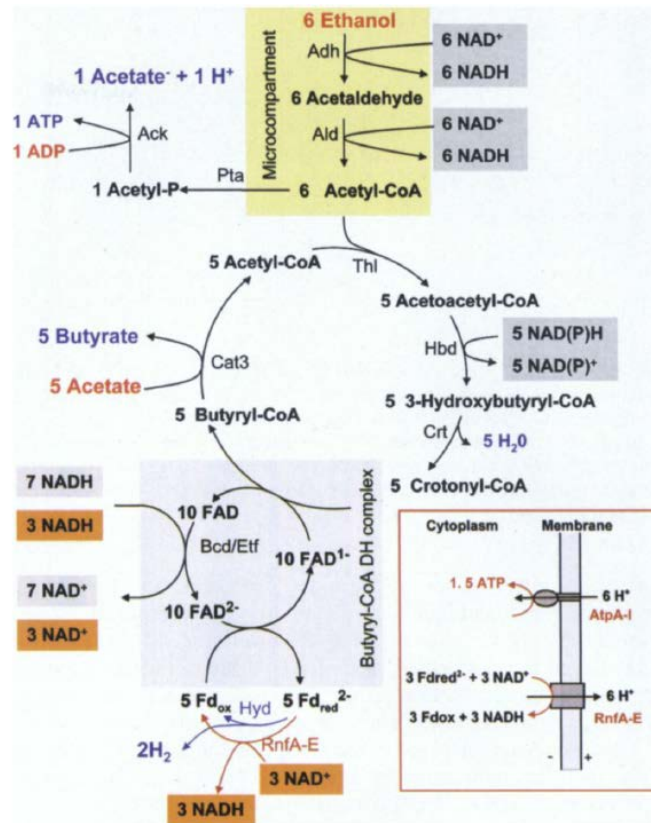


Figure 2.4. Chain elongation of acetate with ethanol as electron donor in *C. kluyveri* adopted from Seedorf et al. (2008).

Caproate production has also been reported with other bacteria. For example, *Megasphaera elsdenii*, producing 5-carbon to 8-carbon medium-chain carboxylic acids (MCCAs) from glucose, lactate, sucrose, and butyrate (Jeon et al., 2016; Marounek et al., 1989; Marx et al., 2011). *Eubacterium limosum*, which forms caproate by growing on methanol (Genthner et al., 1981). *Eubacterium pyruvativorans*, which utilizes amino acids and butyrate, pyruvate or trypticase to produce caproate (Wallace et al., 2004; Wallace et al., 2003). *Peptococcus niger* and *Peptostreptococcus anaerobius*, which produces butyrate and caproate with peptone (Ezaki et al., 2001). And the strain CPB6, affiliated with *Clostridium* cluster IV of

the *Ruminococcaceae* family, which produces a high concentration of caproate from lactate (Zhu et al., 2017). These caproate producing bacteria are mesophilic and can be enriched from rumen culture or partially from the human gut ecosystem. A summary of caproate producers is shown in Table 2.4.

Table 2.4. A summary of caproate producers.

Substrate	Caproate producer	Favorable condition	Reference
Ethanol and acetate	<i>Clostridium kluyveri</i>	pH of 7.2, Temperature of 32 – 35 °C	(Barker et al., 1945)
Propanol and succinate; ethanol and succinate	<i>Clostridium kluyveri</i>	pH of 6.4, Temperature of 35 – 37 °C	(Kenealy & Waselefsky, 1985)
Glucose and lactate	<i>Megasphaera elsdenii</i>	pH of 6.4, Temperature of 35 – 37 °C	(Marounek et al., 1989)
Sucrose and butyrate	<i>Megasphaera elsdenii</i>	pH of 6.0, Temperature of 37 °C	(Choi et al., 2013)
Methanol	<i>Eubacterium limosum</i>	pH of 7.2, Temperature of 37 °C	(Genthner et al., 1981)
Amino acids and butyrate, pyruvate or trypticase	<i>Eubacterium pyruvativorans</i>	pH of 7.0, Temperature of 39 °C	(Wallace et al., 2004; Wallace et al., 2003)
Peptone	<i>Peptococcus niger</i>	Not reported	(Ezaki et al.,

	<i>Peptostreptococcus</i>		2001)
	<i>anaerobius</i>		
Lactate	<i>Ruminococcaceae</i> bacterium CPB6	pH of 5.0 – 6.5, Temperature of 30 – 40 °C	(Zhu et al., 2017)
D-galactitol	<i>Clostridium</i> sp. BS-1	pH of 7.0, Temperature of 37 °C	(Jeon et al., 2010)

The biological pathways of caproate production by different caproate producers has been summarized and demonstrated in Figure 2.5. As reported in the genome of *C. kluyveri*, caproate is directly produced through a substitutional reaction with acetate/butyrate and caproyl-CoA which is catalyzed by Cat3 which has a broad substrate specificity (Seedorf et al., 2008). Caproyl-CoA is formed via a reverse β -oxidation pathway with acetyl-CoA and butyryl-CoA reduction. When butyryl-CoA is reduced from acetyl-CoA, butyrate production could be achieved via two pathways which are catalyzed by either CoA transferases (broad substrate specificity) or a combination of two enzymes, phosphate butyryltransferase and butyrate-kinase via butyryl-phosphate (Pryde et al., 2002). Some bacteria contain only phosphate butyryltransferase and butyrate-kinase other than CoA transferases. This may be one of the reasons that some bacteria produce butyrate but with insignificant caproate production. As shown in Figure 2.5, acetyl-CoA is the central intermediate linking with reoxidation of different electron donors for caproate

production via reverse β -oxidation.

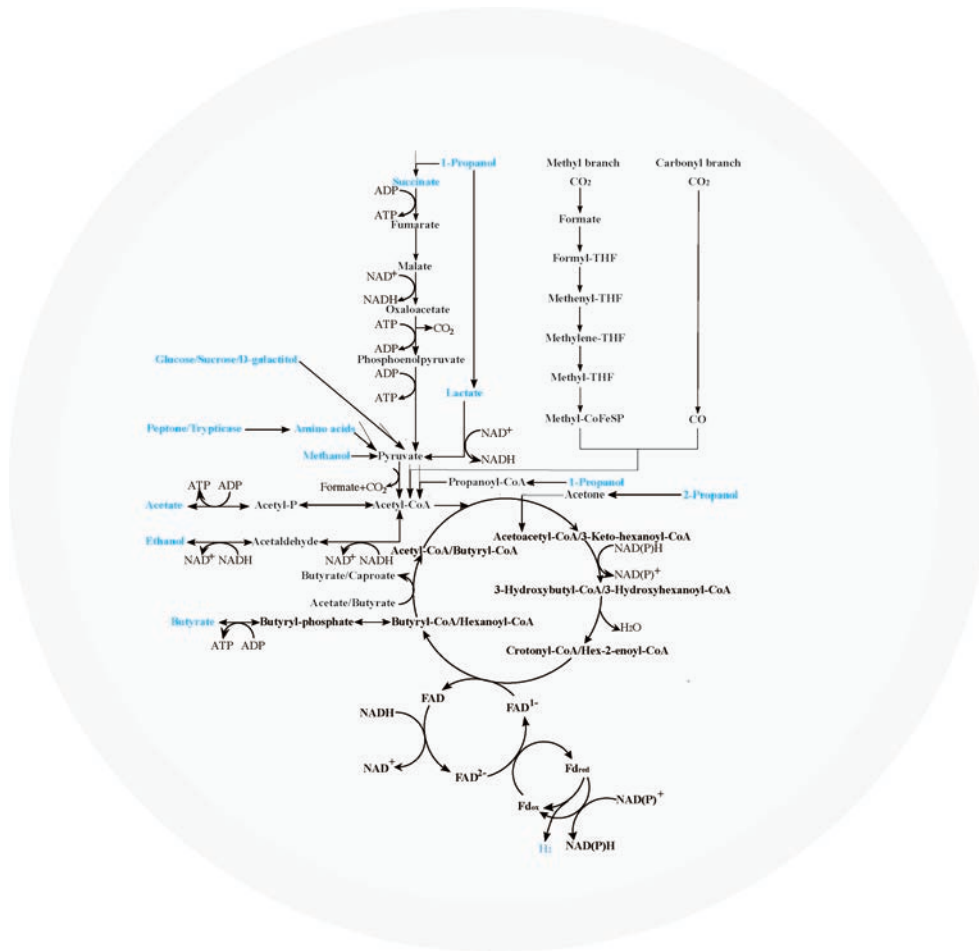


Figure 2.5. Biological pathways of caproate production in different anaerobes (partial).

2.3 Waste-derived reduced compounds for carboxylate chain elongation

The chain elongation of SCFAs into MCFAs within anaerobic reactor microbiomes requires additional electron donors. Some of the reducing compounds, directly donating electrons into chain elongation, including ethanol, methanol, lactate and glucose (Table 2.4), are contained in or could be produced from waste, and (Agler et al., 2012; Ghaffar et al., 2014; Li et al., 2007; Vasudevan et al., 2005). With electrons and carbons transferred from water-soluble compounds (SCFAs and reducing

compounds) into MCFAs of a good separation property, the cost of energy input for the resources recovery from wastes is reduced. In addition, there are also some other waste-derived compounds, such as H₂, syngas (a mixture of CO, H₂ and CO₂) and glycerol, that can provide energy and reducing equivalents for chain elongation indirectly with production of ethanol, lactate and SCFAs as intermediates (Ito et al., 2005; Munasinghe & Khanal, 2010; Sakai et al., 2004). With these reducing compounds, the chain elongation for MCFAs production can be achieved via interspecies cooperation. Chain elongation for caproate and caprylate production from acetate with H₂ as electron donor in anaerobic mixed culture has been achieved by Steinbusch et al. (2011), and syngas fermentation for caproate production via ethanol as intermediates has been reported by Vasudevan et al. (2014). However, MCFAs production with glycerol as electron donor is yet to be investigated.

2.4 Glycerol fermentation

2.4.1 Crude glycerol produced in biodiesel process

Glycerol, the structural component of any lipids, is abundant in nature (da Silva et al., 2009). In the process of biodiesel production with the transesterification of vegetable oils or animals fats, 10 % (w/w) of crude glycerol is produced as a byproduct (Yazdani & Gonzalez, 2007). Therefore, glycerol is presently being generated in surplus with the rapid growth of biodiesel industry, which causes the decline of glycerol price, shown in Figure 2.6. Crude glycerol has been regarded as a waste stream that leads to a disposal cost. Ultimately, removal and recovery of this

byproduct in the biodiesel stream is crucial for the economic viability of the biodiesel industry. Biological conversion of glycerol into different industrial chemicals and solvents has been widely applied due to the high reduced nature of carbon in glycerol and lower capital and operational costs of anaerobic fermentation. Elongation of SCFAs with glycerol as electron donor instead of ethanol is of special interest.

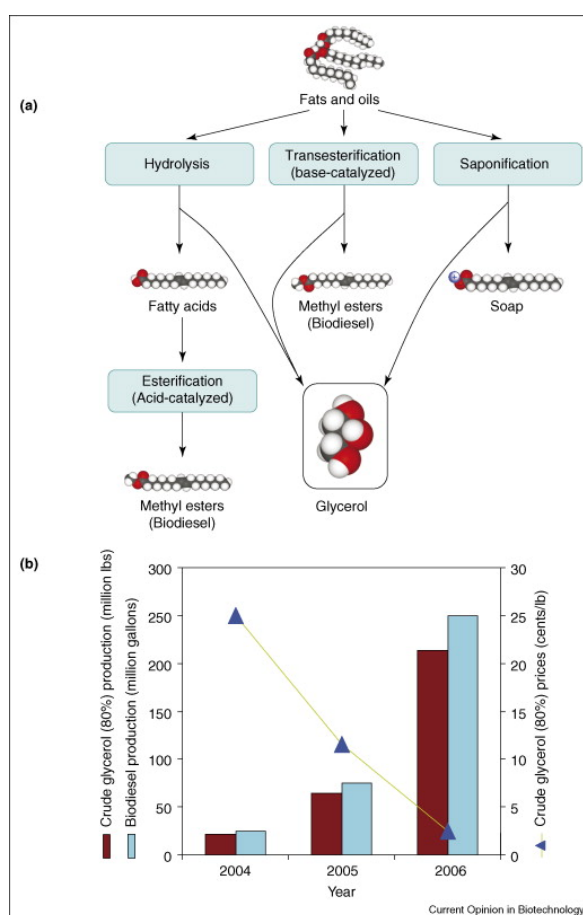


Figure 2.6. Glycerol production as a byproduct in biodiesel process from fats and oils (a); Biodiesel production and its impact on crude glycerol prices in US (b) adopted from Yazdani and Gonzalez (2007).

2.4.2 Glycerol fermentation pathways and microbiomes

One particular and promising choice of the biological conversion of glycerol is to

produce 1,3-PDO which is a monomer applied for all types of polycondensates (polyester and polyurethanes) (Lee et al., 2015). Glycerol fermentation generates other products such as acetate, lactate, butyrate, ethanol, butanol, succinic acid and H₂ in addition to 1,3-PDO (Viana et al., 2014). The common glycerol fermentation microorganisms that have been investigated so far belong to the genera of *Klebsiella*, *Clostridium*, *Citrobacter*, and *Enterobacter* (Yazdani & Gonzalez, 2007). For example, *Klebsiella pneumoniae* anaerobically grows on glycerol for 1,3-PDO production at pH 7 and 37 °C (Menzel et al., 1997); *Klebsiella planticola* produces ethanol and formate from glycerol at pH 7.2 to 7.4 and 37 °C (Jarvis et al., 1997); *Clostridium butyricum* produces 1,3-PDO, butyrate, and acetate with glycerol at pH 7 and 37 °C (Barbirato et al., 1998); *Clostridium pasteurianum* produces 1,3-PDO and butanol from glycerol (Biebl, 2001); *Citrobacter freundii* converts glycerol to 1,3-PDO at around pH 7 and 30 °C (Boenigk et al., 1993); *Enterobacter Aerogenes* produces ethanol from glycerol at pH 7 and 30 °C (Chantoom et al., 2014). A summary of glycerol-fermenting bacteria is shown in Table 2.5. These consortia of glycerol-fermenting bacteria have similar cultivation conditions with chain elongation caproate producing bacteria. Figure 2.7 shows the metabolic pathways for glycerol fermentation in *Clostridia*. The previous study showed that glycerol fermentation obtained a 1,3-PDO and ethanol yield of 0.34 and 0.44 mol per C₃, respectively (Varrone et al., 2012), while chain elongation achieved a caproate yield of 0.6 mol C per mol C with ethanol (Steinbusch et al., 2011). This suggests that if simultaneous glycerol formation and chain elongation can be achieved,

stoichiometric 1,3-PDO and caproate yields of 0.34 and 0.088 mol per mol glycerol are theoretically possible.

Table 2.5. A summary of glycerol-fermenting bacteria.

Products	Microorganism	Favorable condition	Reference
1,3-PDO	<i>Klebsiella pneumoniae</i>	pH of 7.0 and Temperature of 37 °C	(Menzel et al., 1997)
Ethanol	<i>Klebsiella pneumoniae</i> (mutant strain, GEM167)	Temperature of 37 °C	(Oh et al., 2011)
Ethanol and formate	<i>Klebsiella planticola</i>	pH of 7.2 – 7.4 and Temperature of 37 °C	(Jarvis et al., 1997)
1,3-PDO, butyrate, and acetate	<i>Clostridium butyricum</i>	pH of 7.0 and Temperature of 37 °C	(Barbirato et al., 1998)
1,3-PDO and butanol	<i>Clostridium</i> <i>pasteurianum</i>	pH of 4.5 – 7.5, Temperature of 35 °C	(Biebl, 2001)
1,3-PDO	<i>Clostridium beijerinckii</i>	pH of 7.0 and Temperature of 37 °C	(Gungormusler et al., 2011)
Ethanol	<i>Clostridium</i> <i>cellobioparum</i>	pH of 6.0 and Temperature of 35 °C, Microbial Electrolysis Cell (MEC)	(Speers et al., 2014)
1,3-PDO	<i>Citrobacter freundii</i>	pH of 7.0, Temperature of 30 °C	(Boenigk et al., 1993)

Ethanol	<i>Enterobacter Aerogenes</i>	pH of 7.0,	(Chantoom et al.,
		Temperature of 30 °C	2014)
Ethanol, succinate, formate	<i>Escherichia coli</i>	pH of 6.3,	(Murarka et al.,
		Temperature of 37 °C	2008)

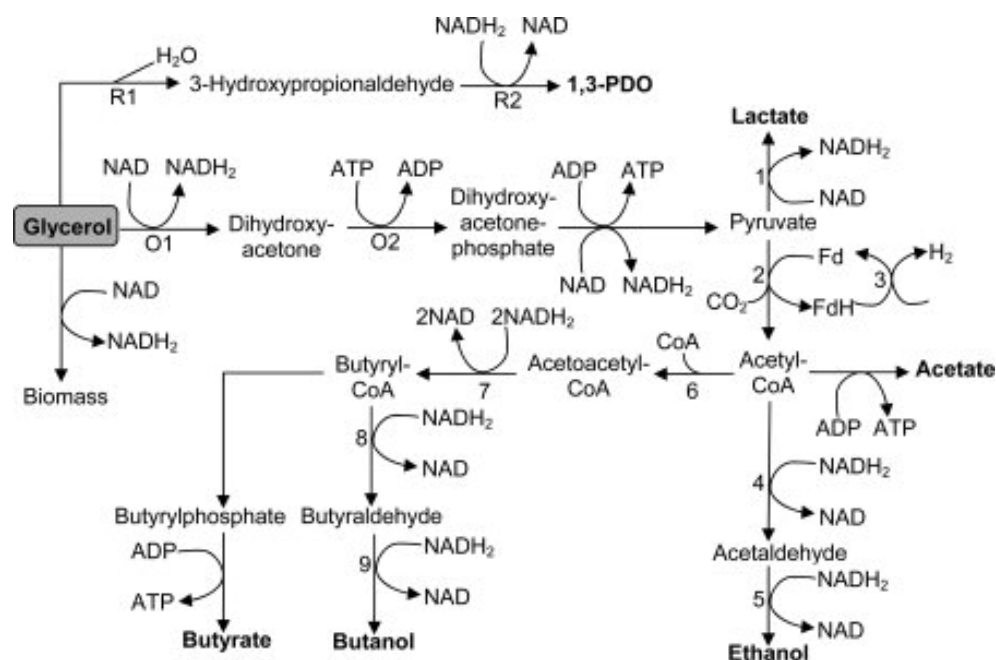


Figure 2.7. Metabolic pathways for glycerol metabolism in *clostridia* adopted from Johnson and Taconi (2007).

As shown in Figure 2.7, two different concurrent metabolic pathways of glycerol dissimilation are demonstrated including the reductive pathway and the oxidative pathway. In the former pathway, 1,3-PDO production from glycerol reduction begins with the transformation of glycerol to 3-hydroxy-propionaldehyde, which is catalyzed by a coenzyme B12-dependent propanediol dehydratase (Forage & Foster, 1982) or a coenzyme B12-dependent glycerol dehydratase (Raynaud et al., 2003).

Then, 3-hydroxy-propionaldehyde is further reduced to 1,3-PDO catalyzed by 1,3-PDO dehydrogenase (Raynaud et al., 2003). The glycerol dehydratase is the rate-limiting step for glycerol reduction to 1,3-PDO (Abbad-Andaloussi et al., 1996; Menzel et al., 1998). In the latter pathway, glycerol is first dehydrogenated to form dihydroxyacetone by glycerol dehydrogenase, followed by the phosphorylation of dihydroxyacetone to dihydroxyacetone-phosphate by glycolytic enzyme dihydroxyacetone kinase, which is then funneled to glycolysis leading to the production of different carboxylic acids and solvents (da Silva et al., 2009; Johnson & Taconi, 2007). Pyruvate is the core intermediate of glycerol oxidation, which is further converted into acetyl-CoA through an oxidation pathway for SCFAs and alcohol production. These two pathways are associated with electron balance of glycerol dissimilation. For example, one molar acetate production from one molar glycerol results in six molar electrons production. Therefore, other reductive reactions such as 1,3-PDO production should occur to balance the reducing equivalents of the system. In addition, the generation of acetate or butyrate will yield higher amount of ATP compared to ethanol or butanol, which promotes higher biomass formation (Johnson & Taconi, 2007).

2.4.3 Glycerol fermentation with undefined mixed culture

In order to reduce the production costs, the use of undefined mixed cultures to convert crude glycerol to value-added chemicals under nonsterile conditions is more prospective. Glycerol fermentation by undefined mixed culture has been widely

investigated for 1,3-PDO, ethanol, propionate and hydrogen production (Chen et al., 2016; Moscoviz et al., 2016; Varrone et al., 2012; Vikromvarasiri et al., 2014). A selective microbial community with functional consortium that adapt to the imposed conditions will dominate after enrichment.

Dietz and Zeng achieved yields of 0.56–0.76 mol 1,3-PDO per mol glycerol with a minimal culture medium containing crude glycerol used mixed cultures from municipal wastewater biogas sludge (Dietz & Zeng, 2014). Selembo et al. achieved 1,3-PDO yield of 0.69 mol 1,3-PDO per mol glycerol along with 0.28 mol H₂ per mol glycerol using heat treated mixed culture (Selembo et al., 2009). Liu et al. used an organic soil mixed culture with heat pretreatment and obtained 1,3-PDO yield of 0.65 mol 1,3-PDO per mol glycerol (Liu et al., 2013). Vikromvarasiri et al. collected mixed culture seed from a full-scale upflow anaerobic sludge blanket (UASB) system and achieved an ethanol yield of 0.81 mol ethanol per mol glycerol operated at 30 °C and pH 7 under anaerobic conditions (Vikromvarasiri et al., 2014). The enriched culture mainly consists of bacteria closely associated with genera of *Enterobacter* and *Klebsiella* (Vikromvarasiri et al., 2014). Chen et al. achieved propionate yield of 0.45 g COD/g COD glycerol with anaerobic sludge from a mesophilic digester treating starch wastewater induced by high ammonium concentration (Chen et al., 2016). Temudo et al. conducted two comparable fermentations of glycerol and glucose with continuous stirred reactors at pH of 8 under undefined mixed culture (Temudo et al., 2008). They found glycerol

fermentation produced more reduced compounds (ethanol and 1,3-PDO) and less biomass than glucose fermentation (Temudo et al., 2008). With limited substrate, the yields of ethanol and formate were higher (60% of the carbon converted) (Temudo et al., 2008). Formate can be further converted into H₂ and CO₂ by the action of formate-H₂ lyase from certain species of enteric bacteria such as *Escherichia coli* and *E. aerogenes* (Viana et al., 2014). With increasing the substrate concentration, the yields of 1,-PDO, acetate increased, and the biomass yield decreased (Temudo et al., 2008). Mixed culture fermentation products spectrum of glycerol are influenced by the NAD⁺/NADH balance.

The pH of undefined mixed culture is a crucial parameter that has a significant impact on the production spectrum. The pH not only affects the growth rate, substrate uptake, efficiency of the substrate conversion, but also determines the fraction of undissociated acids in the solution, which are able to permeate through cell membranes (Temudo et al., 2008). Vikromvarasiri conducted a batch scale experiment to study the pH impact on the bioethanol production from glycerol under mixed culture. They found the neutral pH (6.8 and 7) favored the glycerol utilization and bioethanol production (Vikromvarasiri et al., 2014). Moscoviz et al. investigated the initial pH effect on glycerol fermentation in a batch mixed culture with pH values between 5 and 9 and found that the highest 1,3-PDO production yields was obtained at pH 7 and 8 (Moscoviz et al., 2016).

2.5 Challenges on 1,3-PDO and caproate co-production

To the knowledge of the authors, such a co-production has yet to be realized due to several challenges. First, no organism is known to perform glycerol reduction to 1,3-PDO and glycerol oxidation coupling with chain elongation to caproate concurrently. The chain elongation bacterium, *C. kluyveri*, lacks glycerol utilization capability (Seedorf et al., 2008), and the well-known glycerol fermentation bacteria of the genera *Klebsiella*, *Clostridium*, and *Citrobacter* are also incapable of producing caproate (Barbirato et al., 1998; Biebl, 2001; Boenigk et al., 1993; Jarvis et al., 1997; Menzel et al., 1997). Consequently, the co-production is only possible via interspecies cooperation. This presents a second challenge on the suitability of cultivation matrix to support the co-dominance of 1,3-PDO-producing and caproate-producing microbes. Specifically, ethanol and 1,3-PDO, both of which are products of glycerol fermentation, may have opposing effects on caproate producers. Ethanol is an essential electron donor for caproate production, while 1,3-PDO suppresses the chain elongation activity of *Clostridium* spp (Szymanowska-Powaowska & Kubiak, 2015). Ultimately, achieving a balance of 1,3-PDO and ethanol levels within the cultivation matrix is crucial for supporting the population and activity of caproate producers.

2.6 Bioenergetics of anaerobic microbial metabolism

Electron donor (energy source) can be used by microorganisms for two approaches, converted into reduced products (catabolism), and assimilated for cell synthesis

(anabolism). Cells of microorganism also decay due to normal maintenance or predation. Part of energy is transferred to the acceptors for more energy generation, and the other part is transferred into the non-active organic cell residue, shown in Figure 2.8. A very important facet of the energy partitioning framework is that it is in terms of electron equivalents (Rittmann & McCarty, 2012). Both the reduced products and microorganism cell synthesis can be expressed as electron equivalents. The two major intermediates connecting cell synthesis and reduced products formation are pyruvate and acetyl-CoA. From pyruvate to acetyl-CoA, a formate (CO_2 and H_2) will be generated. In undefined mixed culture, different organisms are co-existing, and some of them are in an obligately mutualistic metabolism. In the case of one partner of organisms living off the products of the other partner of organism, it is termed as syntrophy. Schink suggested that a biological “quantum of energy” minimum exists in syntrophy. It has been postulated that a bacterium needs a minimum energy of about -20 kJ mol^{-1} (one third of that needed for the synthesis of an ATP molecule), which is the smallest quantum of metabolically convertible energy for an ion to transport across the cytoplasmic membrane and the amount (Schink, 1997). However, it was reported that many organisms can survive on much less than the -20 kJ mol^{-1} (McCarty & Bae, 2011).

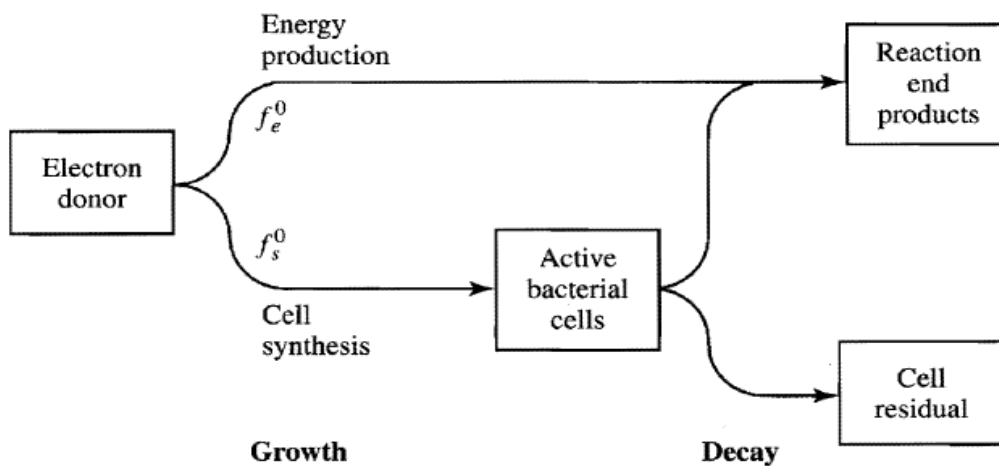


Figure 2.8. Utilization of electron donor for energy production and cell synthesis adopted from Rittmann and McCarty (2012).

2.6.1 Thermodynamics in metabolism

Free energy change of a specific reaction indicates it is spontaneous or not. Thermodynamics of biochemical reactions is more complicated than that of chemical reactions in aqueous solution owing to more independent variables that have to be specified (Alberty, 2005). For example, biochemical reactants often exist in ions, and the activity coefficients of ions are influenced by ionic strength. Therefore, the thermodynamic analysis which is used to compare the free energy change of reactions should involve the association with pH, ionic strength. A transformed thermodynamic model of Gibbs free energies has been well developed (Alberty, 2005). The transformed thermodynamic model with these transformed Gibbs free energies is more appropriate allowing for the simple thermodynamic analysis of multiple forms of biological species in aqueous solution. For example, as the pH and

ionic strength are embedded in the transformed thermodynamic properties, calculating the Gibbs free energy of reaction with varying pH and ionic strength is straight forward with tabulated transformed Gibbs free energy of formation for each species. In general, the thermodynamic strategy can be used to compare the potential of different electron donors and manipulate different reduced products formation from different pathways.

Thermodynamic laws can act as a vital tool to provide the theoretical basis for analyzing experimental results and providing important information regarding bacterial growth and metabolism. Thermodynamics also play an important role in understanding the pathway reversibility. The possible pathway reversibility of specific anaerobic catabolic reactions opens a new paradigm in the development of biofuels and chemicals with high energy density (Leng et al., 2017). As anaerobic bioprocesses occur in an energy-scarce environment, the metabolic pathways take place very close to thermodynamic equilibrium with minimum energy dissipation. Therefore, a slight change in substrate/product concentrations or environmental conditions can alter the direction of the pathway.

2.6.2 Energy conservation in anaerobic syntrophy

Even when the products of syntrophic acetogenesis are at low concentrations, the Gibbs free energy change for syntrophic metabolism is about -15 to -20 kJ mol^{-1} , the smallest quantum of metabolically convertible energy for an ion to transport

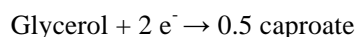
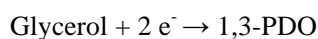
across the cytoplasmic membrane, which is lower than the energy required for the synthesis of ATP from ADP (40–70 kJ per mole of ATP) (McInerney et al., 2009; Schink & Stams, 2013). Syntrophic bacteria couple substrate metabolism directly to ATP synthesis by classical phosphoryl transfer reactions (Jackson & McInerney, 2002), and are well adapted to an energetically stressed lifestyle with low growth rate and low yield. The marginal energy economy of syntrophs based on oxidation of energetically unfavorable substrates requires an efficient interspecies transfer to enable the survival of the microbes involved under thermodynamically demanding conditions; for instance, extremely low H₂ concentrations are required for syntrophic bacteria to acquire energy through the oxidation of energetically challenging substrates (Kouzuma et al., 2015). For thermodynamically unfavorable reduction of protons (H⁺) to hydrogen (H₂), very efficient energy conservation systems are necessary (Narihiro et al., 2016). Whole-genome and metagenome sequencing approaches have been used to investigate how the syntrophic microorganisms conserve energy when their thermodynamic driving force is very low (McInerney et al., 2009).

Reverse electron transfer, an energy conservation system, is a key requirement in syntrophic interactions. Via biochemical mechanisms, microorganism can perform endergonic chemical transformations under prevailing conditions using energy from other, exergonic transformation steps (Stams & Plugge, 2009). In syntrophic methanogenesis, hydrogen and formate formation from electrons generated in the

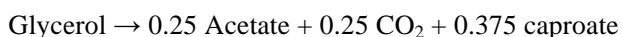
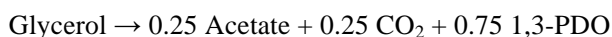
oxidation of acyl-CoA intermediates to their respective enoyl-CoA intermediates is energetically unfavorable and can occur only with energy input from an energy conservation process (Sato et al., 1999).

2.7 Economic analysis of the processes for two value-added chemicals co-production from glycerol

Theoretically, 1 mole of glycerol produces 1 mole of 1,3-PDO with consumption of 2 mole of electrons while 1 mole of glycerol produces 0.5 mole of caproate with consumption of the same electrons.



As the biological reaction of acetate and CO₂ production from glycerol generates the highest amount of electrons (6 mole e⁻ per mole glycerol), the highest conversion rates of 1,3-PDO and caproate were 0.750 and 0.375 mole per mole glycerol, respectively.



For treating 1000 ton of glycerol, the theoretical highest yields for 1,3-PDO and caproate are 620 ton and 473 ton, respectively. The latest market price for refinery and crude glycerol are around US\$ 600 and 70 per ton, respectively (Quispe et al., 2013). The market prices for 1,3-PDO and caproic acid with high purity (above 98%)

are US\$ 900 to 1200 and 2100 to 3600 per ton, respectively. With refinery glycerol as substrate, the feedstock capital is US\$ 600,000. The income for 1,3-PDO production is US\$ 558,000 to 744,000 while that for caproic acid production is US\$ 993,300 to 1,702,800. With crude glycerol as substrate, the benefits are even higher. In general, caproic acid production from the glycerol waste stream is with applicable potential from economic perspective.

Chapter 3. Materials and Methodology

3.1 Thermodynamics calculation of biochemical reactions

The thermodynamic calculations of biochemical reactions were made after Alberty (Alberty, 2005; Hu et al., 2011). The transformed Gibbs free energy, $\Delta_r G'_T$, is as follows,

$$\Delta_r G'_T = \Delta_r G'^0_T + RT \ln Q \quad (1)$$

where $\Delta_r G'^0_T$ is the standard transformed Gibbs free energy of a reaction at a temperature (T) and Q is a factor related to the activities of reactants and products defined as,

$$Q = \frac{(a_A)^a (a_B)^b \dots (a_C)^c}{(a_X)^x (a_Y)^y \dots (a_Z)^z} \quad (2)$$

where the numerator represents the activity of products A , B , C , etc. and the denominator represents the activity of reactants X , Y , Z , etc. The powers are the stoichiometric coefficients of the products and reactants in each reaction.

In order to obtain $\Delta_r G'^0_T$, the standard Gibbs free energy of formation ($\Delta_f G^0$) and standard enthalpy of formation ($\Delta_f H^0$) for each reactant and product at $T=298.15$ K and ionic strength (I)=0 M were found in references, and a T correction for the Gibbs free energies of formation is first required. For example, for a given condition of 310 K, the Gibbs free energy of formation at $T=310$ K, $\Delta_f G^0_{i,310K}$ is adjusted with Eq. 3,

$$\Delta_f G^0_{i,310K} = \left(\frac{310K}{298.15K} \right) \times \Delta_f G^0_{i,298.15K} + \left(1 - \frac{310K}{298.15K} \right) \times \Delta_f H^0_i \quad (3)$$

Subsequently, the standard transformed Gibbs free energies of formation at different pH and ionic strength, $\Delta_f G'^0_{i,310K}(pH, I)$, are calculated as follows:

$$\Delta_f G'^0_{i,310K}(pH, I) = \Delta_f G^0_{i,310K} - N_{H,i}RT \ln 10^{-pH} - RT\alpha(Z_i^2 - N_{H,i})I^{1/2}/(1 + BI^{1/2}) \quad (4)$$

where $RT\alpha = 9.20483 \times 10^{-3}T - 1.28467 \times 10^{-5}T^2 + 4.95199 \times 10^{-8}T^3$, $B = 1.6 \text{ kg}^{1/2} \text{ mol}^{-1/2}$, $N_{H,i}$ is the number of hydrogen atoms in a substance, and Z_i is the charge number (Alberty, 2001).

Finally, with the standard transformed Gibbs free energies of formation of each reactant and product, the standard transformed Gibbs free energy of each biochemical reaction is calculated using Eq. 5,

$$\Delta_r G'^0_T = \sum v_i \times \Delta_f G'^0_{i,T} \quad (5)$$

where v_i is the stoichiometry of each reactant and product.

A MATLAB program for thermodynamics calculation is created as follows,

```
Zi = [0 -1 0 0 0 0 -1 -1 -1 0 -1 -2];
```

```
# Charge number of substances (Reactors and products)
```

```
NH,i = [2 1 2 6 8 8 3 7 11 10 26 27];
```

```
# Number of hydrogen atoms in a substance
```

```
ΔfH0 = [0 -691.99 -285.83 -277.7 -676.55 -480.8 -486.01 -533.8 -583.8 -327.3 0  
-31.94];
```

```
# Standard enthalpy of formation (ΔfH0) at T=298.15 K and I=0 M
```

```
ΔfG0 = [0 -586.77 -237.17 -174.9 -497.48 -327.08 -369.31 -352.63 -335.96 -171.84
```

```

0 22.65];

# Standard gibbs free energy of formation ( $\Delta_f G^0$ ) at T=298.15 K and I=0 M

n = length(Zi);

 $\Delta_f G^0_{i,310K}$  = zeros(n,1);

for i = 1:n

     $\Delta_f G^0_{i,310K}(i) = (310.00/298.15) \times \Delta_f G^0_{i,298.15K} + (1-310.00/298.15) \times \Delta_f H^0_i$ ;

end

# To calculate gibbs free energy of formation at Temperature=310 K

T = 310; B = 1.6;

R = 0.008314;

RTa = 9.20483 × (10-3) × T - 1.28467 × (10-5) × (T2) + 4.95199 × (10-8) × (T3);

I = [0 0.05 0.1 0.15 0.2 0.25]; pH = [4.5 5 5.5 6 7 8];

 $\Delta_f G'^0_{i,310K}$  = zeros(length(I),length(pH),n);

for j = 1:n

    for i = 1:length(I)

        for k = 1:length(pH)

             $\Delta_f G'^0_{i,310K}(i,k,j) = \Delta_f G^0_{i,310K}(j) - N_{H,i}(j) \times R \times T \times \log(10^{(-pH(k))}) - RTa \times (Z_i(j)^2 - N_{H,i}(j))$ 

             $\times (I(i)^{(1/2)}) / (1 + B \times I(i)^{(1/2)})$ ;

        end

    end

```

```

    end

end

# To calculate standard transformed Gibbs free energies of formation at different pH
and ionic strength

 $\Delta_1 G'^0_{310K}$  = zeros(length(I),length(pH)); % R1 as an example

for i = 1:length(I)

    for k = 1:length(pH)

         $\Delta_1 G'^0_{310K}(i,k) =$ 
        -  $\Delta_f G'^0_{i,310K}(i,k,4)$ -  $\Delta_f G'^0_{i,310K}(i,k,7)$ +  $\Delta_f G'^0_{i,310K}(i,k,8)$ +  $\Delta_f G'^0_{i,310K}(i,k,3)$ ;

    end

end

# To calculate the standard transformed gibbs free energy of reactions

 $\Delta_1 G'^0_{310K}*$  =  $\Delta_4 G'^0_{310K}(3,5)$ ; % R1 as an example, fixing pH = 7 and I = 0.1 M

x1 = [0 0.001 0.01 0.1 0.2 0.4 0.6 0.74];

y1 = [0 10 25 50 100 150 250 500];

 $\Delta_1 G'_{310K}$  = zeros(length(x1),length(y1));

```

for i = 1:length(x1)

for k = 1:length(y1)

$$\Delta_1 G'_{310K}(i,k) = \Delta_1 G'^0_{310K} + 0 \times R \times T \times \log(x1(i)) - 1 \times R \times T \times \log(y1(k));$$

end

end

To calculate the transformed gibbs free energy of reactions in terms of the activities of reactants and products

3.2 Inoculum and medium for fermentation

An inoculum of 10% (volume/working volume [v/v]) anaerobic digestion (AD) sludge was collected from Shek Wu Hui (SWH) Sewage Treatment Works in Sheung Shui, Hong Kong. SWH Sewage Treatment Works treated wastewater collected from Sheung Shui and Fanling areas where freshwater is used for toilet flushing. Thus, the seed culture of our study is non-saline AD sludge.

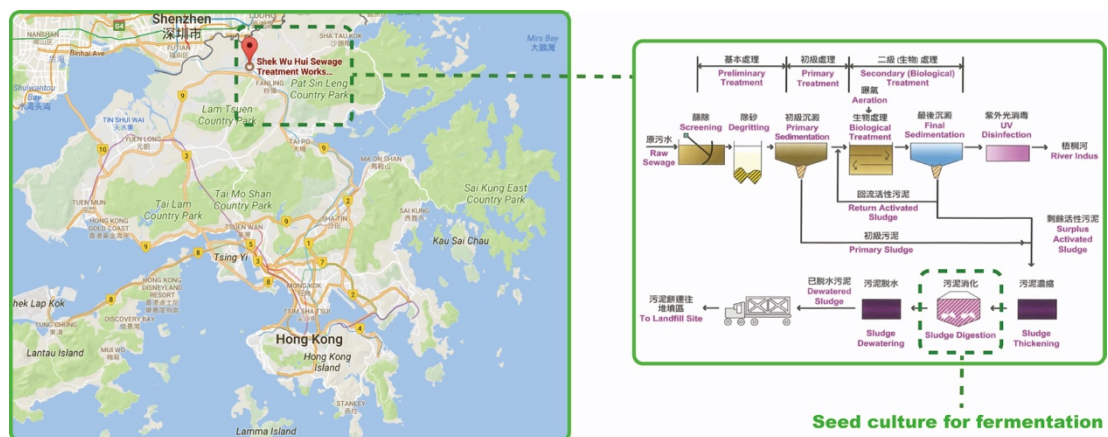


Figure 3.1. Inoculum source for fermentation (Drainage Services Department, Hong Kong).

The composition of the medium included substrates, minerals, trace metals, a reducing agent, a methanogenesis inhibitor, and a redox indicator. One liter of the fermentation medium contained 0.20 g of KH_2PO_4 , 0.50 g of NH_4Cl , 1.00 g of NaCl , 0.24 g of MgSO_4 , 0.50 g of KCl , 0.15 g of $\text{CaCl}_2 \cdot 2\text{H}_2\text{O}$, 2.52 g of NaHCO_3 , 1.50 mg of $\text{Fe}_2\text{Cl} \cdot 4\text{H}_2\text{O}$, 0.30 mg of H_3BO_3 , 0.20 mg of $\text{CoCl}_2 \cdot 4\text{H}_2\text{O}$, 0.05 mg of ZnCl_2 , 0.03 mg of $\text{MnCl}_2 \cdot 4\text{H}_2\text{O}$, 0.03 mg of $\text{Na}_2\text{MoO}_4 \cdot 2\text{H}_2\text{O}$, 0.02 mg of $\text{NiCl}_2 \cdot 6\text{H}_2\text{O}$, 0.01 mg of $\text{CuCl}_2 \cdot 2\text{H}_2\text{O}$, 0.5 g of L-cysteine, 10 g of 2-bromoethanosulfonic acid (BESA), and 1 mL of resazurin (0.1% w/v). The BESA was added to inhibit methanogenesis.

Table 3.1. Medium composition for fermentation.

Mineral		
KH_2PO_4	0.20	g/L
NH_4Cl	0.50	g/L
NaCl	1.00	g/L
MgSO_4	0.24	g/L
KCl	0.50	g/L
$\text{CaCl}_2 \cdot 2\text{H}_2\text{O}$	0.15	g/L
NaHCO_3	2.52	g/L
Trace metal		
$\text{Fe}_2\text{Cl} \cdot 4\text{H}_2\text{O}$	1.50	mg/L
H_3BO_3	0.30	mg/L
$\text{CoCl}_2 \cdot 4\text{H}_2\text{O}$	0.20	mg/L
ZnCl_2	0.05	mg/L
$\text{MnCl}_2 \cdot 4\text{H}_2\text{O}$	0.03	mg/L
$\text{Na}_2\text{MoO}_4 \cdot 2\text{H}_2\text{O}$	0.03	mg/L
$\text{NiCl}_2 \cdot 6\text{H}_2\text{O}$	0.02	mg/L
$\text{CuCl}_2 \cdot 2\text{H}_2\text{O}$	0.01	mg/L
Reducing Agent		
L-cysteine	0.50	g/L
Methanogenesis Inhibitor		
2-bromoethanosulfonic acid (BESA)	10	g/L
Redox indicator		
Resazurin (0.1% w/v)	1	mL/L

3.3 Batch test experiment

3.3.1 Batch tests design for the study in chapter four

Four experimental batches are conducted. The first batch was caproate production from acetate (50 mM) with ethanol or glycerol as electron donor at different molar ratios of ethanol to acetate or glycerol to acetate. The concentration of substrates and products were detected at Day 0 and 35. The second batch was conducted at optimal ratios of ethanol to acetate (50 mM) and glycerol to acetate (50 mM) for catabolism analysis. The third batch was caproate production from acetate with ethanol and glycerol, of which ethanol was added at the beginning or at Day 20. The fourth batch was inoculated with ethanol screened culture and fed with 90 mM ethanol and 30 mM acetate, 120 mM glycerol and 30 mM acetate. The batch fermentation tests were performed in 100 mL anaerobic bottles with rubber stoppers and aluminum caps in duplicate. Each anaerobic bottle was filled with 35 mL working volume, containing carbon source, electron donor, mineral, trace metal, reducing agent, methanogenesis inhibitor, and redox indicator, and then sterilized at 120°C for 20 mins. Before inoculation, the pH was adjusted to 7 with Phosphate Buffer Saline (PBS) solution. After inoculation with 10% (v/v) wet seed culture solution, the anaerobic bottles were capped and closed. The headspace was vacuumed and flushed with nitrogen three times. The anaerobic bottles were incubated at 37°C with agitation at 150 rpm in an incubator.

3.3.2 Batch test design for the study in chapter five

Caproate production from acetate (50 mM) was conducted with ethanol as the electron donor (150 mM). The batch fermentation tests were performed in 250 mL anaerobic bottles with rubber stoppers and plastic caps in duplicate. Each anaerobic bottle was filled with 70 mL medium, and sterilized at 120°C for 20 mins. Before inoculation, the pH was adjusted to 7 using PBS buffer, and maintained around 7 during the entire fermentation process. After inoculated with 10% (v/v) working volume of wet seed, the anaerobic bottles were capped and closed. The headspace was vacuumed and flushed with nitrogen gas for three times to maintain anaerobic condition. The anaerobic bottles were incubated at 37°C with agitation at 150 rpm. Liquid and gas samples were collected periodically and biomass-containing liquid samples were collected at Day 0, 6, 15 and 23.

3.3.3 Batch tests design for the study in chapter six and seven

Caproate production from acetate was conducted with ethanol, glycerol, and a combination of ethanol and glycerol as electron donor(s), respectively. The batch fermentation tests were performed in duplicate in 250-mL anaerobic bottles with rubber stoppers and aluminum caps. Each anaerobic bottle was filled with a 70-mL working volume and then sterilized at 120 °C for 20 min. Before inoculation, the pH was adjusted to 7 with PBS solution, and a pH of around 7 was maintained throughout the fermentation process. After inoculation with 10% (v/v) wet seed, the

anaerobic bottles were capped and closed. The headspace was vacuumed and flushed with nitrogen three times to maintain anaerobic conditions. The anaerobic bottles were incubated at 37 °C with agitation at 150 rpm.

3.4 Semi-continuous fermentation

The semi-continuous fermentation was performed in a 2-L auto-controlled fermenter (Shanghai Bailun Bio. Tech.) with 1.5-L working volume in six stages for 396 days. The fermenter, containing a carbon source, electron donor, minerals, trace metals, reducing agent, methanogenesis inhibitor, and a redox indicator, was sterilized at 120 °C for 20 min before inoculation. After inoculation with 10% (v/v) wet AD sludge, the fermenter became a closed system. The operation was auto-controlled at pH 7 (5 M NaOH and 5 M HCl), 37 °C, and a 150-rpm stirring rate with nitrogen saturation at 1 atm. The semi-continuous fermentation was operated for 96 h per cycle. During each cycle, a 200-mL suspension was decanted and the substrate was supplemented (time 0: substrate feeding, 95 h fermentation, and 1 h settling and rapid effluent removal). Therefore, the flowrate was controlled to 200 mL every 4 days (50 mL/day) and a hydraulic retention time (HRT) of 30 days. Sampling was carried out on Day 0 (influent), Day 2, and Day 4 (effluent).

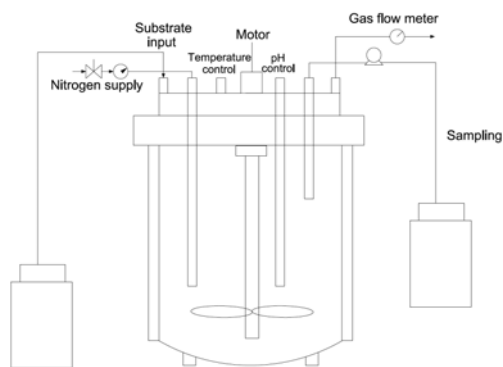


Figure 3.2. Semi-continuous fermentation system.

3.5 Analytical procedures

Liquid samples were taken with a 1-mL syringe, placed into a 2.0-mL centrifuge tube, centrifuged at 6000 rpm for 5 min, and filtered through a 0.20- μ m filter (PVDF syringe, Whatman, Springfield Mill, UK) before analysis. Alcohols and fatty acids were determined using a high-performance liquid chromatography (HPLC) system (SHIMADZU Prominence, MD) equipped with a refractive index detector (RID) and a column (Bio-Rad Aminex HPX-87H column). The operating conditions were 5 mM H₂SO₄ as the mobile phase, a pump flowrate of 0.6 mL/min, 50 °C detector temperature, and 65 °C oven temperature.



Figure 3.3. The HPLC system (SHIMADZU) used for quantification of the target compounds and GC system (Agilent) used for quantification of the target gases.

Gas samples were collected with a 50-mL disposable syringe. The total gas volume was determined at 1 atm. To determine its composition of hydrogen, CO₂, and methane, a 200- μ L gas sample was then analyzed with a gas chromatography (GC) (Agilent 6850 Series II single channel) system equipped with a thermal conductivity detector (TCD) and a carbon molecular sieve-type stationary-phase column (TDX-01, Jing Ke Rui Da Technology, Beijing, China). The operating conditions were helium as the carrier gas, injector temperature of 120°C, oven temperature of 100 °C, detector temperature of 150 °C, pressure control with a 20-psi front inlet pressure, front detector reference flowrate of 15 mL/min, front detector makeup flowrate of 5 mL/min, and total detected flowrate of 41.7 mL/min.

3.6 DNA extraction and high-throughput sequencing

Biomass-containing liquid samples (1 mL) were collected from duplicate cultures and immediately mixed with 100% ethanol at a ratio of 1:1 (v:v) for biomass fixation. The samples were stored at -20°C before DNA extraction (Yang et al., 2013). Total DNA extraction was conducted on the samples centrifugated at 16000g for 10 min using the protocol described by Liu et al. (Liu et al., 1997). The DNA concentrations and the purity were measured using a NanoDrop 2000c UV-vis spectrophotometer (Thermo Scientific). Total DNA samples were sent to BGI (Shenzhen, China) for 16S rRNA genes library construction and high-throughput sequencing on the Illumina MiSeq platform, generating paired-end (PE) reads 300 (Figure 3.4). 16S rRNA amplicon sequencing was conducted using primers 515F (5' GTG CCA GCM GCC GCG GTA A 3') and 806R (5' GGA CTA CHV GGG TWT CTA AT 3'), which targets the V4 variable region (Albertsen et al., 2015). Shotgun metagenomics sequencing was performed on an Hiseq 4000 platform at BGI (Shenzhen, China), generating PE reads with a read length of 151 base pairs (bp). About 5 Gbp of metagenomic data was generated for each DNA sample.

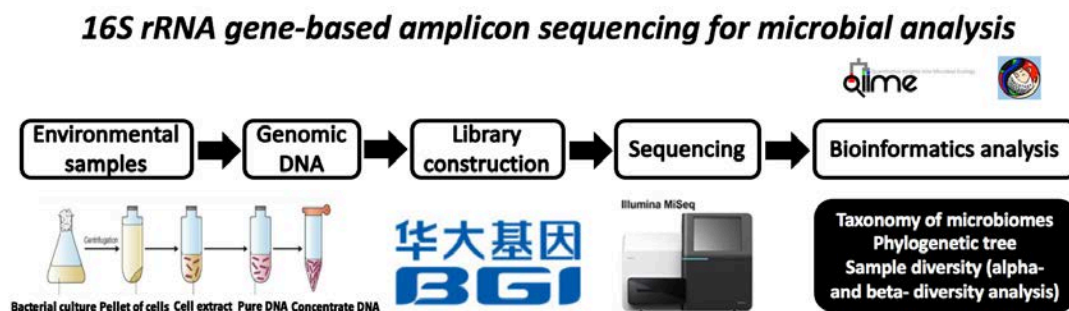


Figure 3.4. Flowchart of 16S rRNA gene-based amplicon sequencing for microbial analysis.

3.7 Bioinformatics analysis

In the study of chapter four, the obtained PE reads were separated to each sample according to barcodes and subsequently processed following the operational taxonomic unit (OTU)-based analysis provided in the MiSeq SOP (Kozich et al., 2013) on the Mothur (v.1.36.1) platform (Schloss et al., 2009). Specifically, we merged pair-end MiSeq reads into contigs and removed those contigs with ambiguous base calls and with read length shorter than 275 bps. The filter contigs were aligned with the SILVA reference database (release 102) and filtered to ensure that the derived contigs were from the V4 region. In addition, chimera contigs identified with UCHIME were removed and the clean sequences were obtained for downstream analyses. Hierarchical clustering of the sludge samples was performed based on all OTUs with an unweighted-pair group mean average (UPGMA) algorithm to generate a newick-formatted tree.

In the study of chapter five, six and seven, for 16S rRNA gene-based analysis, the raw reads were first merged into contigs and screened for ambiguous base calls and read lengths shorter than 400 bp using the Mothur software (v. 1.36.1) (Schloss et al., 2009). The filtered contigs were aligned with the Greengenes reference database in QIIME (MacQIIME 1.9.1) (Caporaso et al., 2010). In addition, the chimera contigs identified with ChimeraSlayer were removed and clean sequences were obtained for downstream analyses (Haas et al., 2011). Taxonomy was assigned with the Greengenes reference database clustered at 97% identity (McDonald et al., 2012). A

neighbor-joining phylogenetic tree was constructed and analyzed in ARB, with SILVA database SSU NR99 as a reference (Ludwig et al., 2004). Hierarchical clustering of the sludge samples was performed based on OTUs with an UPGMA algorithm to generate a newick-formatted tree.

For metagenomic analysis, the raw reads were first trimmed with a minimum quality cutoff of 3 and further screened to be at least 78 bp in length, having an average quality score above 30 and containing less than three ambiguous nucleotides (N's) using trimmomatic (Bolger et al., 2014). Khmer scripts were then used for digital normalization, abundance filtering, and pair and orphan reads splitting (“-k 20”). The trimmed clean PE reads were further *de novo* assembled into long sequence contigs using SPAdes version 3.9.0 based on the de Bruijn graph, with default settings (“-k 19,33,47,61,75 --careful”) (Bankevich et al., 2012; Nurk et al., 2013). The quality of the assembled contigs was evaluated with Quast (Gurevich et al., 2013). Contigs were clustered into taxonomic bins with MaxBin based on an expectation–maximization algorithm (Wu et al., 2014). CheckM was introduced to evaluate the quality of a draft recovered genome bin using a broader set of marker genes specific to the position of a genome within a reference genome tree and information of the collocation of these genes (Parks et al., 2015). The recovered genome bins were matched to the reference phylogenetic tree with PhyloPhlAn (Segata et al., 2013). Protein coding genes were annotated with Prokka version 1.11 (Seemann, 2014). BlastKOALA was used to further characterize individual gene functions and

reconstruct functional pathways (Kanehisa et al., 2016). The flowchart of metagenomic analysis is shown in Figure 3.5.

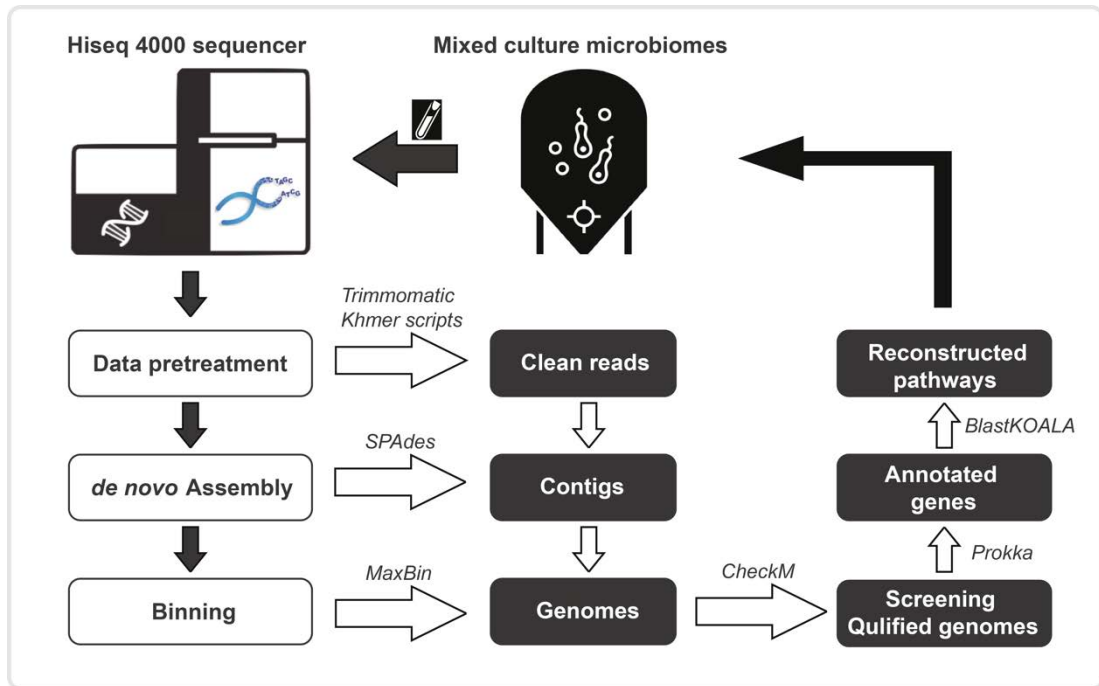


Figure 3.5. Metagenomic analysis flowchart.

Chapter 4. Thermodynamic and physiological study of caproate and 1,3-PDO co-production through glycerol fermentation and fatty acids chain elongation

4.1 Overview

An alternative process for anaerobic wastewater treatment with methane recovery is to elongate the carbon chain of volatile fatty acids (VFAs) with a formation of medium chain carboxylic acids (MCCAs), e.g. *n*-caproic acid with higher monetary value. A potential electron donor is glycerol as a surplus byproduct from the rapid growth of waste-derived biodiesel industry. In the current approach, an industrial chemical, 1,3-PDO is produced from crude glycerol along with a formation of other soluble byproducts including ethanol and VFAs, which necessitates a significant amount of energy input for separation and purification. To circumvent the energy sink requirement and upcycle both the wastewater treatment process and the biodiesel industry, it is highly beneficial to produce a valuable secondary product from the byproducts.

In this chapter, thermodynamic and physiological insights gained into the co-production of 1,3-PDO and caproate from glycerol are reported. Thermodynamics analysis demonstrated that a higher pH range is more favorable when either glycerol or ethanol acting as an electron donor, whereas a high partial pressure (27% at 1 atm) and a low pH (≤ 5.5) are advantageous for caproate formation with hydrogen. With the glycerol-to-acetate molar ratio of 4 and pH of 7, the physiological experiments

achieved a co-production of 1,3-PDO and caproate. However, the caproate yield was low and found to be kinetic-limited. Caproate formation was significantly increased by the intermediate ethanol addition with the optimal mono-caproate formation obtained at the ethanol-to-acetate molar ratio of 3. A synergistic relationship was evinced through microbial characterization, resulting in *C. kluyveri* and some bacteria with function of converting glycerol to VFAs. The knowledge gleaned paves new avenues for the biodiesel industry by upcycling the byproduct crude glycerol into 1,3-PDO and caproate.

4.2 Results and discussion

4.2.1 Thermodynamic analysis of chain elongation with different electron donors

Table 4.1 lists potential stoichiometries for acetate chain elongation with ethanol (Eq. R1 to R6) or H₂ (Eq. R7 and R8), 1,3-PDO/ethanol/butanol formation with glycerol (Eq. R9 to R12), and caproate formation with glycerol (Eq. R13 and R14). To evaluate the thermodynamics of acetate chain elongation for caproate formation with ethanol/glycerol, we developed a generalized stoichiometric model with boundary and assumption of carbon flux balanced in metabolic compounds and a fixed acetate stoichiometry of 1.

Table 4.1. Potential stoichiometry of chain elongation to caproate and glycerol fermentation to 1,3-PDO, ethanol, butanol and caproate.

No.	Electron donor	Stoichiometric molar ratio	Reaction
R1	Ethanol	1:1	$\text{Ethanol} + \text{Acetate}^- \rightarrow \text{Butyrate}^- + \text{H}_2\text{O}$
R2	Ethanol	3:2	$\frac{3}{2} \text{Ethanol} + \text{Acetate}^- \rightarrow \frac{5}{4} \text{Butyrate}^- + \frac{1}{4} \text{H}^+ + \frac{1}{2} \text{H}_2 + \text{H}_2\text{O}$
R3	Ethanol	2:1	$2 \text{Ethanol} + \text{Acetate}^- \rightarrow \text{Butyrate}^- + \frac{1}{3} \text{Caproate}^- + \frac{1}{3} \text{H}^+ + \frac{2}{3} \text{H}_2 + \frac{4}{3} \text{H}_2\text{O}$
R4	Ethanol	3:1	$3 \text{Ethanol} + \text{Acetate}^- \rightarrow \frac{1}{2} \text{Butyrate}^- + \text{Caproate}^- + \frac{1}{2} \text{H}^+ + \text{H}_2 + 2 \text{H}_2\text{O}$
R5	Ethanol	4:1	$4 \text{Ethanol} + \text{Acetate}^- \rightarrow \frac{5}{8} \text{Butyrate}^- + \frac{5}{4} \text{Caproate}^- + \frac{7}{8} \text{H}^+ + \frac{7}{4} \text{H}_2 + \frac{9}{4} \text{H}_2\text{O}$
R6	Ethanol	5:1	$5 \text{Ethanol} + \text{Acetate}^- \rightarrow 0.565 \text{Butyrate}^- + 1.625 \text{Caproate}^- + 1.190 \text{H}^+ + 2.375 \text{H}_2 + 2.625 \text{H}_2\text{O}$
R7	Hydrogen	1:1	$\text{H}_2 + \text{Acetate}^- + \frac{1}{2} \text{H}^+ \rightarrow \frac{1}{2} \text{Butyrate}^- + \text{H}_2\text{O}$
R8	Hydrogen	4:3	$\frac{4}{3} \text{H}_2 + \text{Acetate}^- + \frac{2}{3} \text{H}^+ \rightarrow \frac{1}{3} \text{Caproate}^- + \frac{4}{3} \text{H}_2\text{O}$
R9	Glycerol	-	$\text{Glycerol} \rightarrow \frac{2}{3} \text{1,3-PDO} + \frac{1}{3} \text{Acetate}^- + \frac{2}{3} \text{H}^+ + \frac{1}{3} \text{HCO}_3^- + \frac{1}{3} \text{H}_2$
R10	Glycerol	-	$\text{Glycerol} \rightarrow \frac{1}{2} \text{1,3-PDO} + \frac{1}{4} \text{Butyrate}^- + \frac{3}{4} \text{H}^+ + \frac{1}{2} \text{HCO}_3^- + \frac{1}{2} \text{H}_2$
R11	Glycerol	-	$\text{Glycerol} + \text{H}_2\text{O} \rightarrow \text{Ethanol} + \text{HCO}_3^- + \text{H}_2 + \text{H}^+$
R12	Glycerol	-	$\text{Glycerol} + \frac{1}{2} \text{H}_2\text{O} \rightarrow \frac{1}{2} \text{Butanol} + \text{HCO}_3^- + \text{H}_2 + \text{H}^+$
R13	Glycerol	2:1	$2 \text{Glycerol} + \text{Acetate}^- + \frac{2}{3} \text{H}_2\text{O} \rightarrow \text{Butyrate}^- + \frac{1}{3} \text{Caproate}^- + \frac{7}{3} \text{H}^+ + \frac{8}{3} \text{H}_2 + 2 \text{HCO}_3^-$
R14	Glycerol	3:1	$3 \text{Glycerol} + \text{Acetate}^- + \text{H}_2\text{O} \rightarrow \frac{1}{2} \text{Butyrate}^- + \text{Caproate}^- + \frac{7}{2} \text{H}^+ + 4 \text{H}_2 + 3 \text{HCO}_3^-$

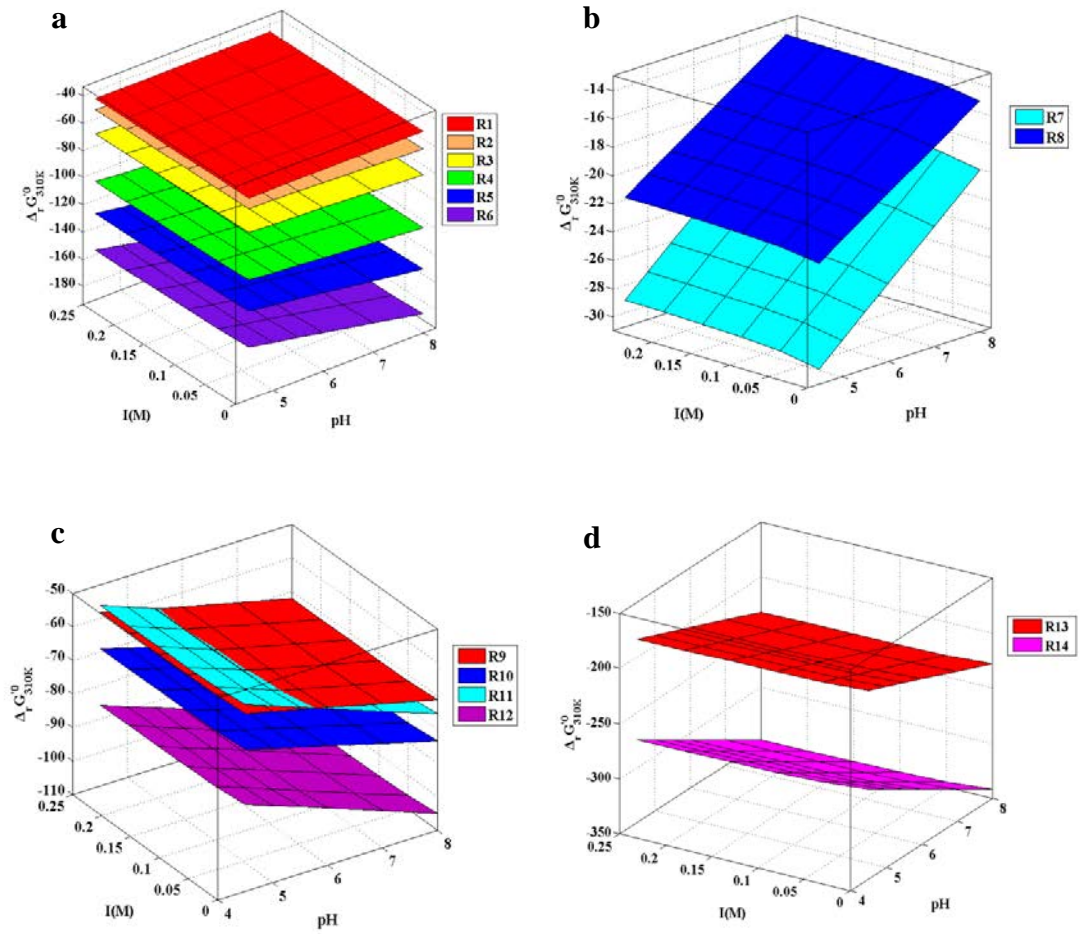


Figure 4.1. Standard transformed Gibbs free energy values ($\Delta_r G'_{310K}$) in KJ mol^{-1} as a function of pH and ionic strength (I) for (a) caproate formation with ethanol (Eq. R1 to R6), (b) caproate formation with H_2 (Eq. R7 and R8), (c) different product formation with glycerol fermentation (Eq. R9 to R12), and (d) caproate formation with glycerol (Eq. R13 and R14).

Fig. 4.1 shows the standard transformed Gibbs free energy values ($\Delta_{R1-14} G'_{310K}$) of the reactions in Table 4.1 (Case 1) as a function of pH and ionic strength (I). $\Delta_{R1-6} G'_{310K}$ for butyrate/caproate formation with a series of stoichiometric ratios of ethanol to acetate, illustrated in Fig. 4.1a, yielded values that were higher than the biological “quantum of energy” minimum of approximately - 20 kJ per mol for cell

survival (Schink, 1997), indicating thermodynamically favorable pathways. More free energy is released with higher ethanol/acetate ratio. Additionally, it is worth noting that higher pH conditions have a positive influence on free energy release for Eqs. R2 to R6, though the influence was negligible for *I*. On the contrary, with H₂, $\Delta_{R7,8}G'_{310K}$ was more negative at lower pH, and $\Delta_{R8}G'_{310K}$ for caproate formation remained at levels higher than the “quantum of energy” minimum only if pH was below 5.5 (Fig. 4.1b). Furthermore, $\Delta_{R9-12}G'_{310K}$ were found to be more negative than the minimum “quantum of energy,” implying that glycerol co-production of 1,3-PDO with acetate or butyrate and mono-production of ethanol or butanol ($\Delta_{R9-12}G'_{310K}$) are all biologically feasible, particularly at higher pH (Fig. 4.1c). Their thermodynamic priorities lie in butanol formation for mono-production and PDO and butyrate formation for co-production. Similarly, the proposed pathways of caproate and butyrate formation with glycerol were energetically possible and more favorable with higher pH, as the $\Delta_{R13-14}G'_{310K}$ values were above the minimal “quantum of energy” (Fig. 4.1d).

In order to better investigate the thermodynamics of different stoichiometries of chain elongation with ethanol and acetate, Gibbs free energy change per electron of each reaction is determined and summarized in Table 4.2 (Case 2).

Table 4.2. Electrons transfer of chain elongation with ethanol and acetate at different ethanol/acetate ratio.

No.	Electron donor	Molar ratio	Reaction	Electrons Transfer per reaction
R1	Ethanol	1:1	$\text{CH}_3\text{CH}_2\text{OH} + \text{CH}_3\text{COO}^- \rightarrow \text{CH}_3(\text{CH}_2)_2\text{COO}^- + \text{H}_2\text{O}$	2.00
R2	Ethanol	3:2	$3/2 \text{CH}_3\text{CH}_2\text{OH} + \text{CH}_3\text{COO}^- \rightarrow 5/4 \text{CH}_3(\text{CH}_2)_2\text{COO}^- + 1/4 \text{H}^+ + 1/2 \text{H}_2 + \text{H}_2\text{O}$	3.00
R3	Ethanol	2:1	$2 \text{CH}_3\text{CH}_2\text{OH} + \text{CH}_3\text{COO}^- \rightarrow \text{CH}_3(\text{CH}_2)_2\text{COO}^- + 1/3 \text{CH}_3(\text{CH}_2)_4\text{COO}^- + 1/3 \text{H}^+ + 2/3 \text{H}_2 + 4/3 \text{H}_2\text{O}$	3.55
R4	Ethanol	3:1	$3 \text{CH}_3\text{CH}_2\text{OH} + \text{CH}_3\text{COO}^- \rightarrow 1/2 \text{CH}_3(\text{CH}_2)_2\text{COO}^- + \text{CH}_3(\text{CH}_2)_4\text{COO}^- + 1/2 \text{H}^+ + \text{H}_2 + 2 \text{H}_2\text{O}$	4.50
R5	Ethanol	4:1	$4 \text{CH}_3\text{CH}_2\text{OH} + \text{CH}_3\text{COO}^- \rightarrow 5/8 \text{CH}_3(\text{CH}_2)_2\text{COO}^- + 5/4 \text{CH}_3(\text{CH}_2)_4\text{COO}^- + 7/8 \text{H}^+ + 7/4 \text{H}_2 + 9/4 \text{H}_2\text{O}$	6.00
R6	Ethanol	5:1	$5 \text{CH}_3\text{CH}_2\text{OH} + \text{CH}_3\text{COO}^- \rightarrow 0.565 \text{CH}_3(\text{CH}_2)_2\text{COO}^- + 1.625 \text{CH}_3(\text{CH}_2)_4\text{COO}^- + 1.190 \text{H}^+ + 2.375 \text{H}_2 + 2.625 \text{H}_2\text{O}$	7.30

As illustrated in Fig. 4.2, ethanol/acetate ratio of 3 has the highest free energy release. Interestingly, when the ratio increases from 3 to 4 or 5, the free energy release drops per electron, which is approaching closely to the “quantum of energy” minimum. It indicates that the optimal ethanol/acetate ratio is 3 in the substrate for chain elongation thermodynamically.

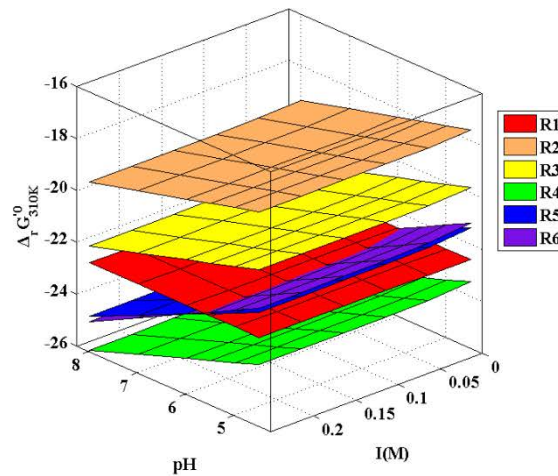


Figure 4.2. Standard transformed Gibbs free energy values ($\Delta_r G'_{310K}$) per electron transfer in KJ mol^{-1} as a function of pH and ionic strength (I) for caproate formation with ethanol as electron donor (Eq. R1 to R6).

The transformed Gibbs free energy values ($\Delta_r G'_{310K}$) at pH 7 and $I = 0.1 \text{ M}$ were determined according to the condition of Case 1. Fig. 4.3a displays $\Delta_{R1-2} G'_{310K}$ as a function of the dissolved H_2 and acetate, demonstrating that the free energy release of the fermentation for butyrate formation is not affected by H_2 concentration when ethanol/acetate ratio is 1. As the ratio approaches to 2 or higher, the caproate is formed in addition to butyrate. As shown in Fig. 4.3b, the higher the relative ratio of ethanol to acetate, the more free energy is released at a wide range of substrate and

compound concentrations in solution suggesting that caproate formation is more favorable at elevated ethanol/acetate ratio. This finding has also been introduced by Angenent with a simple stoichiometry model for stoichiometry and thermodynamics of reverse β oxidation with ethanol based on *C. Kluyveri* (Angenent et al., 2016).

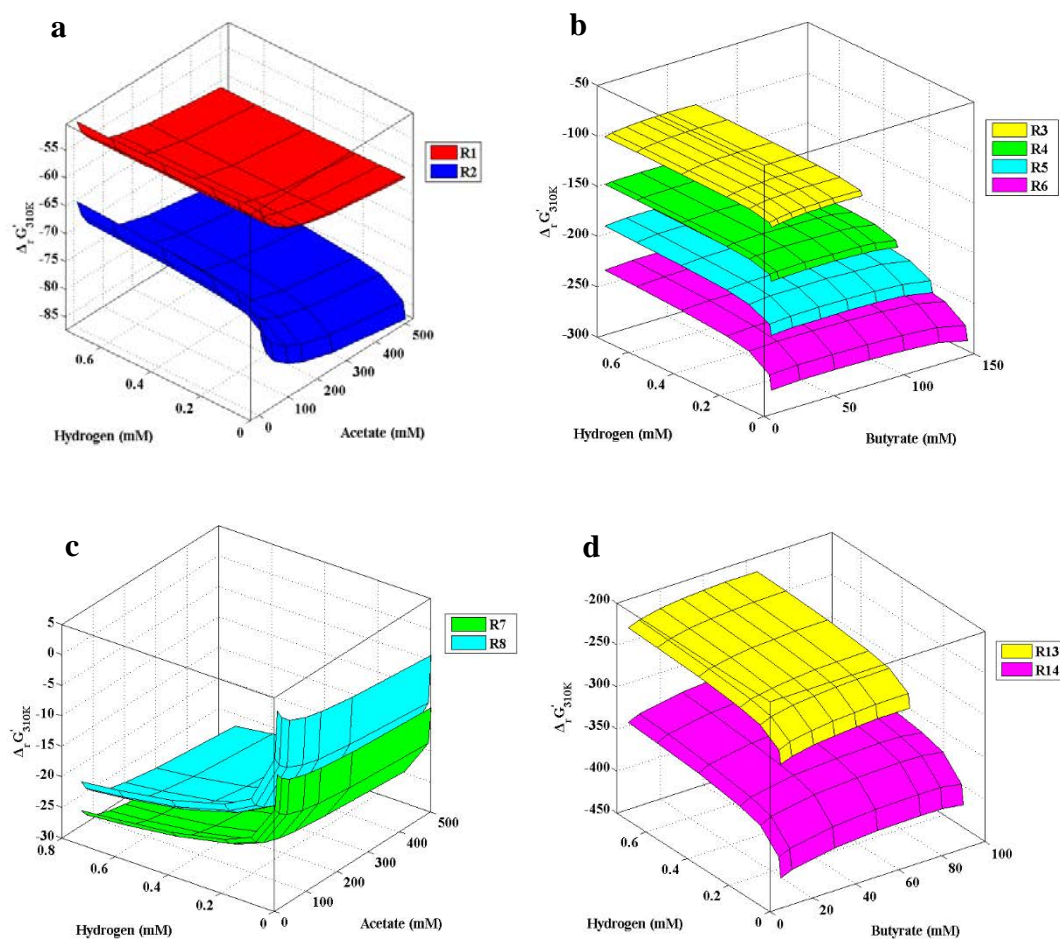


Figure 4.3. Transformed Gibbs free energy values ($\Delta_r G'_{310K}$) in KJ mol^{-1} at a pH of 7, an ionic strength (I) of 0.1 M, a temperature of 310 K and pressure of 1 atm for (a) Eq. R1 and R2 as a function of the dissolved H_2 and acetate; (b) Eq. R3 to R6 as a function of the dissolved H_2 and butyrate, acetate of 50 mM; (c) Eq. R7 and R8 as a function of the dissolved H_2 and acetate; (d) Eq. R13 and R14 as a function of the dissolved H_2 and butyrate, acetate of 50 mM, CO_2 formation of twice of butyrate.

Fig. 4.4 shows that the energy release, as the stoichiometric ratio of ethanol to acetate increased from 3 to 4 or 5, decreased slightly, suggesting the optimal stoichiometric ratio of 3 (Case 2). Chain elongation with H₂ is sensitive to the dissolved H₂ concentration (Fig. 4.3c). By overcoming the minimum “quantum of energy” for caproate formation, there is a “window of opportunity” defining the dissolved H₂ concentration to be increased to levels higher than 0.2 mM (27% gas composition at 1 atm). This is unlikely to occur without additional H₂ supply; as demonstrated by Steinbusch et al., 1.5×10⁵ Pa (1.5 atm) headspace H₂ was provided for caproate formation (Steinbusch et al., 2011). Fig. 4.3d demonstrates that caproate formation from glycerol is thermodynamically feasible at wide ranges of dissolved H₂, and butyrate concentration.

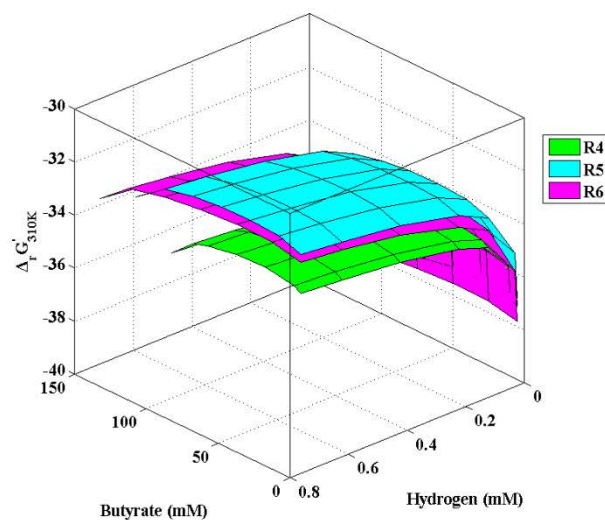


Figure 4.4. Transformed Gibbs free energy values per electron transfer ($\Delta_r G'_{310K}$) in KJ mol^{-1} at pH 7 and ionic strength (I) of 0.1 M for Eq. R4/R5/R6 as a function of the dissolved H₂ and butyrate, [Acetate] = 50 mM.

Table 4.3 lists potential electron flow reactions by various electron donors for the NAD^+/NADH electron carrier pair. Electron transfer from ethanol involves two dehydrogenation steps: ethanol into acetaldehyde (Eq. R15) by a NAD-dependent alcohol dehydrogenase (adh), and acetaldehyde into acetyl-CoA (Eq. R16) by a NAD-dependent acetaldehyde dehydrogenase (ald), overall as described by Eq. R17. Similarly, electron transfer from hydrogen is via the hydrogenase enzyme (Eq. R18), whereas electron transfer from glycerol is via glycerol dehydrogenase and dihydroxyacetone (DHA) kinase to DHA and pyruvate, respectively (Eq. R19 and R20).

Table 4.3. Potential electron production with various electron donors for the NAD^+/NADH electron carrier pair.

No.	Electron donor	Reaction
R15	Ethanol	$\text{CH}_3\text{CH}_2\text{OH} + \text{NAD}_{\text{ox}} \rightarrow \text{CH}_3\text{CHO} + \text{NAD}_{\text{red}}$
R16	Ethanol	$\text{CH}_3\text{CHO} + \text{CoA} + \text{NAD}_{\text{ox}} \rightarrow \text{Acetyl-CoA} + \text{NAD}_{\text{red}}$
R17	Ethanol	$\text{CH}_3\text{CH}_2\text{OH} + \text{CoA} + 2 \text{NAD}_{\text{ox}} \rightarrow \text{Acetyl-CoA} + 2 \text{NAD}_{\text{red}}$
R18	H_2	$\text{H}_2 + \text{NAD}_{\text{ox}} \rightarrow \text{NAD}_{\text{red}}$
R19	Glycerol	$\text{C}_3\text{H}_8\text{O}_3 + \text{NAD}_{\text{ox}} \rightarrow \text{C}_3\text{H}_6\text{O}_3 \text{ (Dihydroxyacetone)} + \text{NAD}_{\text{red}}$
R20	Glycerol	$\text{C}_3\text{H}_8\text{O}_3 + 2 \text{NAD}_{\text{ox}} \rightarrow \text{CH}_3\text{COCOO}^- + 2 \text{NAD}_{\text{red}}$

Fig. 4.5 demonstrates $\Delta_r G^0_{310K}$ for these aforementioned reactions, and the results of Eq. R15 and R19 show that these reactions are thermodynamically unfavorable at all pH and I ranges, suggesting that additional coupled exergonic reactions are needed

for ethanol and glycerol via adh and glycerol dehydrogenase, respectively. As noted above, the electron transfer of Eq. R17 from ethanol to acetyl-CoA tends to occur when pH exceeds 6.5, so that the initial electron-intensive barrier can be overcome for the chain elongation of acetate. The two enzymes (adh and ald) are located in a microcompartment existing as a macromolecular complex in *C. kluyveri* (Seedorf et al., 2008). Results of $\Delta_{R20}G^{\circ}_{310K}$ show that the electron donation of glycerol is thermodynamically achievable, if Eq. R19 is coupled with two further steps for pyruvate formation. Coincidentally, glycerol dehydrogenase and DHA kinase expression are regulated under the same genetic control *dha* system in *Klebsiella sp.* (Forage & Foster, 1982). Jointly, all reactions of the NAD^+/NADH electron carrier pairs presented favors intrinsically at higher pH.

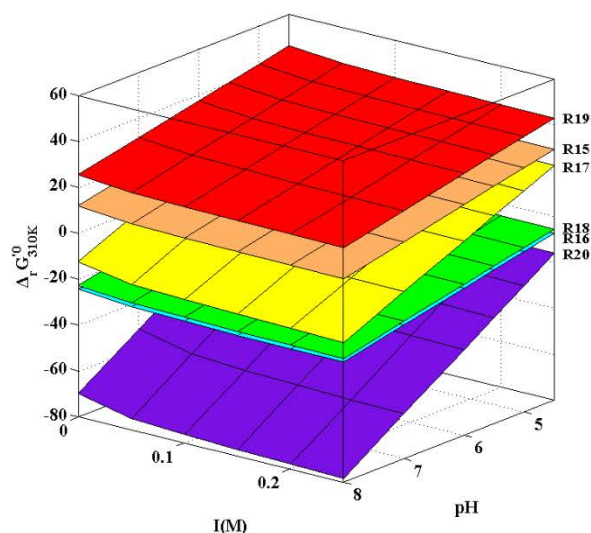


Figure 4.5. Standard transformed Gibbs free energy of reaction ($\Delta_r G^{\circ}_{310K}$) in KJ mol^{-1} as a function of pH and ionic strength (I) for Eq. R15 to R20.

4.2.2 MCFA production with ethanol

The physiological results of MCFA production with ethanol for the fixed acetate of 50 mM were consistent with the aforementioned thermodynamic analyses. As shown in Table 4.4, as the stoichiometric ethanol-to-acetate ratio increased over 1, caproate formed and leveled off at the ratio of 3, which was thermodynamically expected to be the optimal condition. This achieved a caproate conversion rate of around 40% in mol C caproate to mol C substrate corresponding to 0.54 mol C caproate per mol C ethanol. In addition, the stoichiometric ratio tendency for butyrate formation was the reverse, owing to the theoretical increase of chain elongation degree from butyrate to caproate with a higher concentration of electron donors. A similar finding of high ethanol/acetate ratio favored n-caproate and a low ratio favored n-butyrate has been unraveled in pure cultures of by *C. kluyveri* by Barker et al (Barker et al., 1945).

Table 4.4. Butyric acid and caproic acid production with different substrate molar ratios at a fixed theoretical acetate concentration of 50 mM.

Substrate molar ratio Ethanol/Acetic acid	Ethanol (mM C)	Total substrate (mM C)	Caproic acid (mM C)	Butyric acid (mM C)	Acetic acid (mM C)
0.8	79.98±0.0	175.6±0.0	0.0±0.0	4.1±5.8	46.3±1.5
1.0	126.17±1.9	257.6±10.6	0.0±0.0	165.8±80.7	-81.2±23.2
1.5	137.78±3.3	231.3±18.6	27.4±19.4	51.7±40.3	-10.5±10.3
3.0	264.38±4.8	360.3±8.9	143.5±56.7	69.4±1.9	-42.6±8.7
4.0	349.62±0.0	439.2±0.0	133.2±94.2	36.2±25.6	-57.0±52.6

5.0	427.45±0.0	517.0±0.0	144.5±102.2	30.6±21.6	-65.2±65.4
-----	------------	-----------	-------------	-----------	------------

Fig. 4.6a shows caproate formation at the stoichiometric ethanol-to-acetate ratio of 3. The formation of butyrate and caproate was synchronous with H₂ yield, exhibiting a lag phase of 10 to 15 days, which decreased with alcohol-contained lignocellulose solution, as shown in Fig. 4.7 (occurrence within 4 days). A high titer ethanol production solution was obtained from wood using a quasi-simultaneous enzymatic saccharification and combined fermentation method with sulfite pretreatment (Lan et al., 2013). The solutions were diluted to 150 mM ethanol as substrate. In addition to ethanol, the solutions contained some remaining yeast extract powder, lignin, cellulose and 3 mM glucose. This demonstrates that the chain elongation process is hydrogenogenic, because the highest H₂ detected was lower than 12% at 1 atm, which was nowhere near the “window of opportunity” (Ding et al., 2010). When ethanol was completely consumed (Day 25), the concentration of butyrate and caproate levelled off and the amount of H₂ decreased, probably due to a lack of preferred reduced compounds and inactivity of hydrogenic bacteria (Smith & Mccarty, 1989). Concerning the inoculums with fresh AD sludge and ethanol screened culture at the stoichiometric ethanol-to-acetate ratio of 3, the caproate recovery rates were 39.8% and 34.7%, respectively, indicating that chain elongation bacteria are adaptive to ethanol enriched culture and rapidly dominate the anaerobic mixed culture. Due to undetectable methane in the gas phase of batch bottles, we believe methanogenesis was effectively inhibited by 10 g/L of BESA.

Overall, this study concluded that the stoichiometric feed ratio is involved in the central metabolism of caproate formation, and the ratio of 3 is the optimal feed composition, which is very close to the optimized ethanol and acetate loading rates in an upflow anaerobic filter for high rate MCFA production, as suggested by Grootsholten et al. (Grootsholten et al., 2013). These findings provide useful information on the favorable intermediate composition of glycerol fermentation for caproate production; and indicate that the electron of the caproate originated from ethanol rather than from H₂ produced as one of the intermediates.

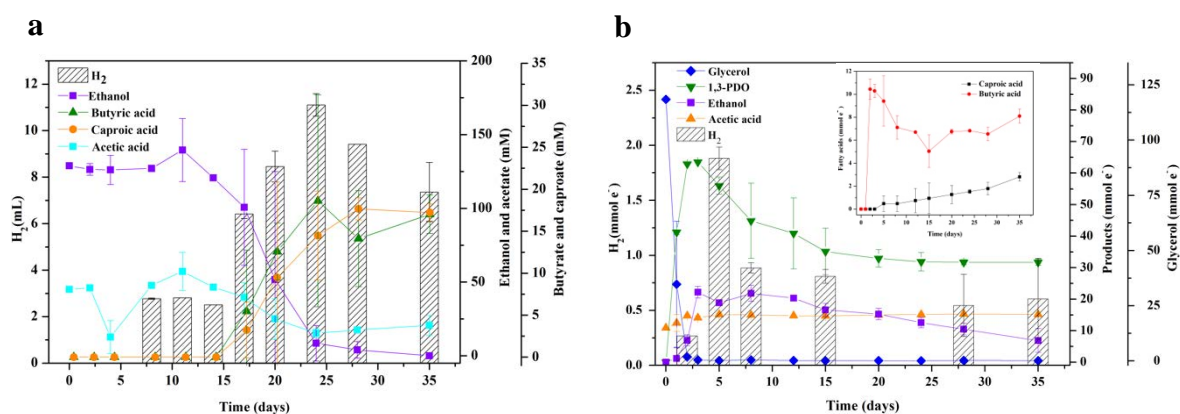


Figure 4.6. (a) Chain elongation of 150 mM ethanol and 50 mM acetate with AD sludge at a pH 7 and 37°C, (b) Product generation of glycerol fermentation in mmol electron with AD sludge at pH 7 and 37°C.

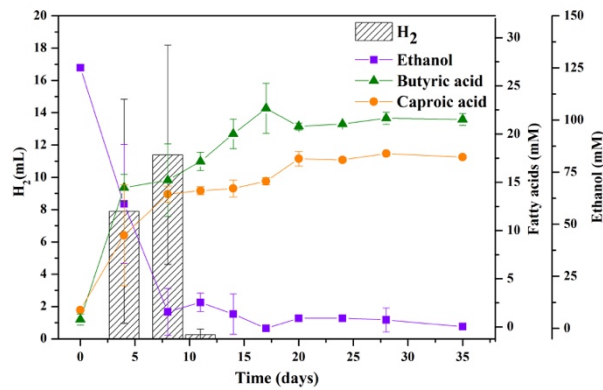


Figure 4.7. Kinetics of butyric acid, caproic acid, and H₂ production with 150 mM alcohol-contained lignocellulose solution and 50 mM acetate at pH 7 and 37°C.

4.2.3 1,3-PDO and MCFA production with glycerol

Fig. 4.8 illustrates that acetate has a positive effect on the formation of butyrate and ethanol in mixed culture glycerol fermentation, and indicates acetate addition is favorable to caproate production. Different molar ratios of glycerol to acetate (i.e., 2, 4, and 6) were performed and the formation of varied products is summarized in Table 4.5.

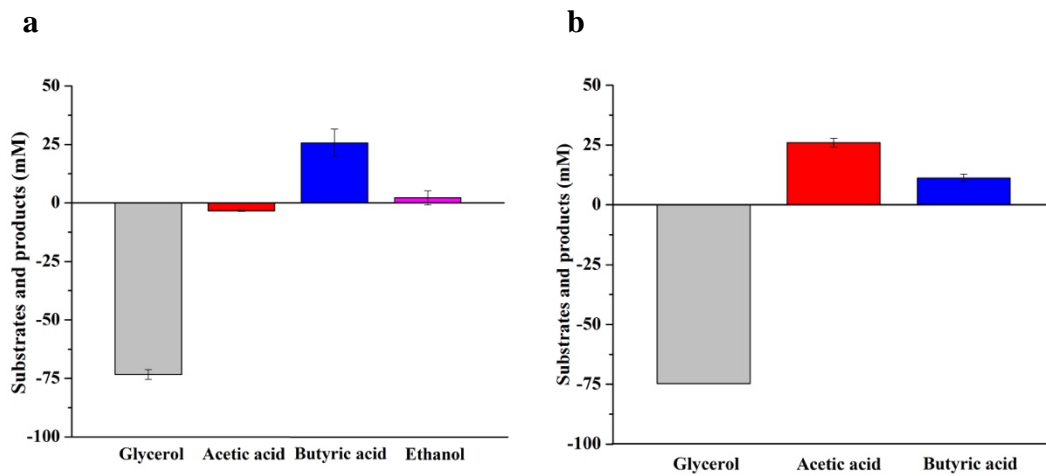


Figure 4.8. Glycerol fermentation with and without acetate.

Caproate and 1,3-PDO co-formation in mixed culture glycerol fermentation was observed, which corroborated the thermodynamic analyses. 1,3-PDO production increased as the ratio grew; however, caproate production was found to have an optimal ratio of 4 which was consistent with the trend of ethanol. This shows a close agreement with the finding of Temudo et al. that ethanol production was mainly associated with a substrate limiting condition, while 1,3-PDO was the dominant product with excess substrate (Temudo et al., 2008). The carbon recovery rates to the compounds in Table 2 were 37.6%, 37.4% and 31.4% for the respective glycerol-to-acetate ratios, which decreased with increasing levels of excess substrate. Fig. 4.6b displays the product formation with glycerol and acetate at a molar ratio of 4. Consumption of glycerol and production of 1,3-PDO, ethanol, butyrate, and H₂ occurred within 3 days, while caproate formation was mainly initiated around 15 days, a similar lag phase to caproate formation with ethanol. Along with caproate formation, primary products including ethanol, 1,3-PDO, and H₂ decreased.

Table 4.5. Product distribution in carbon from glycerol fermentation with acetate (50 mM) at different substrate molar ratios.

Glycerol/ Acetic acid	Substrate (mM C)	1,3-PDO (mM C)	Ethanol (mM C)	Butanol (mM C)	Caproic acid (mM C)	Butyric acid (mM C)	Acetic acid (mM C)
2.0	433.2±0.0	108.8±11.1	8.0±11.4	2.2±0.2	1.9±2.7	41.8±33.5	26.1±30.9
4.0	726.8±0.0	187.8±5.3	32.2±17.8	7.9±4.5	11.7±4.3	32.4±3.5	82.5±0.9
6.0	1144.8±0.0	265.7±13.5	17.7±4.6	16.6±1.4	9.7±3.5	49.9±5.0	16.4±4.8

These findings indicated that Carboxylates Chain Elongation Process (CCEP) is

indirect from glycerol, and the formed reduced products could be utilized when glycerol is completely consumed. Similar findings were reported by Daniel and Perry that the electrons contributed to more thermodynamically favorable products might come first from a high potential electron donor and subsequently from reduced potential intermediates (Smith & Mccarty, 1989). It was concluded that the composition of the primary fermenting products (1,3-PDO, ethanol, acetate, and butyrate) is crucial for the secondary fermenting product (caproate). As indicated in the thermodynamic analysis, the closer the ethanol to acetate molar ratio is to 3, the higher the amount of caproate theoretically produced. In general, it is essential to reduce the lag phase of CCEP and increase the yield of ethanol in the intermediates so as to stimulate the co-production of 1,3-PDO and caproate.

Table 4.6 shows the results for glycerol fermentation inoculated with fresh AD sludge and ethanol screened culture. The results confirmed our conceptual hypothesis and further implied that the microorganisms with the function of 1,3-PDO production from glycerol were easier to be dominant from fresh AD inoculum, while the microorganisms with the function of CCEP preferred to use ethanol and capable of utilizing glycerol for butyrate and caproate production probably in a synergistic pathway.

Table 4.6. Products formation distribution of glycerol fermentation with acetate inoculated with fresh anaerobic digestion sludge and ethanol screened culture.

Inoculum culture	Sub. (mM C)	Caproic acid (mM C)	Butyric acid (mM C)	Acetic acid (mM C)	Ethanol (mM C)	Butanol (mM C)	1,3-PDO (mM C)	Carbon recovery rate (%)
Fresh AD sludge	433.2±0.0	1.9±2.7	41.8±3.5	26.1±3.0	8.0±11.4	2.2±0.2	108.8±1.1	43.6±8.8
Ethanol screened	462.4±0.0	47.2±2.0	136.7±71.4	108.0±60.0	0.0±0.0	3.7±2.6	0.0±0.0	63.9±18.4

4.2.4 1,3-PDO and MCFA production with ethanol and glycerol

Fig. 4.9 shows two batch co-fermentation cases of glycerol with ethanol addition on Day 0 (AD inoculum) and Day 20 (enrichment inoculum from Case 1). 1,3-PDO and caproate are co-produced for both cases. For Case 1, there was still a dynamic formation difference, of which glycerol consumption and 1,3-PDO production occurred within two days, while ethanol consumption and caproate production happened after 20 days (Fig. 4.9a). Compared to caproate production with ethanol, the caproate formation with glycerol and ethanol was further delayed roughly five days in the case of co-existing electron donors, which was nevertheless negligible considering the whole fermentation period. Even though ethanol and butyrate were initially produced along with 1,3-PDO from glycerol, caproate was not concurrently produced. This again indicated that caproate formation from glycerol under mixed culture was probably not a direct bioconversion.

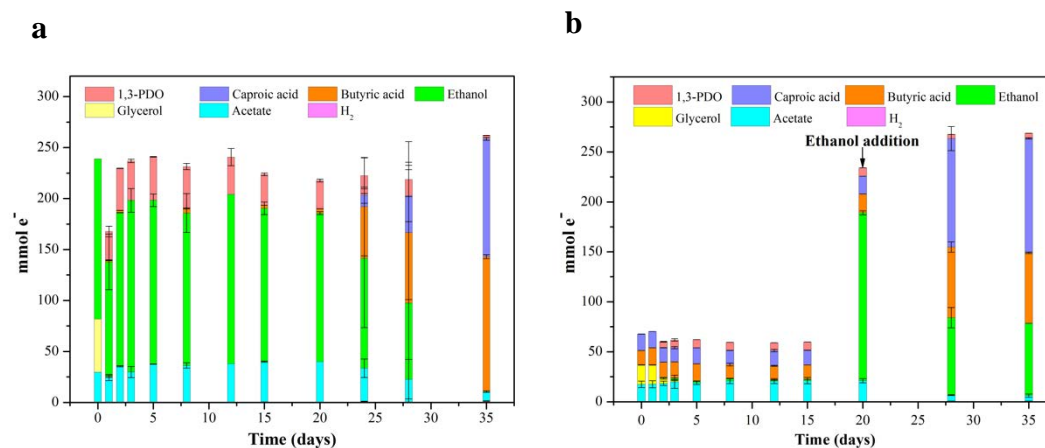


Figure 4.9. 1,3-PDO and caproate co-production with both ethanol and glycerol in the substrate, and the relationship with H₂ level at a pH 7 and 37°C, (a) Ethanol and glycerol addition on Day 0, (b) Ethanol addition on Day 20.

Interestingly, caproate was immediately formed upon ethanol addition on Day 20 (Fig. 4.9b), implying that CCEP microorganisms can be dominant by ethanol addition in glycerol fermentation culture. Unfortunately, 1,3-PDO decreased when CCEP occurred for both cases. The overcoming of kinetics limitation might be stimulated by the existing of lignocellulose, suggested by Kenealy et al. that this promotion is pivotal to the co-cultures of *C. kluyveri* and ruminal cellulolytic bacteria (Kenealy et al., 1995). Further studies to evaluate this mechanism would be beneficial.

4.2.5 Microbial characterization

Five enriched samples were characterized for microbial community composition. Sample G-1, G-2 and E-1 (batch 1) were enriched from AD sludge with 100 mM

glycerol and 50 mM acetate, 200 mM glycerol and 50 mM acetate, 150 mM ethanol and 50 mM acetate, respectively. Sample E-2 and G-3 (batch 4) were enriched from the culture of E-1, fed with 90 mM ethanol and 30 mM acetate, 120 mM glycerol and 30 mM acetate, respectively. The upper panel in Fig. 4.10 displays the distance of their community structure based on all OTUs. According to the clustering tree, G-1 is differentiated from other cultures while G-2 and E-1 are relatively close, and E-2 and G-3 are located in a group. The lower panel of Fig. 4.10 demonstrates that the top 29 most dominant OTUs in genus level covered 97.65%, 94.82%, 96.79%, 43.22% and 62.29% of sequences in G-1, E-2, G-3, E-1, G-2. Most of the genus belong to *Firmicutes* and *Proteobacteria*. The microbial community structure is more diverse when enriched from AD sludge, however, G-1 is exceptional.

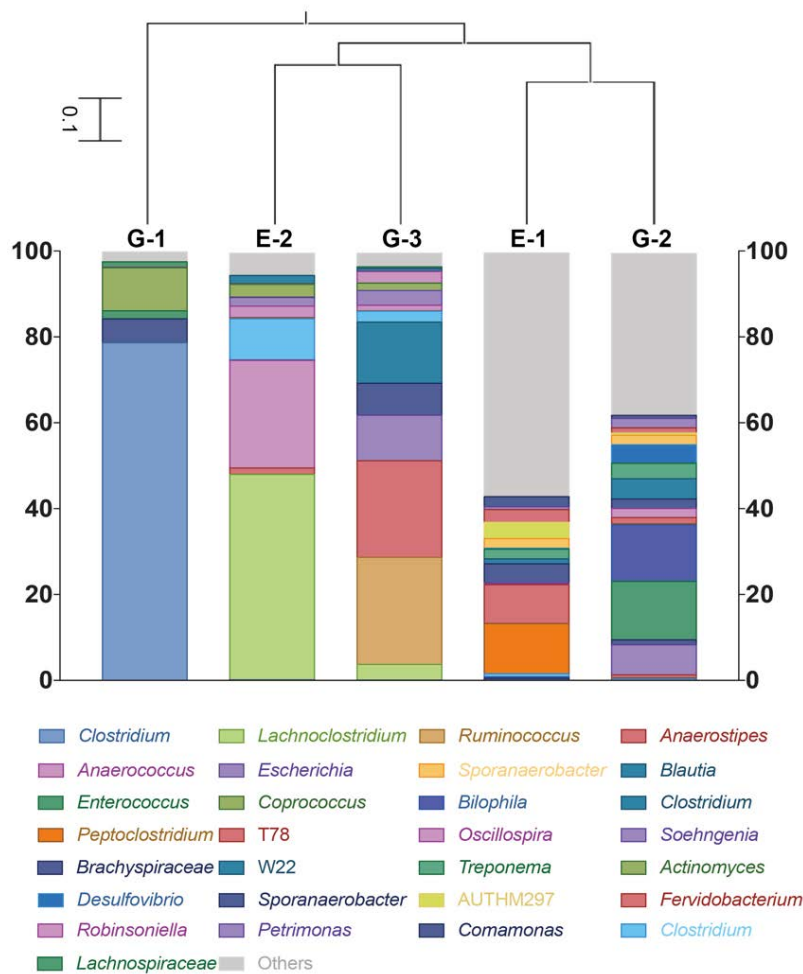


Figure 4.10. Composition of relative abundances of OTUs at Genus level in different sludge samples. Hierarchical clustering of five sludge samples was performed based on all OTUs from the microbial communities with a UPGMA algorithm to generate a newick-formatted tree.

Table 4.7. Abundance of most abundant and functional OTUs of each sample.

	G-1	G-2	E-1	G-3	E-2
<i>Clostridium butyricum</i>	78.68%	0.54%	0.02%	0.06%	0.13%
<i>[Clostridium] indolis</i>	0.01%	0.01%	0.01%	3.71%	47.88%
<i>Anaerostipes caccae</i>	0.00%	0.66%	0.01%	22.51%	1.47%
<i>Escherichia coli</i>	0.00%	7.02%	0.01%	10.62%	0.03%
<i>Blautia producta</i>	0.00%	0.01%	0.00%	14.28%	0.06%

<i>Enterococcus avium</i>	1.87%	13.61%	0.01%	0.00%	0.00%
<i>Clostridium kluyveri</i>	0.00%	0.02%	0.74%	2.54%	9.66%
<i>[Clostridium] sticklandii</i>	0.00%	0.27%	11.73%	0.05%	0.16%

The dominant and functional OTUs are summarized in Table 4.7 and the top 20 abundant OTUs in fresh AD sludge sample are shown in Table 4.8. With blast towards NCBI database, these OTUs were further characterized to species level with over 99% identity. *C. butyricum* was highly dominant in G-1, which is responsible for 1,3-PDO and butyrate production from glycerol fermentation (Saintamans et al., 1994). *Enterococcus avium* with 1.87% abundance in G-1 is capable of utilizing glycerol for acids production (Facklam & Collins, 1989). In contrast, the abundance of *C. butyricum* declined and the abundance of *E. avium* and *E. coli* grew when the substrate level glycerol/acetate ratio increased from 2 to 4. This shift of the microbial community structure explained the decrease of conversion ratios of butyrate and 1,3-PDO and the increase of production rate of ethanol illustrated in Table 4.5 since *E. coli* has been reported to produce ethanol, succinate, and formate from glycerol (Murarka et al., 2008). In terms of *C. kluyveri*, the abundance in G-1 and G-2 were 0.00% and 0.02%, respectively, which results in no caproate and a small amount of caproate production in these two cultures. The ethanol for caproate formation in G-2 was probably produced by *E. coli* as an intermediate through a synergistic pathway. The structure of E-1 includes *C. kluyveri* and high abundance of *[Clostridium] sticklandii*. The butyrate and caproate production with ethanol was consistent with existence of *C. kluyveri* (Seedorf et al., 2008). *[C.] sticklandii* which converts amino

acids together with H₂ and acetate to butyrate might promote the chain elongation pathway (Fonknechten et al., 2010). When the culture was further enriched with ethanol and acetate for one more batch, the abundance of *C. kluyveri* and [*Clostridium*] *indolis* increased while that of [*C.*] *sticklandii* decreased. [*C.*] *indolis* is a sulfate reducer capable of consuming some simple sugars, pectin, pectate, mannitol, and galacturonate, and pyruvate to acetate, formate, ethanol, and butyrate (Biddle et al., 2014). Alcohol dehydrogenase, NADH-dependent aldehyde dehydrogenase and CoA-transferase were also found in the [*C.*] *indolis* genome (Biddle et al., 2014). The relationship of this bacteria and carboxylic acids chain elongation with ethanol is also interesting for further study. The culture of G-3 that utilized glycerol for butyrate and caproate formation instead of 1,3-PDO consists of more comparable abundant OTUs which infers to 22.51% of *Anaerostipes caccae*, 14.28% of *Blautia producta*, 10.62% of *E. coli*, 3.71% of [*C.*] *indolis* and 2.54% of *C. kluyveri*. *A. caccae* is a saccharolytic acetate-utilizing and butyrate-producing bacterium from human faeces (Schwiertz et al., 2002), and *B. producta* is a H₂/CO₂- or CO-utilizing and acetate-producing *Ruminococcus* bacterium (Liew et al., 2016; Liu et al., 2008). In a synergistic network, glycerol consumed by *E. coli* with the formation of ethanol, and formate (H₂ and CO₂). Then *C. kluyveri* utilized ethanol for butyrate and caproate production in CCEP. Meanwhile, *B. producta* produced acetate with H₂ and CO₂ and *A. caccae* further used acetate to generate butyrate. And the butyrate generated in a parallel pathway promoted caproate formation by *C. kluyveri*. The cease of 1,3-PDO production was consistent with the insignificant abundance of *C. butyricum* (0.06%) in G-3 culture. Together with the evidences that caproate

production was found to have an optimal ratio of 4 which was consistent with the trend of ethanol; ethanol production was simultaneous with glycerol consumption and caproate production was simultaneous with ethanol depletion; ethanol addition immediately enhanced caproate production, it concluded that glycerol acting as an electron donor for caproate production was indirectly through the intermediate, ethanol.

Table 4.8. Abundance and taxonomy of the overall top 20 most abundant OTUs in fresh AD sludge sample.

OTU ID	Abundance	Phylum	Class	Order	Family	Genus
12116	0.00%	<i>Firmicutes</i>	<i>Clostridia</i>	<i>Clostridiales</i>	<i>Clostridiaceae</i>	<i>Clostridium</i>
35728	0.00%	<i>Proteobacteria</i>	<i>Deltaproteobacteria</i>	<i>Desulfovibrionales</i>	<i>Desulfovibrionaceae</i>	<i>Desulfovibrio</i>
52828	0.01%	<i>Fusobacteria</i>	<i>Fusobacteriia</i>	<i>Fusobacteriales</i>	<i>Fusobacteriaceae</i>	<i>Fusobacterium</i>
39880	0.01%	<i>Bacteroidetes</i>	<i>Bacteroidia</i>	<i>Bacteroidales</i>	<i>Rikenellaceae</i>	<i>Alistipes</i>
77232	0.01%	<i>Firmicutes</i>	<i>Clostridia</i>	<i>Clostridiales</i>	<i>Clostridiaceae</i>	<i>Proteinclasticum</i>
85382	0.05%	<i>Proteobacteria</i>	<i>Gammaproteobacteria</i>	<i>Enterobacteriales</i>	<i>Enterobacteriaceae</i>	<i>Escherichia</i>
11332	2.50%	<i>Thermotogae</i>	<i>Thermotogae</i>	<i>Thermotogales</i>	<i>Thermotogaceae</i>	AUTHM297
38781	0.00%	<i>Firmicutes</i>	<i>Bacilli</i>	<i>Bacillales</i>	<i>Bacillaceae</i>	Unknown
77487	0.01%	<i>Firmicutes</i>	<i>Clostridia</i>	<i>Clostridiales</i>	<i>Peptostreptococcaceae</i>	<i>Peptoclostridium</i>
60584	2.07%	<i>Proteobacteria</i>	<i>Betaproteobacteria</i>	<i>Burkholderiales</i>	<i>Comamonadaceae</i>	Unknown
49975	0.00%	<i>Actinobacteria</i>	<i>Coriobacteriia</i>	<i>Coriobacteriales</i>	<i>Coriobacteriaceae</i>	Unknown
68739	0.00%	<i>Firmicutes</i>	<i>Clostridia</i>	<i>Clostridiales</i>	<i>[Tissierellaceae]</i>	<i>Sedimentibacter</i>
54933	0.00%	<i>Firmicutes</i>	<i>Clostridia</i>	<i>Clostridiales</i>	<i>Peptostreptococcaceae</i>	<i>Proteocatella</i>
21429	0.00%	<i>Firmicutes</i>	<i>Clostridia</i>	<i>Clostridiales</i>	<i>[Tissierellaceae]</i>	<i>Sporanaerobacte</i>
18980	0.01%	<i>Firmicutes</i>	<i>Clostridia</i>	<i>Clostridiales</i>	<i>Eubacteriaceae</i>	<i>Eubacterium</i>
26494	0.45%	<i>Chloroflexi</i>	<i>Anaerolineae</i>	SHA-20	Unknown	Unknown
17097	0.10%	<i>Proteobacteria</i>	<i>Deltaproteobacteria</i>	<i>Desulfovibrionales</i>	<i>Desulfovibrionaceae</i>	<i>Desulfovibrio</i>
50118	2.95%	WWE1	<i>[Cloacamonae]</i>	<i>[Cloacamonales]</i>	<i>[Cloacamonaceae]</i>	W22
29891	0.03%	<i>Bacteroidetes</i>	<i>Bacteroidia</i>	<i>Bacteroidales</i>	<i>Porphyromonadaceae</i>	<i>Petrimonas</i>
74102	0.42%	<i>Chloroflexi</i>	<i>Anaerolineae</i>	<i>Caldilineales</i>	<i>Caldilineaceae</i>	<i>Caldilinea</i>

In general, interesting synergistic pathways with different interspecies electron transport routes occurred during glycerol-acetate fermentation (Fig. 4.11). Through the holistic thermodynamic and physiological analysis, it is suggested that in chemostat reactor settings, a desired population of organisms could be manipulated by supplying an optimal substrate composition that gives sufficient energy flow for co-production of 1,3-PDO and caproate.

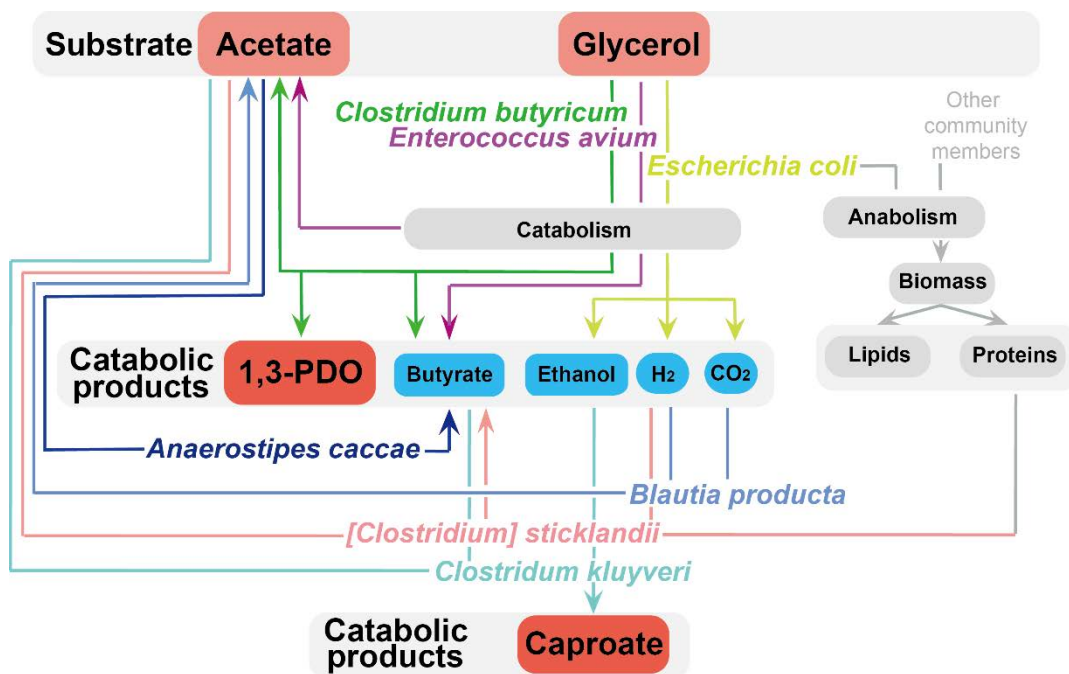


Figure 4.11. Microbial pathways occurred in mixed culture glycerol-acetate fermentation.

4.3 Chapter summary

This chapter reports thermodynamic and physiological insights for co-production of 1,3-PDO and caproate from glycerol and acetate. Detailed energetic analysis demonstrated that caproate can be elongated from acetate with either ethanol or glycerol, favorable at higher pH range, while caproate formation using H₂ as sole

electron donor need to be maintained at lower pH. The optimized conversion rates of mono-caproate and co-production of 1,3-PDO and caproate were achieved at the ethanol/acetate and glycerol/acetate molar ratios of 3 and 4, respectively. The sufficient intermediate ethanol is capable of enhancing caproate formation along with 1,3-PDO. Such a co-production system is pivotal to a synergistic network resulting in the co-existence of *C. butyricum*, *E. coli*, *C. kluyveri* and some other butyrate production bacteria with function of glycerol directly converting to 1,3-PDO and indirectly to caproate. To define and verify the synergistic network, further metagenomic analysis is necessary. The discovery is able to lift up wastewater anaerobic treatment and biodiesel industry and, more significantly, validate thermodynamic aspect to manipulate microbial interspecies interaction for engineering applications.

Chapter 5. Unveiling a new synergistic and syntrophic microbial network for carboxylates chain elongation with ethanol

5.1 Overview

Mixed culture carboxylates chain elongation for caproate formation with ethanol as an electron donor is an attractive option for resource recovery from fatty acids in anaerobic wastewater treatment. Whilst the metabolic pathway of *C. kluyveri* in carboxylates chain elongation has been discovered, the role of other abundant co-existing microbiomes and the synergistic network remained unclear in mixed culture. To this end, we conducted a fresh digestion sludge inoculated ethanol-acetate fermentation experiment at optimal conditions, and both 16S rRNA gene-based amplicon and shotgun metagenomics sequencing were employed to elucidate the mixed culture chain elongation by uncovering the microbes and functional pathways involved. Results revealed a synergistic relationship between *C. kluyveri* and three co-dominant species *Desulfovibrio vulgaris*, *Fusobacterium varium* and *Acetoanaerobium sticklandii*. The co-existence of these three species were able to boost the carboxylates chain elongation by *C. kluyveri*. Draft genomes of *C. kluyveri*, *D. vulgaris* and *A. sticklandii* were successfully recovered, revealing that butyrate and caproate can be directly produced from ethanol and acetate by *C. kluyveri* and indirectly produced through a syntrophic partnership between *D. vulgaris* and *A. sticklandii* with hydrogen serving as a reducing equivalent messenger. This study presents evidences of a syntrophic partnership between bacterial species and unveils an intricate and synergistic microbial network in mixed culture carboxylates chain

elongation.

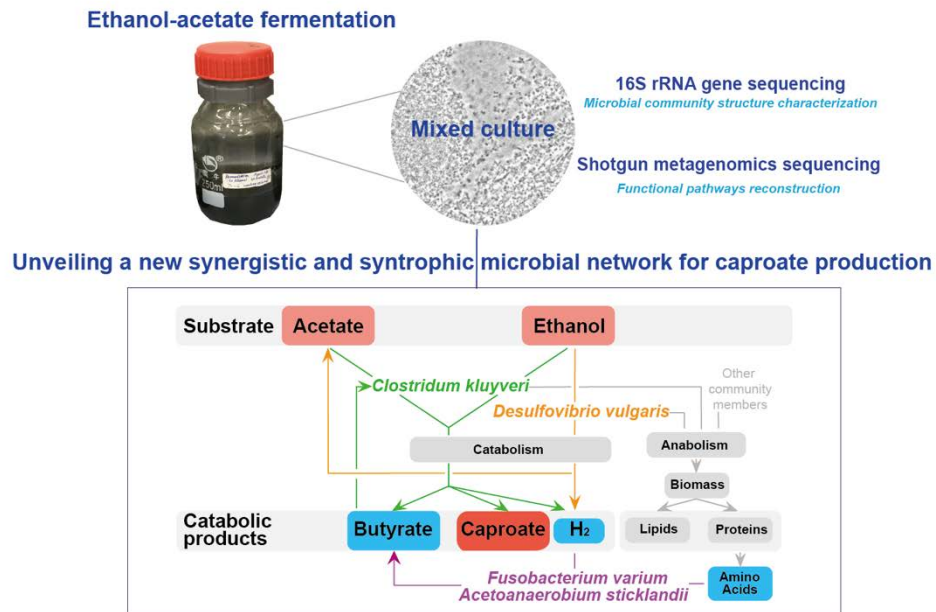


Figure 5.1. Microbial pathways occurred in mixed culture glycerol-acetate fermentation.

5.2 Results and discussion

5.2.1 Microbial community structures under different physiological stages of carboxylate chain elongation with ethanol

Figure 5.2a shows caproate production from ethanol and acetate in a fresh AD enriched culture. Butyrate and caproate formation were initiated on Day 3 and ended on Day 10, which occurred faster and completed within a shorter period of time in comparison to a similar fermentation conducted previously (initiated on Day 10 and ended on Day 25), even though the caproate conversion rate was similar to previous observation in chapter 4 (Leng et al., 2017). During chain elongation, H₂ was produced concurrently while methane was undetectable, and caproate formation

persisted longer (Day 10) than butyrate formation (Day 6).

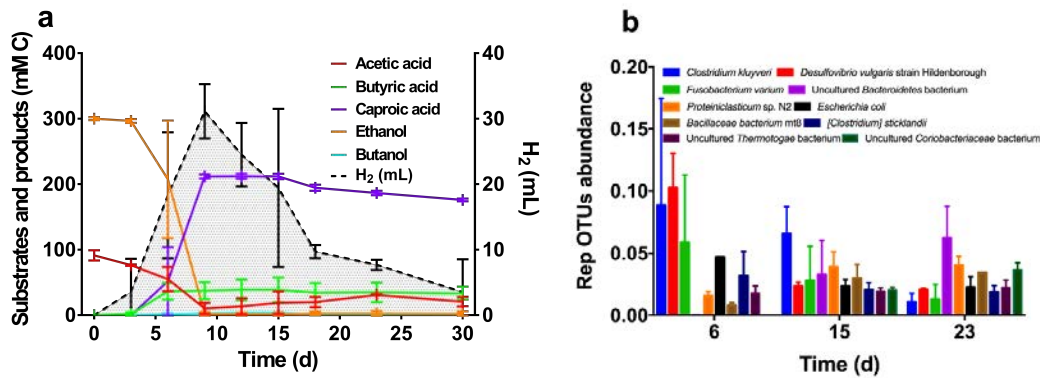


Figure 5.2. Mixed culture carboxylates chain elongation from ethanol with acetate inoculated with fresh AD sludge. The batch fermentation kinetics conducted at 37 °C, pH of 7 and 150 rpm in an incubator with methanogenesis inhibition. Corresponding representative OTUs, collected at three time points, collectively formed 28.25%-37.04% of the bacterial community.

Table 5.1. Summary of processed sequences and results from alpha diversity analysis.

Sample ID	Sequences/sample	Good's coverage	OTU	Shannon index	Inverse simpson index
Day0_1	89920	94.40%	8582	9.719	0.995
Day0_2	89920	94.00%	8890	9.716	0.996
Day6_1	89920	95.90%	6066	7.898	0.976
Day6_2	89920	96.60%	5226	7.106	0.956
Day15_1	89920	96.00%	6018	8.018	0.985
Day15_2	89920	95.80%	6079	7.984	0.983
Day23_1	89920	96.30%	5566	7.921	0.983
Day23_2	89920	96.30%	5681	8.071	0.986

To understand the microbial dynamics during the long chain elongation process, 4 groups of duplicate biomass samples for 16S rRNA gene sequencing were collected on Day 0, 6, 15 and 23. A normalized number of 89,920 sequences were obtained with an average Good's coverage of 95.66 % (Table 5.1).

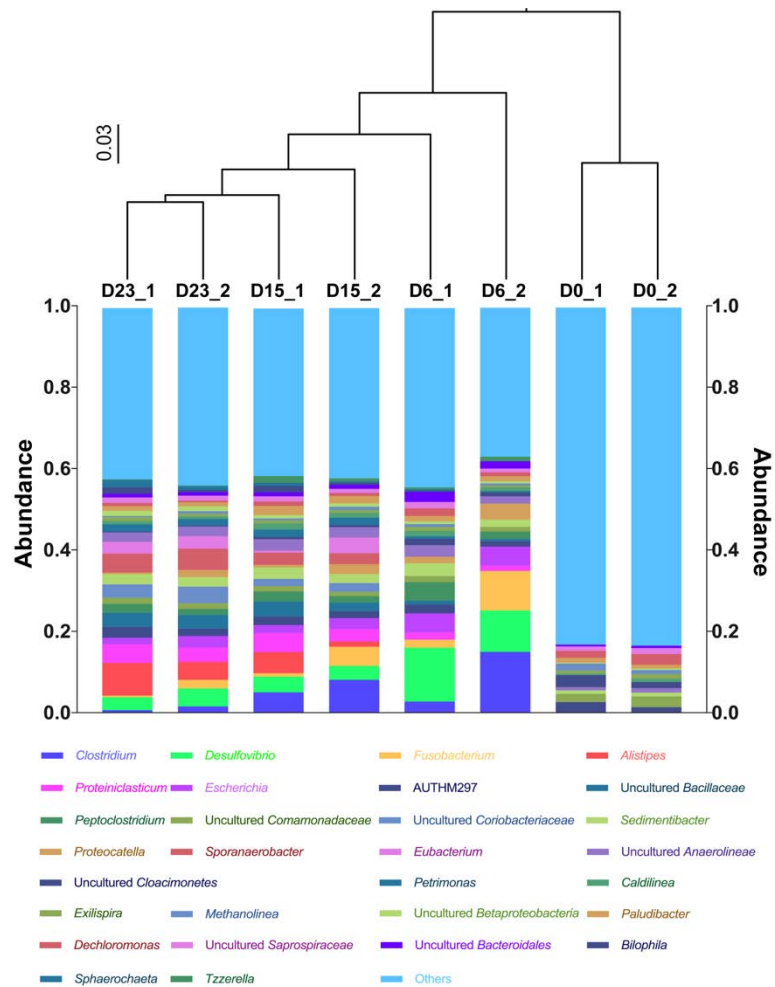


Figure 5.3. Composition of relative abundance of OTUs at the Genus level in different samples.

The different OTUs in the same genus level were combined to show in the columns. Hierarchical clustering of the total 8 samples was performed based on all OTUs from the microbial communities with a UPGMA algorithm to generate a newick-formatted tree. D0_1 and D0_2, D6_1 and D6_2, D15_1 and D15_2, D23_1 and D23_2 represent samples collected at Day 0, Day 6, Day 15 and Day 23 from duplicated bottles, respectively.

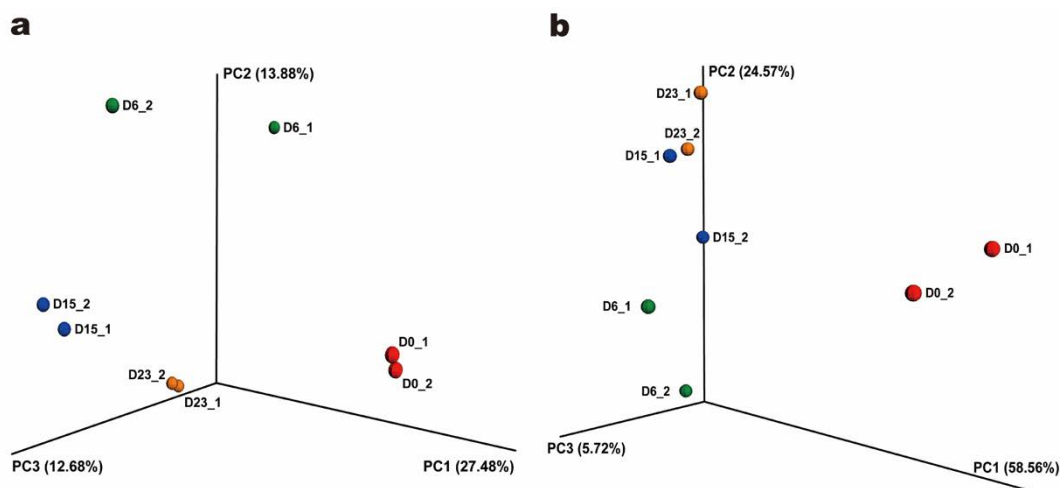


Figure 5.4. UniFrac emperor principal coordinate analysis (PCoA) (a. unweighted, b. weighted) of total 8 samples based on all OTUs from the microbial communities. D0_1 and D0_2, D6_1 and D6_2, D15_1 and D15_2, D23_1 and D23_2 represent samples collected at Day 0, Day 6, Day 15 and Day 23 from duplicated bottles, respectively.

Microbial community structures of the 8 samples were characterized. Based on clustering result, the bacterial community structure in the AD sludge inoculums evolved and became increasingly differentiated with time (Figure 5.3). This was further supported by the principal coordinate analysis (PCoA) (Figure 5.4). PCoA reveals that the microbial community varied during fermentation with consumption of substrates, and formation of intermediates and products. The observed Shannon and inverse Simpson indices indicated that the AD sludge inoculum contained a more diverse microbial community structure with a total of 8582/8890 bacterial OTUs detected (Table 5.1).

Table 5.2. Abundance and taxonomy of top 20 most abundant OTUs in fresh AD sludge samples.

OTU ID	Day0_1	Day0_2	Phylum	Class	Order	Family	Genus
12116	0.00%	0.01%	<i>Firmicutes</i>	<i>Clostridia</i>	<i>Clostridiales</i>	<i>Clostridiaceae</i>	<i>Clostridium</i>
35728	0.00%	0.01%	<i>Proteobacteria</i>	<i>Deltaproteobacteria</i>	<i>Desulfovibrionales</i>	<i>Desulfovibrionaceae</i>	<i>Desulfovibrio</i>
52828	0.01%	0.00%	<i>Fusobacteria</i>	<i>Fusobacteriia</i>	<i>Fusobacteriales</i>	<i>Fusobacteriaceae</i>	<i>Fusobacterium</i>
39880	0.01%	0.01%	<i>Bacteroidetes</i>	<i>Bacteroidia</i>	<i>Bacteroidales</i>	<i>Rikenellaceae</i>	<i>Alistipes</i>
77232	0.01%	0.01%	<i>Firmicutes</i>	<i>Clostridia</i>	<i>Clostridiales</i>	<i>Clostridiaceae</i>	<i>Proteiniclasticum</i>
85382	0.05%	0.01%	<i>Proteobacteria</i>	<i>Gammaproteobacteria</i>	<i>Enterobacteriales</i>	<i>Enterobacteriaceae</i>	<i>Escherichia</i>
11332	2.50%	1.28%	<i>Thermotogae</i>	<i>Thermotogae</i>	<i>Thermotogales</i>	<i>Thermotogaceae</i>	AUTHM297
38781	0.00%	0.01%	<i>Firmicutes</i>	<i>Bacilli</i>	<i>Bacillales</i>	<i>Bacillaceae</i>	Unknown
77487	0.01%	0.01%	<i>Firmicutes</i>	<i>Clostridia</i>	<i>Clostridiales</i>	<i>Peptostreptococcaceae</i>	<i>Peptoclostridium</i>
60584	2.07%	2.66%	<i>Proteobacteria</i>	<i>Betaproteobacteria</i>	<i>Burkholderiales</i>	<i>Comamonadaceae</i>	Unknown
49975	0.00%	0.00%	<i>Actinobacteria</i>	<i>Coriobacteriia</i>	<i>Coriobacteriales</i>	<i>Coriobacteriaceae</i>	Unknown
68739	0.00%	0.01%	<i>Firmicutes</i>	<i>Clostridia</i>	<i>Clostridiales</i>	[<i>Tissierellaceae</i>]	<i>Sedimentibacter</i>
54933	0.00%	0.00%	<i>Firmicutes</i>	<i>Clostridia</i>	<i>Clostridiales</i>	<i>Peptostreptococcaceae</i>	<i>Proteocatella</i>
21429	0.00%	0.01%	<i>Firmicutes</i>	<i>Clostridia</i>	<i>Clostridiales</i>	[<i>Tissierellaceae</i>]	<i>Sporanaerobacte</i>
18980	0.01%	0.01%	<i>Firmicutes</i>	<i>Clostridia</i>	<i>Clostridiales</i>	<i>Eubacteriaceae</i>	<i>Eubacterium</i>
26494	0.45%	0.61%	<i>Chloroflexi</i>	<i>Anaerolineae</i>	SHA-20	Unknown	Unknown
17097	0.10%	0.07%	<i>Proteobacteria</i>	<i>Deltaproteobacteria</i>	<i>Desulfovibrionales</i>	<i>Desulfovibrionaceae</i>	<i>Desulfovibrio</i>
50118	2.95%	1.53%	WWE1	[<i>Cloacamonae</i>]	[<i>Cloacamonales</i>]	[<i>Cloacamonaceae</i>]	W22
29891	0.03%	0.01%	<i>Bacteroidetes</i>	<i>Bacteroidia</i>	<i>Bacteroidales</i>	<i>Porphyromonadaceae</i>	<i>Petrimonas</i>
74102	0.42%	0.84%	<i>Chloroflexi</i>	<i>Anaerolineae</i>	<i>Caldilineales</i>	<i>Caldilineaceae</i>	<i>Caldilinea</i>

The taxonomy of the top 20 abundant OTUs are shown in Table 5.2, and collectively accounted for merely $7.86\% \pm 1.07\%$ of the total bacterial population in AD sludge inoculum. In contrast, the microbial community structure became increasingly specialized under enrichment with the dominance of certain bacterial species. At three time points during enrichment (Day 6, 15 and 23), the number of OTUs decreased to between 5226 and 6079 (Figure 5.3 and Table 5.1), and the top 20 abundant OTUs accounted for more than 50% of the bacterial populations. Specifically, the genera of dominant microorganisms in the ethanol and acetate enriched culture were *Clostridium*, *Desulfovibrio*, *Fusobacterium*, *Alistipes*, and

Proteiniclasticum. Compared with the similar fermentation conducted previously (Leng et al., 2017), the abundance of *Desulfovibrio* and *Fusobacterium* increased significantly in this batch. It implies that a distinctive interspecies association of the carboxylates chain elongation with ethanol and acetate might be involved. The abundance of methanogens was low and not ranked the top 20 counted OTUs. The total abundances of methanogens in fresh AD inoculum, Day 6, Day 15, and Day 23 were 2.175%, 0.978%, 1.099%, 0.841%, respectively.

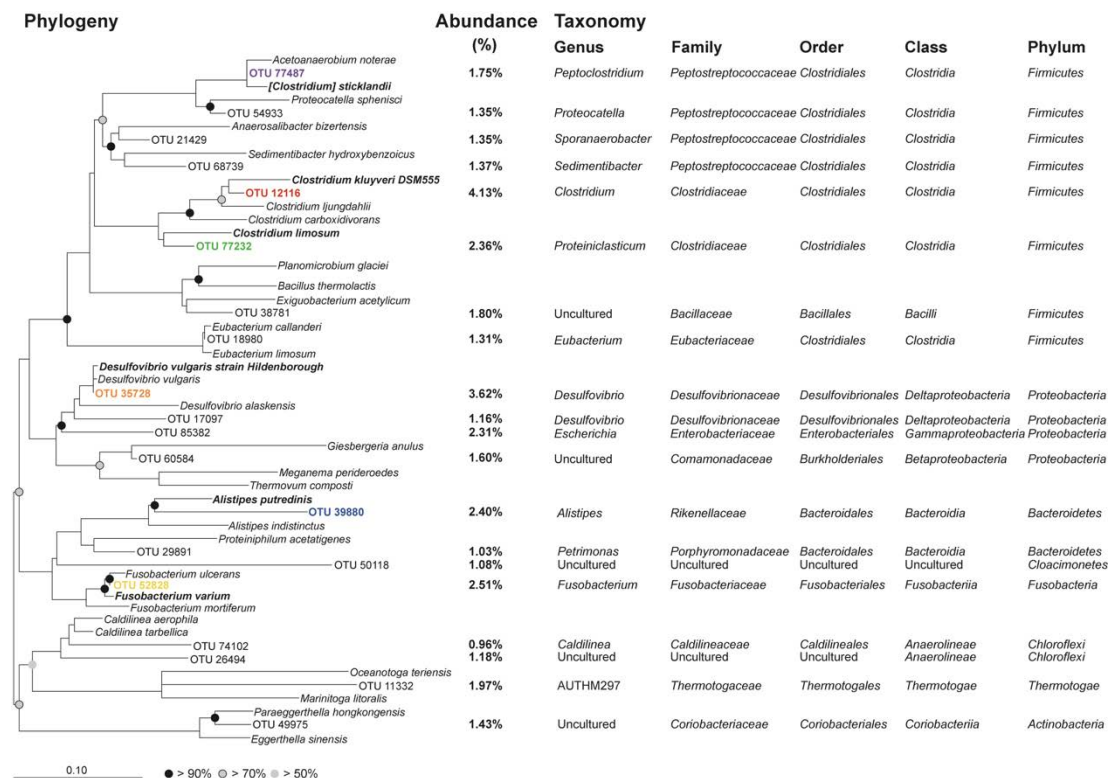


Figure 5.5. Neighbor-joining tree based on 16S rRNA gene sequences and related reference lineages. 20 most abundant OTUs of 8 samples were selected for analysis and shown with average abundance and taxonomy information. The phylogenetic tree (bootstrap 1000: > 90% black node, > 70% gray node with black outline and > 50% gray node) were performed in ARB with SILVA database SSU NR99 as reference.

A 16S rRNA gene-based tree was constructed by neighbor-joining method to decipher the phylogenetic affiliation of the 20 most abundant OTUs and their evolutionary relationships to known lineages (Figure 5.5). The highly abundant OTU 12116 (4.13%) and OTU 35728 (3.62%) are closely associated with *C. kluyveri* and *D. vulgaris* strain Hildenborough, respectively. The other two OTUs that dominated during the active chain elongation period (Day 3 to Day 10), OTU 52828 and 77487, are affiliated to *F. varium* and *Acetoanaerobium sticklandii* (formerly known as *Clostridium sticklandii*) (Galperin et al., 2016), respectively. In addition, the two OTUs, which dominated at the end of or after the active chain elongation period, OTU 77232 and 39880, are closely related to *Clostridium limosum* (95% identity based on Blastn) and *Alistipes putredinis* (87% identity based on Blastn), respectively. *C. limosum*, found in a cluster with other two species, *C. histolyticum* and *C. proteolyticum*, is highly proteolytic and able to produce acetate as the major end product (Collins et al., 1994). *A. putredinis* under the order of *Bacteroidales*, is capable of producing SCFAs, especially succinic acid, from carbohydrate (Rautio et al., 2003).

Figure 5.2b demonstrates the corresponding dominant microbial constituents in the culture on Day 6, 15, and 23. During Day 6 to Day 15, *C. kluyveri*-related organism were predominantly observed at 7–9% composition of the whole microbial consortia, indicating its critical role in caproate production from ethanol and acetate prior to Day 6, and further elongation from ethanol and butyrate until Day 10 (Steinbusch et al., 2011). In the following stages, the caproate concentration decreased slightly with

the depletion of substrate level energy source, but H₂ declined gradually to a low level.

The most abundant OTUs observed on Day 6, corresponding to the peak of chain elongation activity, was closely related to *D. vulgaris* strain Hildenborough (100% similarity in Blastn), a well-known sulfate-reducing bacteria (SRB) in anaerobic ecosystem (Heidelberg et al., 2004). This microorganism typically uses sulfate as an electron acceptor, and H₂, organic acids (i.e., lactate and formate) and ethanol as electron donors for ATP generation through electron transfer-coupled phosphorylation (Heidelberg et al., 2004; Tao et al., 2014). Meanwhile, *D. vulgaris* Hildenborough preferentially utilizes lactate or ethanol over H₂ as the electron donor and produces H₂ constantly unless lactate or ethanol is depleted (Bryant et al., 1977; Tao et al., 2014). Therefore, the occurrence of H₂ peak during active chain elongation was probably contributed by *D. vulgaris* Hildenborough and *C. kluyveri* (Ding et al., 2010; Seedorf et al., 2008). In addition, Bryant et al. revealed a syntrophic relationship between *D. vulgaris* Hildenborough and H₂-utilizing methanogens, in which the electrons transferred from ethanol or lactate could be used for methane production via H₂ without competition from the reduction reaction of sulfate to sulfide in media containing low sulfate (20 mM, corresponding to 1921 mg/L) (Bryant et al., 1977). In other words, the non-saline AD sludge inoculum used in this study (20 mg/L sulfate, low sulfate condition) may induce H₂ production from ethanol by *D. vulgaris* Hildenborough instead of sulfide formation, implying that the electrons generation along with ATP formation from ethanol could also be further

transferred to butyrate and caproate as end products. Specifically, the other two dominant microorganisms, *F. varium* and *A. sticklandii*, are able to consume amino acids and H₂ generated by *D. vulgaris* Hildenborough to produce butyrate for *C. kluyveri*, and the latter was proved to harbor Wood–Ljungdahl pathway (Fonknechten et al., 2010; Potrykus et al., 2008). After Day 10, a slight acetate accumulation was observed (Figure 1a). In comparison with the microbial community structures on Day 6 and 15, the proportions of four organisms related to uncultured *Bacteroidetes* bacterium (clone e03=d04), *Proteiniclasticum* sp., *Bacillaceae* bacterium mt8, and uncultured *Coriobacteriaceae* bacterium increased and dominated during the last stage (Day 23). The uncultured *Bacteroidetes* bacterium-related organisms are frequently found in the human gut microbiome, animal rumen, and sludge-degrading community in slurry composting process (Jung & Regan, 2007; Mohapatra, 2008). Many *Bacteroidetes* species are able to produce acetate and succinate from various carbohydrates, amino acids and lipids (Miller, 1978; Shoaie et al., 2013). The *Proteiniclasticum* sp., 100% identified as a partial sequence of *Proteiniclasticum* sp. N2, is an anaerobic proteolytic bacterium isolated from cellulose-degrading mixed culture with acetate as one of the fermentative products (Gao et al., 2014; Zhang et al., 2010). *Bacillaceae* bacterial species predominate in hydrolysis and acidogenesis (Khanal, 2009). *Coriobacteriaceae* bacterial species are strict anaerobic microbes many of which are usually saccharolytic and possess a variety of aminopeptidases (Clavel et al., 2014). Thus, the acetate accumulation in the last stage may be caused by fermentative degradation of debris compounds (i.e., carbohydrates, proteins, and lipids) derived from dead cell

biomass.

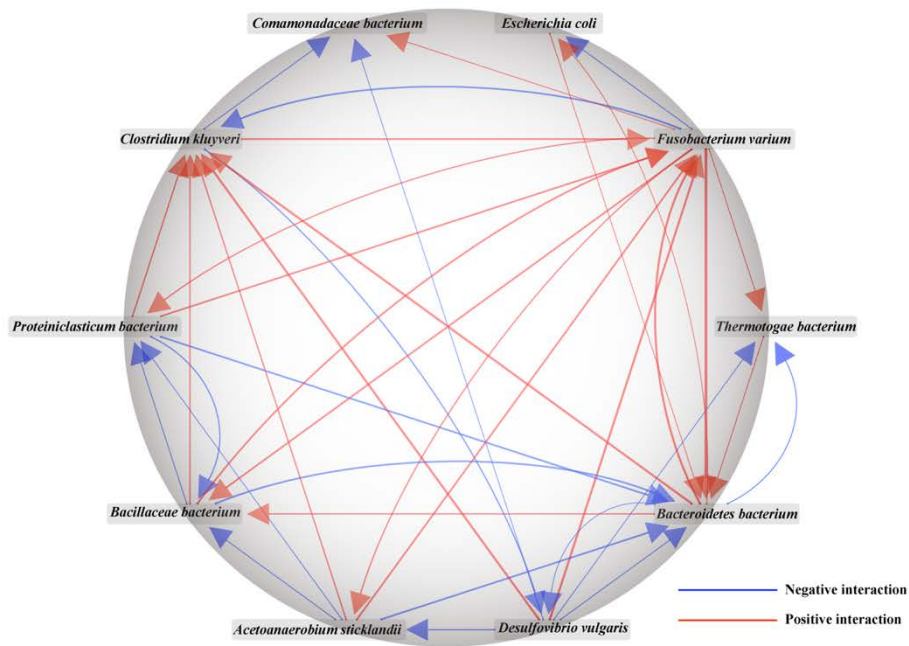


Figure 5.6. Association network among top 10 abundant microbes. Each node represents an OTU and each edge represents a negative (blue) or positive (red) interaction between the two connect nodes. Arrow demonstrates the direction of the influence and the width of edges indicates the strength of the interaction.

Figure 5.6 illustrates the network interaction of the top 10 most abundant OTUs based on microbial community profiles of Day 6, 15, 23. *D. vulgaris* had a positive influence on *C. kluyveri* while *C. kluyveri* had a weak negative effect towards *D. vulgaris*. Although these two microbes compete for the ethanol as electron donor, the acetate generated by *D. vulgaris* could be used by *C. kluyveri*. However, the H₂ formation from ethanol-acetate fermentation by *C. kluyveri* inhibited the ethanol oxidation of *D. vulgaris*. A strong interaction between *D. vulgaris* and *F. varium* was observed, implying that *F. varium* was positively associated with *D. vulgaris*. An

unexpected finding of *A. sticklandii* with low concentration and insignificant dynamics requires further investigation. In addition, this network interaction also explains the difference of the abundant OTUs between previous observation in a similar condition and this study (Leng et al., 2017) (Table 5.3). Compared to OTUs abundance of the previous observation, *C. kluyveri* and *F. varium* increased with the growth of *D. vulgaris*.

Table 5.3. Comparison of abundant OTUs of previous observation with this study.

OTUs	<i>Desulfovibrio vulgaris</i>	<i>Clostridium kluyveri</i>	<i>Fusobacterium varium</i>	[<i>Clostridium</i>] <i>sticklandii</i>	<i>Escherichia coli</i>
Previous observation	0.09%	0.74%	0.00%	11.73%	0.01%
This study	4.84%	5.51%	3.35%	2.34%	3.08%

5.2.2 Metagenomics-based metabolic pathways characterization

To verify our proposed synergistic metabolic network for caproate production in the microcosm (Figure 5.7), we performed shotgun sequencing and *de novo* assembly. The recovered metagenomic bins were phylogenetically identified by genomic comparison using PhyloPhlAn, which indicated that Bin 001, Bin 002 and Bin 045 likely represent the draft genomes of *D. vulgaris*, *C. kluyveri* and *A. sticklandii*, respectively (Figure 5.8) (Segata et al., 2013). Table 5.4 summarized the features of these three recovered bins, whose chromosome size are 2.78 Mb, 4.37 Mb, and 2.33 Mb, respectively, and guanine-cytosine (G+C) content are 63.5%, 31.3%, 34.9%, respectively. The circular chromosome sizes and G+C % of genomes of *D. vulgaris*, *C. kluyveri* and *A. sticklandii* are 3.57 Mb, 3,96 Mb, 2.72 Mb, respectively, and

63.2%, 32.0%, 33.3%, respectively (Devereux et al., 1997; Fonknechten et al., 2010; Heidelberg et al., 2004; Seedorf et al., 2008). The similar genome sizes and G+C percentages further indicate high similarity between recovered bins and the genomes of known isolates. The completeness of these three bins were between 90% and 95%, and were thus considered as substantially complete genomes. Gene annotation was further performed to illuminate the chain elongation metabolic pathways for caproate formation in mixed culture.

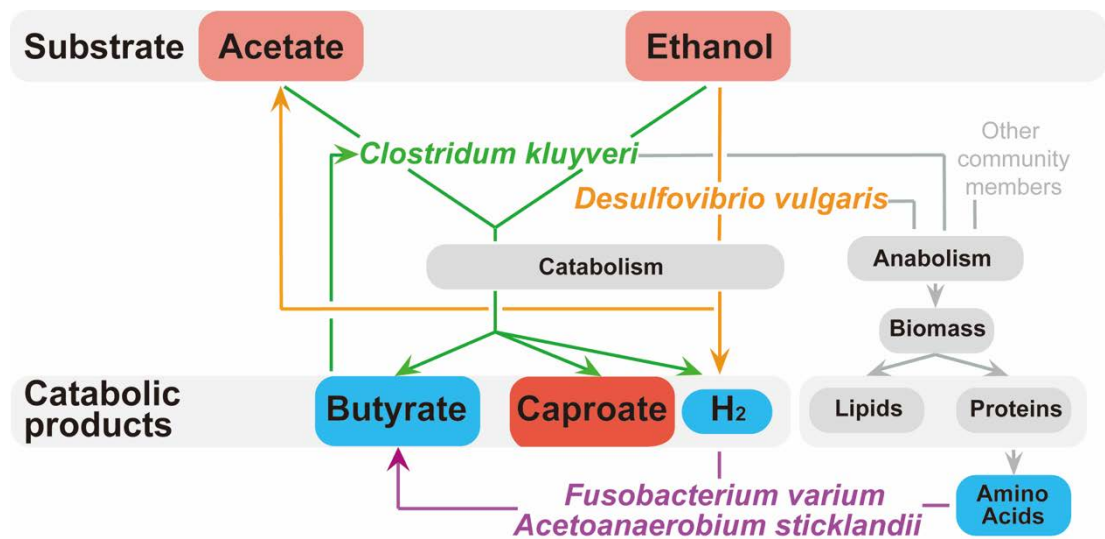


Figure 5.7. The proposed synergistic and syntrophic network during the active phase of mixed culture carboxylates chain elongation with ethanol.

Table 5.4. A summary of genomes recovered from shotgun *de-novo* assembly.

Genome	Chromosome size (bp)	GC content (%)	Completeness (%)	Contamination (%)	Strain heterogeneity (%)
<i>Desulfovibrio vulgaris</i>	2,777,217	63.5	90	4.45	44.44

<i>Clostridium</i>					
<i>kluyveri</i>	4,373,507	31.3	95	0.95	0
<i>Acetoanaerobium</i>					
<i>sticklandii</i>	2,325,435	34.9	95	28.42	24.49

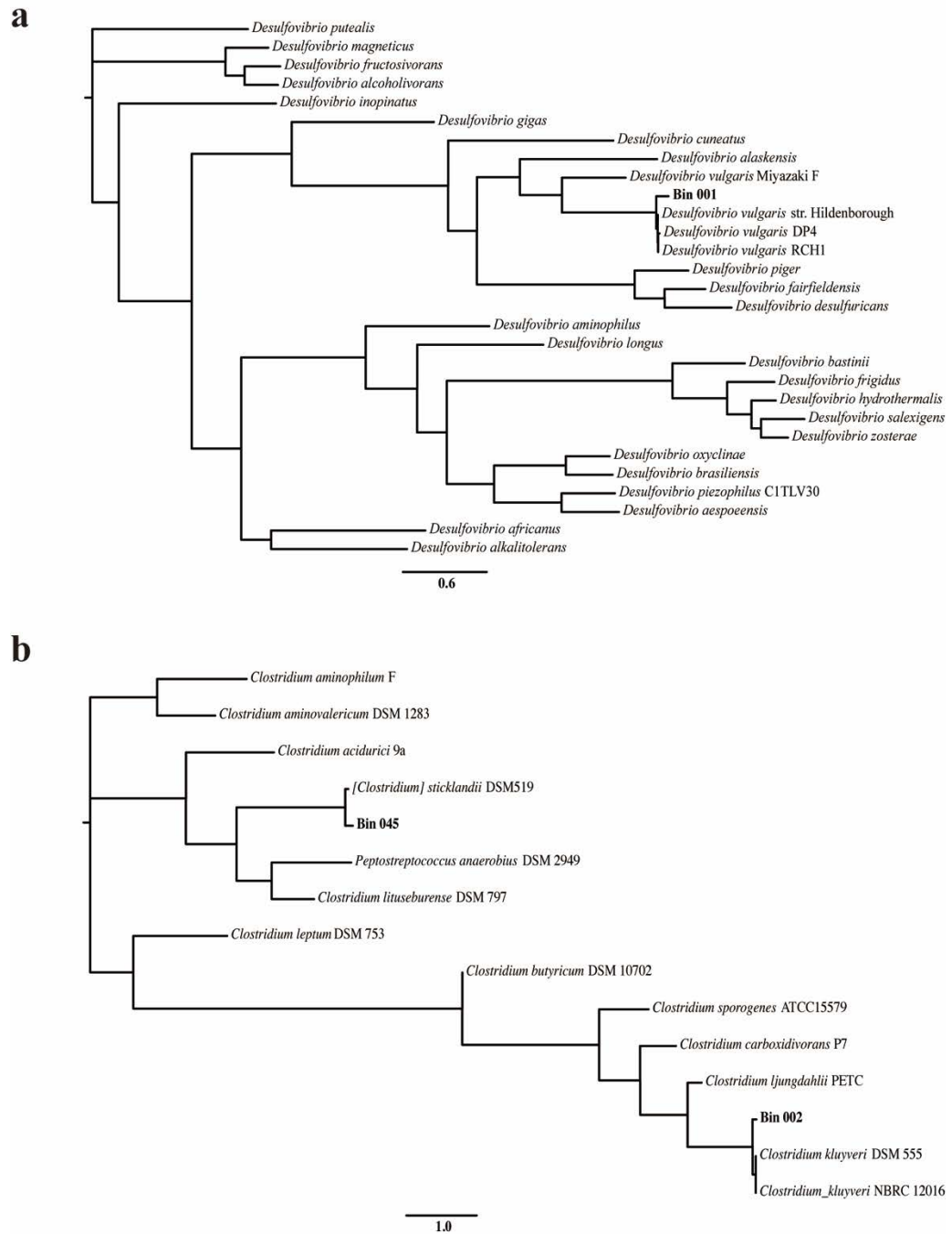


Figure 5.8. Phylogenetic tree based on whole-genome sequence using PhyloPhlAn.

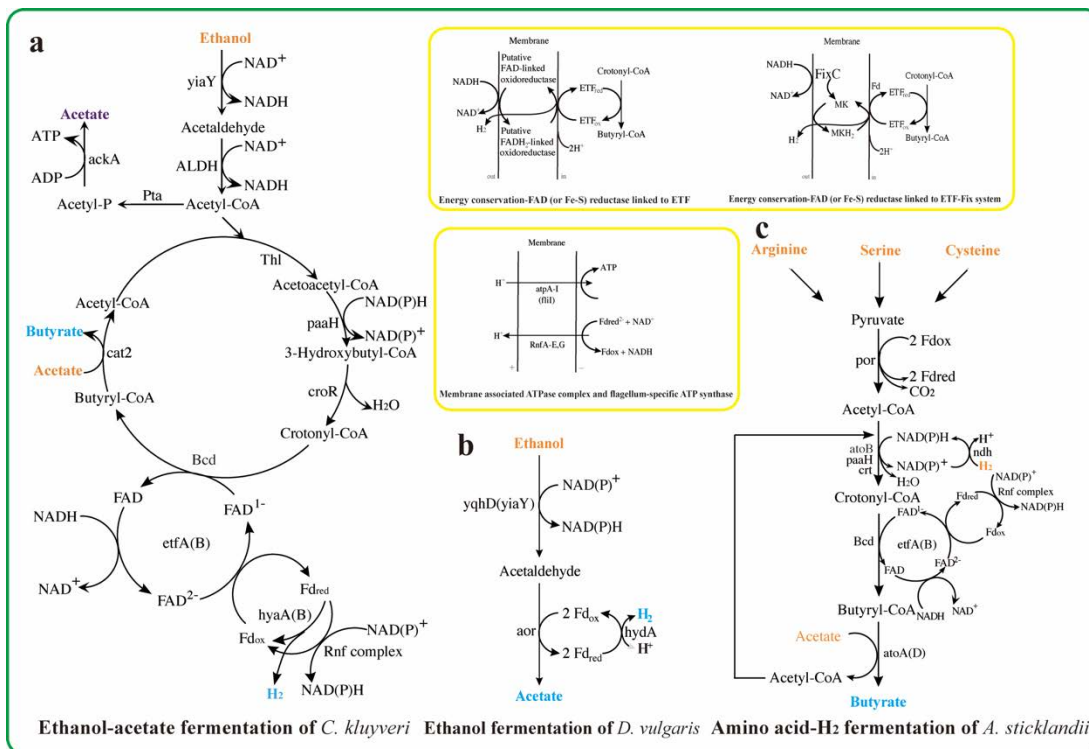


Figure 5.9. The carboxylates chain elongation pathways of *C. kluyveri* or a syntrophic partnership of *D. vulgaris* and *A. sticklandii*. (a) Ethanol-**acetate** fermentation to butyrate along with H₂ formation; (b) Ethanol oxidation to **acetate** and H₂; (c) Amino-acids-**acetate**-H₂ fermentation to butyrate.

Ethanol and acetate are known to be fermented by *C. kluyveri* with the production of butyrate and caproate (Smith et al., 1985). Although the genome of *C. kluyveri* DSM 555 revealed that the bacterium could perform the metabolism entirely on its own (Seedorf et al., 2008), the gene annotation of the three recovered bins revealed an intricate interspecies pathway of ethanol-**acetate** fermentation in mixed culture (Appendix I Table and Figure 5.9a). The pathway of *C. kluyveri* bin starts with ethanol oxidation via acetaldehyde to acetyl-CoA catalyzed by NAD-dependent iron-containing alcohol dehydrogenases (*yiaY* and *adhE*; CK_01148, CK_01212, CK_02184, CK_02636, CK_03254, CK_04032, and CK_04084) and a

NAD(P)-dependent acetaldehyde dehydrogenase (ALDH; CK_03374). These genes are not discovered to be located in the same cluster with microcompartment-associated genes (CK_02630–02631), differing from the strain DSM 555 genome (Seedorf et al., 2008). In the following step, acetate formation from acetyl-CoA via acetyl-phosphate is catalyzed by putative phosphotransacetylase (*pta*; CK_03900) and acetate kinase (*ackA*; CK_00062). Meanwhile, two acetyl-CoA proceeds to form acetoacetyl-CoA catalyzed by acetoacetyl-CoA thiolase (*thl*; CK_00443–00445). Subsequently, butyryl-CoA formation proceeds from the acetoacetyl-CoA via 3-hydroxybutyryl-CoA and crotonyl-CoA through reverse β -oxidation pathway. This process involves three enzymes, 3-hydroxybutyryl-CoA dehydrogenase (PaaH), 3-hydroxybutyryl-CoA dehydratase (CroR/Crt) and NAD-dependent butyryl-CoA dehydrogenase/electron transfer flavoprotein (ETF) complex (Bcd/EtfAB). These β -oxidation-related genes are located in a gene cluster (CK_01045–01049). These coding DNA sequences (CDS) are also capable of forming caproyl-CoA (hexanoyl-CoA) (Figure 5.10) (Seedorf et al., 2008). The formed butyryl-CoA reacts with acetate to form butyrate in a reaction catalyzed by CoA-transferases (*cat2*; CK_00295). Similarly, caproate could be formed from caproyl-CoA and butyrate/acetate catalyzed by Cat2 (Figure 5.10). A membrane-bound energy converting systems are also found in the *C. kluyveri* bin (*Appendix II* Table). Along with the conversion of crotonyl-CoA to butyryl-CoA, catalyzed by Bcd/EtfAB complex, the reduced ferredoxin (Fd_{red}) generated is oxidized with NAD(P)^+ catalyzed by *Rhodobacter* nitrogen fixation (Rnf) complex (CK_01888–01893). In addition, we found two additional membrane-associated

energy conservation systems: ETF-linked iron-sulfur binding reductase (CK_03656–03658) and ETF dehydrogenase (*fixABCX*; CK_02710–02713). These membrane-bound energy conservation systems consume protons while protons are generated along with ATP formation catalyzed by another membrane associated enzymes ATPase complex (CK_00434–00442) and a flagellum-specific ATP synthase (*flil*; CK_01313). The surplus Fd_{red} could be oxidized with H_2 production catalyzed by periplasmic hydrogenase subunit (CK_02733–02741) and cytoplasmic iron-only hydrogenases (CK_00654 and CK_00728).

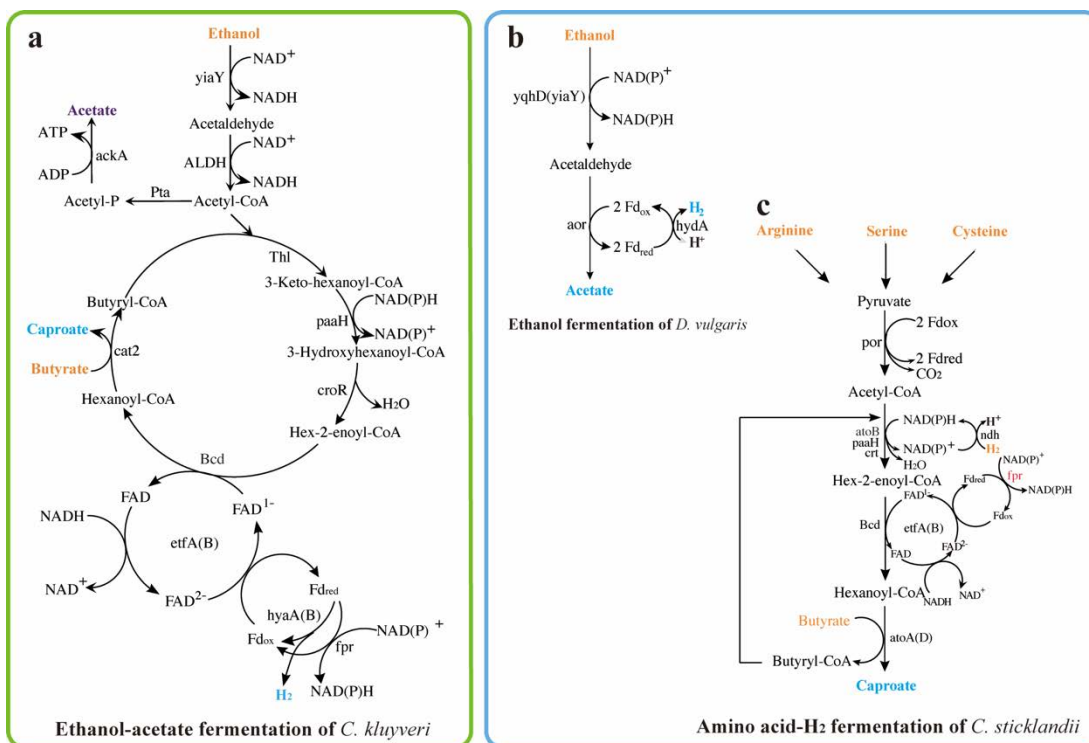


Figure 5.10. The carboxylates chain elongation pathways of *C. kluyveri* or a syntrophic partnership of *D. vulgaris* and *A. sticklandii*. (a) Ethanol-butyrate fermentation to caproate along with H_2 formation; (b) Ethanol oxidation to acetate and H_2 ; (c) Amino-acids-butyrate- H_2 fermentation to caproate.

As discussed above, *D. vulgaris* Hildenborough could utilize ethanol to produce H₂ for synergistic-associated methanogens in the absence of the competing sulfate to sulfide reaction in low sulfate media. However, the oxidation of ethanol to acetate with H₂ formation rather than with sulfate as electron acceptor has not been well delineated. Genes encoded in the *D. vulgaris*-related bin 001 was annotated to verify the pathway (*Appendix I* Table and Figure 5.9b). The fermentation proceeds with ethanol oxidation via acetaldehyde to acetate catalyzed by five alcohol dehydrogenases (*yqhD* and *yiaY*; DV_00409, DV_01064, DV_01916, DV_02002, and DV_02751), an aldehyde dehydrogenase (DV_00071–00072 and DV_01138) and an aldehyde:ferredoxin oxidoreductase (*aor*; DV_02212). None of the five alcohol dehydrogenase genes are located close to the *aor* gene. The H₂ formation cooperated with a periplasmic [NiFe] hydrogenase was also identified with high amino acid identity to that found in the genome of strain Hildenborough (*Appendix II* Table).

The unexpected finding on ethanol oxidation to acetate and H₂ could be thermodynamically infeasible as shown in the calculation using a thermodynamic model of biochemical reactions (Table 5.5) (Alberty, 2005). Due to the biological “quantum of energy”, where a minimum of approximately -20 kJ per mol is required for cell survival of a microorganism, *D. vulgaris* Hildenborough is unable to produce acetate and H₂ from ethanol without external thermodynamics impetus (Schink, 1997). However, this biochemical reaction could proceed when a syntrophic microorganism exists in the culture. *F. varium* and *A. sticklandii* are found to be

abundant at the ethanol fermentation stage. They could utilize amino acids and H₂ as energy sources to achieve acetate-butyrate pathways (Fonknechten et al., 2010; Potrykus et al., 2008). Butyrate formation from acetate and H₂ is thermodynamically feasible (Table 5.5). As the products are rapidly consumed by the syntrophic partners, the low concentration of products, especially H₂, would enable the biochemical reaction of ethanol oxidation by *D. vulgaris* Hildenborough to become thermodynamically feasible. The overall reaction of the two in Table 5.5 yields a value of Gibbs free energy that is higher than twice of the biological “quantum of energy” and supports this syntrophy thermodynamically.

Syntrophic relationship is well known between hydrogen-producing acetogens and methanogenic archaea, in which acetate and H₂ are intermediates and low H₂ partial pressure is essential for acetogenic reactions to be thermodynamically favorable (Schink, 1997). Nevertheless, our findings raised an important notion that syntrophy in mixed culture is not only confined to bacteria and archaea, but could also be extended to inter-bacterial species. Co-culture studies of Men et al. and Harding et al. also illustrate the sustainable syntrophy between *Dehalococcoides ethenogenes* strain 195 (DE195) and *D. vulgaris* Hildenborough and *Dehalococcoides mccartyi* 195 (Dhc195) and *D. vulgaris* Hildenborough, respectively in dechlorination (Harding et al., 2013; Men et al., 2012).

Table 5.5. Standard transformed Gibbs free energy ($\Delta_r G^{\circ}_{310K}$) of ethanol oxidation to acetate and H₂ by *D. vulgaris*, and butyrate formation from acetate and H₂ by *A. sticklandii*.

Reaction: Ethanol + H ₂ O → Acetate ⁻ + H ⁺ + 2 H ₂						
Ionic strength (M)	pH 4.5	pH 5	pH 5.5	pH 6	pH 7	pH 8
0	14.69	11.73	8.76	5.79	-0.14	-6.08
0.05	13.67	10.71	7.74	4.77	-1.16	-7.10
0.1	13.39	10.43	7.46	4.49	-1.44	-7.38
0.25	12.97	10.01	7.04	4.07	-1.86	-7.80

Reaction: 2 Acetate ⁻ + 2 H ₂ + H ⁺ → Butyrate ⁻ + 2 H ₂ O						
Ionic strength (M)	pH 4.5	pH 5	pH 5.5	pH 6	pH 7	pH 8
0	-59.89	-56.93	-53.96	-50.99	-45.06	-39.12
0.05	-58.87	-55.91	-52.94	-49.97	-44.04	-38.10
0.1	-58.59	-55.63	-52.66	-49.69	-43.76	-37.82
0.25	-58.18	-55.21	-52.24	-49.27	-43.34	-37.40

Unit: KJ mol⁻¹

The genes of *A. sticklandii*-related metagenome bin 045 are annotated. As illustrated in *Appendix I* Table, *Appendix III* Table and Figure 5.9c, amino acids such as arginine, serine and cysteine can be fermented to pyruvate (Fonknechten et al., 2010). In addition, alanine can be oxidized to pyruvate by alanine dehydrogenase

(CS_00093) coupled with the reduction of glycine to acetate via Stickland reaction employing glycine reductase complex (CS_00283–00284, CS_00993–00998, CS_01071–01073, and CS_01780–01781). Following which, pyruvate is oxidized to acetyl-CoA catalyzed by pyruvate-ferredoxin/flavodoxin oxidoreductase (*por*; CS_00432 and CS_00649) along with CO₂ production. The following pathway for butyrate formation is similar to the pathway of *C. kluyveri*. Butyryl-CoA formation from acetyl-CoA proceeds via the intermediates of acetoacetyl-CoA, 3-hydroxybutyryl-CoA, crotonyl-CoA, and butyryl-CoA. The involved enzymes include acetyl-CoA C-acetyltransferase (*atoB*; CS_01299 and CS_01905), 3-hydroxybutyryl-CoA dehydrogenase (*paaH*; CS_00222 and CS_00704), enoyl-CoA hydratase (*crt*; CS_00221) and NAD-dependent butyryl-CoA dehydrogenase complex (*bcd/etfAB*; CS_01444 and CS_01937, partial). The formed butyryl-CoA reacting with acetate results in butyrate formation, catalyzed by acetate CoA/acetoacetate CoA-transferase subunits (*atoAD*; CS_00212–00213). According to the abovementioned genes, *A. sticklandii* also has the potential of caproate formation (Figure 5.10).

As for *Fusobacterium*, no recovered bin was closely associated with the genome of *F. varium* or *F. ulcerans*. The BLAST analysis of 16S rRNA gene sequences showed that the OTU52828 has 99.6% identity to the *F. varium* ATCC 27725, 99.6% identity to the type strain of *F. varium* JSM 6320 (=ATCC 8501) and 99.2% identity to the *F. ulcerans* ATCC 49185 (type strain of *F. ulcerans*). In order to verify an amino acids-acetate-H₂ fermentation pathway of *F. varium*, the genome of *F. varium* ATCC

27725 obtained from Integrated Microbial Genomes (IMG) system of U.S. Department of Energy Joint Genome Institute (DOE JGI) was annotated (McGuire et al., 2014). *F. varium* ATCC 27725 is able to utilize multiple amino acids such as glycine, serine, and threonine (*Appendix IV* Table). The pyruvate generated from amino acids is oxidized to acetyl-CoA catalyzed by pyruvate-ferredoxin/flavodoxin oxidoreductase (*por*; 646284783 and 646284198-646284201) along with CO₂ production (*Appendix IV* Table). Butyryl-CoA formation from acetyl-CoA proceeds via the intermediates of acetyl-CoA C-acetyltransferase, 3-hydroxybutyryl-CoA, crotonyl-CoA, and butyryl-CoA. The involved enzymes include acetyl-CoA C-acetyltransferase (*atoB*; 646283343 and 646283326), 3-hydroxybutyryl-CoA dehydrogenase (*paaH*; 646284062 and 646283324), 3-hydroxybutyryl-CoA dehydratase (*croR*; 646285345, 646284822 and 646283189), enoyl-CoA hydratase (*crt*; 646283325) and butyryl-CoA dehydrogenase complex (*bcd/etfAB*; 646283190, 646283191 and 646283192) (*Appendix IV* Table). The formed butyryl-CoA reacting with acetate results in butyrate formation, catalyzed by acetate CoA/acetoacetate CoA-transferase subunits (*atoAD*; 646284367 and 646284366) or CoA-transferases (*cat2*; 646284915) (*Appendix IV* Table). According to these annotated genes, the caproate formation by *F. varium* ATCC 27725 is also possible.

The abovementioned metagenomic features of dominant microbiomes in the mixed culture demonstrate a synergistic and syntrophic metabolic network for caproate production through reconstructed pathways. It proves that butyrate and caproate can be directly produced from ethanol and acetate in the presence of *C. kluyveri* under

mixed culture. In addition, a syntrophic partnership of *D. vulgaris* and *A. sticklandii* (*F. varium*) relying on H₂ as a reducing equivalent messenger, for the first time, was unveiled to indirectly achieve carboxylates chain elongation in low sulfate mixed culture (Figure 5.9). The former pathway of *C. kluyveri* starts with ethanol oxidation and produces caproate by reverse β -oxidation. In this pathway, the reduction of crotonyl-CoA to butyryl-CoA by NADH, catalyzed by Bcd/EtfAB complex, is coupled with the reduction of ferredoxin by NADH. Reduced ferredoxin can be reoxidized by NAD⁺ mediated by the Rnf system which generates an electrochemical proton gradient for ATP synthesis. H₂ production is catalyzed by periplasmic hydrogenase subunit and cytoplasmic iron-only hydrogenases for surplus Fd_{red} reoxidation. The latter pathway starts with ethanol oxidation by *D. vulgaris* along with H₂ generation by a periplasmic [NiFe] hydrogenase coupled to an aldehyde:ferredoxin oxidoreductase. The H₂ is then utilized by *A. sticklandii* through NADH dehydrogenase involved in the reverse β -oxidation pathway.

5.3 Chapter summary

The abundant bacteria, *D. vulgaris*, *F. varium*, and *A. sticklandii*, which are co-existent with *C. kluyveri* accelerated the carbon and electron flows of carboxylates chain elongation with ethanol. *D. vulgaris* oxidizes ethanol to acetate and thereby the formed H₂ is used by the two amino acid degrading bacteria for the production of butyrate. The interspecies H₂ transfer takes place, which has been hitherto commonly known for the interaction between syntrophic bacteria and methanogenic archaea. The disclosed metabolic pathways by metagenomic analysis

suggested that the synergy network could be technically applied with the potential to upcycle the mixed culture anaerobic processes for value-added chemicals production. Finally, prior to implementing this mixed culture anaerobic process in practice, additional research must be conducted to (1) identify an optimal bacterial composition for efficient caproate production in a mixture of pure culture strains and (2) test an optimal H₂ partial pressure to maintain the synergistic and syntrophic network in a continuous fermentation reactor.

Chapter 6. 1,3-PDO and Caproate co-production through glycerol fermentation and carboxylate chain elongation by shaping microbial consortia

6.1 Overview

Glycerol is presently being generated in surplus with the rapid growth of biodiesel industry and the demand for 1,3-PDO-based polymers is constantly increasing. Biological reduction of glycerol to 1,3-PDO concurrently produces byproducts which limit its purity and cause the cost for distillation. This pioneering study successfully enriched a microbial community capable of efficiently converting glycerol to 1,3-PDO and producing a water-slightly-soluble and value-added chemical, caproate, from the byproducts of glycerol fermentation through carboxylate chain elongation. A co-production of 6.38 mM C 1,3-PDO d⁻¹ and 2.95 mM C caproate d⁻¹ was achieved in a 2-L semi-continuous fermenter with a glycerol-ethanol-acetate stoichiometric ratio of 4:3:1. Microbimes, *E. limosum*, *C. kluyveri* and *M. senegalense*, utilize a unique combination of metabolic pathways to facilitate the above conversion. Based on metagenomics, *E. limosum* is capable of converting glycerol to 1,3-PDO, ethanol and H₂, and also redirecting the electron potential of H₂ into acetate via the Wood–Ljungdahl pathway for chain elongation. *C. kluyveri* worked synergistically with *E. limosum* by consuming ethanol and acetate for caproate production. *M. senegalense* encodes for ethanol oxidation to acetate and butyrate, facilitating the generation of these intermediates for elongation to caproate by *C. kluyveri*. During the transition between fermentation and elongation, an unexpected phenomenon of poly-β-hydroxybutyrate (PHB) formation and

reutilization by *M. senegalense* was observed, which may be associated with butyrate formation for further caproate generation. Significant ethanol production as an intermediate of glycerol dissimilation and the non-inhibiting level of 1,3-PDO production, which allows the dominance of *C. kluyveri*, are key to increasing caproate production. The knowledge gleaned from the substrate constitute, microbial consortium and their metabolism creates a valuable resource recovery potential for the biodiesel industry.

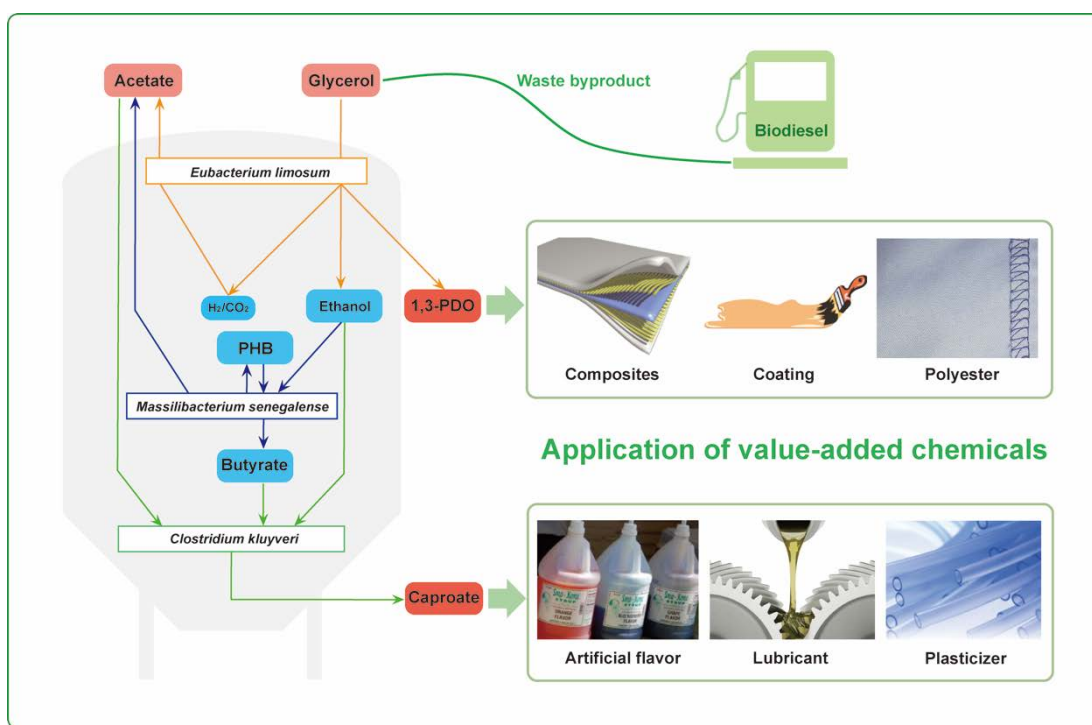


Figure 6.1. Two value-added chemicals, 1,3-PDO and caproate, co-production through glycerol fermentation and carboxylate chain elongation.

6.2 Results and discussion

6.2.1 Glycerol fermentation in a semi-continuous reactor

Glycerol fermentation with mixed culture enriched from non-saline AD sludge was first conducted for three stages in a semi-continuous reactor (Figure 6.2). Fermentation was constantly carried out with methanogenesis inhibition with an HRT of 30 days, controlling temperature at 37 °C, and pH at 7. In the three stages, a gradual increase of glycerol with a constant amount of acetate was fed into the fermenter (Figures 6.2a), resulting in 1,3-PDO, butyrate and acetate as major products (Figures 6.2b). At stage 3, we achieved the highest 1,3-PDO production rate of 13.90 mM C d⁻¹ and butyrate and acetate (net) yields of 5.48 and 4.06 mM C d⁻¹, respectively, from 45 mM C d⁻¹ of glycerol. The conversion rates of 1,3-PDO and butyrate were 31% ($\text{mol}_{1,3\text{-PDO}} / \text{mol}_{\text{glycerol}}^{-1}$) and 10% ($\text{mol}_{\text{butyrate}} / \text{mol}_{\text{glycerol}}$), respectively. The electron flow balance in this stage indicated that around 60% of glycerol was catabolized into 1,3-PDO, butyrate and acetate. Correspondingly, 16S rRNA gene-based analysis of the microbial constituents (Figure 6.2c) at the middle and late periods of stage 3 show that organisms associated with *E. limosum* (100% identity based on Blastn), *Proteiniphilum acetatigenes* (100%), *Actinomyces* sp. MD1 (100%), and *A. caccae* (100%) dominated. Based on the corresponding genome bin recovered (S3_Bin001), *E. limosum* is likely converting glycerol to acetate oxidatively (via GldA–DhaL/K) and 1,3-PDO (via PduC/D/E–DhaT) reductively (Figure 6.12 and Table 6.4) (Lin, 1976). *A. caccae* (S3_Bin003) encodes for glycerol oxidation to butyrate (via GldA–DhaL/K– –Cat2/3) (Louis & Flint, 2009).

Unexpectedly, the commonly known 1,3-PDO-producing bacteria (*C. butyricum* and *K. pneumoniae*) only contributed a small proportion of the microbial constituents in this stage.

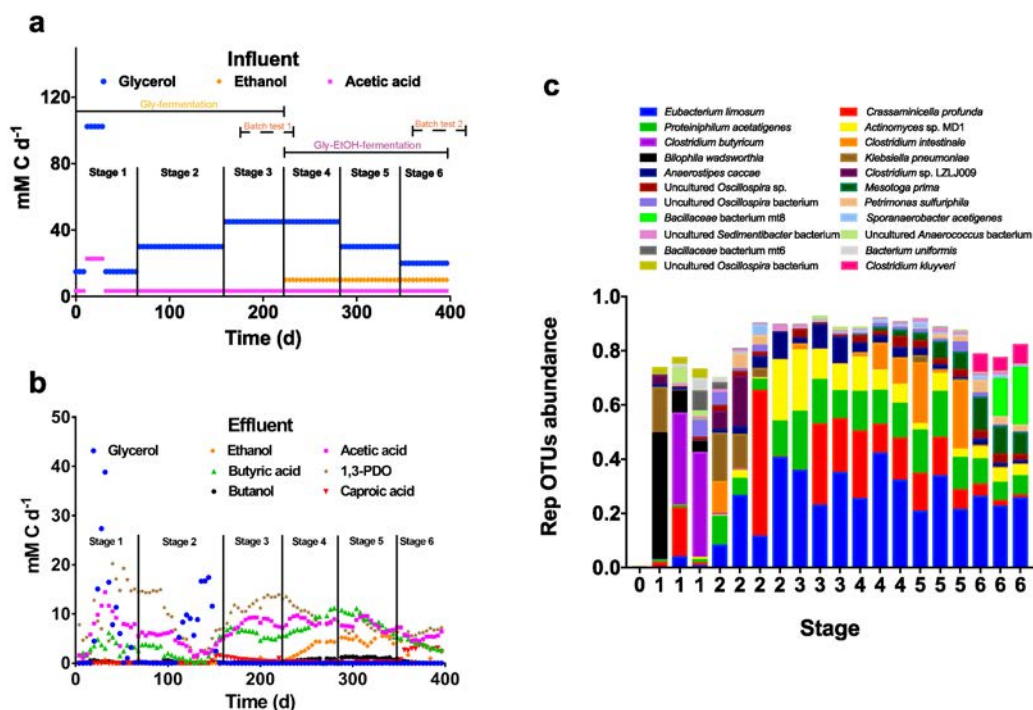


Figure 6.2. Physiologic performance and microbial characterization of semi-continuous mixed culture fermentation at 37 °C, pH of 7, stirring rate of 150 rpm and HRT of 30 days with methanogenesis inhibition. Substrates in influent (a) and products in effluent (b) of the six stages differ from substrate compositions. Corresponding representative OTUs are covered 63.04%–73.56%, 63.54%–86.63%, 65.32%–79.73%, 73.99%–82.40%, 79.21%–86.62%, and 70.44%–77.43% of the whole sequence at each stage, respectively (c).

In contrast, *C. butyricum* dominated with a large proportion of 34.06% to 38.64% when the glycerol in the influent was much higher (102 mM C d⁻¹) at stage 1 (Figure 6.2). Nevertheless, such a high glycerol load could not be completely consumed by

the mixed culture in the fermenter. In addition, in the first half of stage 2, *K. pneumoniae* showed a high abundance of 12.68% to 17.86%, consistently resulting in a high 1,3-PDO yield of 14.97 mM C d⁻¹ from 30 mM C d⁻¹ of glycerol. However, the fermentation became inefficient in the second half of stage 2, accumulating a large amount of glycerol due to fermenter operation fluctuations. In general, a stable microbial community effectively facilitating glycerol dissimilation to 1,3-PDO, butyrate and acetate was enriched during Stage 1 to 3. However, questions remained as to how the fermenter microbiota could be manipulated to achieve a concurrent chain elongation of acetate and butyrate to caproate along with 1,3-PDO production, and how the microorganisms interact to accomplish such metabolisms.

6.2.2 Effect of substrates on caproate and 1,3-PDO formation

To figure out how to link caproate production with glycerol fermentation, three batch tests were performed: glycerol fermentation with acetate (Case 1), glycerol fermentation with ethanol and acetate (Case 2), and ethanol-acetate fermentation (Case 3). Compared with glycerol fermentation in semi-continuous fermenter, the butyrate production was much lower but 1,3-PDO yield was higher in Case 1 (Figure 6.3a). Chain elongation for caproate production only occurred in Case 2 and Case 3 (Figure 6.3b–c).

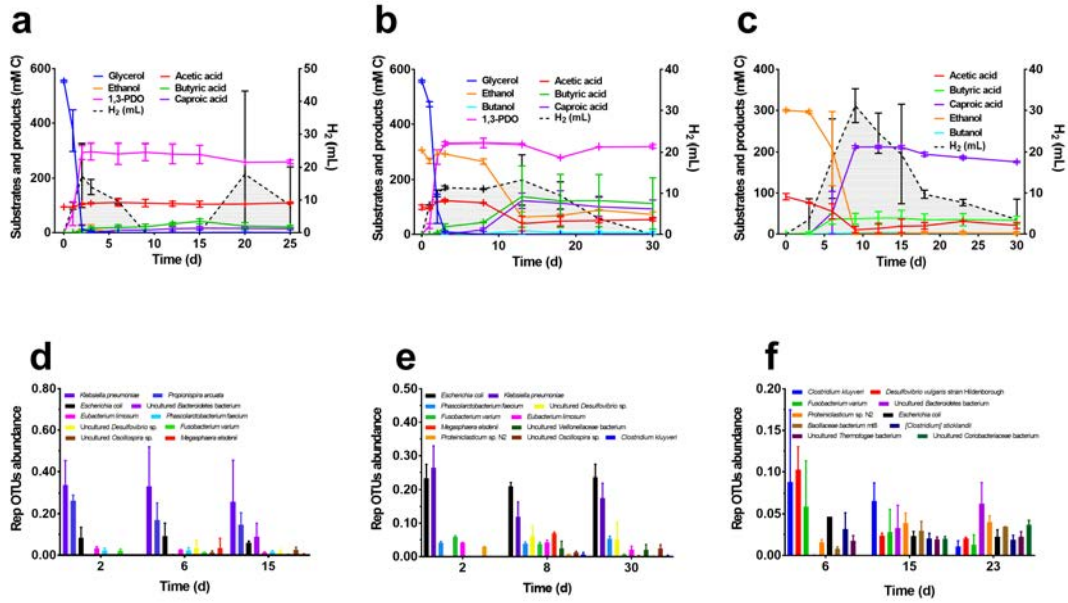


Figure 6.3. Mixed culture fermentation from different substrates inoculated with fresh AD sludge: glycerol with acetate (a), ethanol and glycerol with acetate (b), ethanol with acetate (c). Corresponding representative OTUs collected at three time points are covered 63.23%–76.59%, 59.31%–67.21%, and 28.25%–37.04% of the sequences from each culture, respectively (d–f).

As illustrated in Figure 6.3a, within 3 days, glycerol was completely consumed, resulting in a high amount of 1,3-PDO (0.54 mol C/mol C glycerol) and an insignificant formation of acetate, butyrate and ethanol. After the depletion of glycerol, the ethanol was used immediately with a small yield of butyrate (0.08 mol C/mol C glycerol) and caproate (0.03 mol C/mol C glycerol) in the following days. The H₂ amount in the system showed two peaks, which were associated with glycerol dissimilation and butyrate and 1,3-PDO consumption, respectively. At Day 2 (Figure 6.3e), two dominant microorganisms were identified, which were closely associated with *K. pneumoniae* (100%) and *Propionispira arcuata* (100%). At Day 6, two organisms, uncultured *Desulfovibrio* sp. (100%) and *Megasphaera elsdenii*

(100%), increased. The high abundance of *K. pneumoniae* contributed to the high production of 1,3-PDO. *M. elsdenii* was reportedly associated with butyrate and caproate (low) production (Marounek et al., 1989).

Figure 6.3b demonstrates two stages of the fermentation. Glycerol consumption occurred quickly within 3 days with the release of a large amount of 1,3-PDO (0.60 mol C/mol C glycerol) and some acetate, butyrate, and ethanol. In the second stage, from Day 4 to Day 12, ethanol and acetate were consumed to form butyrate (0.56 mol C/mol C ethanol) and caproate (0.50 mol C/mol C ethanol). The H₂ amount increased with continued glycerol fermentation, and it remained level until the ethanol declined to a low concentration. However, the chain elongation process was unanticipated to cease after 12 days before ethanol and acetate were depleted. As shown in Figure 6.3f, the microbial community structure at Day 2 was mainly constructed by *K. pneumoniae* (100%) and *E. coli* (100%). *E. limosum* also co-existed with an abundance of 4.16 %. In this case, *K. pneumoniae* and *E. limosum* facilitated 1,3-PDO production from glycerol. At Day 8 within the second stage, *M. elsdenii* (100%) and uncultured *Desulfovibrio* sp. (100%) increased significantly. *C. kluyveri* also showed a small increase during the butyrate and caproate formation stage. A co-production of 1,3-PDO and caproate was achieved from glycerol fermentation with ethanol and acetate, and the ethanol addition did not depress the 1,3-PDO production.

Comparing the microbial community with Case 1, the major differences during

glycerol consumption stage were the increase of *E. coli* and the disappearance of *P. arcuata* in Case 2. The dominance of *E. coli* over *P. arcuata* was probably because *E. coli* is capable of converting glycerol to ethanol (Murarka et al., 2008) and better adapting to ethanol-containing culture. Comparing the microbial community of day 8 in Case 2 to day 6 in Case 1, a synergistic network for chain elongation was constructed in Case 2. The synergistic network is hypothesized: The *Desulfovibrio* sp. consumed ethanol to produce acetate and butyrate. The *F. varium* utilized amino acids and H₂ for butyrate production. The synergistic-associated *M. elsdenii* and *C. kluyveri* could then elongate butyrate to caproate. At Day 30, the *M. elsdenii* amount significantly decreased, which was consistent with the cessation of caproate formation. The remaining ethanol at a certain level might be related to the breaking down of such a synergistic network.

In general, ethanol addition or increase of ethanol production from glycerol is one of the keys to facilitate the chain elongation for caproate production followed by glycerol fermentation. The kinetics difference of glycerol fermentation and chain elongation is another issue which may cause the electron loss during the leisure time.

In Case 3 (Figures 6.3c and 6.3g), at Day 12, butyrate and caproate formation were initiated on Day 3 and reached peak conversion rates of 0.13 (mol C/mol C of ethanol) and 0.71 (mol C/mol C of ethanol), respectively on Day 12. In comparison with Case 2, the chain elongation occurred more promptly and a complete utilization of ethanol and acetate were achieved with very similar ethanol and acetate levels.

The more caproate production over butyrate in Case 3 than that in Case 2 occurred with a higher H₂ formation indicating a higher reducing potential in the system. Notably, *C. kluyveri* predominated on Day 6 (Detailed discussion in Chapter 5).

In batch test, glycerol-acetate fermentation resulted in a significant production of 1,3-PDO with low amount of acetate, butyrate and H₂ formation (Case 1); glycerol-ethanol-acetate fermentation produced high amount of 1,3-PDO and butyrate with low amounts of caproate and H₂ generation (Case 2); ethanol-acetate fermentation achieved high caproate and H₂ formation with low amount of butyrate production (Case 3). The comparison between Case 2 and Case 3 on caproate production is reflective of an antagonistic effect of glycerol on chain elongation. A big difference on the organism responsible for chain elongation was also observed in that *M. elsdenii* was chosen over *C. kluyveri* in Case 2 while *C. kluyveri* was dominant in Case 3. This indicated that *C. kluyveri* is more efficient in chain elongation for caproate production. The reason why *M. elsdenii* was selectively enriched over *C. kluyveri* in the presence of glycerol is crucial to improve caproate production in glycerol fermentation. Importance was found *M. elsdenii* cannot metabolize glycerol (Marounek et al., 1989) and hence, its enrichment is not directly stimulated by glycerol. On Day 3 in Case 2 and Day 0 in Case 3, the ethanol and acetate levels were very similar, suggesting it was not substrate availability. The only apparent difference was the generation of 1,3-PDO from glycerol degradation between Day 1–3 in Case 2, which suggested that 1,3-PDO toxicity may be a major factor driving the selection of organisms capable of chain elongation. A previous

study has reported that 10–15 g/L 1,3-PDO can be inhibitory for *Clostridium* spp. (Szymanowska-Powaowska & Kubiak, 2015) and the highest concentration of 1,3-PDO in Case 2 was close to 10 g/L and that in Stage 3 was above it. The inhibitory effect of 1,3-PDO thus created a selective pressure against *C. kluyveri* and provided a window of opportunity for the enrichment of *M. elsdenii*.

Aside from the finding that ethanol addition facilitated concurrent chain elongation and glycerol fermentation, these findings also led us to conclude that an efficient 1,3-PDO and caproate co-production needs (1) a lower glycerol loading to control 1,3-PDO at a non-inhibitory level to allow for 1,3-PDO-sensitive chain elongation bacteria (i.e. *C. kluyveri*) to grow; (2) a glycerol fermenter that produces less 1,3-PDO by converting more glycerol to ethanol (a less oxidized product than acetate), and/or by generating more H₂ to consume excess reducing power through an alternative route; (3) a H₂ consumer who supports H₂ formation from glycerol to maximize the use of glycerol-derived energy.

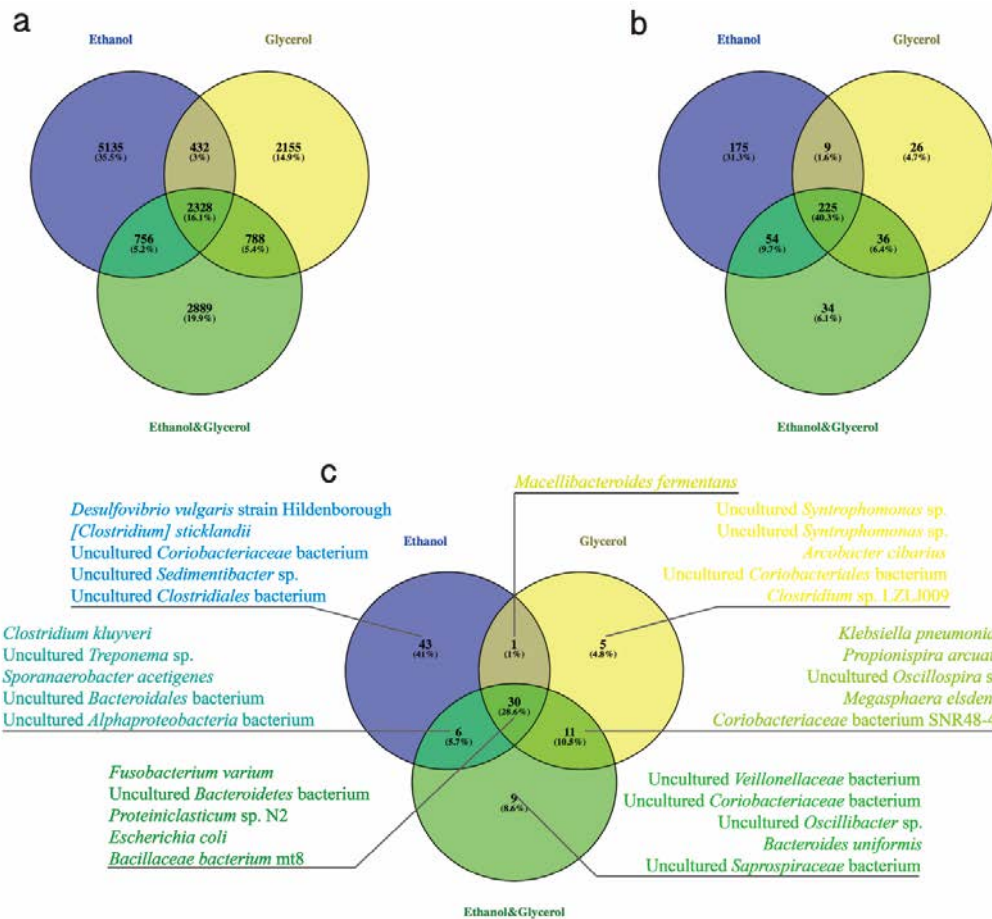


Figure 6.4. Venn diagrams (Oliveros, 2007-2015) of OTUs from three different substrate-enriched cultures in batch fermentation conducted at 37 °C, pH of 7, and 150 rpm with methanogenesis inhibition. Each culture includes 6 samples taken at three time points in duplicate. All OTUs involved (a), OTUs with reads higher than 100 of each culture involved (b), and OTUs with reads higher than 1000 of each culture involved (c).

The relationship of the microbial constituents among these three cases is illustrated with Venn diagrams (Figure 6.4). The diagram that includes all OTUs (Figure 6.4a) demonstrates that the three cultures shared 2,328 OTUs, corresponding to 16.1% of the total population. The culture enriched with ethanol harbors a relatively large number of unique OTUs (35.5%) compared with enrichment cultures with glycerol

(14.9%) or co-electron donors (glycerol and ethanol, 19.9%). Focusing on the abundant OTUs having more 100 and 1000 reads (Figures 6.4b and 6.4c, respectively), similar results could be concluded. Specifically, according to the major OTUs having more than 1000 reads (Figure 6.4c), the three-parties-shared part possesses 28.6% of all parts, which includes *F. varium*, uncultured *Bacteroidetes* bacterium, *Proteiniclasticum* sp., *E. coli*, and *Bacillaceae* bacterium mt8. As discussed above, *F. varium*, uncultured *Bacteroidetes* bacterium, and *Proteiniclasticum* sp. can produce SCFAs using amino acids, probably from biomass degradation. The *Bacillaceae* are a family of heterotrophic bacteria that predominate in the hydrolysis and acidogenesis stage of AD, mainly hydrolyzing proteins into amino acids (Khanal, 2009). As to *E. coli* growing anaerobically, it also contains membrane-bound enzymes such as hydrogenase, fumarate reductase, and formate dehydrogenase, in addition to essential enzymes for glycerol oxidation (Gray et al., 1966). Between the ethanol- and glycerol-fed cultures in this criteria, there was only one shared OTU, *Macellibacteroides fermentans* (100%), which belongs to the *Porphyromonadaceae* family and was initially isolated from an up-flow anaerobic filter treating abattoir wastewater (Jabari et al., 2012). Jabari et al. revealed that this novel obligate anaerobic bacterium uses carbohydrates as electron donors and catalyzes the production of acetate, lactate, and butyrate from glucose (Jabari et al., 2012). In general, these commonly shared OTUs are mainly with functions of hydrolysis, acidogenesis, and acetogenesis, which is similar to traditional AD (Khanal, 2009). *C. kluyveri*, which produces caproate with ethanol and acetate, is only shared by cultures enriched with ethanol and co-electron donors, whereas *K.*

pneumoniae, with function of 1,3-PDO production from glycerol, is only shared by cultures enriched with glycerol and co-electron donors. These results indicate their critical role in the production of caproate and 1,3-PDO. Potential MCCA-producing *M. elsdenii*-related OTUs are only shared by cultures enriched with glycerol and co-electron donors. Miyazaki et al. reported that ethanol inhibited the growth of *M. elsdenii* under weakly acidic–neutral conditions (pH 6.0 to 6.8) (Miyazaki et al., 1991). Although acetate had a stimulating effect on its growth, even in the presence of ethanol at low pH (6.0), the integrated influence on neutral pH was insignificant (Miyazaki et al., 1991), especially in a competitive environment. *D. vulgaris* Hildenborough and *A. sticklandii* were owned only by the culture enriched with ethanol in this criteria. The shorter lag phase of chain elongation in the culture enriched with ethanol compared to that enriched with co-electron donors was probably associated with a synergistic network involving *D. vulgaris* Hildenborough, *A. sticklandii*, and *C. kluyveri*. Although *D. vulgaris* Hildenborough possesses glycerol utilization genes (glycerol kinase and glycerol-3-phosphate dehydrogenase) (Clark et al., 2012; Heidelberg et al., 2004; Rajeev et al., 2012), the growth of *D. vulgaris* Hildenborough on glycerol was relatively slow (Kremer & Hansen, 1987). The absence of *D. vulgaris* Hildenborough in the co-electron donor culture might have been caused by comprehensive factors, including its poor glycerol consumption, low sulfate concentration, and lack of synergistic partners.

6.2.3 Fermenter microbiome enrichment and physiological performance with

an ethanol addition

With the findings from the batch tests, we tested the addition of ethanol while gradually decreasing glycerol loading in the influent of the semi-continuous fermenter (Figure 6.2a) to enrich ethanol-consuming caproate producer and ethanol-tolerant/-producing glycerol degraders. As ethanol is contained in the brewery wastewater which needs to be treated, adding the ethanol-containing brewery wastewater also shows a prospect in economic and environmental considerations for such a practice.

As shown in Figure 6.2b, only half of the ethanol in the influent could be used at the beginning, the glycerol decrease and ethanol addition in the influent caused a decline of 1,3-PDO production but an increase in the butyrate yield, especially at stage 4. The average conversion rate of 1,3-PDO from glycerol was $0.23 \text{ mol}_{1,3\text{-PDO}} \text{ mol}_{\text{glycerol}}^{-1}$ at stages 4 and 5, which is a slight decrease compared to the conversion rate at stage 3 ($0.26 \text{ mol}_{1,3\text{-PDO}} \text{ mol}_{\text{glycerol}}^{-1}$). During these two stages, the microbial consortia showed an obvious increase in the abundance of *Clostridium intestinale* (100%) (Figure 6.2c). *C. intestinale* is a butyrate-producing hydrogen producer that can grow on saccharides and glycerol but not on ethanol (Gossner et al., 2006; Kalia, 2016; Moscoviz et al., 2016; Viana et al., 2014). In stage 6, the fermentation achieved the optimized function of 1,3-PDO and caproate co-production with glycerol-ethanol-acetate stoichiometric ratio of 4:3:1 when the reduced glycerol loading resulted in a lower 1,3-PDO production. The complete consumption of

glycerol and ethanol (20 and 10 mM C d⁻¹, respectively) resulted in 6.38 and 2.95 mM C d⁻¹ of 1,3-PDO and caproate, respectively (Table 6.1). The average conversion rate of 1,3-PDO from glycerol increased to 0.32 mol_{1,3-PDO} mol⁻¹_{glycerol}. The most abundant organisms were *E. limosum* and *C. kluyveri* as well as *Bacillaceae* bacterium mt8 in Stage 6 (Figure 6.2c). Based on the recovered genome bins from metagenomics sequencing (Figure 6.12 and Table 6.4), *E. limosum* (S6_Bin003) is one of the few organisms capable of converting glycerol (via GldA–DhaL/K) to 1,3-PDO (via PduC/D/E–DhaT), ethanol (via AdhE and Adh2) and H₂. *E. limosum* is also capable of oxidizing H₂ to acetate via the Wood–Ljungdahl pathway, which efficiently redirects the energy of H₂ back into chain elongation. The gene annotation results of S6_Bin012 were consistent with the well-known pathway of *C. kluyveri*, which uses ethanol and acetate to produce butyrate and caproate (via Cat2). *Massilibacterium senegalense* (*Bacillaceae* bacterium mt8, S6_Bin004) encodes for ethanol oxidation (via Adh2/YiaY and ALDH) for acetate (via Pta and AckA) and butyrate (via AtoD) production, facilitating carboxylate chain elongation of *C. kluyveri*. In contrast to Case 2 of the batch tests, the enrichment of microorganisms in the semi-continuous fermenter selectively excluded facultative pathogens, such as *E. coli* and *K. pneumoniae*, but still accomplished the 1,3-PDO and caproate co-production with a straightforward biological process of glycerol fermentation and chain elongation.

Table 6.1. Average concentrations of substrates and products in stage 6 of semi-continuous fermenter. Standard deviation is given in parentheses.

Stage 6	Glycerol	Acetic acid	Butyric acid	Caproic acid	Ethanol	Butanol	1,3-PDO
Influent	20.00	3.33	/	/	10.00	/	/
Effluent	0.00 (0.00)	5.30 (0.58)	3.87 (0.95)	2.95 (0.39)	0.31 (0.54)	0.10 (0.15)	6.38 (0.56)

Unit: mM C d⁻¹

The affinity of the 15 most-abundant OTUs in stage 6 and some other related known lineages were deciphered with a phylogenetic tree (Figure 6.5). OTU 106782 with the highest abundance of 24.67% is close to *E. limosum*. As discussed above, the H₂ and CO₂ produced from glycerol could be used by *E. limosum* for acetate and butyrate formation, which would be further utilized by *C. kluyveri* for carboxylates chain elongation. The other abundant OTUs, such as OTU 20679 and OTU 9264, were also involved in such synergetic network. They are able to consume amino acids, sugars and pyruvate in the system to produce acetate and butyrate (S. Y. Chen & Dong, 2005; Nesbo et al., 2012; Zhaxybayeva et al., 2012).

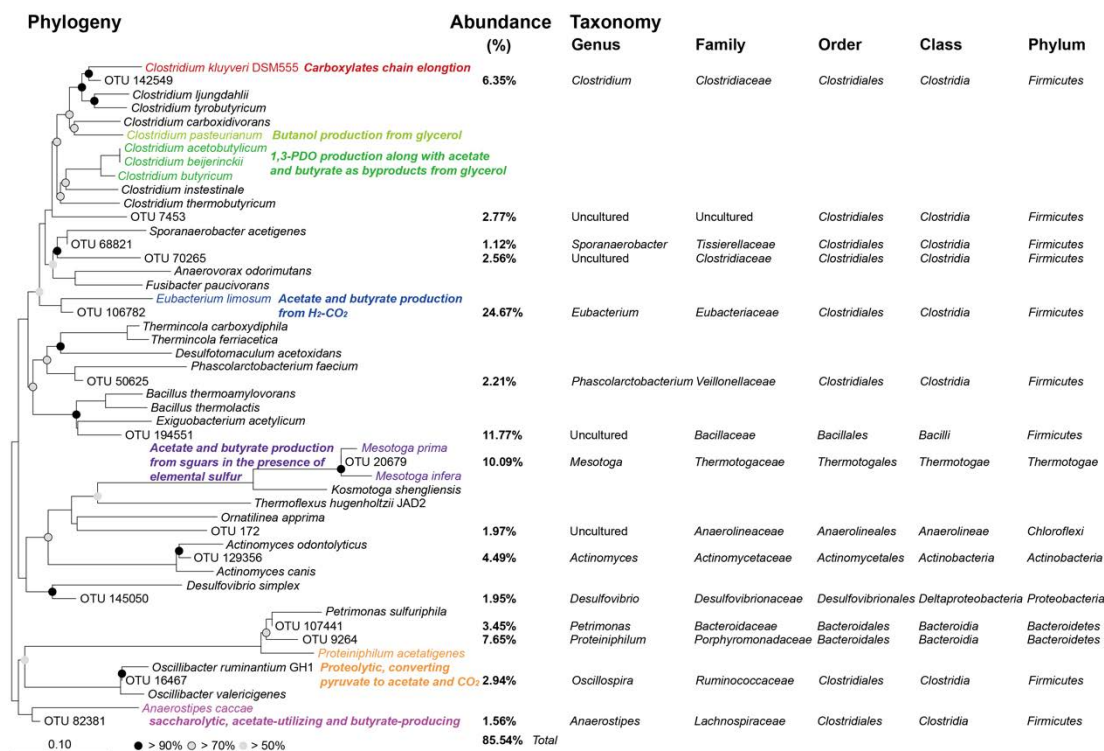


Figure 6.5. Neighbor-joining tree based on 16S rRNA gene sequences determined in stage 6 of semi-continuous fermenter and related reference lineages. 15 most abundant OTUs were selected for analysis and shown with abundance and taxonomy information. The phylogenetic tree (bootstrap 1000: > 90% black node, > 70% gray node with black outline and > 50% gray node) were performed in ARB with SILVA database SSU NR99 as reference.

Comparing the microbial community of stage 3 and stage 6, the glycerol decrease and ethanol addition lead to the decrease of *C. profunda*, *Actinomyces* sp. MD1 and *A. caccae*, and the increase of *Bacillaceae* bacterium mt8 and *C. kluyveri*. The metabolic pathways of these two stages are discussed in detail in the metagenomic analysis part. In contrast to the Case 2 of the batch test, the enrichment of microorganisms in the semi-continuous fermenter selectively excluded facultative pathogens, such as *E. coli* and *K. pneumoniae*, but still accomplished the 1,3-PDO

and caproate co-production with more appropriate metabolic pathways.

6.2.4 Microbial community structure analysis

Thirty-nine enriched samples were characterized for microbial community composition and structural differences. The upper panel in Figure 6.6 displays the distances of the 39 samples based on all OTUs of their communities with a UPGMA algorithm. According to the clustering tree, the 39 enriched cultures formed two groups, one group of fermenter-based semi-continuous fermentation and the other group a batch test in anaerobic bottles together with fresh AD sludge. These results reveal that the sample structure was significantly influenced by the fermentation process. In the batch test group, subgroups are mainly differentiated by substrates. The two seed cultures, fresh AD sludge samples, are close to samples enriched with ethanol as an electron donor, which is probably due to their common relative diverse traits (lower panel). In contrast, the samples enriched with co-electron donors and with glycerol are more similar in structure, with abundant dominant OTUs. These results indicate that the glycerol-utilizing bacteria and their related synergistic bacteria are more dominant than those enriched with ethanol in the mixed culture.

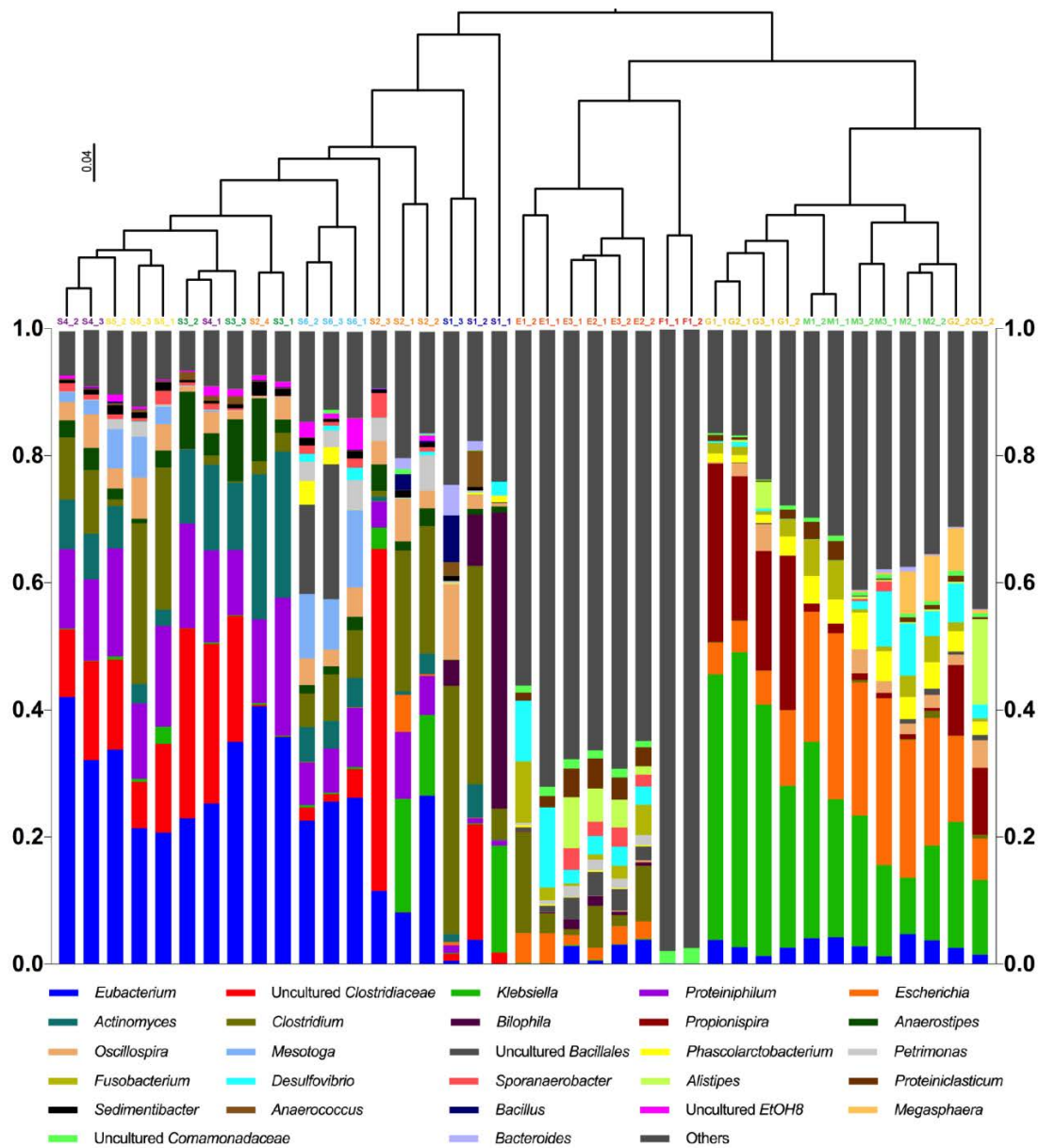


Figure 6.6. Composition of relative abundance of OTUs at genus level in different sludge samples.

Hierarchical clustering of a total of 39 samples was performed based on all OTUs from the microbial communities with a UPGMA algorithm to generate a newick-formatted tree. For sample labels, F represents fresh AD sludge; E is batch test with ethanol as electron donor; G is batch test with glycerol as electron donor; M is batch test with both ethanol and glycerol as electron donors; S stands for semi-continuous fermentation. The numbers represent stage and order (E1_1: stage 1, parallel number 1; S1_1: stage 1, phase 1).

Specifically, the dominant bacteria in the glycerol-enriched culture belong to the genera of *Klebsiella*, *Propionispira*, *Escherichia*, and *Eubacterium*. The two distinguished samples, G2_2 and G3_2, include additional dominant genera of *Megasphaera*, *Desulfovibrio*, and *Alistipes*. As discussed in the previous section, *Klebsiella* and *Escherichia* are responsible for the glycerol dissimilation and 1,3-PDO, ethanol, succinate, and formate (H₂ and CO₂) production. *Eubacterium* then uses H₂ and CO₂ for acetate and butyrate formation. *Propionispira* facilitates glycerol dissimilation to acetate and propionate. In the adjacent culture enriched with co-electron donors, the dominant bacteria are from the genera *Escherichia*, *Klebsiella*, *Phascolarctobacterium*, *Desulfovibrio*, *Eubacterium*, *Fusobacterium*, and *Megasphaera*. In addition to the shared genera, some species of *Phascolarctobacterium* can use succinate for propionate production (Stackebrandt & Osawa, 2015; Watanabe et al., 2012), and the dominance of *Megasphaera* corresponds with caproate production in this culture. The genera of the dominant bacteria in the ethanol-enriched culture are *Clostridium*, *Desulfovibrio*, *Fusobacterium*, *Alistipes*, *Proteiniclasticum*, and *Escherichia*. The dominance of *Clostridium* is responsible for carboxylate chain elongation with ethanol.

Considering the semi-continuous fermentation group, the subgroups are mainly separated by stage with different substrate loadings. The dominant bacteria of the first three stages are the genera of *Eubacterium*, *Clostridium*, *Proteiniphilum*, *Actinomyces*, *Bilophila*, *Klebsiella*, and *Anaerostipes*, whereas those of the last three stages belong to genera of *Eubacterium*, *Proteiniphilum*, *Clostridium*, *Actinomyces*,

Mesotoga, and *Oscillospira*. It is clear that the major dominant genus remained in the system from the stages of single glycerol as an electron donor to the co-electron donor stages. It is apparent that the ethanol addition in the glycerol-enriched culture does not shift the microbial communities significantly and that the ethanol-favorable bacteria grow slowly and are less competitive for space in the co-electron donor condition. *Klebsiella* with function of glycerol to 1,3-PDO only dominated in single electron donor of glycerol. *Mesotoga*, which is capable of fermenting carbohydrates into acetate and butyrate, and *Oscillospira* species, which were found in rumen bacteria with unknown metabolism, were dominant in the stages fed with co-electron donors. (Kamagata, 2015; Mackie et al., 2003)

As illustrated in Figure 6.7, the microbial structure difference of the 39 samples was further analyzed with PCoA. Both weighted (Figure 6.7a) and unweighted (Figure 6.7b) UniFrac distances were performed to reveal the differences in terms of OTUs with and without abundance information. First, the seed cultures (F1_1 and F1_2) were apparently separated from the batch-based ethanol-enriched culture by weighted but not unweighted PCoA, which suggests that the difference lies the OTU abundance. Similar results were found between batch-based glycerol-enriched and co-electron donor-enriched cultures. The distances among the fermenter-based samples were similar with the two analyses. However, the samples of stage 2 were even more differentiated from the others in unweighted analysis, which implies that this difference lies not on abundant OTUs.

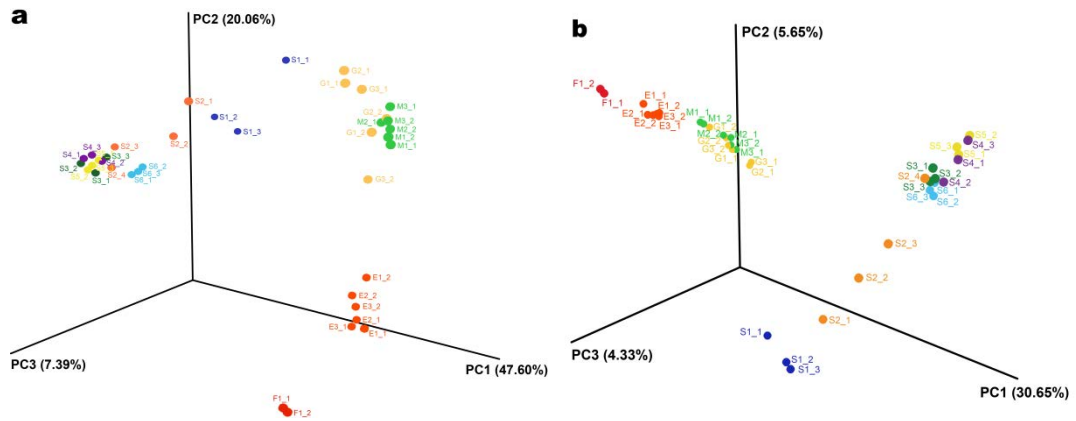


Figure 6.7. UniFrac emperor PCoA (a. weighted, b. unweighted) of a total of 39 samples based on all OTUs from the microbial communities. For sample labels, F represents fresh AD sludge; E is batch test with ethanol as electron donor; G is batch test with glycerol as electron donor; M is batch test with both ethanol and glycerol as electron donors; S stands for semi-continuous fermentation. The numbers represent stage and order (E1_1: stage 1, parallel number 1; S1_1: stage 1, phase 1).

To investigate the influence of environmental variables (substrate difference) on sample structure, especially the dominant microorganisms, canonical correspondence analysis (CCA) was performed with four constrained axes accounting for 71.45% of the explained variance. The ordination biplot of the first two axes accounting for 42.10% of the explained variance are shown in Figure 6.8.

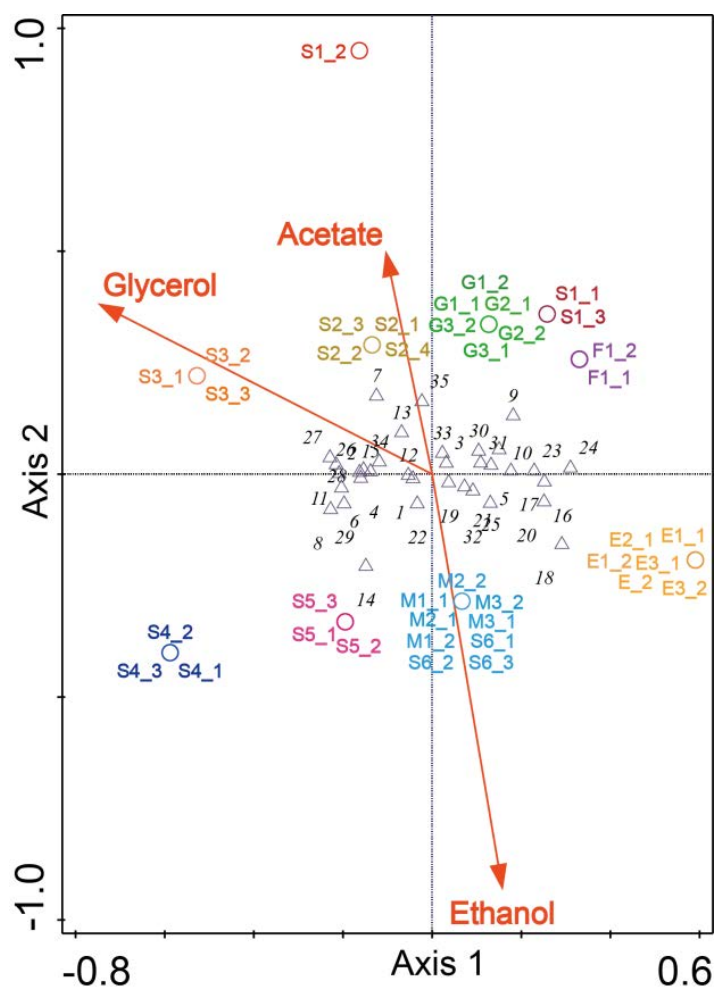


Figure 6.8. CCA of microbial community structure with fermentation operational conditions.

Arrows represent the three substrate-based environmental variables, glycerol, ethanol, and acetate, and indicate the direction and magnitude of variables associated with the microbial community structure. The 39 samples, including both batch and semi-continuous fermentation, are demonstrated by circles. Triangles with numbers stand for the 35 most-abundant OTUs of all 39 samples. Axes 1 and 2 account for 36.07% and 6.03% of the variation, respectively.

CCA revealed that the environmental variable ethanol was highly positively correlated to axis 2, whereas acetate was highly negatively correlated to this axis.

The correlation of glycerol towards axis 2 was not apparent, but it was negatively

correlated to axis 1. We now consider the sample position and assembly of the ethanol-influenced batch-based samples enriched with ethanol and co-electron donors and the second half three stages of the fermenter-based semi-continuous fermentation samples. The batch-based samples enriched with co-electron donors and the semi-continuous samples of stage 6 are assembled together. These results are consistent with the fermentation conditions and their corresponding performance. Acetate slightly affected the batched-based samples enriched with glycerol and the first half three stages of the fermenter-based semi-continuous fermentation samples. In addition, the effect of glycerol increased from stage 1 to stage 3 but then it decreased from stage 4 to stage 6 of the fermenter-based semi-continuous fermentation samples. These results indicate the sample structure was mostly affected by glycerol in stage 3, but the effect gradually decreased after ethanol addition. However, the glycerol influence on the batch-based samples enriched with glycerol and co-electron donors was insignificant in these two constrained axes.

Table 6.2. Label and taxonomic information of 35 most-abundant OTUs in Figure 6.7.

Number	Taxonomic information
1	<i>Eubacterium limosum</i>
2	<i>Crassaminicella profunda</i> strain Ra1766H
3	<i>Klebsiella pneumoniae</i>
4	<i>Proteiniphilum acetatigenes</i>
5	<i>Escherichia coli</i>
6	<i>Actinomyces</i> sp MD1
7	<i>Clostridium butyricum</i>
8	<i>Clostridium intestinale</i>
9	<i>Bilophila wadsworthia</i>
10	<i>Propionispira arcuata</i> strain WK011
11	<i>Anaerostipes caccae</i>

12	Uncultured <i>Oscillospira</i> sp
13	<i>Clostridium</i> sp LZLJ009
14	<i>Mesotoga prima</i>
15	Uncultured <i>Oscillospira</i> bacterium
16	<i>Bacillaceae</i> bacterium mt8
17	<i>Phascolarctobacterium faecium</i>
18	<i>Clostridium kluyveri</i>
19	<i>Petrimonas sulfuriphila</i>
20	<i>Fusobacterium varium</i> strain JCM 6320
21	Uncultured <i>Desulfovibrio</i> sp clone ADSV51
22	<i>Sporanaerobacter acetigenes</i> strain DSM 13106
23	Uncultured <i>Bacteroidetes</i> bacterium
24	<i>Desulfovibrio vulgaris</i> strain Hildenborough
25	<i>Proteiniclasticum</i> sp N2
26	Uncultured <i>Sedimentibacter</i> sp
27	Uncultured <i>Anaerococcus</i> sp
28	<i>Bacillaceae</i> bacterium mt6
29	Uncultured <i>Clostridiales</i> bacterium
30	Uncultured <i>Clostridium</i> sp clone 5926
31	Uncultured <i>Brachymonas</i> sp clone
32	<i>Megasphaera elsdenii</i>
33	<i>Clostridium propionicum</i> DSM 1682
34	Uncultured <i>Actinomyces</i> bacterium
35	<i>Bacteroides uniformis</i>

The CCA of environmental variables with the 35 most-abundant OTUs disclosed significant correlations for numerous taxonomic groups (Table 6.2). Specifically, OTUs of number 14 and 18 were identified as *M. prima* and *C. kluyveri*, respectively. The high correlation of *C. kluyveri* towards ethanol proved that the carboxylate chain elongation with ethanol was conducted by *C. kluyveri*. As to *M. prima*, which was dominant in the second half three stages of the semi-continuous fermentation, the high correlation towards ethanol indicated that it was involved in the synergistic network with ethanol fermentation bacteria. However, Hania revealed that ethanol

did not support the growth of a novel *M. prima* species (*Mesotoga* strain PhosAc3) (Ben Hania et al., 2015). The arrow length of acetate is relatively short, which implies that the influence of acetate on these microorganisms is slight. OTUs of numbers 7, 35, and 9, which are mildly correlated to acetate, were identified as *C. butyricum*, *Bacteroides uniformis*, and *Bilophila wadsworthia*. Acetate addition increases the biomass of *C. butyricum* and promotes butyrate formation from glycerol (Colin et al., 2001), whereas *B. uniformis* and *B. wadsworthia* are acetogenic bacteria (Eggerth & Gagnon, 1933; Laue et al., 1997). OTUs of number 27, 26, 7, and 11 were significantly correlated to glycerol. The first two OTUs were uncultured bacteria in the genera of *Anaerococcus* and *Sedimentibacter*. The other two OTUs were identified as *C. butyricum* and *A. caccae*. In addition to *C. butyricum*, the other three OTUs are not directly involved in glycerol dissimilation, but they are often found in mixed cultures in which intermediates of glycerol fermentation are utilized (Breitenstein et al., 2002; Li et al., 2013; Schwiertz et al., 2002).

6.2.5 Genome reconstruction and metabolic pathways characterization

The high-quality PE reads of two samples from the third phase of stages 3 and 6 were collected for shotgun metagenomic sequencing and assembled through *de novo* assembly, resulting in 24,150 and 30,114 contigs with lengths ranging from 1000 to 404,416 bp (N50: 4034 bp) and 1000 to 647,900 bp (N50: 4320 bp), respectively. Seventeen (17) and 21 genome bins with high completeness were recovered from the contigs, as shown in Table 6.3.

Table 6.3. High-quality recovered genome bins.

Bin name	Completeness	Genome size	GC content
S3_Bin008.fasta	100.00%	3887005	68.1
S3_Bin011.fasta	100.00%	3628321	37.7
S3_Bin003.fasta	97.50%	3539365	44.2
S3_Bin004.fasta	97.50%	2836163	41.4
S3_Bin006.fasta	97.50%	2796871	64.4
S3_Bin013.fasta	97.50%	3941282	43.9
S3_Bin014.fasta	97.50%	3251808	67
S3_Bin016.fasta	97.50%	4427423	63.7
S3_Bin018.fasta	97.50%	4341524	52.9
S3_Bin019.fasta	97.50%	1251484	33.3
S3_Bin020.fasta	97.50%	2406510	49.8
S3_Bin001.fasta	95.00%	4115771	47.9
S3_Bin021.fasta	95.00%	2778211	65.7
S3_Bin012.fasta	90.00%	2774731	55.7
S3_Bin002.fasta	87.50%	2923495	70.1
S3_Bin009.fasta	87.50%	4000309	56.6
S3_Bin015.fasta	87.50%	3491606	66.1
S6_Bin002.fasta	100.00%	3121049	65.5
S6_Bin003.fasta	100.00%	4570359	47.2
S6_Bin004.fasta	100.00%	3077359	35.8
S6_Bin007.fasta	100.00%	4967574	63.9
S6_Bin012.fasta	100.00%	3978715	31.2
S6_Bin015.fasta	100.00%	2150534	44.5
S6_Bin017.fasta	100.00%	4873951	36.7
S6_Bin018.fasta	100.00%	3378214	57.6
S6_Bin001.fasta	97.50%	2918299	69.9
S6_Bin005.fasta	97.50%	2408517	41.8
S6_Bin008.fasta	97.50%	3712876	55.3
S6_Bin010.fasta	97.50%	4762934	43.4
S6_Bin011.fasta	97.50%	2872656	64.6
S6_Bin013.fasta	97.50%	3263496	44.4
S6_Bin020.fasta	97.50%	2874281	55.4
S6_Bin025.fasta	97.50%	2421834	49.7
S6_Bin016.fasta	95.00%	2457566	63.4
S6_Bin019.fasta	95.00%	2817586	66.5
S6_Bin021.fasta	95.00%	2935508	46.6
S6_Bin023.fasta	95.00%	3449208	40.7
S6_Bin006.fasta	87.50%	2355869	45.3

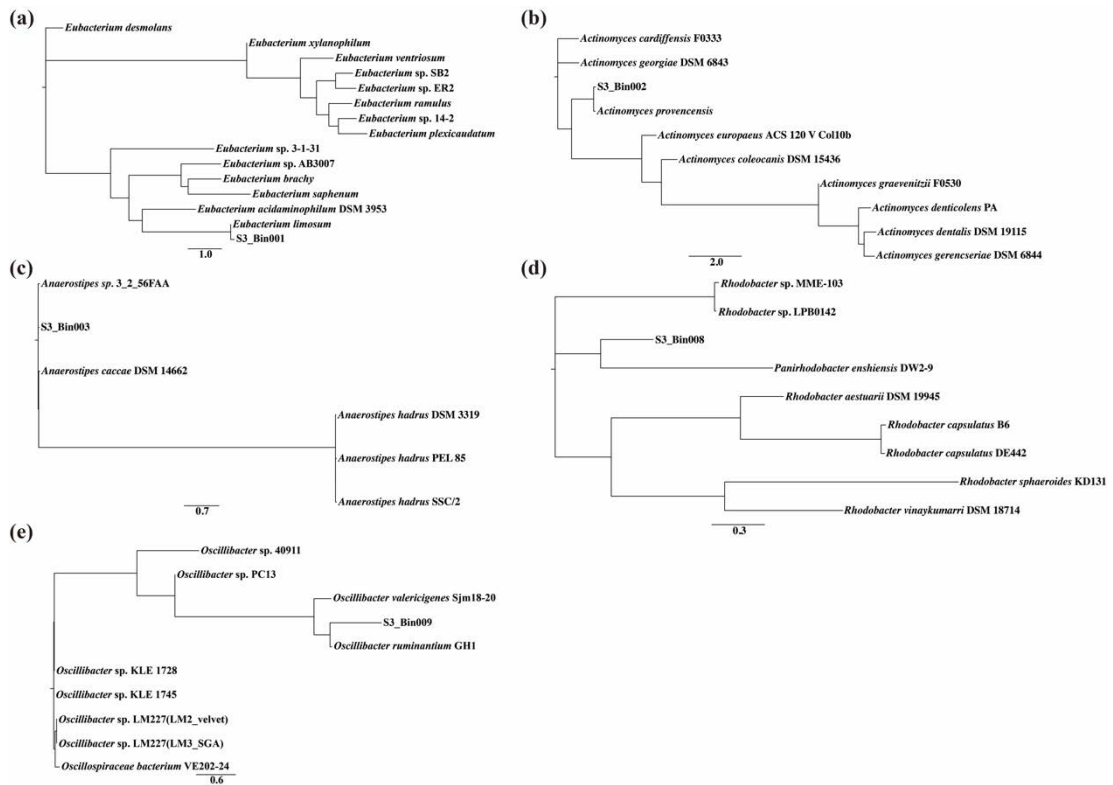


Figure 6.9. Phylogenetic tree of genome bins in stage 3 using PhyloPhlAn.

The genome bins, which were phylogenetically identified by genomic comparison using PhyloPhlAn, showed that S3_Bin 001, S3_Bin 002, S3_Bin003 S3_Bin008, and S3_Bin009 were closely related to the draft genomes of *E. limosum*, *Actinomyces provencensis*, *A. caccae*, *Paenirhodobacter enshiensis*, and *Oscillibacter ruminantium* in stage 3 (Figure 6.9), whereas S6_Bin001, S6_Bin003, S6_Bin004, S6_Bin006, S6_Bin0012, and S6_Bin0013 were closely related to the draft genomes of *A. provencensis*, *E. limosum*, *Massilibacterium senegalense* (*Bacillaceae bacterium* mt8), *Mesotoga infera*, *C. kluyveri*, and *A. caccae* in stage 6 (Figure 6.10). In addition, S3_Bin004, S3_Bin013, S6_Bin005, and S6_Bin010 were identified to be *Bacteroidia bacteria* (Figure 6.11), among which S3_Bin013 and S6_Bin010 are closely related to *P. acetatigenes* and *Bacteroidia bacterium* 43-41, respectively. These recovered genome bins are highly consistent with the abundant

OTUs of the 16S rRNA gene analysis.

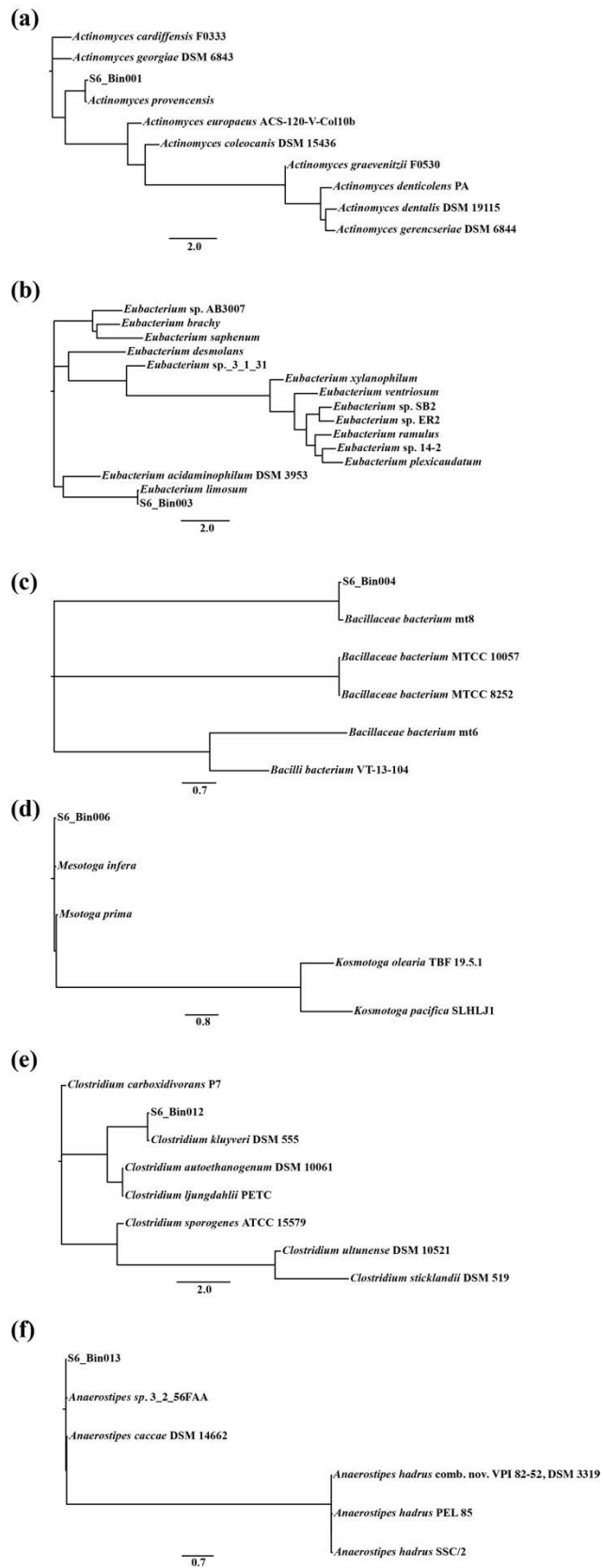


Figure 6.10. Phylogenetic tree of genome bins in stage 6 using PhyloPhlAn.

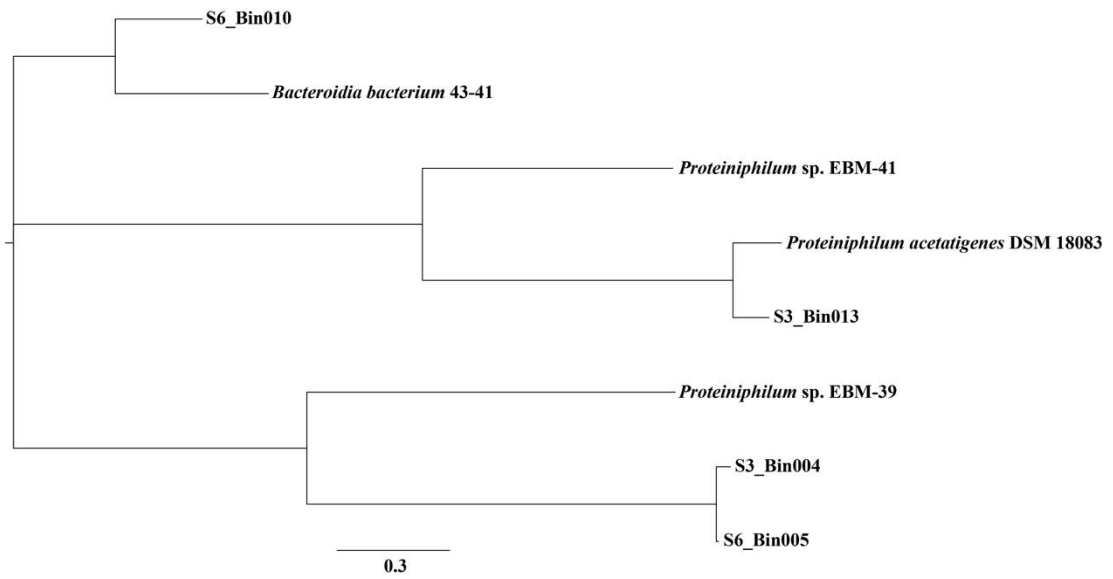


Figure 6.11. Phylogenetic tree of genome bins closely related to *Bacteroidia* bacteria using PhyloPhlAn.

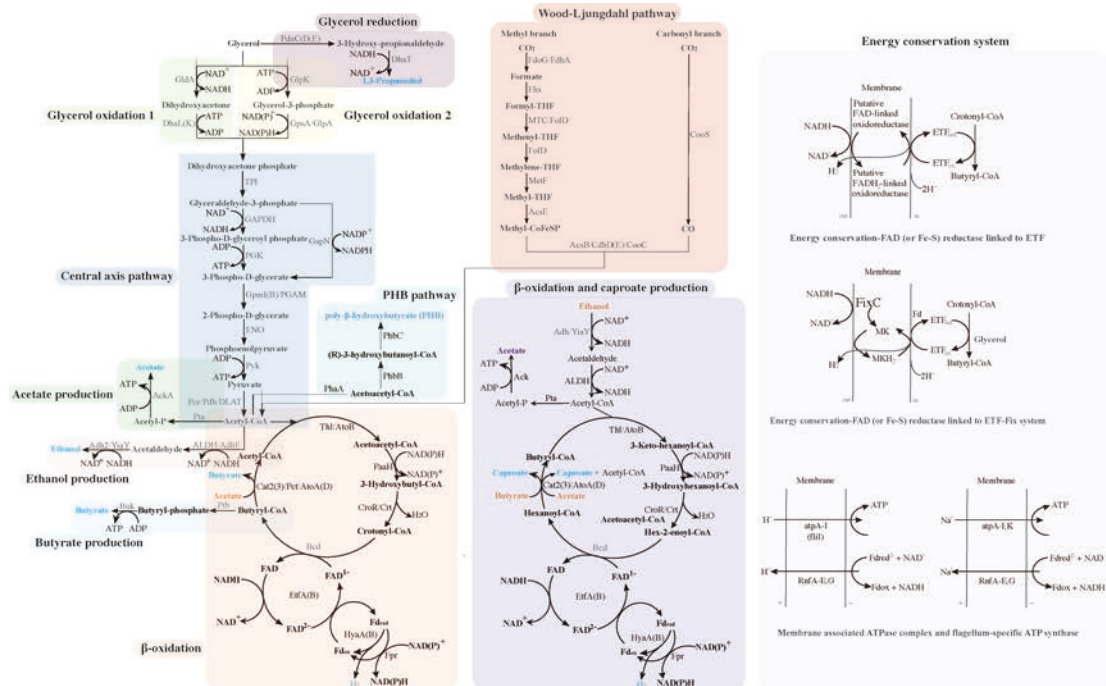


Figure 6.12. Annotated metabolic pathways of glycerol fermentation and carboxylate chain elongation in the system.

The gene content of the reconstructed highly abundant genome bins was annotated,

thereby illuminating the potential functional properties of the microbial species. Figure 6.12 and *Appendix V* Table illustrate the annotated glycerol fermentation and carboxylate chain elongation pathways. There are two pathways for glycerol oxidation. One starts with dehydrogenation catalyzed by glycerol dehydrogenase (GldA), which is followed by phosphorylation catalyzed by dihydroxyacetone kinase [DhaL(K)], and the other starts with phosphorylation catalyzed by glycerol kinase (GlpK), which is followed by dehydrogenation catalyzed by glycerol-3-phosphate dehydrogenase (GlpA) or glycerol-3-phosphate dehydrogenase [NAD(P)⁺] (GpsA) (Lin, 1976). Both pathways result in dihydroxyacetone phosphate (DHA-P) production. Different bacterial species are equipped with different glycerol oxidation pathways. For example, *C. butyricum* exclusively uses the former (Gonzalez-Pajuelo et al., 2006; Raynaud et al., 2011), whereas *E. coli* has been described to use glycerol through the latter (Richey & Lin, 1972; Voegelé et al., 1993). *K. pneumoniae* has been reported to be equipped with both pathways, of which the former is normally inducible anaerobically and the latter is responsible for glycerol oxidation aerobically (Forage & Foster, 1982; Forage & Lin, 1982; Jin et al., 1982). DHA-P is then converted to glyceraldehyde-3-phosphate (glyceraldehyde-3-P) catalyzed by triosephosphate isomerase (TPI), which is followed by a glycolytic pathway resulting in pyruvate formation via the intermediates of 3-phospho-D-glycerate, 2-phospho-D-glycerate, and phosphoenolpyruvate. The involved enzymes include glyceraldehyde-3-phosphate dehydrogenase (NADP⁺) (GapN), glyceraldehyde 3-phosphate dehydrogenase (GAPDH), phosphoglycerate kinase (PGK), phosphoglycerate mutase (GpmI(B), PGAM), enolase (ENO), and

pyruvate kinase (Pyk). Pyruvate oxidation to acetyl-CoA is catalyzed by pyruvate ferredoxin oxidoreductase (Por) or pyruvate dehydrogenase (Pdh). The acetyl-CoA formation then leads to different downstream products. Glycerol reduction to 1,3-PDO begins with the transformation of glycerol to 3-hydroxy-propionaldehyde, which is catalyzed by a coenzyme B12-dependent propanediol dehydratase [PduC(D,E)]. This transformation could also be catalyzed by a coenzyme B12-dependent glycerol dehydratase such as in *K. pneumoniae* (Forage & Foster, 1982) and *C. butyricum* (Raynaud et al., 2003), although it was not found in the recovered genomes bins of our system. The intermediate, 3-hydroxy-propionaldehyde, is further transformed to 1,3-PDO catalyzed by 1,3-PDO dehydrogenase (DhaT).

Acetate formation from acetyl-CoA via acetyl-phosphate is catalyzed by putative phosphotransacetylase (Pta) and acetate kinase (AckA). Ethanol production from acetyl-CoA via acetaldehyde is catalyzed by acetaldehyde dehydrogenase (AdhE) and alcohol dehydrogenase (Adh2). The other two functional enzymes, aldehyde dehydrogenase (NAD⁺) and alcohol dehydrogenase (YiaY), acting on acetyl-CoA to ethanol, were also recovered in the genomes bins of our system. The ethanol production pathway is reversible, which could also have worked on ethanol oxidation in our system. Two acetyl-CoAs form acetoacetyl-CoA catalyzed by acetoacetyl-CoA thiolase (Thl/AtoB). Butyryl-CoA formation then proceeds from the acetoacetyl-CoA via 3-hydroxybutyryl-CoA and crotonyl-CoA through a reverse β -oxidation pathway. This process involves three enzymes, 3-hydroxybutyryl-CoA

dehydrogenase (PaaH), 3-hydroxybutyryl-CoA dehydratase (CroR/Crt), and an NAD-dependent butyryl-CoA dehydrogenase/electron transfer flavoprotein (ETF) complex (Bcd/EtfAB). These CDS are also capable of forming caproyl-CoA (hexanoyl-CoA). The formed butyryl-CoA reacting with acetate to form butyrate in a substitution reaction is possibly catalyzed by 4-hydroxybutyrate CoA-transferase (Cat2), butyryl CoA:acetate CoA transferase (YdiF/Cat3), propionate CoA-transferase (Pct), and acetate CoA/acetoacetate CoA-transferase subunits [AtoA(D)]. Among these CoA-transferases, Pct is a general CoA-transferase that can mediate the exchange of acetate/butyryl-CoA and butyrate/acetyl-CoA (Prabhu et al., 2012). Caproate could be produced from caproyl-CoA substituted with butyrate/acetate possibly catalyzed by Cat2, Cat3, and AtoA(D). In addition, an alternative pathway for butyrate formation from butyryl-CoA via butyryl-phosphate is catalyzed by phosphate butyryltransferase (Ptb) and butyrate kinase (Buk). Table 6.4 summarizes the ownership of the above-mentioned glycerol fermentation and carboxylate chain elongation pathways for some high-quality recovered genome bins.

Table 6.4. Glycerol fermentation and carboxylate chain elongation pathways in some high-quality recovered genome bins.

Sample ID	Closely related species	Glycerol oxidation 1	Glycerol oxidation 2	DHA-P to glyceraldehyde-3-P	Glycolytic pathway	Pyruvate to acetyl-CoA	Acetate production	Butyrate production	Caproate production	Glycerol reduction to 1,3-PDO	Ethanol production/oxidation	PHB production/utilization
S3_Bin001	<i>Eubacterium limosum</i>	+	+	+	+	+	+	+	-	+	+	-
S3_Bin002	<i>Actinomyces provencensis</i>	-	+	+	-	+	+	-	-	-	+	-
S3_Bin003	<i>Anaerostipes caccae</i>	+	+	+	+	+	+	+	+	-	+	-
S3_Bin008	<i>Paenirhodobacter enshiensis</i>	-	+	+	+	+	+	+	+	-	+	-
S3_Bin009	<i>Oscillibacter ruminantium</i>	-	+	+	+	+	+	+	+	-	-	-
S3_Bin011	<i>Clostridiales</i> bacterium	+	+	+	+	+	-	+	+	-	+	-
S3_Bin013	<i>Proteiniphilum acetatigenes</i>	-	-	-	-	+	+	+	-	-	-	-
S6_Bin001	<i>Actinomyces provencensis</i>	-	+	+	+	+	+	-	-	-	+	-
S6_Bin003	<i>Eubacterium limosum</i>	+	+	+	+	+	+	+	-	+	+	-
S6_Bin004	<i>Massilibacterium senegalense</i>	-	+	+	+	+	+	+	-	-	+	+
S6_Bin006	<i>Mesotoga infera</i>	-	+	+	+	+	+	-	-	-	-	-
S6_Bin010	<i>Bacteroidia</i> bacterium 43-41	-	-	-	-	+	+	+	+	-	-	-
S6_Bin012	<i>Clostridium kluyveri</i>	-	-	-	-	-	+	+	+	-	+	-
S6_Bin013	<i>Anaerostipes caccae</i>	+	+	+	+	+	+	+	+	-	+	-

Gene annotation of the recovered genome bin S3_Bin001 (*E. limosum*) and S6_Bin003 (*E. limosum*) both showed that it is possible to produce acetate, butyrate, and ethanol through glycerol oxidation and to generate 1,3-PDO by glycerol reduction. Wood–Ljungdahl pathway is annotated in these two recovered genome bins. Previous researchers also identified *E. limosum* to be an anaerobic acetogen that utilizes H₂/CO₂, CO, and a variety of organic substrates for acetate, butyrate, and ethanol production (Kelly et al., 2016; Lindley et al., 1987; Roh et al., 2011). Lindley et al. proposed that butyrate production from butyryl-CoA is due to the action of phosphate acyltransferase and butyrate kinase (Lindley et al., 1987), whereas Kelly et al. found that butyrate formation is catalyzed by Cat3 in the absence of *Buk* based on their isolated *E. limosum* SA11 genome from the rumen of a New Zealand sheep (Kelly et al., 2016). S3_Bin001 does not have the *Buk* gene, and the CoA transferase was identified to be Pct. A previous study indicated that caproate production might be possible in *E. limosum*, as evidenced by physiological observation that caproate was produced from methanol dissimilatory flux with a high butyrate supplement by Lindley et al. and the gene information (Cat3) of *E. limosum* SA11 by Kelly et al. However, we could not say that caproate production is related to S3_Bin001 in our system due to the absence of Cat3 in the recovered genome bin. To the best of our knowledge, the evidence that *E. limosum* produces 1,3-PDO from glycerol is reported here for the first time. The reference close-related genomes, *E. limosum* KIST612, *E. limosum* 8486cho, *E. limosum* ATCC8486 do not include propanediol dehydratase and 1,3-PDO dehydrogenase genes for 1,3-PDO production with glycerol reduction. *E. limosum* SA11 includes propanediol dehydratase gene but no

1,3-PDO dehydrogenase gene. *E. limosum* 32-A2 is capable of producing 1,3-PDO with genes of glycerol dehydratase and 1,3-PDO dehydrogenase. *A. provencensis* was a newly isolated facultative anaerobic species from fresh stools of obese French patients (Ndongo et al., 2017), and its metabolic function has not yet been reported. Gene annotation of S3_Bin003 (*A. provencensis*) and S6_Bin001 (*A. provencensis*) illustrates that these two recovered genome bins can oxidize glycerol through a GlpK–GpsA/GlpA pathway and produce acetate and ethanol. According to the 16S rRNA gene sequencing, the abundance of *Actinomyces* bacteria decreased after adding ethanol as one of the substrates. Therefore, *A. provencensis* was more likely to produce ethanol beyond its utilization. In our system. In S3_Bin003, the *ENO* gene in glycolysis was missing; it was, however, found in S6_Bin001. S3_Bin003 and S6_Bin013, which are closely related to *A. caccae*, contain the genes needed to conduct all the pathways given in Table 6.4 except for glycerol reduction. Although Louis and Flint discovered that Cat3 works on the final step of butyrate synthesis other than Buk in *A. caccae* (Louis & Flint, 2009), caproate formation of *A. caccae* was not reported. In S3_Bin003 and S6_Bin013, Cat2, Cat3, Pct, and AtoA(D) were all annotated. S3_Bin008 (*P. enshiensis*) has the genes of glycerol uptake (GlpK–GpsA/GlpA pathway), acetate, butyrate [gene *AtoA(D)*], and ethanol production. Wang et al. investigated the phenotypic characteristics of strain DW2-9^T and showed that *P. enshiensis* strain DW2-9^T could utilize acetate, pyruvate, propionate, fumarate, malate, citrate, succinate, D-glucose, D-fructose, D-xylose, maltose as sole carbon sources, and sodium sulfate, cysteine as electron donors, whereas it could not use glycerol as a sole carbon source (Wang et al., 2014). The gene content of S3_Bin009

(*O. ruminantium*) shows that it is predicted to oxidize glycerol through the GlpK–GpsA pathway and produce acetate and butyrate. The *O. ruminantium* strain GH1 was isolated from the rumen of Korean native cattle and identified to be a strict anaerobe producing butyrate from carbohydrates (Lee et al., 2012; Lee et al., 2013). Because the GlpK–GpsA pathway for glycerol oxidation is anaerobically deficient in some bacteria (Jacobs & VanDemark, 1960), the glycerol uptake by *O. ruminantium* needs further study. In terms of butyrate formation, genes *Pct* and *AtoD* were annotated in S3_Bin009, whereas genes *Ptb* and *Buk* were not. The function of gene *AtoD* working on caproate formation needs further evidence. S3_Bin013 was identified as being closely related to *P. acetatigenes*, containing the genes for pyruvate uptake, acetate production, and butyrate formation (Ptk–Buk pathway). *P. acetatigenes* strains were isolated from the granule sludge of an upflow anaerobic sludge blanket reactor treating brewery wastewater, which is a proteolytic, strictly anaerobic bacteria capable of acetate, NH₃, and CO₂ production (Chen & Dong, 2005). S6_Bin010 is another *Bacteroidia* bacterium (*Bacteroidia* bacterium 43-41) that contains the genes for pyruvate uptake, acetate production, and butyrate formation (Ptk–Buk pathway). In addition, gene *AtoA* was also annotated in S6_Bin010 for butyrate formation. S3_Bin011, which could not be closely related to a specific species, nevertheless is under the order of *Clostridiales*. Its gene annotation shows that glycerol oxidation for butyrate, caproate, and ethanol production is possible. Interestingly, it also includes the genes *PduC(D,E)* for glycerol reduction to 3-hydroxy-propionaldehyde. However, gene *DhaT* was not annotated for 1,3-PDO production. Gene *AckA* for acetate production was missing in

this recovered genome bin. S6_Bin004 (*M. senegalense*) contains genes *GlpK* and *GpsA/GlpA* to oxidize glycerol, genes *Pta* and *AckA* to produce acetate, and genes *ALDH* and *Adh2/YiaY* for ethanol oxidation/production. A phenotypic study of *M. senegalense* strain mt8^T resulted in a negative reaction of it with glycerol incubated at 37 °C in aerobic conditions (Tidjani Alou et al., 2016), and an insignificant abundance of OTUs related to *M. senegalense* were observed in the first three stages, with only glycerol as the electron donor and carbon source in the substrate. Therefore, these results indicate that S6_Bin004 might be responsible for ethanol oxidation to acetate and H₂. The gene content of S6_Bin006 shows that it is possible to oxidize glycerol through the GlpK–GlpA pathway and produce acetate. *Mesotoga infera* Strain VNs100^T and *Mesotoga prima* strain PhosAc3 were reported to only utilize simple sugars and organic acids in the presence of elemental sulfur as a terminal electron acceptor for acetate, CO₂, and sulfide production (Ben Hania et al., 2013), whereas *Mesotoga prima* strain MesG1.Ag.4.2^T ferments sugars for acetate, butyrate, isobutyrate, isovalerate, and e-methyl-butyrate production (Ben Hania et al., 2015). Therefore, the growth of S6_Bin006 in our system is probably related to the element sulfur, and it contributes to glycerol oxidation for acetate CO₂ production in the system. The annotation results of S6_Bin010 shows that it is unable to use either glycerol or ethanol; however, pyruvate uptake for acetate and butyrate formation is possible. The gene annotation results of S6_Bin012 are consistent with the well-known pathway of *C. kluyveri*, which uses ethanol and acetate to produce butyrate and caproate. In S6_Bin012, butyrate and caproate production was catalyzed by Cat2 rather than Cat3, which was previously reported by Seedorf et al. (Seedorf et

al., 2008).

Three modes of energy conservation are generally known, including substrate-level phosphorylation (SLP), electron transport phosphorylation (ETP), and flavin-based electron bifurcation (FBEB) (Buckel & Thauer, 2013; Thauer et al., 1977). SLP is a metabolic reaction coupling with the phosphorylation of ADP with a phosphoryl (PO_3) group, which is directly transferred from another phosphorylated compound, for ATP formation. ETP, in most cases known as chemiosmotic ion gradient-driven phosphorylation, uses the electrochemical potential between redox partners to drive the ATP synthesis by a membrane-bound ATP synthase (Thauer et al., 1977). Specifically, the generation of the transmembrane electrochemical ion gradient (an electrical and/or ion gradient) across the membrane is induced by an electron-transfer reaction of different redox partners (Schuchmann & Muller, 2014). FBEB is initially introduced in *C. kluyveri* including a butyryl-CoA dehydrogenase (Bcd) with two closely located subunits of an electron transferring flavoprotein (EtfAB), forming a complex and binding a flavin cofactor (FMN or FAD) (Li et al., 2008). The mechanism of FBEB peculiarly involves endergonic redox reactions coupled to exergonic redox reactions, where exergonic reduction reactions of one acceptor drives the endergonic reduction of the second acceptor (Schuchmann & Muller, 2014). For example, in clostridial, an endergonic ferredoxin reduction with NADH is coupled to an exergonic crotonyl-CoA reduction with NADH catalyzed by the Bcd/Etf complex (Buckel & Thauer, 2013).

Figure 6.11 demonstrate that SLP energy conservation in glycerol fermentation is catalyzed by PGK and Pyk in a glycolytic pathway, AckA of acetate production, and Buk of butyrate formation. These kinases directly induce a phosphoryl (PO_3) group transformation from a phosphorylated compound to ADP for ATP generation. In addition, the H^+ - and Na^+ -motive forces generated by a redox reaction of ferredoxin with NADH drive the synthesis of ATP (Figure 6.12). This ETP energy conservation is catalyzed by a Rnf complex coupling with a H^+/Na^+ translocating ATPase (Tremblay et al., 2013). FBEB energy conservation occurs in the reversed beta-oxidation pathway of carboxylate chain elongation (Figure 6.12). The reduction of crotonyl-CoA to butyryl-CoA by NADH, which is highly exergonic and irreversible under physiological conditions, conserves energy through the redox reaction of ferredoxin with NAD(P)^+ that is further catalyzed by an Rnf complex (Herrmann et al., 2008). In addition, we found two additional FBEB membrane-associated energy conservation systems: ETF-linked iron-sulfur binding reductase and ETF dehydrogenase (Figure 6.12). These membrane-bound energy conservation systems consume protons while protons are generated along with ATP formation catalyzed by another membrane-associated enzyme, ATPase complex, and a flagellum-specific ATP synthase, FliI. The surplus Fd_{red} could be oxidized with H_2 production catalyzed by a periplasmic hydrogenase subunit and cytoplasmic iron-only hydrogenases.

Table 6.5 summarizes the energy conservation modules of the recovered genome bins.

E. limosum (S3_Bin001 and S6_Bin003), *A. caccae* (S3_Bin003 and S6_Bin013), *P.*

acetatigenes (S3_Bin013), *M. senegalense* (S6_Bin004), and *Bacteroidia bacterium* 43-41 (S6_Bin010), hold the Bcd/Etf complex for energy conservation, which is similar to *C. kluyveri* (S6_Bin012). *E. limosum* (S3_Bin001 and S6_Bin003), *A. caccae* (S3_Bin003 and S6_Bin013), and *C. kluyveri* (S6_Bin012) also include FAD (or Fe-S) reductase linked to the ETF system for energy conservation. *C. kluyveri* (S6_Bin012) particularly contains FAD (or Fe-S) reductase linked to the ETF-Fix system. Most of the recovered genome bins conserved energy through ETP module. As shown in Table 6.5, Rnf coupling with V/A-type H⁺/Na⁺-transporting ATPase was found in *E. limosum* (S3_Bin001 and S6_Bin003), *A. caccae* (S3_Bin003 and S6_Bin013), *P. acetatigenes* (S3_Bin013), and *Bacteroidia bacterium* 43-41 (S6_Bin010), whereas Rnf coupling with F-type H⁺-transporting ATPase was included in *A. caccae* (S3_Bin003 and S6_Bin013), *O. ruminantium* (S3_Bin009), *Clostridiales bacterium* (S3_Bin011), *Bacteroidia bacterium* 43-41 (S6_Bin010), and *C. kluyveri* (S6_Bin012).

Table 6.5. Energy conservation modes (excluding substrate-level phosphorylation) of recovered genome bins.

Bin name	Electron Transport Phosphorylation (ETP)	Flavin-based Electron Bifurcation (FBEB)
S3_Bin001	Rnf coupling with V/A-type H ⁺ /Na ⁺ -transporting ATPase	Bcd/Etf complex FAD (or Fe-S) reductase linked to ETF
S3_Bin003	Rnf coupling with V/A-type H ⁺ /Na ⁺ -transporting ATPase Rnf coupling with F-type H ⁺ -transporting ATPase	Bcd/Etf complex FAD (or Fe-S) reductase lined to ETF

S3_Bin008	F-type H ⁺ -transporting ATPase	-
S3_Bin009	Rnf coupling with F-type H ⁺ -transporting ATPase	-
S3_Bin011	Rnf coupling with F-type H ⁺ -transporting ATPase	-
S3_Bin013	Rnf coupling with V/A-type H ⁺ /Na ⁺ -transporting ATPase	Bcd/Etf complex
S6_Bin003	Rnf coupling with V/A-type H ⁺ /Na ⁺ -transporting ATPase	Bcd/Etf complex FAD (or Fe-S) reductase linked to ETF
S6_Bin004	-	Bcd/Etf complex
S6_Bin010	Rnf coupling with V/A-type H ⁺ /Na ⁺ -transporting ATPase Rnf coupling with F-type H ⁺ -transporting ATPase	Bcd/Etf complex
S6_Bin012	Rnf coupling with F-type H ⁺ -transporting ATPase	Bcd/Etf complex FAD (or Fe-S) reductase lined to ETF FAD (or Fe-S) reductase lined to ETF-Fix system
S6_Bin013	Rnf coupling with V/A-type H ⁺ /Na ⁺ -transporting ATPase Rnf coupling with F-type H ⁺ -transporting ATPase	Bcd/Etf complex FAD (or Fe-S) reductase lined to ETF

Syntrophomonas wolfei was reported to produce and utilize poly-β-hydroxyalkanoate (PHA) for intracellular energy regulation in both pure culture and coculture with *Methanospirillum hungatei* (Amos & Mcinerney, 1989). Proteomic analysis of *S. wolfei* revealed that the PHA-associated mechanism is supported by enzymes including PhaR, poly-(3-hydroxyalkanoic acid) synthase, acyl-CoA dehydratase, enoyl-CoA hydratase, acetoacetyl-CoA reductase (Sieber et al., 2015). In the recovered genome bin associated with *M. senegalense* (S6_Bin004), three detected genes are very likely related to PHB production/utilization including an acetyl-CoA

acetyltransferase gene (*atoB/phaA*), a 3-oxoacyl-[acyl-carrier-protein] reductase gene (*phbB*) and a poly-beta-hydroxybutyrate polymerase gene (*phbC*) (Figure 6.12 and Appendix VI Table). These gene-expressed enzymes can catalyze acetotyl-CoA to PHB through acetoacetyl-CoA and (R)-3-hydroxybutanoyl-CoA. It is hypothesized that PHA-associated endogenous energy balance regulation for syntrophic bacteria occurs when the concentrations of H₂ or acetate are too high for the degradation of the growth substrate to be thermodynamically favorable (Mcinerney et al., 1992). This PHB formation and reutilization by *M. senegalense* was further proven by the detection of PHB at 1.94 % cell dry mass (CDM) in phase 3 of Stage 6 whereas it was not detected in the culture without the dominance of *M. senegalense* (i.e. phase 2 of Stage 2) as a reference. It is not clear why PHB was produced rather than generating more butyrate during glycerol fermentation and then utilized during the leisure phase between glycerol fermentation and carboxylates chain elongation, and also why it was produced during the carboxylates chain elongation. One hypothesis is that high accumulated acetate and H₂ need a sink to store temporally and promote the ethanol oxidation to be thermodynamically favorable. *M. senegalense* paired ethanol oxidation, PHB production, and butyrate production to balance electrons. However, there is little experimental evidence yet for this hypothesis. A better understanding of the PHB system involved in such glycerol fermentation and carboxylates chain elongation system will be of importance since this leads to an energy-efficient process for 1,3-PDO and caproate co-production.

The metabolic pathways in difference stages or batch cases are hypothesized. In

stage 3 of semi-continuous fermentation, *E. limosum* converted glycerol to 1,3-PDO, acetate and butyrate, and *A. caccae* facilitate butyrate production from glycerol; In Case 1 of batch test, *K. pneumoniae* dominated and contributed to 1,3-PDO production from glycerol, however, butyrate formation decreased significantly and glycerol oxidizing to some worthless compounds; In Case 2 of batch test, there are two main phases in which *K. pneumoniae* converted glycerol to 1,3-PDO at the beginning together with dominance of *E. coli* which converted glycerol to ethanol and acetate, and a synergistic network of *Desulfovibrio* sp., *F. varium*, *M. elsdenii*, *C. kluyveri* facilitated carboxylates chain elongation with ethanol and acetate; In Case 3 of batch test, a synergistic relationship between *C. kluyveri* and the three co-dominant species, *D. vulgaris*, *F. varium*, and *A. sticklandii* were found to boost the carboxylate chain elongation for caproate production from ethanol and acetate; In stage 4 and 5 of semi-continuous fermentation, *E. limosum* still dominated and converted glycerol to 1,3-PDO, acetate and butyrate. In addition to *A. caccae*, *C. intestinale* also dominated and facilitated butyrate production from glycerol. In stage 6 of semi-continuous fermentation, *E. limosum* converted glycerol to 1,3-PDO, acetate and butyrate. *M. senegalense* oxidized ethanol to acetate and butyrate. *C. kluyveri* accomplished carboxylates chain elongation with ethanol, acetate and butyrate.

6.3 Chapter summary

1,3-PDO and caproate co-production were demonstrated in batch- and semi-continuous scale fermentation that use glycerol, glycerol-ethanol or ethanol as

electron donors. In batch test, glycerol-acetate fermentation resulted in a significant production of 1,3-PDO with an insignificant formation of acetate, butyrate and H₂ (Case 1). *K. pneumoniae* facilitated high 1,3-PDO production from glycerol. Glycerol-ethanol-acetate fermentation produced high amount of 1,3-PDO and butyrate with low amounts of caproate and H₂ generation (Case 2). *K. pneumoniae* and *E. limosum* facilitated high 1,3-PDO production from glycerol while *M. elsdenii* associated with butyrate and low caproate production. Ethanol-acetate fermentation achieved high caproate and H₂ formation with low amount of butyrate production (Case 3), *C. kluyveri* associated with high caproate and low butyrate production. The comparison of Case 2 and Case 3 on caproate production is reflective of an antagonistic effect of glycerol on chain elongation. A big difference on the organism responsible for chain elongation: *M. elsdenii* associated with caproate production was chosen over *C. kluyveri* in Case 2 while *C. kluyveri* was dominant in Case 3. *C. kluyveri* is more efficient in chain elongation for caproate production. In Case 2, glycerol led to high 1,3-PDO production which is toxic to *C. kluyveri*. With the knowledge of batch tests, ethanol addition can technically facilitate chain elongation for caproate production, and an efficient 1,3-PDO and caproate co-production needs (1) a glycerol fermenter that produces less 1,3-PDO by converting more glycerol to ethanol (a less oxidized product than acetate), and/or by generating more H₂ to consume excess reducing power through an alternative route; (2) a lower glycerol loading to reduce 1,3-PDO production to allow for 1,3-PDO-sensitive chain elongation bacteria (i.e. *C. kluyveri*) to grow; (3) a H₂ consumer who supports H₂ formation from glycerol to not waste glycerol-derived energy.

In the semi-continuous glycerol fermentation, caproate production was stimulated with an ethanol addition and a gradual decrease of glycerol loading. The complete consumption of glycerol and ethanol (20 and 10 mM C d⁻¹) resulted in average production rates of 6.38 and 2.95 mM C d⁻¹ for 1,3-PDO and caproate, respectively. The conversion rates were 0.32 mol_{1,3-PDO} mol⁻¹_{glycerol} and 0.10 mol_{caproate} mol⁻¹_{ethanol} (0.30 mol C caproate/mol C ethanol). The microbiomes, *E. limosum*, *C. kluyveri* as well as *M. senegalense* predominated. The concomitant enrichment of *E. limosum* and gradual decrease of the glycerol loading indeed allowed *C. kluyveri* to predominate. *E. limosum* is one of the few organisms capable of converting glycerol to 1,3-PDO, ethanol and H₂ and also oxidizing H₂ to acetate via the Wood–Ljungdahl pathway, whereby efficiently redirecting the energy of H₂ back into chain elongation. *C. kluyveri* uses ethanol and acetate to produce butyrate and caproate. *M. senegalense* encodes for ethanol oxidation for acetate and butyrate production. In contrast to the Case 2 of the batch test, the enrichment of microorganisms in the semi-continuous fermenter selectively excluded facultative pathogens, such as *E. coli* and *K. pneumoniae*, but still accomplished the 1,3-PDO and caproate co-production with more appropriate metabolic pathways.

Three modes of energy conservation, including substrate-level phosphorylation (SLP), electron transport phosphorylation (ETP), and flavin-based electron bifurcation (FBEB), were annotated in both stages of the system. *E. limosum*, *A. caccae*, *P. acetatigenes*, *M. senegalense*, and *Bacteroidia bacterium* 43-41 held the

Bcd/Etf complex for energy conservation, which is similar to *C. kluyveri*. *E. limosum*, *A. caccae*, and *C. kluyveri* also included FAD (or Fe-S) reductase linked to the ETF system for energy conservation. *C. kluyveri* particularly contains FAD (or Fe-S) reductase linked to the ETF–Fix system.

Chapter 7. Co-production of 1,3-PDO and caproate from glycerol with enriched microbial community

7.1 Overview

Co-production of 1,3-PDO and caproate in a semi-continuous fermenter with glycerol-ethanol-acetate stoichiometric ratio of 4:3:1 has been introduced in the previous chapter. The metagenomics of the enriched microbial community reconstructed the pathway of ethanol production from glycerol (i.e. *E. limosum*). Nonetheless, whether the enriched versatile glycerol degrader, *E. limosum*, could convert glycerol-derived energy to ethanol and H₂ in a balance with 1,3-PDO and acetate and redirect the energy of H₂ back into chain elongation needs further evidence. An investigation on electron flux of glycerol fermentation and chain elongation with ethanol self-sufficiency inoculated by the fermenter-enriched microbial community could help answer the question. In addition, this study also investigated whether the ethanol could be further utilized for caproate production through chain elongation within the cultivation matrix. A batch test inoculated with the fermenter-enriched culture and fed with glycerol and acetate with different concentrations were conducted. The co-production of 1,3-PDO and caproate in glycerol–acetate fermentation was achieved with a favorable glycerol/acetate stoichiometric ratio. Significant ethanol production from glycerol oxidation is the main reason for the caproate production enhancement. A dynamic balance of three dominant microbiomes, *E. limosum*, *M. senegalense*, and *C. kluyveri*, could complete the multiple stages co-production process. The physiological performance and dynamic microbial community disclosed a unique combination of metabolic

pathways successfully facilitated the hypothesized conversion.

7.2 Results and discussion

7.2.1 Physiological performance of batch tests

The enriched culture collected from the late period of stage 6 of the semi-continuous fermentation was used as the seed for a new batch test fed with glycerol and acetate. The physiological performance of two cases (Case 4 and Case 5) with different initial substrate concentrations is shown in Figure 7.1. In general, 1,3-PDO was produced in Case 4 (Figure 7.1a) while a co-production of 1,3-PDO and caproate was achieved in Case 5 (Figure 7.1b). For both cases, glycerol fermentation resulted in 1,3-PDO and ethanol formation within 4 days. The difference lies on acetate concentration increased along with glycerol consumption in Case 4 while that decreased and much more ethanol was produced in Case 5. The electrons from glycerol in Case 4 were not capable of producing enough ethanol to be further utilized for caproate production through carboxylates chain elongation. During the ethanol consumption stage, butyrate was produced in Case 4 along with H₂ decrease while caproate and butyrate were generated in Case 5 along with H₂ increase. It indicates that carboxylates chain elongation did not occur in Case 4 because chain elongation is a H₂ formation process.

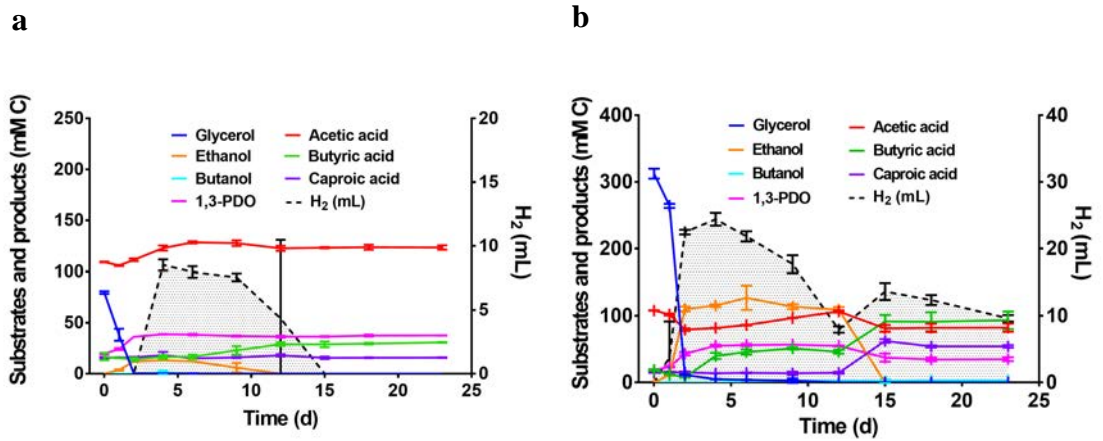


Figure 7.1. Glycerol fermentation with fermenter-enriched culture.

Here we investigated Case 5 in details. Compared to Case 1 (Chapter 6), a significant amount of ethanol was produced in addition to 1,3-PDO along with glycerol consumption (Days 1–4) and a delayed butyrate production was also observed (Days 2–6). With a lag phase of around 12 days, the produced ethanol and the acetate in the system were then used for caproate and butyrate formation. The chain elongation metabolism ceased when ethanol was depleted even though a high amount of butyrate remained in the system. This novel result indicates the importance of ethanol production as an intermediate of glycerol dissimilation before carboxylate chain elongation for caproate production. There are two increases in hydrogen (Days 0–4; Days 12–15) and two decreases (Days 4–12; Days 15–23), and we also divided the whole process into the four phases for analysis. (P1) The first increase correlates to glycerol degradation to ethanol and 1,3-PDO, with delayed accumulation of butyrate. (P2) The first decrease correlates to gradual acetate accumulation. (P3) The second increase correlates with sudden ethanol consumption and production of butyrate and caproate. (P4) The second decrease correlates to a slight increase of

acetate and butyrate.

7.2.2 Microbial community of glycerol fermentation for two value-added chemicals co-production

The mixed culture of three time points was collected for 16S rRNA gene-based analysis in order to identify the microbial community dynamics in Case 5. A 16S rRNA gene-based tree was constructed by neighbor-joining method to decipher the phylogenetic affiliation of the overall 20 most abundant OTUs and their evolutionary relationships to known lineages (Figure 7.2). Together with blastn identification of OTUs, the microbial community of P1–3 of Case 5 is shown in Figure 7.3. Top 10 representative OTUs at three time points are covered 72.04%–89.14% of the total sequences, which is more enriched compared with Case 1–3 (Chapter 6). The microbial community mainly includes *Bacillaceae* bacterium mt8 (*Massilibacterium senegalense*) and *E. limosum* in P1; *Bacillaceae* bacterium mt8 in P2. And *C. kluyveri* increased significantly in P3. How these dynamic microbiomes worked and cooperated to complete the co-production pathways is discussed in the following section.

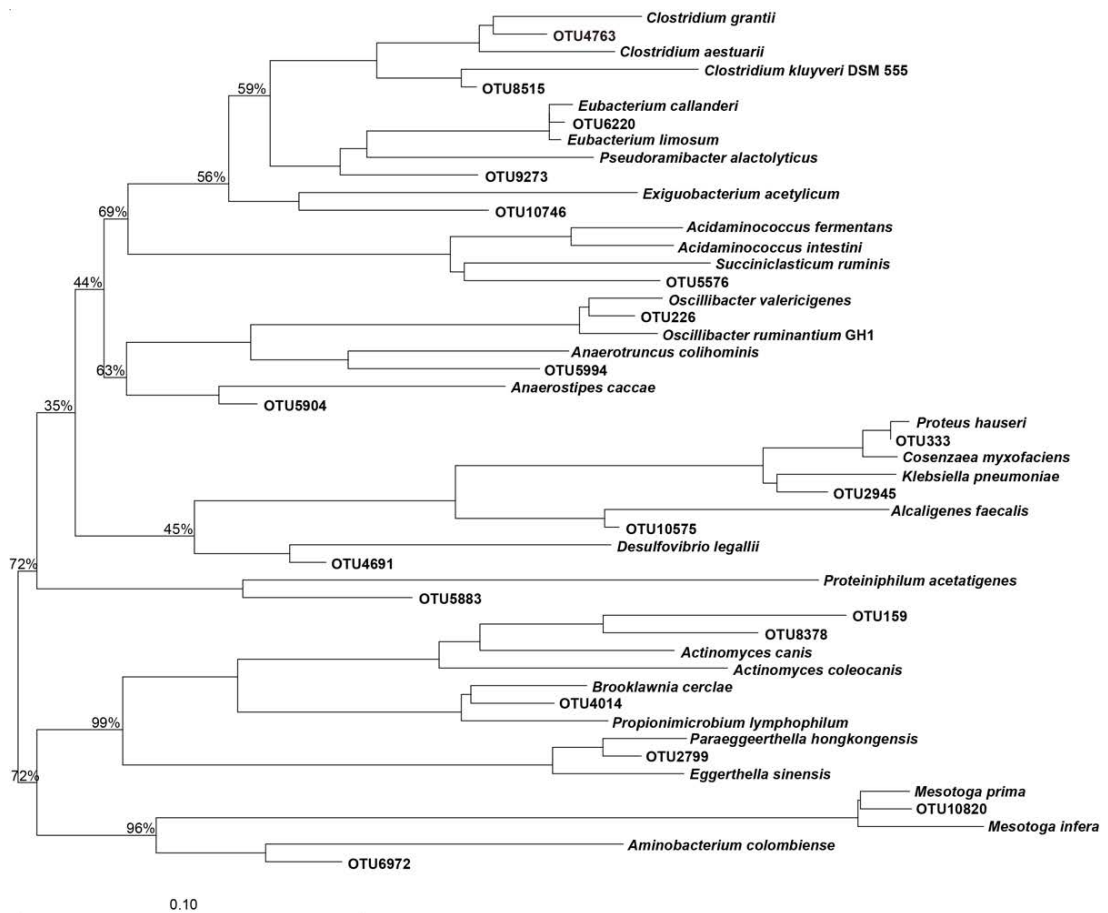


Figure 7.2. Neighbor-joining tree based on 16S rRNA gene sequences and related reference lineages. 20 most abundant OTUs were selected for analysis and shown with average abundance and taxonomy information. The phylogenetic tree was performed in ARB with SILVA database SSU NR99 as reference.

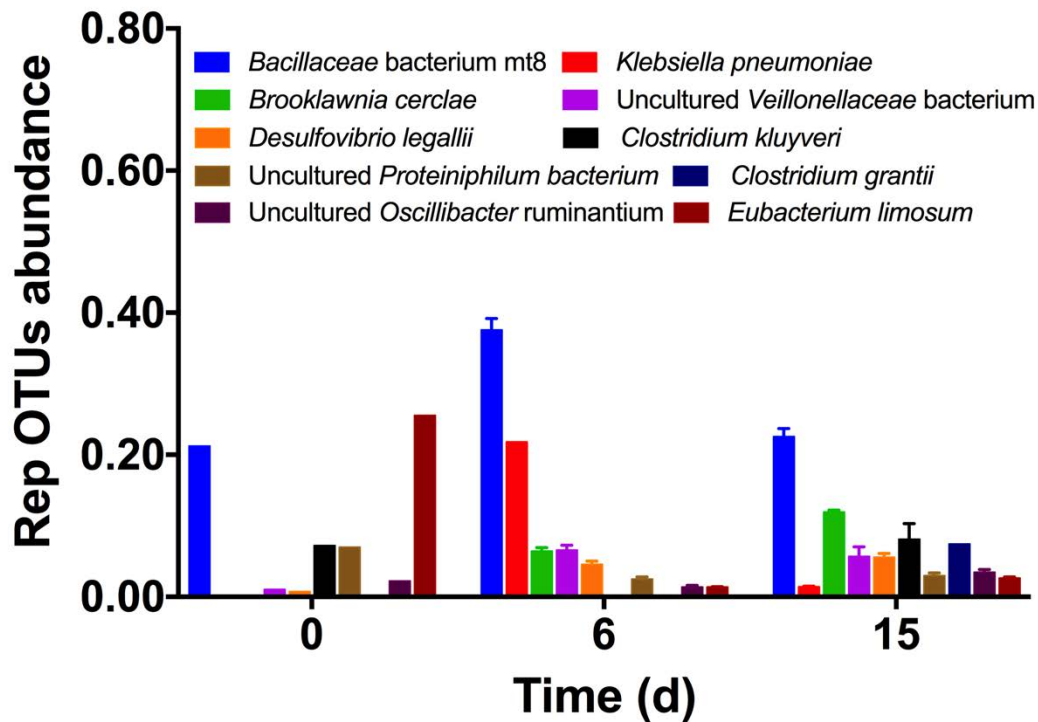


Figure 7.3. Physiologic performance of enriched culture from stage 6 with glycerol in batch.

Corresponding representative OTUs at four time points are covered 72.04%–89.14% of the total sequences.

7.2.3 Electron flow of glycerol fermentation

The electron flow-based biochemical reactions are summarized in Table 7.1. In P1, 1,3-PDO production from glycerol is net reduction (R1), ethanol production from glycerol is a net oxidation (R2), and H₂ production is also a reductive process (R6). Since a slight consumption of acetate and delayed butyrate production occurred, we assume that some acetate was converted to butyrate reductively and the butyrate was temporarily stored in the cells and released slowly into solution (R9). However, these four reactions in total could not balance the electrons and there is a significant amount of reductive reactions not accounted for. Plus, the acetate should be one of

the byproducts in glycerol fermentation but a net acetate consumption in P1 and a gradual accumulation of acetate in P2 were observed, which indicates acetate is probably stored temporarily in some compounds, such as poly- β -hydroxybutyrate (PHB). Glycerol oxidation to acetate and CO₂ (R3), Reduction of CO₂ to acetate (R8), and PHB production (R11) are assumed to balance the electron and acetate in P1 (Table 7.1). In the same phase of Case 1, there is a significant amount of oxidative reactions not accounted for, which leads to a big net electron consumption of the total anticipated reactions. The unanticipated oxidized compounds from glycerol in Case 1 reduced the carbon flow to ethanol, and further inhibited the chain elongation for caproate production. Comparing P1 of Case 1 and 5, glycerol converting to ethanol in Case 5 is probably associated with *Bacillaceae* bacterium mt8 and *E. limosum* which were not detected in Case 1. In P2, ethanol oxidation to acetate (R5), H₂ oxidation (R7), acetate reduction to butyrate (R9) were detected. The electron flow analysis showed that reduction of CO₂ to acetate (R8) and PHB consumption (R12) are probably occurred concurrently to balance the electron flow. It further proves the PHB production and consumption happened in the process. The most dominant bacteria in P2 of Case 5 was *Bacillaceae* bacterium mt8. In P3, chain elongation related reactions occurred, including R5, R6, R9 and R10. Reduction of CO₂ to acetate (R8) and PHB production (R12) are probably occurred concurrently to balance the electron flow. Compared with the same phase of Case 1, the dominance of *Bacillaceae* bacterium mt8 and *C. kluyveri* in Case 5 are believed to make the major difference.

Table 7.1. Electron flow calculation of glycerol fermentation with enriched culture.

	P.1	P.2	P.3	P.4	
R1	Glycerol + 2e ⁻ → 1,3-PDO	12.08	0.00	0.00	0.00
R2	Glycerol → Ethanol + CO ₂ + 2e ⁻	57.61	0.00	0.00	0.00
R3	Glycerol → Acetate + CO ₂ + 6e ⁻	<u>6.00</u>	0.00	0.00	0.00
R4	Acetate + 4e ⁻ → Ethanol	0.00	0.00	0.00	0.00
R5	Ethanol → Acetate + 4e ⁻	0.00	2.96	54.65	0.00
R6	2H ⁺ + 2e ⁻ → H ₂	13.70	0.00	3.20	0.00
R7	H ₂ → 2H ⁺ + 2e ⁻	0.00	9.24	0.00	2.25
R8	2CO ₂ + 8e ⁻ → Acetate	<u>8.00</u>	<u>4.00</u>	<u>9.00</u>	0.55
R9	2Acetate + 4e ⁻ → Butyrate	5.32	1.55	19.38	0.00
R10	Acetate + Butyrate + 4e ⁻ → Caproate	0.00	0.00	7.99	0.00
R11	PHB(N) + 2Acetate + 2e ⁻ → PHB(N+1)	<u>8.25</u>	0.00	<u>15.00</u>	0.00
R12	PHB(N+1) → PHB(N) + 2Acetate + 2e ⁻	0.00	<u>4.00</u>	0.00	0.00
Calculated change based on electron involved reactions					
	Glycerol	-75.69	0.00	0.00	0.00
	1,3-PDO	12.08	0.00	0.00	0.00
	Ethanol	57.61	-2.96	-54.65	0.00
	Acetate	-13.14	11.87	-13.11	0.55
	Butyrate	5.32	1.55	11.39	0.00
	Caproate	0.00	0.00	7.99	0.00
	H ₂	13.70	-9.24	3.20	-2.25
	e ⁻	-2.12	0.16	0.69	0.10
Detected change					
	dGlycerol	-102.47	-1.68	0.00	0.00
	dEthanol	57.61	-2.96	-54.65	0.00
	dAcetate	-13.14	12.38	-12.65	0.55
	dButyrate	5.32	1.55	11.39	0.42
	dH ₂	13.70	-9.24	3.20	-2.25

Assumptions are labeled with underline, Unit: mM

In Case 5 of batch test, *E. limosum* utilized glycerol to produce both 1,3-PDO, acetate and butyrate, and also produce acetate from CO₂ and H₂ via the Wood–Ljungdahl pathway. *M. senegalense* oxidized ethanol to acetate and H₂, which pairs a PHB formation to store acetate and electrons temporally and a delayed butyrate formation from acetate and H₂ in the first phase. During the leisure period between

glycerol fermentation and carboxylates chain elongation, PHB was utilized to generate acetate and release electrons by *M. senegalense*. Meanwhile, some acetate together with H₂ was utilized by *M. senegalense* for butyrate production. In the carboxylates chain elongation phase, *M. senegalense* and *C. kluyveri* worked together for caproate production with ethanol and acetate.

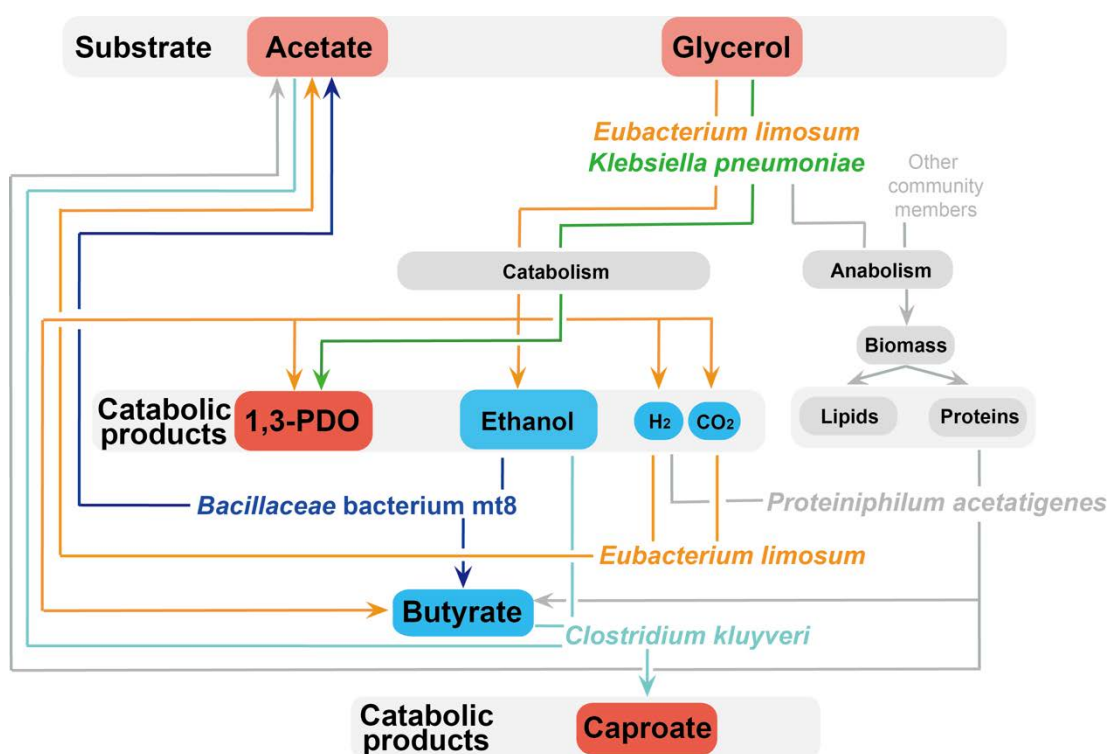


Figure 7.4. Metabolic pathway of caproate and 1,3-PDO co-production from glycerol with enriched mixed culture.

7.3 Chapter summary

The co-production of 1,3-PDO and caproate in glycerol–acetate fermentation was achieved in batch test inoculated with the fermenter-enriched culture and fed with a favorable glycerol/acetate stoichiometric ratio. Significant ethanol production from

glycerol oxidation is the main reason for the caproate production enhancement, which indicates the importance of ethanol production as an intermediate of glycerol dissimilation prior to carboxylate chain elongation for caproate production. The increase of ethanol production rather than other worthless products from glycerol oxidation could balance electron flow in an efficient way with glycerol reduction to 1,3-PDO and further transfer the electrons to caproate. A dynamic balance of three dominant microbiomes, *E. limosum*, *M. senegalense*, and *C. kluyveri*, could complete the multiple stages co-production process. In addition to the metabolism described in Chapter 6, *E. limosum* is proved to utilized glycerol for ethanol production. *M. senegalense* oxidized ethanol to acetate and H₂, which pairs a PHB formation to store acetate and electrons temporally for further utilization in the leisure period between glycerol fermentation and carboxylates chain elongation. In the carboxylates chain elongation phase, *M. senegalense* and *C. kluyveri* worked together for caproate production with ethanol and acetate. A significant ethanol production from glycerol oxidation and a non-inhibiting level of 1,3-PDO production towards *C. kluyveri* are crucial to realize the co-production process.

Chapter 8. Conclusions and Recommendations

8.1 Conclusions

In this thesis, an environmental friendly biological process for the recovery of two value-added chemicals, 1,3-PDO and caproate, from waste(water) was proposed and investigated in depth by examining its thermodynamic feasibility, physiological performance, corresponding microbial communities, and metabolic pathways. Results showed that 1,3-PDO production can be achieved with glycerol reduction, and caproate is able to be produced from SCFAs and ethanol which is generated with glycerol oxidation. A microbial community was successfully enriched to efficiently convert glycerol to 1,3-PDO and utilize the SCFAs and ethanol for caproate production through carboxylate chain elongation. Organisms *E. limosum*, *M. senegalense*, *C. kluyveri* associated with the fermenter utilize a unique combination of metabolic pathways to facilitate the above conversion. The discovery is able to lift up wastewater anaerobic treatment and biodiesel industry downstream technology.

Firstly, it reports thermodynamic and physiological insights for co-production of 1,3-PDO and caproate from glycerol and acetate. Detailed energetic analysis demonstrated that caproate can be elongated from acetate with either ethanol or glycerol, favorable at higher pH range. The optimized conversion rates of mono-caproate and co-production of 1,3-PDO and caproate were achieved at the ethanol/acetate and glycerol/acetate molar ratios of 3 and 4, respectively. A lag phase between 1,3-PDO and caproate production was observed. The sufficient intermediate

ethanol is capable of enhancing caproate formation along with 1,3-PDO. Such a co-production system is pivotal to a synergistic network resulting in the co-existence of *C. butyricum*, *E. coli*, *C. kluyveri* and some other butyrate production bacteria with function of glycerol directly converting to 1,3-PDO and indirectly to caproate.

Secondly, a synergistic network of *D. vulgaris*, *F. varium*, and *A. sticklandii*, which are co-existent with *C. kluyveri* was disclosed to accelerate the carbon and electron flows of carboxylates chain elongation with ethanol so as to shorten the lag phase between 1,3-PDO and caproate production. *D. vulgaris* oxidizes ethanol to acetate and thereby the formed H₂ is used by the two amino acid degrading bacteria for the production of butyrate. The interspecies H₂ transfer takes place, which has been hitherto commonly known for the interaction between syntrophic bacteria and methanogenic archaea. The disclosed metabolic pathways by metagenomic analysis suggested that the synergy network could be technically applied with the potential to upcycle the mixed culture anaerobic processes for value-added chemicals production.

Furthermore, 1,3-PDO and caproate production were demonstrated in batch- and semi-continuous scale fermentation that use glycerol and glycerol-ethanol as electron donors. In batch test, glycerol-acetate fermentation resulted in significant production of 1,3-PDO with low amounts of acetate, butyrate and H₂ formation (Case 1), *K. pneumoniae* facilitated high 1,3-PDO production from glycerol. Glycerol-ethanol-acetate fermentation produced high amount of 1,3-PDO and butyrate with low amounts of caproate and H₂ generation (Case 2). *K. pneumoniae*

and *E. limosum* facilitated high 1,3-PDO production from glycerol while *M. elsdenii* associated with butyrate and low caproate production. Ethanol-acetate fermentation achieved high caproate and H₂ formation with low amount of butyrate production (Case 3), *C. kluyveri* associated with high caproate and low butyrate production. The comparison of Case 2 and Case 3 on caproate production is reflective of an antagonistic effect of glycerol on chain elongation. A big difference on the organism responsible for chain elongation: *M. elsdenii* associated with caproate production was chosen over *C. kluyveri* in Case 2 while *C. kluyveri* was dominant in Case 3. *C. kluyveri* is more efficient in chain elongation for caproate production. In Case 2, glycerol led to high 1,3-PDO production which is toxic to *C. kluyveri*. With the knowledge of batch tests, ethanol addition can technically facilitate chain elongation for caproate production, and an efficient 1,3-PDO and caproate co-production needs (1) a glycerol fermenter that produces less 1,3-PDO by converting more glycerol to ethanol (a less oxidized product than acetate), and/or by generating more H₂ to consume excess reducing power through an alternative route; (2) a lower glycerol loading to reduce 1,3-PDO production to allow for 1,3-PDO-sensitive chain elongation bacteria (i.e. *C. kluyveri*) to grow; (3) a H₂ consumer who supports H₂ formation from glycerol to not waste glycerol-derived energy. In the semi-continuous glycerol fermentation, caproate production was stimulated with an ethanol addition and a gradual decrease of glycerol loading. The complete consumption of glycerol and ethanol (20 and 10 mM C d⁻¹) resulted in average production rates of 6.38 and 2.95 mM C d⁻¹ for 1,3-PDO and caproate, respectively. The conversion rates were 0.32 mol_{1,3-PDO} mol⁻¹_{glycerol} and 0.10 mol_{caproate} mol⁻¹_{ethanol} (0.30 mol C caproate/mol C

ethanol). The microbiomes *E. limosum*, *C. kluyveri* as well as *M. senegalense* predominated. The concomitant enrichment of *E. limosum* and gradually decrease of the glycerol loading indeed allowed *C. kluyveri* to predominate. *E. limosum* is one of the few organisms capable of converting glycerol to 1,3-PDO, ethanol and H₂ and also oxidizing H₂ to acetate via the Wood–Ljungdahl pathway, whereby efficiently redirecting the energy of H₂ back into chain elongation. *C. kluyveri* uses ethanol and acetate to produce butyrate and caproate. *M. senegalense* encodes for ethanol oxidation for acetate and butyrate production. In contrast to the Case 2 of the batch test, the enrichment of microorganisms in the semi-continuous fermenter selectively excluded facultative pathogens, such as *E. coli* and *K. pneumoniae*, but still accomplished the 1,3-PDO and caproate co-production with more appropriate metabolic pathways.

Finally, the co-production of 1,3-PDO and caproate in glycerol–acetate fermentation was achieved in batch test when the seed culture was inoculated with the semi-continuous fermenter in the glycerol–ethanol–acetate fermentation stage. Significant ethanol production from glycerol oxidation is the main reason for the caproate production enhancement, which indicates the importance of ethanol production as an intermediate of glycerol dissimilation prior to carboxylate chain elongation for caproate production. The increase of ethanol production rather than other worthless products from glycerol oxidation could balance electron flow in an efficient way with glycerol reduction to 1,3-PDO and further transfer the electrons to caproate. A dynamic balance of three dominant microbiomes, *E. limosum*, *M.*

senegalense, and *C. kluyveri*, could complete the multiple stages co-production process. *M. senegalense* oxidized ethanol to acetate and H₂, which pairs a PHB formation to store acetate and electrons temporally for further utilization in the leisure period between glycerol fermentation and carboxylates chain elongation. In the carboxylates chain elongation phase, *M. senegalense* and *C. kluyveri* worked together for caproate production with ethanol and acetate. Significant ethanol production from glycerol oxidation is the main reason for the caproate production enhancement.

8.2 Recommendations for Future Work

Prior to implementing this mixed culture anaerobic process in application, additional research must be conducted to (1) optimize 1,3-PDO and caproate co-production yields in a continuous anaerobic reactor with crude glycerol and SCFAs-contained wastewater combined in line products extraction, (2) and test the stability and resilience of the reactor microbiomes to withstand operating upsets which probably occur in industrial application. To further prove the syntroph in carboxylate chain elongation, a co-culture cultivation of *D. vulgaris*, *A. sticklandii* and *C. kluyveri* needs to be conducted.

Appendix I Table

CDS	Predicted function	Gene name	Enzyme commission	Identity (%)	e-value	Accession no.	Closely related protein
<i>Clostridium kluyveri</i>-Ethanol metabolism							
CK_01148	Iron containing alcohol dehydrogenase	<i>yiaY</i>	EC:1.1.1.1	93.7	0	BAH07172	hypothetical protein CKR 2121 [<i>Clostridium kluyveri</i> NBRC 12016]
CK_01212	Predicted iron containing alcohol dehydrogenase	<i>yiaY</i>	EC:1.1.1.1	93.6	0	EDK35008	Predicted iron containing alcohol dehydrogenase [<i>Clostridium kluyveri</i> DSM 555]
CK_02184	Predicted iron containing alcohol dehydrogenase	<i>yiaY</i>	EC:1.1.1.1	95.4	0	EDK34986	Predicted iron containing alcohol dehydrogenase [<i>Clostridium kluyveri</i> DSM 555]
CK_02636	Predicted iron containing alcohol dehydrogenase	<i>yiaY</i>	EC:1.1.1.1	68.5	0	EDK34986	Predicted iron containing alcohol dehydrogenase [<i>Clostridium kluyveri</i> DSM 555]
CK_03254	alcohol dehydrogenase	<i>yiaY</i>	EC:1.1.1.1	100.0	0	WP_012102403	ethanolamine utilization protein EutG [<i>Clostridium kluyveri</i>]
CK_04032	Aldehyde-alcohol dehydrogenase	<i>adhE</i>	EC:1.2.1.10; 1.1.1.1	96.2	1E-26	BAH06031	hypothetical protein CKR_0980 [<i>Clostridium kluyveri</i> NBRC 12016]
CK_04084	Predicted iron containing alcohol dehydrogenase	<i>yiaY</i>	EC:1.1.1.1	96.7	0	BAH08081	hypothetical protein CKR 3030 [<i>Clostridium kluyveri</i> NBRC 12016]

dehydrogenase

CK_02630	ethanolamine utilization protein EutL	<i>eutL</i>		100.0	0	WP_073538121	microcompartment protein PduB [<i>Clostridium kluyveri</i>]
CK_02631	ethanolamine utilization protein EutM	<i>eutM</i>		100.0	9E-57	WP_012101449	carboxysome shell protein [<i>Clostridium kluyveri</i>]
CK_03374	Aldehyde dehydrogenase AlkH	<i>alkH</i> (ALDH)	EC:1.2.1.3	96.0	0	WP_012102549	aldehyde dehydrogenase [<i>Clostridium kluyveri</i>]

***Clostridium kluyveri*-reverse β -oxidation**

CK_03900	putative phosphotransacetylase	<i>pta</i>	EC:2.3.1.8	98.6	2.00E-156	WP_011989412	propanediol utilization phosphotransacetylase [<i>Clostridium kluyveri</i>]
CK_00062	acetate kinase	<i>ackA</i>	EC:2.7.2.1	99.0	0	BAH06338	hypothetical protein CKR 1287 [<i>Clostridium kluyveri</i> NBRC 12016]
CK_00443	acetoacetyl-CoA thiolase	<i>thl</i>	EC:2.3.1.9	91.3	0	WP_012104014	acetyl-CoA acetyltransferase [<i>Clostridium kluyveri</i>]
CK_00444	acetoacetyl-CoA thiolase	<i>thl</i>	EC:2.3.1.9	97.4	0	WP_012104015	acetyl-CoA acetyltransferase [<i>Clostridium kluyveri</i>]
CK_00445	acetoacetyl-CoA thiolase	<i>thl</i>	EC:2.3.1.9	99.2	0	WP_012104016	acetyl-CoA acetyltransferase [<i>Clostridium kluyveri</i>]
CK_01526	3-hydroxybutyryl-CoA dehydrogenase	<i>hbd (paaH)</i>	EC:1.1.1.157	96.9	0	WP_012103136	3-hydroxybutyryl-CoA dehydrogenase [<i>Clostridium kluyveri</i>]
CK_01183	3-hydroxybutyryl-CoA dehydratase	<i>croR</i>	EC:4.2.1.55	97.1	3.00E-93	WP_012103365	enoyl-CoA hydratase [<i>Clostridium kluyveri</i>]

CK_00295	CoA-transferases	<i>cat2</i>	EC:2.8.3.-	99.1	0	WP_012103918	4-hydroxybutyrate CoA-transferase [<i>Clostridium kluyveri</i>]
CK_01045	3-hydroxybutyryl-CoA dehydrogenase	<i>hbd (paaH)</i>	EC:1.1.1.157	97.9	0	BAH05454	hypothetical protein CKR 0403 [<i>Clostridium kluyveri</i> NBRC 12016]
CK_01046	Acryloyl-CoA reductase electron transfer subunit gamma	<i>etfA</i>		98.2	0	WP_011989026	electron transfer flavoprotein subunit alpha [<i>Clostridium kluyveri</i>]
CK_01047	Acryloyl-CoA reductase electron transfer subunit beta	<i>etfB</i>		98.8	0	WP_011989025	electron transfer flavoprotein subunit beta [<i>Clostridium kluyveri</i>]
CK_01048	butyryl-CoA dehydrogenase	<i>bcd</i>	EC:1.3.8.1	95.8	0	WP_011989024	acyl-CoA dehydrogenase [<i>Clostridium kluyveri</i>]
CK_01049	3-hydroxybutyryl-CoA dehydratase	<i>crt</i>	EC:4.2.1.55	98.5	0	WP_011989023	crotonase [<i>Clostridium kluyveri</i>]

***Desulfovibrio vulgaris*-Ethanol metabolism**

DV_00409	NADP-dependent alcohol dehydrogenase	<i>yqhD</i>	EC:1.1.-.-	97.9	0	WP_010939476	NADH-dependent alcohol dehydrogenase [<i>Desulfovibrio vulgaris</i>]
DV_01064	NADP-dependent alcohol dehydrogenase	<i>yqhD</i>	EC:1.1.-.-	100.0	0	WP_010939476	NADH-dependent alcohol dehydrogenase [<i>Desulfovibrio vulgaris</i>]
DV_01916	alcohol dehydrogenase, iron-containing	<i>adh</i>	EC:1.1.1.1	99.1	7.00E-153	WP_010940145	alcohol dehydrogenase [<i>Desulfovibrio vulgaris</i>]
DV_02002	3-deoxy-alpha-D-manno-octulosonate	<i>kdnB</i>	EC:1.1.3.48	100.0	3.00E-71	WP_010937660	alcohol dehydrogenase [<i>Desulfovibrio vulgaris</i>]

	8-oxidase						
DV_02751	alcohol dehydrogenase	<i>yiaY</i>	EC:1.1.1.1	100.0	0	WP_010939677	alcohol dehydrogenase [<i>Desulfovibrio vulgaris</i>]
DV_02212	aldehyde:ferredoxin oxidoreductase	<i>aor</i>	EC:1.2.7.5	99.6	3.00E-179	WP_011792756	aldehyde ferredoxin oxidoreductase [<i>Desulfovibrio vulgaris</i>]
DV_01138	aldehyde dehydrogenase, iron-sulfur subunit			99.0	0	WP_011792354	4Fe-4S ferredoxin [<i>Desulfovibrio vulgaris</i>]
DV_00071	aldehyde oxidoreductase (FAD-independent)	<i>mop</i>	EC:1.2.99.7	99.9	0	WP_011792353	aldehyde oxidoreductase [<i>Desulfovibrio vulgaris</i>]
DV_00072	molybdopterin biosynthesis protein			100.0	0	WP_010938852	molybdopterin biosynthesis protein [<i>Desulfovibrio vulgaris</i>]
<hr/>							
<i>Acetoanaerobium sticklandii</i>-pyruvate to acetyl-CoA							
CS_00432	pyruvate-ferredoxin/flavodoxin oxidoreductase	<i>porI</i>	EC:1.2.7.1	98.0	0	WP_013362125	pyruvate:ferredoxin (flavodoxin) oxidoreductase [[<i>Clostridium</i>] <i>sticklandii</i>]
CS_00649	pyruvate-ferredoxin/flavodoxin oxidoreductase	<i>por</i>	EC:1.2.7.1	96.3	0	SCG83877	putative pyruvate-flavodoxin oxidoreductase [<i>Proteiniborus</i> sp. DW1]

***Acetoanaerobium sticklandii*-reverse β -oxidation**

CS_00221	enoyl-CoA hydratase-isomerase	<i>paaF</i>	EC:4.2.1.17	98.4	0	WP_013361345	crotonase [[<i>Clostridium</i>] <i>sticklandii</i>]
CS_00222	3-hydroxybutyryl-CoA dehydrogenase	<i>paaH</i>	EC:1.1.1.157	99.6	0	CBH21253	3-hydroxybutyryl-CoA dehydrogenase [[<i>Clostridium</i>] <i>sticklandii</i>]
CS_00704	3-hydroxyacyl-CoA dehydrogenase precursor		EC:1.1.1.35	99.0	0	WP_013360419	3-hydroxyacyl-CoA dehydrogenase [[<i>Clostridium</i>] <i>sticklandii</i>]
CS_00929	NADH dehydrogenase	<i>ndh</i>	EC:1.6.99.3	99.7	0	WP_013361632	pyridine nucleotide-disulfide oxidoreductase [[<i>Clostridium</i>] <i>sticklandii</i>]
CS_01444	Acyl-CoA dehydrogenase, short-chain specific	<i>ACADS</i>	EC:1.3.8.1	100.0	0	WP_013361348	acyl-CoA dehydrogenase [[<i>Clostridium</i>] <i>sticklandii</i>]
CS_01937	Acryloyl-CoA reductase electron transfer subunit beta	<i>etfA</i>		99.7	0	WP_013361350	electron transfer flavoprotein subunit alpha [[<i>Clostridium</i>] <i>sticklandii</i>]
CS_01298	Acetate CoA-transferase subunit alpha	<i>atoD</i>	EC:2.8.3.8; 2.8.3.9	94.9	8.00E-136	SCG81852	butyrate-acetoacetate CoA-transferase [<i>Proteiniborus</i> sp. DW1]
CS_01299	Acetyl-CoA acetyltransferase	<i>atoB</i>	EC:2.3.1.9	84.7	0	SHK32546	acetyl-CoA C-acetyltransferase [<i>Caminicella sporogenes</i> DSM 14501]
CS_01905	Acetyl-CoA acetyltransferase	<i>atoB</i>	EC:2.3.1.9	97.1	2.00E-167	WP_013361347	acetyl-CoA acetyltransferase [[<i>Clostridium</i>] <i>sticklandii</i>]

CS_00212	acetate	CoA/acetoacetate	<i>atoD</i>	EC:2.8.3.8; 2.8.3.9	99.1	1.00E-150	WP_013361336	acetyl CoA-acetoacetyl-CoA transferase subunit alpha [[<i>Clostridium sticklandii</i>]]
	CoA-transferase alpha subunit							
CS_00213	acetate	CoA/acetoacetate	<i>atoA</i>	EC:2.8.3.8; 2.8.3.9	100.0	7.00E-152	WP_013361337	succinyl-CoA-3-ketoacid-CoA transferase [[<i>Clostridium sticklandii</i>]]
	CoA-transferase beta subunit							
CS_00230	phosphate butyryltransferase		<i>ptb</i>	EC:2.3.1.19	98.0	0	WP_013360706	phosphate butyryltransferase [[<i>Clostridium sticklandii</i>]]
CS_00338	phosphate butyryltransferase		<i>ptb</i>	EC:2.3.1.19	99.0	0	WP_013360427	phosphate butyryltransferase [[<i>Clostridium sticklandii</i>]]
CS_01302	phosphate butyryltransferase		<i>ptb</i>	EC:2.3.1.19	99.7	0	WP_013361368	phosphate butyryltransferase [[<i>Clostridium sticklandii</i>]]
CS_00229	butyrate kinase		<i>buk</i>	EC:2.7.2.7	99.4	0	CBH20614	putative butyrate kinase (BK) (Branched-chain carboxylic acid kinase) [[<i>Clostridium sticklandii</i>]]
CS_00231	butyrate kinase		<i>buk</i>	EC:2.7.2.7	99.4	0	WP_013360705	butyrate kinase [[<i>Clostridium sticklandii</i>]]
CS_00537	butyrate kinase		<i>buk</i>	EC:2.7.2.7	97.2	0	WP_013360976	butyrate kinase [[<i>Clostridium sticklandii</i>]]
CS_01543	butyrate kinase		<i>buk</i>	EC:2.7.2.7	91.3	0	SCG84000	butyrate kinase [<i>Proteiniborus</i> sp. DW1]
CS_02050	butyrate kinase		<i>buk</i>	EC:2.7.2.7	91.9	0	SCG84002	butyrate kinase [<i>Proteiniborus</i> sp. DW1]

CS_00363	NADH dehydrogenase		EC:1.6.5.3	100.0	5.00E-110	WP_013361876	NADH dehydrogenase [[<i>Clostridium</i>] <i>sticklandii</i>]
CS_01380	NADH dehydrogenase	<i>ndh</i>	EC:1.6.99.3	94.8	2.00E-126	SCG83971	NADH dehydrogenase [<i>Proteiniborus</i> sp. DW1]
CS_01647	NADPH dehydrogenase	<i>namA</i>	EC 1.6.99.1	76.9	0	SDY55985	NADPH2 dehydrogenase [<i>Proteiniborus ethanoligenes</i>]
CS_01567	NAD(P)H dehydrogenase (quinone)	<i>wrbA</i>	EC 1.6.5.2	75.9	1.00E-114	WP_005587815	flavoprotein WrbA [[<i>Clostridium</i>] <i>sticklandii</i>]
CS_00663	NADP-thioredoxin reductase	<i>trxB</i>	EC 1.8.1.9	98.8	0	WP_013361651	pyridine nucleotide-disulfide oxidoreductase [[<i>Clostridium</i>] <i>sticklandii</i>]
CS_01384	Ferredoxin--NADP reductase			31.8	1.8	XP_002956436	hypothetical protein VOLCADRAFT_121523 [<i>Volvox carteri</i> f. <i>nagariensis</i>]

Appendix II Table

CDS	Predicted function	Gene name	Enzyme commission	Identity (%)	e-value	Accession no.	Closely related protein
<i>Clostridium kluyveri</i>-Membrane proteins involved in energy conservation-Rnf complex							
CK_01888	Electron transport complex protein RnfC	<i>rnfC</i>		98.9	0	BAH06211	hypothetical protein CKR 1160 [<i>Clostridium kluyveri</i> NBRC 12016]
CK_01889	Electron transport complex protein RnfD	<i>rnfD</i>		100.0	0	WP_012101651	NADH:ubiquinone oxidoreductase [<i>Clostridium kluyveri</i>]
CK_01890	Electron transport complex protein RnfG	<i>rnfG</i>		99.5	3.00E-128	BAH06213	hypothetical protein CKR 1162 [<i>Clostridium kluyveri</i> NBRC 12016]
CK_01891	Electron transport complex protein RnfE	<i>rnfE</i>		99.5	1.00E-148	WP_012101653	electron transport complex subunit RxsE [<i>Clostridium kluyveri</i>]
CK_01892	Electron transport complex protein RnfA	<i>rnfA</i>		99.0	2.00E-127	WP_012101654	electron transport complex subunit RxsA [<i>Clostridium kluyveri</i>]
CK_01893	Electron transport complex protein RnfB	<i>rnfB</i>		97.9	0	WP_012101655	protein RnfB [<i>Clostridium kluyveri</i>]
<i>Clostridium kluyveri</i>-Membrane proteins involved in energy conservation-FAD (or Fe-S) reductase linked to ETF							
CK_03656	putative FAD-linked oxidoreductase			98.9	0	BAH08153	hypothetical protein CKR 3102 [<i>Clostridium kluyveri</i> NBRC 12016]; FAD/FMN-containing dehydrogenase [Energy production and conversion];
CK_03657	Acryloyl-CoA reductase electron transfer subunit beta	<i>etfB</i>		96.4	0	WP_012103838	electron transfer flavoprotein subunit alpha [<i>Clostridium kluyveri</i>]

CK_03658	Acryloyl-CoA reductase electron transfer subunit gamma	<i>etfA</i>		95.7	9.00E-142	WP_012103839	hypothetical protein [<i>Clostridium kluyveri</i>]
----------	--	-------------	--	------	-----------	--------------	--

***Clostridium kluyveri*-Membrane proteins involved in energy conservation-FAD (or Fe-S) reductase linked to ETF-Fix system**

CK_02710	6-hydroxynicotinate reductase	<i>fixX</i>		90.7	2.00E-60	WP_012101891	4Fe-4S ferredoxin [<i>Clostridium kluyveri</i>]
CK_02711	Electron transfer flavoprotein-ubiquinone oxidoreductase	<i>fixC</i>	EC:1.5.5.-	82.1	0	WP_063553767	nitrogen fixation protein FixC [<i>Clostridium ljungdahlii</i>]
CK_02712	electron transfer flavoprotein alpha subunit	<i>fixB</i>		73.0	0	WP_066622777	electron transfer flavoprotein subunit alpha [<i>Clostridium magnum</i>]
CK_02713	electron transfer flavoprotein beta subunit	<i>fixA</i>		82.2	1.00E-164	WP_058953659	electron transfer flavoprotein subunit beta [<i>Clostridium tyrobutyricum</i>]

***Clostridium kluyveri*-Membrane proteins involved in energy conservation-FAD (or Fe-S) reductase linked to ETF-Fix system-ATPase**

CK_00434	F-type H ⁺ -transporting ATPase subunit epsilon	<i>atpC</i>		96.2	2.00E-85	WP_012104005	ATP synthase epsilon chain [<i>Clostridium kluyveri</i>]
CK_00435	F-type H ⁺ -transporting ATPase subunit beta	<i>atpD</i>	EC:3.6.3.14	99.4	0	BAH08304	hypothetical protein CKR 3253 [<i>Clostridium kluyveri</i> NBRC 12016]
CK_00436	F-type H ⁺ -transporting ATPase subunit gamma	<i>atpG</i>		97.9	0	WP_012104007	ATP synthase subunit gamma [<i>Clostridium kluyveri</i>]
CK_00437	F-type H ⁺ -transporting ATPase subunit alpha	<i>atpA</i>	EC:3.6.3.14	99.2	0	WP_012621009	ATP synthase subunit alpha [<i>Clostridium kluyveri</i>]
CK_00438	F-type H ⁺ -transporting ATPase subunit delta	<i>atpH</i>		96.1	2.00E-119	WP_012104009	ATP synthase subunit delta [<i>Clostridium kluyveri</i>]

CK_00439	F-type H ⁺ -transporting ATPase subunit b	<i>atpF</i>		98.1	9.00E-108	BAH08308	hypothetical protein CKR 3257 [<i>Clostridium kluyveri</i> NBRC 12016]
CK_00440	F-type H ⁺ -transporting ATPase subunit c	<i>atpE</i>		100.0	5.00E-47	WP_012104011	ATP synthase F0 subunit C [<i>Clostridium kluyveri</i>]
CK_00441	F-type H ⁺ -transporting ATPase subunit a	<i>atpB</i>		98.7	9.00E-158	WP_012104012	F0F1 ATP synthase subunit A [<i>Clostridium kluyveri</i>]
CK_00442	ATP synthase protein I	<i>atpI</i>		100.0	9.00E-78	WP_073540696	ATP synthase subunit I [<i>Clostridium kluyveri</i>]
CK_01313	flagellum-specific ATP synthase	<i>fliI</i>	EC:3.6.3.14	98.9	0	WP_012101535	flagellar protein export ATPase FliI [<i>Clostridium kluyveri</i>]
CK_01044	ferredoxin-NADP ⁺ reductase	<i>fpr</i>	EC:1.18.1.2	98.3	0	WP_011989028	ferredoxin-NADP ⁺ reductase subunit alpha [<i>Clostridium kluyveri</i>]

***Clostridium kluyveri*-Hydrogenases-Periplasmic [NiFeSe] hydrogenase complex**

CK_02733	Hydrogenase expression/formation protein HypE	<i>hypE</i>		73.9	0	WP_053240720	hydrogenase expression/formation protein HypE [<i>Clostridium</i> sp. DMHC 10]
CK_02734	Hydrogenase isoenzymes formation protein HypD	<i>hypD</i>		59.5	6.00E-153	WP_016206877	hydrogenase formation protein HypD [<i>Clostridium sartagoforme</i>]
CK_02735	Hydrogenase isoenzymes formation protein HypC	<i>hypC</i>		83.3	8.00E-35	WP_053240721	hydrogenase assembly protein HypC [<i>Clostridium</i> sp. DMHC 10]
CK_02736	Carbamoyltransferase HypF	<i>hypF</i>		53.1	0	WP_065418234	carbamoyltransferase HypF [<i>Clostridium beijerinckii</i>]
CK_02737	hydrogenase nickel incorporation protein HypA			72.9	2.00E-35	WP_011989104	hypothetical protein [<i>Clostridium kluyveri</i>]

CK_02738	Cytochrome b5-like Heme/Steroid binding domain protein (putative)			60.3	3.00E-50	AF323616_4	HypQ3 (plasmid) [<i>Clostridium acetobutylicum</i> ATCC 824]
CK_02739	Hydrogenase 3 maturation protease	<i>hyaD</i>	EC:3.4.23.-	63.7	2.00E-59	KZL89330	hydrogenase 2 maturation endopeptidase [<i>Clostridium magnum</i> DSM 2767]
CK_02740	Periplasmic [NiFeSe] hydrogenase large subunit	<i>hyaA</i>	EC:1.12.99.6	74.9	0	WP_066023448	Ni/Fe hydrogenase [<i>Clostridium pasteurianum</i>]
CK_02741	Periplasmic [NiFeSe] hydrogenase small subunit precursor	<i>hyaB</i>	EC:1.12.99.6	82.5	0	WP_066023447	Ni/Fe hydrogenase [<i>Clostridium pasteurianum</i>]

***Clostridium kluyveri*-Hydrogenases-Iron hydrogenase**

CK_00654	ferredoxin hydrogenase	<i>hyaA</i>	EC:1.12.7.2	98.4	0	WP_012102599	ferredoxin [<i>Clostridium kluyveri</i>]
CK_00728	Iron hydrogenase 1			98.0	0	WP_011988737	iron hydrogenase [<i>Clostridium kluyveri</i>]

***Desulfovibrio vulgaris*-Hydrogenase**

DV_01116	Periplasmic [NiFe] hydrogenase large subunit	<i>hyaA</i>	EC:1.12.2.1	99.6	0	WP_010939208	hydrogenase 2 large subunit [<i>Desulfovibrio vulgaris</i>]
DV_01117	Hydrogenase 1 maturation protease	<i>hyaD</i>	EC:3.4.23.-	100.0	2.00E-115	WP_010939209	hydrogenase expression/formation protein [<i>Desulfovibrio vulgaris</i>]
DV_01118	Hydrogenase-2 operon protein HybG			100.0	1.00E-51	WP_010939210	hydantoin utilization protein B [<i>Desulfovibrio vulgaris</i>]
DV_01335	Periplasmic [NiFe] hydrogenase large subunit	<i>hyaA</i>	EC:1.12.2.1	100.0	0	WP_010939796	hydrogenase 2 large subunit [<i>Desulfovibrio vulgaris</i>]

DV_01367	Hydrogenase 1 maturation protease	<i>hyaD</i>	EC:3.4.23.-	100.0	2.00E-110	WP_010939205	HybD peptidase [<i>Desulfovibrio vulgaris</i>]
DV_01368	Periplasmic [NiFeSe] hydrogenase large subunit	<i>hyaB</i>	EC:1.12.99.6	99.7	0	2WPN_B	Chain B, Structure Of The Oxidised, As-isolated Nifese Hydrogenase From <i>D. Vulgaris</i> Hildenborough
DV_01409	putative Ni/Fe-hydrogenase 2 b-type cytochrome subunit			100.0	0	WP_010937840	hypothetical protein [<i>Desulfovibrio vulgaris</i>]
DV_01809	NAD(P)H-quinone oxidoreductase subunit J, chloroplastic			100.0	6.00E-91	WP_010937738	ech hydrogenase subunit EchD [<i>Desulfovibrio vulgaris</i>]
DV_01810	Formate hydrogenlyase subunit 7			100.0	2.00E-109	WP_010937739	NADH ubiquinone oxidoreductase [<i>Desulfovibrio vulgaris</i>]
DV_01811	Hydrogenase-4 component C			100.0	0	WP_010937740	ech hydrogenase subunit EchB [<i>Desulfovibrio vulgaris</i>]
DV_01981	Cytochrome c3			100.0	3.00E-98	WP_014524526	cytochrome c [<i>Desulfovibrio vulgaris</i>]
DV_01982	[NiFe] hydrogenase small subunit	<i>hyaA</i>	EC:1.12.2.1	99.1	0	WP_014524527	[NiFe] hydrogenase small subunit [<i>Desulfovibrio vulgaris</i>]
DV_02012	Hydrogenase-4 component B			99.7	0	WP_011791959	oxidoreductase [<i>Desulfovibrio vulgaris</i>]
DV_02291	Hydrogenase isoenzymes nickel incorporation protein HypB	<i>hypB</i>		100.0	5.00E-118	WP_010939602	hydrogenase nickel incorporation protein HypB [<i>Desulfovibrio vulgaris</i>]
DV_02299	Hydrogenase expression/formation protein HypE	<i>hypE</i>		100.0	0	2Z1T_A	Chain A, Crystal Structure Of Hydrogenase Maturation Protein Hype
DV_02318	Iron-sulfur protein			100.0	3.00E-122	WP_010939568	iron-sulfur protein [<i>Desulfovibrio vulgaris</i>]

DV_02319	Hydrogenase/urease nickel incorporation protein HypA	<i>hypA</i>		99.2	4.00E-79	WP_010939567	hydrogenase nickel incorporation protein HypA [<i>Desulfovibrio vulgaris</i>]
DV_02320	Formate hydrogenlyase subunit 5			99.3	3.00E-98	WP_011791954	carbon monoxide-induced hydrogenase [<i>Desulfovibrio vulgaris</i>]
DV_02634	Formate dehydrogenase subunit alpha	<i>fdnG-1</i>	EC:1.2.1.2	100.0	0	WP_010937890	formate dehydrogenase-N subunit alpha [<i>Desulfovibrio vulgaris</i>]

***Desulfovibrio vulgaris*-Membrane proteins involved in energy conservation**

DV_00397	electron transport complex protein RnfE	<i>rnfE</i>		99.0	2.00E-64	WP_010940061	electron transport complex subunit RnxE [<i>Desulfovibrio vulgaris</i>]
DV_00398	electron transport complex protein RnfA	<i>rnfA</i>		100.0	1.00E-133	WP_010940062	electron transport complex protein RnfA [<i>Desulfovibrio vulgaris</i>]
DV_00399	electron transport complex protein RnfB	<i>rnfB</i>		100.0	0	WP_010940063	ferredoxin [<i>Desulfovibrio vulgaris</i>]
DV_00959		<i>cytC</i>		100.0	0	WP_010940057	cytochrome c [<i>Desulfovibrio vulgaris</i>]
DV_00960	electron transport complex protein RnfC	<i>rnfC</i>		100.0	0	WP_010940058	electron transport complex protein RnfC [<i>Desulfovibrio vulgaris</i>]
DV_00961	electron transport complex protein RnfD	<i>rnfD</i>		100.0	0	WP_010940059	electron transport complex protein RnfD [<i>Desulfovibrio vulgaris</i>]
DV_00604	ATP synthase subunit b, sodium ion specific	<i>atpF</i>		100.0	1.00E-91	WP_011792709	ATP synthase F0 subunit B' [<i>Desulfovibrio vulgaris</i>]
DV_00605	ATP synthase subunit b	<i>atpF</i>		100.0	7.00E-132	WP_011792710	ATP synthase subunit B [<i>Desulfovibrio vulgaris</i>]

DV_00606	ATP synthase subunit delta	<i>atpH</i>		100.0	7.00E-126	WP_010938079	ATP synthase subunit delta [<i>Desulfovibrio vulgaris</i>]
DV_00607	ATP synthase subunit alpha	<i>atpA</i>	EC:3.6.3.14	100.0	0	WP_010938078	ATP synthase subunit alpha [<i>Desulfovibrio vulgaris</i>]
DV_00608	ATP synthase gamma chain	<i>atpG</i>		100.0	0	WP_010938077	ATP synthase subunit gamma [<i>Desulfovibrio vulgaris</i>]
DV_00609	ATP synthase subunit beta	<i>atpD</i>	EC:3.6.3.14	100.0	0	WP_010938076	ATP synthase subunit beta [<i>Desulfovibrio vulgaris</i>]
DV_01506	flagellum-specific ATP synthase	<i>fliI</i>	EC:3.6.3.14	100.0	0	WP_010937617	flagellum-specific ATP synthase FliI [<i>Desulfovibrio vulgaris</i>]

***Acetoanaerobium sticklandii*-ATP synthase complex**

CS_00193	V-type ATP synthase subunit H			96.2	5.00E-59	WP_013362530	hypothetical protein [[<i>Clostridium</i>] <i>sticklandii</i>]
CS_00194	V/A-type H ⁺ /Na ⁺ -transporting ATPase subunit C	<i>atpC</i>		94.5	0	WP_013362529	V-type sodium ATP synthase subunit C [[<i>Clostridium</i>] <i>sticklandii</i>]
CS_00195	V/A-type H ⁺ /Na ⁺ -transporting ATPase subunit I	<i>atpI</i>		96.8	0	WP_013362528	V-type ATP synthase subunit I [[<i>Clostridium</i>] <i>sticklandii</i>]
CS_00196	V/A-type H ⁺ /Na ⁺ -transporting ATPase subunit K	<i>atpK</i>		100.0	1.00E-87	WP_013362527	ATPase [[<i>Clostridium</i>] <i>sticklandii</i>]
CS_00197	V/A-type H ⁺ /Na ⁺ -transporting ATPase subunit F	<i>atpF</i>		100.0	2.00E-67	CBH22435	Vacuolar H ⁺ -transporting two-sector ATPase, F subunit [[<i>Clostridium</i>] <i>sticklandii</i>]
CS_00198	V/A-type H ⁺ /Na ⁺ -transporting ATPase subunit E	<i>atpE</i>		98.6	1.00E-144	WP_013362525	hypothetical protein [[<i>Clostridium</i>] <i>sticklandii</i>]

CS_00199	V/A-type H ⁺ /Na ⁺ -transporting ATPase subunit A	<i>atpA</i>	EC:3.6.3.14; 3.6.3.15	99.5	0	WP_013362524	ATP synthase subunit A [[<i>Clostridium</i>] <i>sticklandii</i>]
CS_00200	V/A-type H ⁺ /Na ⁺ -transporting ATPase subunit B	<i>atpB</i>		99.8	0	WP_013362523	V-type ATP synthase subunit B [[<i>Clostridium</i>] <i>sticklandii</i>]
CS_00201	V/A-type H ⁺ /Na ⁺ -transporting ATPase subunit D	<i>atpD</i>		99.0	8.00E-142	WP_013362522	ATPase [[<i>Clostridium</i>] <i>sticklandii</i>]
CS_00312	F-type H ⁺ -transporting ATPase subunit alpha	<i>atpA</i>	EC:3.6.3.14	100.0	4.00E-84	WP_013362330	ATP synthase subunit alpha [[<i>Clostridium</i>] <i>sticklandii</i>]
CS_00313	F-type H ⁺ -transporting ATPase subunit gamma	<i>atpG</i>		98.6	0	WP_013362329	ATP synthase F1 subunit gamma [[<i>Clostridium</i>] <i>sticklandii</i>]
CS_00314	F-type H ⁺ -transporting ATPase subunit beta	<i>atpD</i>	EC:3.6.3.14	99.1	0	WP_013362328	ATP synthase subunit beta [[<i>Clostridium</i>] <i>sticklandii</i>]
CS_00315	F-type H ⁺ -transporting ATPase subunit epsilon	<i>atpC</i>		97.0	1.00E-87	WP_013362327	ATP synthase F1 subunit epsilon [[<i>Clostridium</i>] <i>sticklandii</i>]
CS_00416	F-type H ⁺ -transporting ATPase subunit delta	<i>atpH</i>		96.1	2.00E-118	WP_013362331	F0F1 ATP synthase subunit delta [[<i>Clostridium</i>] <i>sticklandii</i>]
CS_00417	F-type H ⁺ -transporting ATPase subunit b	<i>atpF</i>		98.2	3.00E-112	WP_013362332	ATP synthase F0 subunit B [[<i>Clostridium</i>] <i>sticklandii</i>]
CS_00418	F-type H ⁺ -transporting ATPase subunit c	<i>atpE</i>		97.6	2.00E-47	WP_013362333	ATP synthase F0 subunit C [[<i>Clostridium</i>] <i>sticklandii</i>]
CS_00419	F-type H ⁺ -transporting ATPase subunit a	<i>atpB</i>		93.7	1.00E-136	WP_013362334	ATP synthase F0 subunit A [[<i>Clostridium</i>] <i>sticklandii</i>]
CS_00420	ATP synthase subunit I	<i>atpI</i>		76.0	2.00E-59	WP_013362335	ATP synthase I [[<i>Clostridium</i>] <i>sticklandii</i>]

CS_00421	ATP synthase protein I	<i>atpI</i>		79.8	3.00E-45	CBH22244	protein of unknown function [<i>[[Clostridium] sticklandii]</i>]
CS_01451				87.9	0	WP_073028149	hypothetical protein [<i>Lutispora thermophila</i>]
CS_01977				96.5	8.00E-53	SCG83516	UPF0296 protein [<i>Proteiniborus</i> sp. DW1]
CS_01984	V/A-type H ⁺ /Na ⁺ -transporting ATPase subunit C	<i>atpC</i>		72.5	1.00E-26	WP_072975129	hypothetical protein [<i>Tissierella praeacuta</i>]

***Acetoanaerobium sticklandii*-Hydrogenase (putative electron-bifurcating hydrogenase)**

CS_00402	NADH-quinone oxidoreductase subunit G	<i>nuoG</i>	EC:1.6.5.3	99.1	0	WP_013361125	NADH:ubiquinone oxidoreductase [<i>[[Clostridium] sticklandii]</i>]
CS_00403	NADH-quinone oxidoreductase subunit F	<i>nuoF</i>	EC:1.6.5.3	99.2	0	WP_013361126	NADH dehydrogenase [<i>[[Clostridium] sticklandii]</i>]
CS_00404	NADH-quinone oxidoreductase subunit E	<i>nuoE</i>	EC:1.6.5.3	99.3	4.00E-96	WP_013361127	NADH:ubiquinone oxidoreductase [<i>[[Clostridium] sticklandii]</i>]

***Acetoanaerobium sticklandii*-Formate dehydrogenase**

CS_00819	formate dehydrogenase major subunit	<i>fdhH</i>	EC:1.2.1.2	98.8	0	CBH20954	Formate dehydrogenase alpha chain [<i>[[Clostridium] sticklandii]</i>]
CS_00820	formate dehydrogenase-H, [4Fe-4S] ferredoxin subunit	<i>fdhB</i>		98.3	3.00E-123	WP_013361048	electron transporter HydN [<i>[[Clostridium] sticklandii]</i>]

Appendix III Table

CDS	Predicted function	Gene name	Enzyme commission	Identity (%)	e-value	Accession no.	Closely related protein
<i>Acetoanaerobium sticklandii</i>-amino acid metabolism-serine metabolism							
CS_00099	D-serine dehydratase	<i>dsdA</i>	EC:4.3.1.18	97.6	0	WP_013360725	D-serine ammonia-lyase [[<i>Clostridium</i>] <i>sticklandii</i>]
CS_00564	L-serine dehydratase			95.8	0	WP_013362579	hypothetical protein [[<i>Clostridium</i>] <i>sticklandii</i>]
CS_01160	L-serine dehydratase	<i>sdhA</i>	EC:4.3.1.17	82.1	1.00E-166	SDZ22446	L-serine dehydratase [<i>Proteiniborus ethanoligenes</i>]
CS_01161	L-serine dehydratase	<i>sdhA</i>	EC:4.3.1.17	92.4	4.00E-147	SCG82933	L-serine dehydratase, iron-sulfur-dependent, beta subunit [<i>Proteiniborus</i> sp. DW1]
<i>Acetoanaerobium sticklandii</i>-amino acid metabolism-arginine deiminase							
CS_01599	arginine utilization regulatory protein	<i>rocR</i>		85.4	0	SCG81785	Arginine utilization regulatory protein rocR [<i>Proteiniborus</i> sp. DW1]
CS_00041	ornithine carbamoyltransferase	<i>arcB</i>	EC:2.1.3.3	98.4	0	WP_013361145	ornithine carbamoyltransferase [[<i>Clostridium</i>] <i>sticklandii</i>]
CS_01695	ornithine carbamoyltransferase	<i>arcB</i>	EC:2.1.3.3	92.1	0	SDZ19422	ornithine carbamoyltransferase [<i>Proteiniborus ethanoligenes</i>]
CS_00040	carbamate kinase	<i>arcC</i>	EC:2.7.2.2	99.7	0	WP_013361146	carbamate kinase [[<i>Clostridium</i>] <i>sticklandii</i>]

Acetoanaerobium sticklandii-amino acid metabolism-cysteine metabolism

CS_01387	4,5-DOPA dioxygenase extradiol	<i>DOPA</i>	EC:1.13.11.-	96.4	4.00E-179	WP_041487119	dioxygenase [[<i>Clostridium</i>] <i>sticklandii</i>]
CS_01758	cystathione beta-lyase	<i>patB</i>	EC:4.4.1.8	95.9	5.00E-133	SCG82539	aminotransferase [<i>Proteiniborus</i> sp. DW1]
CS_00259	cysteine desulfurase	<i>iscS</i>	EC:2.8.1.7	99.5	0	WP_013361707	cysteine desulfurase NifS [[<i>Clostridium</i>] <i>sticklandii</i>]
CS_00920	cysteine desulfurase	<i>iscS</i>	EC:2.8.1.7	99.2	0	WP_013361658	cysteine desulfurase (tRNA sulfurtransferase), PLP-dependent [[<i>Clostridium</i>] <i>sticklandii</i>]
CS_01415	cysteine synthase A	<i>cysK</i>	EC:2.5.1.47	91.7	4.00E-142	SCG83572	cysteine synthase A [<i>Proteiniborus</i> sp. DW1]

Acetoanaerobium sticklandii-Alanine metabolism for Stickland reaction (D-Ala >>> L-Ala >>> pyruvate)

CS_00093	alanine dehydrogenase	<i>ald</i>	EC:1.4.1.1	97.9	0	WP_013360731	alanine dehydrogenase [[<i>Clostridium</i>] <i>sticklandii</i>]
CS_00318	Alanine racemase	<i>alr</i>	EC:5.1.1.1	98.7	0	WP_013362324	alanine racemase [[<i>Clostridium</i>] <i>sticklandii</i>]
CS_00360	Alanine racemase			97.0	2.00E-163	WP_013362093	YggS family pyridoxal phosphate enzyme [[<i>Clostridium</i>] <i>sticklandii</i>]
CS_01609	Alanine racemase	<i>alr</i>	EC:5.1.1.1	94.5	4.00E-123	SCG82786	alanine racemase [<i>Proteiniborus</i> sp. DW1]

Acetoanaerobium sticklandii-Glycine/betaine/sarcosine reductase complex and transporter

CS_00283	glycine reductase		EC:1.21.4.2	99.5	0	WP_013361329	glycine/betaine reductase C [[<i>Clostridium</i>] <i>sticklandii</i>]
CS_00284	glycine reductase		EC:1.21.4.2	99.2	0	WP_013361328	glycine/betaine reductase C [[<i>Clostridium</i>] <i>sticklandii</i>]
CS_00993	thioredoxin 1	<i>trxA</i>		100.0	1.00E-70	WP_013361324	thiol reductase thioredoxin [[<i>Clostridium</i>] <i>sticklandii</i>]
CS_00994	glycine reductase		EC:1.21.4.2	99.1	0	WP_013361325	glycine reductase complex component B subunits alpha and beta [[<i>Clostridium</i>] <i>sticklandii</i>]
CS_00995	glycine/sarcosine/betaine reductase		EC:1.21.4.2; 1.21.4.3; 1.21.4.4	100.0	3.00E-22	GRDA_CLOSD	Glycine/sarcosine/betaine reductase complex component A
CS_00996	glycine/sarcosine/betaine reductase		EC:1.21.4.2; 1.21.4.3; 1.21.4.4	97.2	4.00E-71	WP_041487122	glycine/betaine reductase A [[<i>Clostridium</i>] <i>sticklandii</i>]
CS_00997	glycine reductase		EC:1.21.4.2	98.0	0	CAC14301	47 subunit of Protein B [[<i>Clostridium</i>] <i>sticklandii</i> DSM 519]
CS_00998	glycine reductase		EC:1.21.4.2	100.0	1.00E-47	WP_041487124	glycine reductase [[<i>Clostridium</i>] <i>sticklandii</i>]
CS_01071	glycine reductase		EC:1.21.4.2	100.0	5.00E-50	WP_041487117	glycine reductase complex protein B subunit gamma [[<i>Clostridium</i>] <i>sticklandii</i>]
CS_01072	glycine reductase		EC:1.21.4.2	100.0	0	CBH21180	Betaine reductase complex component B subunit beta (Selenoprotein PB beta) [[<i>Clostridium</i>] <i>sticklandii</i>]
CS_01073	glycine reductase		EC:1.21.4.2	99.1	0	WP_013361272	betaine reductase complex component B subunit alpha (Selenoprotein PB alpha) [[<i>Clostridium</i>] <i>sticklandii</i>]
CS_01780	glycine reductase		EC:1.21.4.2	72.8	5.00E-103	WP_025437076	beta-aspartate methyltransferase [<i>Peptoclostridium acidaminophilum</i>]

CS_01781	glycine reductase		EC:1.21.4.2	81.6	6.00E-37	WP_028331194	glycine reductase [<i>Brachyspira alvinipulli</i>]
CS_01682	glycine betaine transporter	<i>opuD</i>		76.5	0	WP_025640443	choline transporter [[<i>Clostridium</i>] <i>ultunense</i>]
CS_01407	osmoprotectant transport system ATP-binding protein	<i>opuA</i>		95.9	0	CBH20160	putative transporter subunit: ATP-binding component of ABC superfamily transporter [[[<i>Clostridium</i>] <i>sticklandii</i>]

Appendix IV Table

Gene name	Predicted function	Enzyme commission number	CDS	Identity (%)	e-value	Closely related protein
<i>sdaA</i>	L-serine dehydratase	EC:4.3.1.17	646283639	100.0	0	EES64001.1 L-serine ammonia-lyase [<i>Fusobacterium varium</i> ATCC 27725]
<i>dsdA</i>	D-serine dehydratase	EC:4.3.1.18	646283243	100.0	0	EES64271.1 D-serine ammonia-lyase [<i>Fusobacterium varium</i> ATCC 27725]
<i>tdcB</i>	threonine dehydratase	EC:4.3.1.19	646284129	98.3	3.85E-158	OFL90702.1 threonine ammonia-lyase, partial [<i>Fusobacterium</i> sp. HMSC073F01]
<i>tdcB</i>	threonine dehydratase	EC:4.3.1.19	646283773	100.0	2.31E-70	EES63836.2 threonine ammonia-lyase domain protein, partial [<i>Fusobacterium varium</i> ATCC 27725]
<i>tdcB</i>	threonine dehydratase	EC:4.3.1.19	646283262	100.0	8.73E-70	EES63836.2 threonine ammonia-lyase domain protein, partial [<i>Fusobacterium varium</i> ATCC 27725]
<i>glyA</i>	glycine hydroxymethyltransferase	EC:2.1.2.1	646282649	100.0	0	EES65216.1 glycine hydroxymethyltransferase [<i>Fusobacterium varium</i> ATCC 27725]
<i>ltaE</i>	threonine aldolase	EC:4.1.2.48	646284449	100.0	0	EES62548.1 Beta-eliminating lyase [<i>Fusobacterium varium</i> ATCC 27725]
<i>por</i>	pyruvate-ferredoxin/flavodoxin oxidoreductase	EC:1.2.7.1	646284783	100.0	0	EES62881.1 pyruvate synthase [<i>Fusobacterium varium</i> ATCC 27725]
<i>porG</i>	pyruvate ferredoxin oxidoreductase gamma subunit	EC:1.2.7.1	646284201	100.0	8.47E-127	EES63528.2 2-oxoacid:acceptor oxidoreductase, gamma subunit, pyruvate/2-ketoisovalerate family [<i>Fusobacterium varium</i> ATCC 27725]
<i>porD</i>	pyruvate ferredoxin oxidoreductase delta subunit	EC:1.2.7.1	646284200	100.0	3.09E-67	EES63527.1 2-oxoacid:acceptor oxidoreductase, delta subunit, pyruvate/2-ketoisovalerate family [<i>Fusobacterium varium</i> ATCC 27725]

<i>porA</i>	pyruvate ferredoxin oxidoreductase alpha subunit	EC:1.2.7.1	646284199	99.7	0	OFL89337.1 pyruvate ferredoxin oxidoreductase [<i>Fusobacterium</i> sp. HMSC073F01]
<i>porB</i>	pyruvate ferredoxin oxidoreductase beta subunit	EC:1.2.7.1	646284198	100.0	0	EES63525.2 thiamine pyrophosphate enzyme, C-terminal TPP binding domain protein [<i>Fusobacterium varium</i> ATCC 27725]
<i>atoB</i>	acetyl-CoA C-acetyltransferase	EC:2.3.1.9	646283343	100.0	0	EES64371.1 acetyl-CoA C-acetyltransferase [<i>Fusobacterium varium</i> ATCC 27725]
<i>atoB</i>	acetyl-CoA C-acetyltransferase	EC:2.3.1.9	646283326	100.0	0	EES64354.2 acetyl-CoA C-acetyltransferase [<i>Fusobacterium varium</i> ATCC 27725]
<i>hbd (paaH)</i>	3-hydroxybutyryl-CoA dehydrogenase	EC:1.1.1.157	646284062	100.0	0	EES63755.1 putative 3-hydroxybutyryl-CoA dehydrogenase [<i>Fusobacterium varium</i> ATCC 27725]
<i>hbd (paaH)</i>	3-hydroxybutyryl-CoA dehydrogenase	EC:1.1.1.157	646283324	100.0	0	EES64352.1 3-hydroxybutyryl-CoA dehydrogenase [<i>Fusobacterium varium</i> ATCC 27725]
<i>croR</i>	3-hydroxybutyryl-CoA dehydratase	EC:4.2.1.55	646285345	100.0	5.46E-91	WP_005948437.1 enoyl-CoA hydratase [<i>Fusobacterium varium</i>]
<i>croR</i>	3-hydroxybutyryl-CoA dehydratase	EC:4.2.1.55	646284822	100.0	1.11E-91	WP_005947840.1 enoyl-CoA hydratase [<i>Fusobacterium varium</i>]
<i>croR</i>	3-hydroxybutyryl-CoA dehydratase	EC:4.2.1.55	646283189	100.0	9.49E-93	WP_005946704.1 MULTISPECIES: enoyl-CoA hydratase [<i>Fusobacterium</i>]
<i>crt</i>	enoyl-CoA hydratase	EC:4.2.1.17	646283325	100.0	0	EES64353.1 3-hydroxybutyryl-CoA dehydratase [<i>Fusobacterium varium</i> ATCC 27725]
<i>bcd</i>	butyryl-CoA dehydrogenase	EC:1.3.8.1	646283190	100.0	0	EES65026.1 butyryl-CoA dehydrogenase [<i>Fusobacterium varium</i> ATCC 27725]
<i>etfB</i>	electron transfer flavoprotein beta subunit		646283191	100.0	0	EES65027.1 electron transfer flavoprotein subunit beta [<i>Fusobacterium varium</i> ATCC 27725]

<i>etfA</i>	electron transfer flavoprotein alpha subunit		646283192	100.0	0	EES65028.1 electron transfer flavoprotein subunit alpha [<i>Fusobacterium varium</i> ATCC 27725]
<i>cat2</i>	CoA-transferases	EC:2.8.3.-	646284915	100.0	0	EES63001.1 putative butyryl-CoA:acetate CoA-transferase [<i>Fusobacterium varium</i> ATCC 27725]
<i>atoA</i>	acetate CoA/acetoacetate CoA-transferase beta subunit	EC:2.8.3.8 2.8.3.9	646284367	100.0	1.65E-155	EES62466.1 butyrate--acetoacetate CoA-transferase subunit B [<i>Fusobacterium varium</i> ATCC 27725]
<i>atoD</i>	acetate CoA/acetoacetate CoA-transferase alpha subunit	EC:2.8.3.8 2.8.3.9	646284366	100.0	1.63E-150	EES62465.1 butyrate--acetoacetate CoA-transferase subunit A [<i>Fusobacterium varium</i> ATCC 27725]

Appendix V Table

CDS	Predicted function	Gene name	Enzyme commission	Identity (%)	e-value	Accession no.	Closely related protein
S3_Bin001-Eubacterium limosum-Wood Ljungdahl pathway							
EL_0481	formate dehydrogenase major subunit	fdoG	EC:1.2.1.2	99.9	0	WP_038352620.1	molybdopterin oxidoreductase [<i>Eubacterium limosum</i>]
EL_2901	formate dehydrogenase major subunit	fdoG	EC:1.2.1.2	99.6	0	WP_038354071.1	formate dehydrogenase subunit alpha [<i>Eubacterium limosum</i>]
EL_1797	formate--tetrahydrofolate ligase	fhs	EC:6.3.4.3	100.0	0	WP_038351869.1	formate--tetrahydrofolate ligase [<i>Eubacterium limosum</i>]
EL_1799	methylenetetrahydrofolate dehydrogenase (NADP+) / methenyltetrahydrofolate cyclohydrolase	folD	EC:1.5.1.5 3.5.4.9	100.0	0	WP_038351867.1	methylenetetrahydrofolate dehydrogenase [<i>Eubacterium limosum</i>]
EL_0761	methylenetetrahydrofolate reductase (NADPH)	metF	EC:1.5.1.20	99.6	0	WP_038351520.1	5,10-methylenetetrahydrofolate reductase [<i>Eubacterium limosum</i>]
EL_2312	5-methyltetrahydrofolate corrinoid/iron sulfur protein methyltransferase	acsE	EC:2.1.1.258	100.0	0	ADO38562.1	putative methyltetrahydrofolate:corrinoid/iron-sulfur protein methyltransferase [<i>Eubacterium limosum</i> KIST612]
EL_2310	CO dehydrogenase maturation factor	cooC		100.0	0	WP_038352889.1	carbon monoxide dehydrogenase [<i>Eubacterium limosum</i>]
EL_2311	carbon-monoxide dehydrogenase catalytic subunit	cooS	EC:1.2.7.4	100.0	0	WP_038352890.1	carbon-monoxide dehydrogenase catalytic subunit [<i>Eubacterium limosum</i>]
EL_0437	CO dehydrogenase maturation factor	cooC		83.0	1.67E-146	WP_026393828.1	cobyrinic acid a,c-diamide synthase [<i>Acetobacterium dehalogenans</i>]
EL_3306	CO dehydrogenase maturation factor	cooC		100.0	0	WP_038352894.1	carbon monoxide dehydrogenase [<i>Eubacterium limosum</i>]
EL_2364	CO dehydrogenase/acetyl-CoA synthase	acsB	EC:2.3.1.169	100.0	4.29E-92	ALU15664.1	CO dehydrogenase/acetyl-CoA synthase complex beta subunit CdhC [<i>Eubacterium limosum</i>]
EL_2770	acetyl-CoA decarbonylase/synthase complex subunit delta	cdhD	EC:2.1.1.245	100.0	0	WP_038352892.1	acetyl-CoA synthase subunit delta [<i>Eubacterium limosum</i>]
EL_3477	ferredoxin	fer		100.0	1.53E-34	WP_038353543.1	ferredoxin [<i>Eubacterium limosum</i>]
S3_Bin001-Eubacterium limosum-Glycerol oxidation 1							
EL_1252	glycerol dehydrogenase	gldA	EC:1.1.1.6	99.0	6.55E-140	WP_038353946.1	glycerol dehydrogenase [<i>Eubacterium limosum</i>]
EL_2236	glycerol dehydrogenase	gldA	EC:1.1.1.6	100.0	0	ADO38429.1	glycerol dehydrogenase [<i>Eubacterium limosum</i> KIST612]

EL_2306	dihydroxyacetone kinase, C-terminal domain	dhaL	EC:2.7.1.-	100.0	1.31E-154	WP_038351073.1	dihydroxyacetone kinase subunit L [<i>Eubacterium limosum</i>]
EL_2307	dihydroxyacetone kinase, N-terminal domain	dhaK	EC:2.7.1.-	99.7	0	SFO23221.1	dihydroxyacetone kinase DhaK subunit [<i>Eubacterium callanderi</i>]
EL_2319	dihydroxyacetone kinase, C-terminal domain	dhaL	EC:2.7.1.-	99.5	8.06E-151	SHL37728.1	dihydroxyacetone kinase DhaL subunit [<i>Eubacterium callanderi</i>]
EL_2320	dihydroxyacetone kinase, N-terminal domain	dhaK	EC:2.7.1.-	100.0	0	ALU13806.1	dihydroxyacetone kinase DhaK subunit [<i>Eubacterium limosum</i>]
EL_3187	dihydroxyacetone kinase, C-terminal domain	dhaL	EC:2.7.1.-	99.5	4.23E-149	WP_038352007.1	DAK2 domain-containing protein [<i>Eubacterium limosum</i>]
EL_2730	dihydroxyacetone kinase, N-terminal domain	dhaK	EC:2.7.1.-	100.0	0	SFO97100.1	dihydroxyacetone kinase, N-terminal domain [<i>Eubacterium callanderi</i>]
S3_Bin001-Eubacterium limosum-Glycerol oxidation 2							
EL_0172	glycerol kinase	glpK	EC:2.7.1.30	100.0	0	WP_038351422.1	glycerol kinase [<i>Eubacterium limosum</i>]
EL_1833	glycerol kinase	glpK	EC:2.7.1.30	100.0	0	SFO34581.1	glycerol kinase [<i>Eubacterium callanderi</i>]
EL_2689	glycerol kinase	glpK	EC:2.7.1.30	99.8	0	WP_038353941.1	glycerol kinase [<i>Eubacterium limosum</i>]
EL_3206	glycerol kinase	glpK	EC:2.7.1.30	99.2	0	ALU15928.1	carbohydrate kinase FGGY family [<i>Eubacterium limosum</i>]
EL_1275	glycerol-3-phosphate dehydrogenase (NAD(P)+)	gpsA	EC:1.1.1.94	100.0	0	WP_038350631.1	glycerol-3-phosphate dehydrogenase [<i>Eubacterium limosum</i>]
EL_2612	glycerol-3-phosphate dehydrogenase (NAD(P)+)	gpsA	EC:1.1.1.94	100.0	0	SHL05067.1	glycerol-3-phosphate dehydrogenase (NAD(P)+) [<i>Eubacterium callanderi</i>]
EL_1253	glycerol-3-phosphate dehydrogenase	glpA	EC:1.1.5.3	99.3	0	SFP62776.1	glycerol-3-phosphate dehydrogenase [<i>Eubacterium callanderi</i>]
EL_2328	glycerol-3-phosphate dehydrogenase	glpA	EC:1.1.5.3	99.2	2.50E-79	WP_038353344.1	FAD/NAD(P)-binding oxidoreductase [<i>Eubacterium limosum</i>]
EL_2688	glycerol-3-phosphate dehydrogenase	glpA	EC:1.1.5.3	99.8	0	WP_052237462.1	FAD-dependent oxidoreductase [<i>Eubacterium limosum</i>]
EL_3153	glycerol-3-phosphate dehydrogenase	glpA	EC:1.1.5.3	99.8	0	WP_038350670.1	FAD/NAD(P)-binding oxidoreductase [<i>Eubacterium limosum</i>]
EL_3213	glycerol-3-phosphate dehydrogenase	glpA	EC:1.1.5.3	99.5	0	WP_038351061.1	FAD/NAD(P)-binding oxidoreductase [<i>Eubacterium limosum</i>]
EL_3227	glycerol-3-phosphate dehydrogenase	glpA	EC:1.1.5.3	99.6	0	WP_038351204.1	FAD/NAD(P)-binding oxidoreductase [<i>Eubacterium limosum</i>]
EL_3453	glycerol-3-phosphate dehydrogenase	glpA	EC:1.1.5.3	99.3	0	ALU15927.1	FAD-dependent oxidoreductase [<i>Eubacterium limosum</i>]
EL_3629	glycerol-3-phosphate dehydrogenase	glpA	EC:1.1.5.3	100.0	2.37E-180	WP_052237143.1	hypothetical protein [<i>Eubacterium limosum</i>]
S3_Bin001-Eubacterium limosum-Central axis pathway							
EL_0336	triosephosphate isomerase	TPI	EC:5.3.1.1	97.9	1.28E-168	WP_038351440.1	triose-phosphate isomerase [<i>Eubacterium limosum</i>]

EL_1779	triosephosphate isomerase	TPI	EC:5.3.1.1	99.4	9.43E-121	WP_038351075.1	triose-phosphate isomerase [<i>Eubacterium limosum</i>]
EL_2048	triosephosphate isomerase	TPI	EC:5.3.1.1	98.8	1.40E-175	WP_038350858.1	triose-phosphate isomerase [<i>Eubacterium limosum</i>]
EL_2221	triosephosphate isomerase	TPI	EC:5.3.1.1	99.6	2.02E-167	WP_038353251.1	triose-phosphate isomerase [<i>Eubacterium limosum</i>]
EL_2050	glyceraldehyde 3-phosphate dehydrogenase	GAPDH	EC:1.2.1.12	100.0	0	WP_038350860.1	type I glyceraldehyde-3-phosphate dehydrogenase [<i>Eubacterium limosum</i>]
EL_2049	phosphoglycerate kinase	PGK	EC:2.7.2.3	99.5	0	SFO29749.1	phosphoglycerate kinase [<i>Eubacterium callanderi</i>]
EL_0942	probable phosphoglycerate mutase	gpmB	EC:5.4.2.12	99.6	6.77E-165	WP_038350984.1	histidine phosphatase family protein [<i>Eubacterium limosum</i>]
EL_3566	2,3-bisphosphoglycerate-independent phosphoglycerate mutase	gpmI	EC:5.4.2.12	99.3	1.17E-98	WP_038350857.1	2,3-bisphosphoglycerate-independent phosphoglycerate mutase [<i>Eubacterium limosum</i>]
EL_1404	2,3-bisphosphoglycerate-dependent phosphoglycerate mutase	PGAM	EC:5.4.2.11	99.4	2.03E-126	WP_038351252.1	phosphoglyceromutase [<i>Eubacterium limosum</i>]
EL_2137	enolase	ENO	EC:4.2.1.11	99.2	0	SDO52761.1	enolase [<i>Eubacterium limosum</i>]
EL_2047	pyruvate kinase	pyk	EC:2.7.1.40	99.3	0	ADO38040.1	pyruvate kinase [<i>Eubacterium limosum</i> KIST612]
EL_3535	pyruvate dehydrogenase E2 component (dihydrolipoamide acetyltransferase)	DLAT/pdhc	EC:2.3.1.12	100.0	2.40E-69	WP_038351974.1	hypothetical protein [<i>Eubacterium limosum</i>]
EL_3377	pyruvate dehydrogenase E1 component beta subunit	PDHB	EC:1.2.4.1	100.0	0	WP_038351975.1	alpha-ketoacid dehydrogenase subunit beta [<i>Eubacterium limosum</i>]
EL_3375	pyruvate dehydrogenase E1 component alpha subunit	PDHA	EC:1.2.4.1	100.0	0	SHL32931.1	pyruvate dehydrogenase E1 component alpha subunit [<i>Eubacterium callanderi</i>]
EL_0124	pyruvate ferredoxin oxidoreductase gamma subunit	porG	EC:1.2.7.1	100.0	2.88E-128	ALU13014.1	2-ketoisovalerate ferredoxin oxidoreductase gamma subunit [<i>Eubacterium limosum</i>]
EL_0125	pyruvate ferredoxin oxidoreductase delta subunit	porD	EC:1.2.7.1	99.0	5.47E-67	WP_038351933.1	pyruvate ferredoxin oxidoreductase [<i>Eubacterium limosum</i>]
EL_0126	pyruvate ferredoxin oxidoreductase alpha subunit	porA	EC:1.2.7.1	99.7	0	WP_038351932.1	pyruvate ferredoxin oxidoreductase [<i>Eubacterium limosum</i>]
EL_0127	pyruvate ferredoxin oxidoreductase beta subunit	porB	EC:1.2.7.1	99.7	0	WP_038351931.1	2-ketoisovalerate ferredoxin oxidoreductase [<i>Eubacterium limosum</i>]
EL_2451	pyruvate ferredoxin oxidoreductase alpha subunit	porA	EC:1.2.7.1	99.5	0	WP_038353372.1	pyruvate ferredoxin oxidoreductase [<i>Eubacterium limosum</i>]
EL_2452	pyruvate ferredoxin oxidoreductase beta subunit	porB	EC:1.2.7.1	99.7	0	WP_038353373.1	pyruvate ferredoxin oxidoreductase [<i>Eubacterium limosum</i>]
EL_3198	pyruvate ferredoxin oxidoreductase delta subunit	porD	EC:1.2.7.1	100.0	1.07E-67	WP_038353371.1	ferredoxin [<i>Eubacterium limosum</i>]

EL_3199	pyruvate ferredoxin oxidoreductase gamma subunit	porG	EC:1.2.7.1	100.0	2.61E-138	WP_038353370.1	pyruvate synthase [<i>Eubacterium limosum</i>]
S3_Bin001-Eubacterium limosum-Acetate production							
EL_2856	putative phosphotransacetylase	Pta	EC:2.3.1.8	99.1	1.53E-74	WP_041690457.1	MULTISPECIES: phosphate propanoyltransferase [<i>Clostridiales</i>]
EL_3750	putative phosphotransacetylase	Pta	EC:2.3.1.8	99.5	3.62E-144	WP_038352709.1	phosphate propanoyltransferase [<i>Eubacterium limosum</i>]
EL_2391	acetate kinase	ackA	EC:2.7.2.1	100.0	0	WP_038354231.1	acetate kinase [<i>Eubacterium limosum</i>]
S3_Bin001-Eubacterium limosum-Butyrate production							
EL_0510	putative acetyltransferase	yiaC	EC:2.3.1.-	68.6	5.37E-67	WP_033143003.1	GNAT family N-acetyltransferase [<i>Blautia producta</i>]
EL_0991	acetyltransferase	EpsM	EC:2.3.1.-	94.8	2.07E-141	SFP55793.1	sugar O-acyltransferase, sialic acid O-acetyltransferase NeuD family [<i>Eubacterium callanderi</i>]
EL_1705	putative acetyltransferase	yjgM	EC:2.3.1.-	99.4	2.30E-115	WP_038351624.1	N-acetyltransferase [<i>Eubacterium limosum</i>]
EL_3474	acetyltransferase	EpsM	EC:2.3.1.-	89.3	2.38E-118	WP_038352497.1	hypothetical protein [<i>Eubacterium limosum</i>]
EL_2590	3-hydroxybutyryl-CoA dehydrogenase	paaH	EC:1.1.1.157	100.0	0	SFO26749.1	3-hydroxybutyryl-CoA dehydrogenase [<i>Eubacterium callanderi</i>]
EL_2589	enoyl-CoA hydratase	crt	EC:4.2.1.17	100.0	3.40E-101	ADO35554.1	3-hydroxybutyryl-CoA dehydratase [<i>Eubacterium limosum</i> KIST612]
EL_1565	butyryl-CoA dehydrogenase	bcd	EC:1.3.8.1	96.4	0	ADO35336.1	acyl-coa dehydrogenase [<i>Eubacterium limosum</i> KIST612]
EL_2591	butyryl-CoA dehydrogenase	bcd	EC:1.3.8.1	100.0	0	SFO26775.1	butyryl-CoA dehydrogenase [<i>Eubacterium callanderi</i>]
EL_2676	butyryl-CoA dehydrogenase	bcd	EC:1.3.8.1	98.9	5.64E-123	WP_038353017.1	acyl-CoA dehydrogenase [<i>Eubacterium limosum</i>]
EL_3828	butyryl-CoA dehydrogenase	bcd	EC:1.3.8.1	99.3	0	OEZ04909.1	acyl-CoA dehydrogenase [[<i>Butyribacterium</i>] <i>methylotrophicum</i>]
EL_2592	electron transfer flavoprotein beta subunit	etfB		100.0	0	WP_038350951.1	electron transfer flavoprotein subunit beta [<i>Eubacterium limosum</i>]
EL_2593	electron transfer flavoprotein alpha subunit	etfA		100.0	0	ALU16220.1	electron transfer flavoprotein alpha subunit [<i>Eubacterium limosum</i>]
EL_3536	propionate CoA-transferase	pct	EC:2.8.3.1	99.4	0	WP_038353018.1	3-oxoacid CoA-transferase [<i>Eubacterium limosum</i>]
EL_0598	phosphate butyryltransferase	ptb	EC:2.3.1.19	99.3	0	WP_038352195.1	phosphate butyryltransferase [<i>Eubacterium limosum</i>]
EL_2569	phosphate butyryltransferase	ptb	EC:2.3.1.19	100.0	0	WP_052237430.1	phosphate butyryltransferase [<i>Eubacterium limosum</i>]
S3_Bin001-Eubacterium limosum-Ethanol production/oxidation							
EL_1813	propionaldehyde dehydrogenase	pduP	EC:1.2.1.87	99.4	1.84E-120	WP_058696328.1	aldehyde dehydrogenase EutE [<i>Eubacterium limosum</i>]

EL_3666	acetaldehyde dehydrogenase / alcohol dehydrogenase	adhE	EC:1.2.1.10 1.1.1.1	99.7	0	SFO36846.1	hypothetical protein SAMN04487888_101644 [<i>Eubacterium callanderi</i>]
EL_3755	acetaldehyde dehydrogenase / alcohol dehydrogenase	adhE	EC:1.2.1.10 1.1.1.1	99.7	0	WP_038353188.1	butanol dehydrogenase [<i>Eubacterium limosum</i>]
EL_1064	alcohol dehydrogenase	adh2	EC:1.1.1.-	100.0	0	SFP64208.1	alcohol dehydrogenase [<i>Eubacterium callanderi</i>]
S3_Bin001-Eubacterium limosum-Glycerol reduction to 1,3-PDO							
EL_1849	propanediol dehydratase small subunit	pduE	EC:4.2.1.28	100.0	1.50E-118	WP_038352519.1	propanediol dehydratase [<i>Eubacterium limosum</i>]
EL_1850	propanediol dehydratase medium subunit	pduD	EC:4.2.1.28	100.0	2.87E-159	ALU13308.1	propanediol dehydratase medium subunit PduD [<i>Eubacterium limosum</i>]
EL_1851	propanediol dehydratase large subunit	pduC	EC:4.2.1.28	100.0	0	SFP43929.1	propanediol dehydratase large subunit [<i>Eubacterium callanderi</i>]
EL_3115	1,3-propanediol dehydrogenase	dhaT	EC:1.1.1.202	99.8	0	OEZ04839.1	1,3-propanediol dehydrogenase [[<i>Butyribacterium methylophilicum</i>]]
S3_Bin001-Eubacterium limosum-Membrane proteins involved in energy conservation-Rnf complex							
EL_2763	electron transport complex protein RnfC	rnfC		100.0	0	WP_038351329.1	electron transporter RnfC [<i>Eubacterium limosum</i>]
EL_2764	electron transport complex protein RnfD	rnfD		99.7	0	ADO37623.1	RnfD [<i>Eubacterium limosum</i> KIST612]
EL_2765	electron transport complex protein RnfG	rnfG		99.5	8.40E-146	WP_052237107.1	electron transporter [<i>Eubacterium limosum</i>]
S3_Bin001-Eubacterium limosum-Membrane proteins involved in energy conservation-FAD (or Fe-S) reductase linked to ETF							
EL_2516	Acryloyl-CoA reductase electron transfer subunit beta	etfA		91.8	0	SHL94193.1	electron transfer flavoprotein alpha subunit apoprotein [<i>Eubacterium callanderi</i>]
EL_2515	Acryloyl-CoA reductase electron transfer subunit gamma	etfB		98.5	0	WP_038352172.1	hypothetical protein [<i>Eubacterium limosum</i>]
EL_2514	putative FAD-linked oxidoreductase			96.7	0	WP_038352173.1	FAD-binding oxidoreductase [<i>Eubacterium limosum</i>]
S3_Bin001-Eubacterium limosum-Hydrogenases and coupling enzymes							
EL_0587	NADP-reducing hydrogenase subunit HndC	HndC	EC:1.12.1.3	100.0	0	ADO35860.1	NADH dehydrogenase (quinone) [<i>Eubacterium limosum</i> KIST612]

EL_0588	NADP-reducing hydrogenase subunit HndB	HndB	EC:1.12.1.3	100.0	5.63E-88	SDP44400.1	NAD(P)-dependent iron-only hydrogenase iron-sulfur protein [<i>Eubacterium limosum</i>]
EL_2881	Iron hydrogenase 1			99.4	9.33E-106	WP_038352187.1	ferredoxin [<i>Eubacterium limosum</i>]
EL_3665	Ferredoxin, 2Fe-2S			100.0	1.94E-54	ADO36201.1	NADH dehydrogenase subunit E [<i>Eubacterium limosum</i> KIST612]
S3_Bin001-Eubacterium limosum-ATPase							
EL_0572	V/A-type H ⁺ /Na ⁺ -transporting ATPase subunit D	ATPVD		100.0	4.51E-150	SHL59650.1	V/A-type H ⁺ -transporting ATPase subunit D [<i>Eubacterium callanderi</i>]
EL_0573	V/A-type H ⁺ /Na ⁺ -transporting ATPase subunit B	ATPVB		100.0	0	SHL59622.1	V/A-type H ⁺ -transporting ATPase subunit B [<i>Eubacterium callanderi</i>]
EL_0574	V/A-type H ⁺ /Na ⁺ -transporting ATPase subunit A	ATPVA	[EC:3.6.3.14; 3.6.3.15]	99.8	0	SHL59593.1	V/A-type H ⁺ -transporting ATPase subunit A [<i>Eubacterium callanderi</i>]
EL_0575	V/A-type H ⁺ /Na ⁺ -transporting ATPase subunit F	ATPVF		100.0	8.02E-69	SHL59561.1	V/A-type H ⁺ -transporting ATPase subunit F [<i>Eubacterium callanderi</i>]
EL_0576	V/A-type H ⁺ /Na ⁺ -transporting ATPase subunit C	ATPVC		99.7	0	WP_038351649.1	hypothetical protein [<i>Eubacterium limosum</i>]
EL_0577	V/A-type H ⁺ /Na ⁺ -transporting ATPase subunit E	ATPVE		100.0	1.47E-139	WP_038351650.1	hypothetical protein [<i>Eubacterium limosum</i>]
EL_0578	V/A-type H ⁺ /Na ⁺ -transporting ATPase subunit K	ATPVK		100.0	1.18E-99	ALU14703.1	V-type ATP synthase subunit K [<i>Eubacterium limosum</i>]
EL_0579	V/A-type H ⁺ /Na ⁺ -transporting ATPase subunit I	ATPVI		99.7	0	SHL59440.1	V/A-type H ⁺ -transporting ATPase subunit I [<i>Eubacterium callanderi</i>]
EL_0580	V/A-type H ⁺ /Na ⁺ -transporting ATPase subunit G/H	ATPVG		100.0	3.89E-61	SHL59409.1	V/A-type H ⁺ -transporting ATPase subunit G/H [<i>Eubacterium callanderi</i>]
S3_Bin002-Actinomyces provencensis-Glycerol oxidation 2							
AP_0600	glycerol kinase	glpK	EC:2.7.1.30	97.0	0	WP_043535862.1	glycerol kinase [<i>Actinomyces polynesiensis</i>]
AP_1408	glycerol-3-phosphate dehydrogenase (NAD(P) ⁺)	gpsA	EC:1.1.1.94	97.6	0	WP_075890310.1	glycerol-3-phosphate acyltransferase [<i>Actinomyces provencensis</i>]
AP_1337	glycerol-3-phosphate dehydrogenase subunit C	glpC	EC:1.1.5.3	100.0	0	WP_052450782.1	sn-glycerol-3-phosphate dehydrogenase subunit C [<i>Actinomyces polynesiensis</i>]

AP_1338	glycerol-3-phosphate dehydrogenase subunit B	glpB	EC:1.1.5.3	99.0	0	WP_075888552.1	anaerobic glycerol-3-phosphate dehydrogenase subunit B [<i>Actinomyces provencensis</i>]
AP_1339	glycerol-3-phosphate dehydrogenase	glpA	EC:1.1.5.3	99.1	0	WP_075888554.1	sn-glycerol-3-phosphate dehydrogenase subunit A [<i>Actinomyces provencensis</i>]
AP_2140	glycerol-3-phosphate dehydrogenase	glpA	EC:1.1.5.3	98.1	0	WP_075890934.1	glycerol-3-phosphate dehydrogenase [<i>Actinomyces provencensis</i>]
AP_2141	glycerol uptake facilitator protein	GLPF		97.4	0	WP_043535861.1	glycerol transporter [<i>Actinomyces polynesiensis</i>]
S3_Bin002-Actinomyces provencensis-Central axis pathway							
AP_0084	triosephosphate isomerase (TIM)	TPI	EC:5.3.1.1	45.4	1.47E-61	WP_025733286.1	triose-phosphate isomerase [<i>Carnimonas nigrificans</i>]
AP_0330	triosephosphate isomerase (TIM)	TPI	EC:5.3.1.1	99.4	1.31E-116	WP_075889582.1	triose-phosphate isomerase [<i>Actinomyces provencensis</i>]
AP_1462	glyceraldehyde 3-phosphate dehydrogenase	GAPDH	EC:1.2.1.12	92.5	0	WP_043535446.1	type I glyceraldehyde-3-phosphate dehydrogenase [<i>Actinomyces polynesiensis</i>]
AP_2270	glyceraldehyde 3-phosphate dehydrogenase	GAPDH	EC:1.2.1.12	98.8	0	WP_075889586.1	type I glyceraldehyde-3-phosphate dehydrogenase [<i>Actinomyces provencensis</i>]
AP_2271	phosphoglycerate kinase	PGK	EC:2.7.2.3	97.5	0	WP_075889584.1	phosphoglycerate kinase [<i>Actinomyces provencensis</i>]
AP_0092	probable phosphoglycerate mutase	gpmB	EC:5.4.2.12	99.6	7.27E-164	WP_075889274.1	hypothetical protein [<i>Actinomyces provencensis</i>]
AP_0589	probable phosphoglycerate mutase	gpmB	EC:5.4.2.12	98.3	1.48E-165	WP_043536912.1	histidine phosphatase family protein [<i>Actinomyces polynesiensis</i>]
AP_1075	2,3-bisphosphoglycerate-dependent phosphoglycerate mutase	PGAM	EC:5.4.2.11	100.0	4.81E-180	WP_075892264.1	phosphoglyceromutase [<i>Actinomyces provencensis</i>]
AP_2479	pyruvate, orthophosphate dikinase	ppdK	EC:2.7.9.1	99.5	0	WP_075892335.1	pyruvate, phosphate dikinase [<i>Actinomyces provencensis</i>]
AP_2496	Pyruvate kinase	pyk	EC:2.7.1.40	99.7	0	WP_075889634.1	pyruvate kinase [<i>Actinomyces provencensis</i>]
AP_1108	pyruvate dehydrogenase E1 component beta subunit	PDHB	EC:1.2.4.1	99.6	4.35E-174	WP_075891946.1	alpha-ketoacid dehydrogenase subunit beta [<i>Actinomyces provencensis</i>]
AP_1552	pyruvate dehydrogenase E1 component	aceE	EC:1.2.4.1	98.1	0	WP_075888434.1	pyruvate dehydrogenase (acetyl-transferring), homodimeric type [<i>Actinomyces provencensis</i>]
AP_2544	pyruvate dehydrogenase E1 component alpha subunit	PDHA	EC:1.2.4.1	99.7	0	WP_075891944.1	ABC transporter substrate-binding protein [<i>Actinomyces provencensis</i>]

AP_1107	pyruvate dehydrogenase E2 component (dihydrolipoamide acetyltransferase)	DLAT	EC:2.3.1.12	97.4	0	WP_075891948.1	diaminohydroxyphosphoribosylaminopyrimidine deaminase [<i>Actinomyces provencensis</i>]
S3_Bin002-Actinomyces provencensis-Acetate production							
AP_0652	phosphate acetyltransferase	pta	EC:2.3.1.8	71.9	0	ENO18742.1	phosphate acetyltransferase [<i>Actinomyces cardiffensis</i> F0333]
AP_0653	acetate kinase	ackA	EC:2.7.2.1	99.7	0	WP_078062518.1	acetate kinase [<i>Actinomyces provencensis</i>]
S3_Bin002-Actinomyces provencensis-Ethanol production/oxidation							
AP_0159	acetaldehyde dehydrogenase / alcohol dehydrogenase	adhE	EC:1.2.1.10 1.1.1.1	98.4	0	WP_078062118.1	hypothetical protein [<i>Actinomyces provencensis</i>]
S3_Bin002-Actinomyces provencensis-Membrane proteins involved in energy conservation-Fix system							
AP_1658	electron transfer flavoprotein beta subunit	fixA		100.0	0	WP_075888696.1	electron transfer flavoprotein subunit beta [<i>Actinomyces provencensis</i>]
AP_1659	electron transfer flavoprotein alpha subunit	fixB		100.0	0	WP_075888694.1	electron transporter [<i>Actinomyces provencensis</i>]
AP_1631	electron transfer flavoprotein beta subunit	fixA		99.6	0	WP_075889900.1	hypothetical protein [<i>Actinomyces provencensis</i>]
AP_1632	electron transfer flavoprotein alpha subunit	fixB		99.3	0	WP_052450841.1	hypothetical protein [<i>Actinomyces polynesiensis</i>]
AP_1633	electron transfer flavoprotein-quinone oxidoreductase	fixC	EC:1.5.5.-	97.7	0	WP_075889897.1	hypothetical protein [<i>Actinomyces provencensis</i>]
AP_1634	ferredoxin like protein	fixX		99.0	1.05E-66	WP_043536735.1	MULTISPECIES: hypothetical protein [<i>Actinomyces</i>]
S3_Bin003-Anaerostipes caccae-Glycerol oxidation 1							
AC_1263	Glycerol dehydrogenase	gldA	EC:1.1.1.6	100.0	0	CDC34132.1	glycerol dehydrogenase [<i>Anaerostipes</i> sp. CAG:276]
AC_2829	Glycerol dehydrogenase	gldA	EC:1.1.1.6	100.0	0	WP_006567890.1	MULTISPECIES: glycerol dehydrogenase [<i>Anaerostipes</i>]
AC_1206	dihydroxyacetone kinase, C-terminal domain	dhaL	EC:2.7.1.-	100.0	3.54E-145	EFV23311.1	DAK2 domain-containing protein [<i>Anaerostipes</i> sp. 3_2_56FAA]
AC_1207	dihydroxyacetone kinase, N-terminal domain	dhaK	EC:2.7.1.-	100.0	0	EFV23312.1	Dak1 domain-containing protein [<i>Anaerostipes</i> sp. 3_2_56FAA]
AC_1210	dihydroxyacetone kinase, N-terminal domain	dhaK	EC:2.7.1.-	100.0	0	EFV23315.1	Dak1 domain-containing protein [<i>Anaerostipes</i> sp. 3_2_56FAA]
AC_1938	dihydroxyacetone kinase, C-terminal domain	dhaL	EC:2.7.1.-	100.0	1.75E-151	EFV22428.1	DAK2 domain-containing protein [<i>Anaerostipes</i> sp. 3_2_56FAA]
AC_1936	dihydroxyacetone kinase, N-terminal domain	dhaK	EC:2.7.1.-	100.0	0	EFV22430.1	Dak1 domain-containing protein [<i>Anaerostipes</i> sp. 3_2_56FAA]

AC_2476	dihydroxyacetone kinase, C-terminal domain	dhaL	EC:2.7.1.-	100.0	2.78E-151	EFV21282.1	DAK2 domain-containing protein [<i>Anaerostipes</i> sp. 3_2_56FAA]
AC_2477	dihydroxyacetone kinase, N-terminal domain	dhaK	EC:2.7.1.-	99.4	0	EDR98779.1	DAK1 domain protein [<i>Anaerostipes caccae</i> DSM 14662]
S3_Bin003-Anaerostipes caccae-Glycerol oxidation 2							
AC_1043	Glycerol kinase	glpK	EC:2.7.1.30	100.0	0	EFV23466.1	glycerol kinase [<i>Anaerostipes</i> sp. 3_2_56FAA]
AC_2316	glycerol-3-phosphate dehydrogenase (NAD(P)+)	gpsA	EC:1.1.1.94	100.0	0	EDR98278.1	putative glycerol-3-phosphate dehydrogenase [NAD(P)+] [<i>Anaerostipes caccae</i> DSM 14662]
AC_2751	glycerol-3-phosphate dehydrogenase (NAD(P)+)	gpsA	EC:1.1.1.94	99.7	0	EFV20853.1	NAD-dependent glycerol-3-phosphate dehydrogenase [<i>Anaerostipes</i> sp. 3_2_56FAA]
AC_2771	glycerol-3-phosphate dehydrogenase (NAD(P)+)	gpsA	EC:1.1.1.94	100.0	0	EDR96703.1	NAD-dependent glycerol-3-phosphate dehydrogenase C-terminal domain protein [<i>Anaerostipes caccae</i> DSM 14662]
AC_2774	glycerol-3-phosphate dehydrogenase	glpA	EC:1.1.5.3	100.0	0	EDR96700.1	FAD dependent oxidoreductase [<i>Anaerostipes caccae</i> DSM 14662]
S3_Bin003-Anaerostipes caccae-Central axis pathway							
AC_2282	triosephosphate isomerase (TIM)	TPI	EC:5.3.1.1	100.0	0	WP_039930792.1	MULTISPECIES: triose-phosphate isomerase [<i>Anaerostipes</i>]
AC_2625	triosephosphate isomerase (TIM)	TPI	EC:5.3.1.1	100.0	8.82E-167	EDR98634.1	triose-phosphate isomerase [<i>Anaerostipes caccae</i> DSM 14662]
AC_2905	triosephosphate isomerase (TIM)	TPI	EC:5.3.1.1	99.6	8.81E-166	EFV22551.1	triose-phosphate isomerase [<i>Anaerostipes</i> sp. 3_2_56FAA]
AC_2280	glyceraldehyde 3-phosphate dehydrogenase	GAPDH	EC:1.2.1.12	100.0	0	EFV20889.1	glyceraldehyde-3-phosphate dehydrogenase [<i>Anaerostipes</i> sp. 3_2_56FAA]
AC_2281	phosphoglycerate kinase	PGK	EC:2.7.2.3	100.0	0	EDR96773.1	phosphoglycerate kinase [<i>Anaerostipes caccae</i> DSM 14662]
AC_1377	probable phosphoglycerate mutase	gpmB	EC:5.4.2.12	100.0	1.08E-147	EFV23711.1	phosphoglycerate mutase [<i>Anaerostipes</i> sp. 3_2_56FAA]
AC_1628	probable phosphoglycerate mutase	gpmB	EC:5.4.2.12	100.0	0	CDC34743.1	phosphoglycerate mutase family protein [<i>Anaerostipes</i> sp. CAG:276]
AC_2285	2,3-bisphosphoglycerate-independent phosphoglycerate mutase	gpmI	EC:5.4.2.12	100.0	0	EDR96770.1	2,3-bisphosphoglycerate-independent phosphoglycerate mutase [<i>Anaerostipes caccae</i> DSM 14662]
AC_2393	2,3-bisphosphoglycerate-independent phosphoglycerate mutase	apgM	EC:5.4.2.12	99.7	0	EFV22357.1	proposed homoserine kinase [<i>Anaerostipes</i> sp. 3_2_56FAA]
AC_2286	enolase	ENO	EC:4.2.1.11	100.0	0	EFV20895.1	phosphopyruvate hydratase [<i>Anaerostipes</i> sp. 3_2_56FAA]

AC_0934	pyruvate kinase	PK	EC:2.7.1.40	100.0	0	CDC35279.1	pyruvate kinase [<i>Anaerostipes</i> sp. CAG:276]
AC_2439	pyruvate-ferredoxin/ flavodoxin oxidoreductase	por	EC:1.2.7.1 1.2.7.-	100.0	0	CDC36269.1	pyruvate-flavodoxin oxidoreductase [<i>Anaerostipes</i> sp. CAG:276]
S3_Bin003-Anaerostipes caccae-Acetate production							
AC_0919	phosphate acetyltransferase	pta	EC:2.3.1.8	100.0	0	EDR99093.1	phosphate acetyltransferase [<i>Anaerostipes caccae</i> DSM 14662]
AC_0918	Acetate kinase	ackA	EC:2.7.2.1	100.0	0	CDC35243.1	acetate kinase [<i>Anaerostipes</i> sp. CAG:276]
S3_Bin003-Anaerostipes caccae-Butyrate and caproate production							
AC_3098	Acetyl-CoA acetyltransferase	atoB	EC:2.3.1.9	100.0	0	WP_039930536.1	acetyl-CoA acetyltransferase [<i>Anaerostipes</i> sp. 3_2_56FAA]
AC_3096	3-hydroxybutyryl-CoA dehydrogenase	paaH	EC:1.1.1.157	100.0	0	EFV21686.1	3-hydroxyacyl-CoA dehydrogenase [<i>Anaerostipes</i> sp. 3_2_56FAA]
AC_2405	3-hydroxybutyryl-CoA dehydratase	croR	EC:4.2.1.55	100.0	4.26E-103	WP_006568567.1	MULTISPECIES: enoyl-CoA hydratase [<i>Anaerostipes</i>]
AC_2590	3-hydroxybutyryl-CoA dehydratase	croR	EC:4.2.1.55	100.0	7.77E-94	WP_009290664.1	enoyl-CoA hydratase [<i>Anaerostipes</i> sp. 3_2_56FAA]
AC_3097	enoyl-CoA hydratase	crt	EC:4.2.1.17	100.0	0	EDR99005.1	3-hydroxybutyryl-CoA dehydratase [<i>Anaerostipes caccae</i> DSM 14662]
AC_3178	enoyl-CoA hydratase	crt	EC:4.2.1.17	100.0	0	EFV23880.1	enoyl-CoA hydratase/isomerase [<i>Anaerostipes</i> sp. 3_2_56FAA]
AC_0139	butyryl-CoA dehydrogenase	bcd	EC:1.3.8.1	100.0	0	EDR97724.1	acyl-CoA dehydrogenase, C-terminal domain protein [<i>Anaerostipes caccae</i> DSM 14662]
AC_0429	butyryl-CoA dehydrogenase	bcd	EC:1.3.8.1	100.0	0	EDR98937.1	acyl-CoA dehydrogenase, C-terminal domain protein [<i>Anaerostipes caccae</i> DSM 14662]
AC_0474	butyryl-CoA dehydrogenase	bcd	EC:1.3.8.1	100.0	0	EFV23995.1	acyl-CoA dehydrogenase domain-containing protein [<i>Anaerostipes</i> sp. 3_2_56FAA]
AC_0842	butyryl-CoA dehydrogenase	bcd	EC:1.3.8.1	100.0	0	EDR96341.1	acyl-CoA dehydrogenase, C-terminal domain protein [<i>Anaerostipes caccae</i> DSM 14662]
AC_3095	butyryl-CoA dehydrogenase	bcd	EC:1.3.8.1	100.0	0	EFV21687.1	acyl-CoA dehydrogenase domain-containing protein [<i>Anaerostipes</i> sp. 3_2_56FAA]
AC_3177	butyryl-CoA dehydrogenase	bcd	EC:1.3.8.1	100.0	0	EFV23879.1	acyl-CoA dehydrogenase domain-containing protein [<i>Anaerostipes</i> sp. 3_2_56FAA]

								sp. 3_2_56FAA]
AC_2406	propionate CoA-transferase	pct	EC:2.8.3.1	100.0	0	CDC36734.1	acetate CoA-transferase YdiF [<i>Anaerostipes</i> sp. CAG:276]	
AC_3179	propionate CoA-transferase	pct	EC:2.8.3.1	100.0	0	CDC38503.1	acetate CoA-transferase YdiF [<i>Anaerostipes</i> sp. CAG:276]	
AC_2592	4-hydroxybutyrate CoA-transferase	cat2	EC:2.8.3.-	100.0	0	CDC37756.1	acetyl-CoA hydrolase/transferase domain-containing protein [<i>Anaerostipes</i> sp. CAG:276]	
AC_1067	acetate CoA/acetoacetate CoA-transferase alpha subunit	atoD	EC:2.8.3.8 2.8.3.9	100.0	5.51E-174	EFV23538.1	coenzyme A transferase [<i>Anaerostipes</i> sp. 3_2_56FAA]	
AC_1577	acetate CoA-transferase	ydiF	EC:2.8.3.8	99.8	0	CDC36559.1	acetate CoA-transferase YdiF [<i>Anaerostipes</i> sp. CAG:276]	
AC_3093	electron transfer flavoprotein alpha subunit	etfA		100.0	0	EFV21689.1	electron transfer flavoprotein FAD-binding domain-containing protein [<i>Anaerostipes</i> sp. 3_2_56FAA]	
AC_3094	electron transfer flavoprotein beta subunit	etfB		100.0	0	EDR99002.1	electron transfer flavoprotein domain protein [<i>Anaerostipes caccae</i> DSM 14662]	
S3_Bin003-<i>Anaerostipes caccae</i>-Ethanol production/oxidation								
AC_0262	aldehyde dehydrogenase (NAD+)	ALDH	EC:1.2.1.3	100.0	0	CDC37217.1	aldehyde dehydrogenase [<i>Anaerostipes</i> sp. CAG:276]	
AC_0555	alcohol dehydrogenase	adh2	EC:1.1.1.-	100.0	0	CDC36055.1	iron-containing alcohol dehydrogenase [<i>Anaerostipes</i> sp. CAG:276]	
AC_1073	alcohol dehydrogenase	adh2	EC:1.1.1.-	100.0	0	EDR96137.1	alcohol dehydrogenase, iron-dependent [<i>Anaerostipes caccae</i> DSM 14662]	
AC_1564	alcohol dehydrogenase	adh2	EC:1.1.1.-	100.0	0	CDC36582.1	iron-containing alcohol dehydrogenase [<i>Anaerostipes</i> sp. CAG:276]	
AC_1780	alcohol dehydrogenase	adh2	EC:1.1.1.-	99.7	0	CDC38414.1	alcohol dehydrogenase iron-dependent [<i>Anaerostipes</i> sp. CAG:276]	
AC_2010	alcohol dehydrogenase	yiaY	EC:1.1.1.1	100.0	0	EFV21981.1	iron-containing alcohol dehydrogenase [<i>Anaerostipes</i> sp. 3_2_56FAA]	
AC_2521	alcohol dehydrogenase	adh2	EC:1.1.1.-	100.0	0	EDR97981.1	alcohol dehydrogenase, iron-dependent [<i>Anaerostipes caccae</i> DSM 14662]	
AC_2544	alcohol dehydrogenase	adh2	EC:1.1.1.-	100.0	0	EFV22801.1	iron-containing alcohol dehydrogenase [<i>Anaerostipes</i> sp. 3_2_56FAA]	

AC_3251	alcohol dehydrogenase	adh2	EC:1.1.1.-	100.0	0	EFV23191.1	iron-containing alcohol dehydrogenase [<i>Anaerostipes</i> sp. 3_2_56FAA]
S3_Bin003-<i>Anaerostipes caccae</i>-Membrane proteins involved in energy conservation-Rnf complex							
AC_0354	electron transport complex protein RnfB	rnfB		100.0	0	EDR98046.1	electron transport complex, RnfABCDGE type, B subunit [<i>Anaerostipes caccae</i> DSM 14662]
AC_0355	electron transport complex protein RnfA	rnfA		100.0	3.37E-129	EDR98047.1	electron transport complex, RnfABCDGE type, A subunit [<i>Anaerostipes caccae</i> DSM 14662]
AC_0356	electron transport complex protein RnfE	rnfE		100.0	1.60E-164	EDR98048.1	electron transport complex, RnfABCDGE type, E subunit [<i>Anaerostipes caccae</i> DSM 14662]
AC_0357	electron transport complex protein RnfG	rnfG		100.0	4.20E-141	EDR98049.1	electron transport complex, RnfABCDGE type, G subunit [<i>Anaerostipes caccae</i> DSM 14662]
AC_0358	electron transport complex protein RnfD	rnfD		100.0	0	EFV22725.1	electron transport complex [<i>Anaerostipes</i> sp. 3_2_56FAA]
AC_0359	electron transport complex protein RnfC	rnfC		100.0	0	EFV22726.1	electron transport complex [<i>Anaerostipes</i> sp. 3_2_56FAA]
S3_Bin003-<i>Anaerostipes caccae</i>-Membrane proteins involved in energy conservation-FAD (or Fe-S) reductase lined to ETF							
AC_0138	putative FAD-linked oxidoreductase			100.0	0	EFV23038.1	glycolate oxidase [<i>Anaerostipes</i> sp. 3_2_56FAA]
AC_0140	Acryloyl-CoA reductase electron transfer subunit gamma			100.0	0	EDR97725.1	electron transfer flavoprotein subunit beta [<i>Anaerostipes caccae</i> DSM 14662]
AC_0141	Acryloyl-CoA reductase electron transfer subunit beta			100.0	0	EFV23041.1	electron transfer flavoprotein FAD-binding domain-containing protein [<i>Anaerostipes</i> sp. 3_2_56FAA]
AC_0143	Acryloyl-CoA reductase electron transfer subunit gamma			100.0	0	EFV23044.1	electron transfer flavoprotein domain-containing protein [<i>Anaerostipes</i> sp. 3_2_56FAA]
AC_0144	Acryloyl-CoA reductase electron transfer subunit beta			100.0	0	EFV23045.1	electron transfer flavoprotein FAD-binding domain-containing protein [<i>Anaerostipes</i> sp. 3_2_56FAA]
AC_0145	putative FAD-linked oxidoreductase			100.0	0	CDC38868.1	putative glycolate oxidase subunit GlcD [<i>Anaerostipes</i> sp.]

CAG:276]

S3_Bin003-Anaerostipes caccae-Ethanol production/oxidation-ATPase

AC_0980	Ca ²⁺ -transporting ATPase	EC:3.6.3.8	100.0	0	EFV21858.1	ATPase [<i>Anaerostipes</i> sp. 3_2_56FAA]
AC_0981	F-type H ⁺ -transporting ATPase subunit epsilon		100.0	2.78E-96	EDR95658.1	ATP synthase F1, epsilon subunit [<i>Anaerostipes caccae</i> DSM 14662]
AC_0982	F-type H ⁺ -transporting ATPase subunit beta	EC:3.6.3.14	100.0	0	EDR95659.1	ATP synthase F1, beta subunit [<i>Anaerostipes caccae</i> DSM 14662]
AC_0983	F-type H ⁺ -transporting ATPase subunit gamma		100.0	0	EDR95660.1	ATP synthase F1, gamma subunit [<i>Anaerostipes caccae</i> DSM 14662]
AC_0984	F-type H ⁺ -transporting ATPase subunit alpha	EC:3.6.3.14	100.0	0	EFV21853.1	ATP synthase F1 [<i>Anaerostipes</i> sp. 3_2_56FAA]
AC_0985	F-type H ⁺ -transporting ATPase subunit delta		100.0	1.02E-118	EFV21852.1	ATP synthase F1 [<i>Anaerostipes</i> sp. 3_2_56FAA]
AC_0986	F-type H ⁺ -transporting ATPase subunit b		100.0	9.39E-110	EDR95663.1	ATP synthase F0, B subunit [<i>Anaerostipes caccae</i> DSM 14662]
AC_0987	F-type H ⁺ -transporting ATPase subunit c		100.0	2.73E-39	EDR95664.1	ATP synthase F0, C subunit [<i>Anaerostipes caccae</i> DSM 14662]
AC_0988	F-type H ⁺ -transporting ATPase subunit a		100.0	1.28E-157	EDR95665.1	ATP synthase F0, A subunit [<i>Anaerostipes caccae</i> DSM 14662]
AC_0264	V/A-type H ⁺ /Na ⁺ -transporting ATPase subunit D	ATPVD	100.0	6.28E-149	EFV22893.1	ATP synthase subunit D protein [<i>Anaerostipes</i> sp. 3_2_56FAA]
AC_0265	V/A-type H ⁺ /Na ⁺ -transporting ATPase subunit B	ATPVB	99.8	0	EDR97894.1	ATP synthase ab domain protein [<i>Anaerostipes caccae</i> DSM 14662]
AC_0266	V/A-type H ⁺ /Na ⁺ -transporting ATPase subunit A	ATPVA	99.5	0	EDR97895.1	ATP synthase ab domain protein [<i>Anaerostipes caccae</i> DSM 14662]
AC_0267	V/A-type H ⁺ /Na ⁺ -transporting ATPase subunit E	ATPVE	100.0	2.82E-136	EDR97896.1	hypothetical protein ANACAC_01519 [<i>Anaerostipes caccae</i> DSM 14662]
AC_0268	V/A-type H ⁺ /Na ⁺ -transporting ATPase subunit F	ATPVF	100.0	1.66E-65	EFV22897.1	ATP synthase subunit protein [<i>Anaerostipes</i> sp. 3_2_56FAA]
AC_0269	V/A-type H ⁺ /Na ⁺ -transporting ATPase subunit K	ATPVK	99.3	1.56E-89	EFV22898.1	ATP synthase subunit C protein [<i>Anaerostipes</i> sp. 3_2_56FAA]
AC_0270	V/A-type H ⁺ /Na ⁺ -transporting ATPase subunit I	ATPVI	100.0	0	EFV22899.1	V-type ATPase 116kDa subunit protein [<i>Anaerostipes</i> sp. 3_2_56FAA]
AC_0271	V/A-type H ⁺ /Na ⁺ -transporting ATPase subunit C	ATPVC	99.4	0	CDC37134.1	aTP synthase subunit C [<i>Anaerostipes</i> sp. CAG:276]
AC_1187	F-type H ⁺ -transporting ATPase subunit epsilon		100.0	1.27E-93	EDR96894.1	ATP synthase F1, epsilon subunit [<i>Anaerostipes caccae</i> DSM

							14662]
AC_1188	F-type H ⁺ -transporting ATPase subunit beta		EC:3.6.3.14	100.0	0	EDR96895.1	ATP synthase F1, beta subunit [<i>Anaerostipes caccae</i> DSM 14662]
AC_1189	F-type H ⁺ -transporting ATPase subunit gamma			100.0	0	EFV23294.1	ATP synthase F1 [<i>Anaerostipes</i> sp. 3_2_56FAA]
AC_1190	F-type H ⁺ -transporting ATPase subunit alpha		EC:3.6.3.14	100.0	0	EDR96897.1	ATP synthase F1, alpha subunit [<i>Anaerostipes caccae</i> DSM 14662]
AC_1191	F-type H ⁺ -transporting ATPase subunit delta			100.0	4.81E-124	EFV23296.1	ATP synthase delta subunit protein [<i>Anaerostipes</i> sp. 3_2_56FAA]
AC_1192	F-type H ⁺ -transporting ATPase subunit b			100.0	6.26E-116	EFV23297.1	ATP synthase F0 [<i>Anaerostipes</i> sp. 3_2_56FAA]
AC_1193	F-type H ⁺ -transporting ATPase subunit c			100.0	1.70E-51	EDR96900.1	ATP synthase F0, C subunit [<i>Anaerostipes caccae</i> DSM 14662]
AC_1194	F-type H ⁺ -transporting ATPase subunit a			100.0	7.93E-174	EFV23299.1	ATP synthase subunit A protein [<i>Anaerostipes</i> sp. 3_2_56FAA]
AC_1195	ATP synthase protein I	atpI		100.0	3.57E-97	EDR96902.1	hypothetical protein ANACAC_02131 [<i>Anaerostipes caccae</i> DSM 14662]
AC_2203	ferredoxin--NADP ⁺ reductase	fpr	EC:1.18.1.2	99.6	0	EFV22008.1	oxidoreductase NAD-binding domain-containing protein [<i>Anaerostipes</i> sp. 3_2_56FAA]
S3_Bin008-Paenirhodobacter enshiensis-Glycerol oxidation 2							
PE_2877	Glycerol kinase	glpK	EC:2.7.1.30	72.1	0	SDE30209.1	glycerol kinase [<i>Rhodobacter capsulatus</i>]
PE_2128	glycerol-3-phosphate dehydrogenase (NAD(P) ⁺)	gpsA	EC:1.1.1.94	81.1	5.70E-173	WP_068766473.1	glycerol-3-phosphate dehydrogenase [<i>Paenirhodobacter</i> sp. MME-103]
PE_0132	glycerol-3-phosphate dehydrogenase	glpA	EC:1.1.5.3	77.6	0	SDF96460.1	homodimeric glycerol 3-phosphate dehydrogenase (quinone) [<i>Celeribacter baekdonensis</i>]
PE_1158	glycerol-3-phosphate dehydrogenase	glpA	EC:1.1.5.3	57.7	0	WP_071833009.1	hypothetical protein [<i>Rhizobium</i> sp. 59]
PE_2876	glycerol-3-phosphate dehydrogenase	glpA	EC:1.1.5.3	75.6	0	KFI30710.1	glycerol-3-phosphate dehydrogenase [<i>Paenirhodobacter enshiensis</i>]
S3_Bin008-Paenirhodobacter enshiensis-Central axis pathway							
PE_2190	triosephosphate isomerase (TIM)	TPI	EC:5.3.1.1	83.1	1.10E-144	AOZ71005.1	triose-phosphate isomerase [<i>Rhodobacter</i> sp. LPB0142]
PE_0467	glyceraldehyde 3-phosphate dehydrogenase	GAPDH	EC:1.2.1.12	76.7	0	OHC59378.1	type I glyceraldehyde-3-phosphate dehydrogenase [<i>Rhodobacteriales</i> bacterium RIFCSPHIGHO2_02_FULLL_62_130]
PE_0491	glyceraldehyde 3-phosphate dehydrogenase	GAPDH	EC:1.2.1.12	94.9	0	AOZ69693.1	type I glyceraldehyde-3-phosphate dehydrogenase [<i>Rhodobacter</i> sp.]

							LPB0142]
PE_0493	glyceraldehyde 3-phosphate dehydrogenase	GAPDH	EC:1.2.1.12	90.4	0	ETD00999.1	glyceraldehyde-3-phosphate dehydrogenase [<i>Rhodobacter capsulatus</i> DE442]
PE_1588	glyceraldehyde 3-phosphate dehydrogenase	GAPDH	EC:1.2.1.12	73.4	1.57E-172	ESW60866.1	glyceraldehyde-3-phosphate dehydrogenase [<i>Rhodobacter</i> sp. CACIA14H1]
PE_1384	phosphoglycerate kinase	PGK	EC:2.7.2.3	87.6	0	WP_068765213.1	phosphoglycerate kinase [<i>Paenirhodobacter</i> sp. MME-103]
PE_1172	probable phosphoglycerate mutase	gpmB	EC:5.4.2.12	56.4	1.26E-49	SFA48950.1	probable phosphoglycerate mutase [<i>Paracoccus halophilus</i>]
PE_2093	2,3-bisphosphoglycerate-independent phosphoglycerate mutase	gpmI	EC:5.4.2.12	88.1	0	SIS72234.1	phosphoglycerate mutase [<i>Rhodobacter aestuarii</i>]
PE_1391	enolase	ENO	EC:4.2.1.11	94.1	0	SIS80968.1	enolase [<i>Rhodobacter aestuarii</i>]
PE_1761	pyruvate kinase	PK	EC:2.7.1.40	78.6	0	ETD02924.1	pyruvate kinase [<i>Rhodobacter capsulatus</i> DE442]
PE_3496	pyruvate kinase	PK	EC:2.7.1.40	91.5	0	AOZ68411.1	pyruvate kinase [<i>Rhodobacter</i> sp. LPB0142]
PE_1379	pyruvate dehydrogenase E2 component (dihydrolipoamide acetyltransferase)	DLAT	EC:2.3.1.12	83.2	0	WP_068765208.1	pyruvate dehydrogenase complex dihydrolipoamide acetyltransferase [<i>Paenirhodobacter</i> sp. MME-103]
PE_2364	pyruvate dehydrogenase E2 component (dihydrolipoamide acetyltransferase)	DLAT	EC:2.3.1.12	71.8	1.89E-108	SFA84632.1	pyruvate dehydrogenase E2 component (dihydrolipoamide acetyltransferase) [<i>Poseidonocella pacifica</i>]
PE_1380	pyruvate dehydrogenase E1 component beta subunit	PDHB	EC:1.2.4.1	83.1	0	AMY69898.1	pyruvate dehydrogenase subunit beta [<i>Deftuimonas alba</i>]
PE_1381	pyruvate dehydrogenase E1 component alpha subunit	PDHA	EC:1.2.4.1	89.5	0	AOZ69278.1	pyruvate dehydrogenase (acetyl-transferring) E1 component subunit alpha [<i>Rhodobacter</i> sp. LPB0142]
PE_2361	pyruvate dehydrogenase E1 component alpha subunit	PDHA	EC:1.2.4.1	79.9	0	AKO98504.1	Pyruvate/2-oxoglutarate dehydrogenase complex, dehydrogenase component, eukaryotic type [<i>Marinovum algicola</i> DG 898]
PE_2362	pyruvate dehydrogenase E1 component beta subunit	PDHB	EC:1.2.4.1	88.5	0	SFR18622.1	pyruvate dehydrogenase E1 component beta subunit [<i>Poseidonocella sedimentorum</i>]
S3_Bin008-Paenirhodobacter enshiensis-Acetate production							
PE_1307	phosphate acetyltransferase	pta	EC:2.3.1.8	77.1	0	AOZ71023.1	enoyl-CoA hydratase [<i>Rhodobacter</i> sp. LPB0142]
PE_1308	Acetate kinase	ackA	EC:2.7.2.1	84.6	0	WP_068766622.1	acetate kinase [<i>Paenirhodobacter</i> sp. MME-103]

S3_Bin008-Paenirhodobacter enshiensis-Butyrate and caproate production

PE_1057	acetyl-CoA C-acetyltransferase	atoB	EC:2.3.1.9	83.9	0	KFE34529.1	acetyl-CoA acyltransferase [<i>Thioclava atlantica</i>]
PE_1075	acetyl-CoA C-acetyltransferase	atoB	EC:2.3.1.9	86.4	0	WP_068765357.1	acetyl-CoA acetyltransferase [<i>Paenirhodobacter</i> sp. MME-103]
PE_1122	acetyl-CoA C-acetyltransferase	atoB	EC:2.3.1.9	87.6	0	SEO38001.1	acetyl-CoA C-acetyltransferase [<i>Paracoccus alcaliphilus</i>]
PE_1262	acetyl-CoA C-acetyltransferase	atoB	EC:2.3.1.9	90.8	0	SIS65056.1	acetyl-CoA acetyltransferase [<i>Rhodobacter vinaykumarii</i>]
PE_1642	acetyl-CoA C-acetyltransferase	atoB	EC:2.3.1.9	80.5	0	SFQ30065.1	acetyl-CoA C-acetyltransferase [<i>Donghicola eburneus</i>]
PE_1791	acetyl-CoA C-acetyltransferase	atoB	EC:2.3.1.9	94.3	0	WP_068767177.1	acetyl-CoA acetyltransferase [<i>Paenirhodobacter</i> sp. MME-103]
PE_0778	3-hydroxybutyryl-CoA dehydrogenase	paaH	EC:1.1.1.157	65.4	5.76E-132	WP_010138125.1	3-hydroxybutyryl-CoA dehydrogenase [<i>Oceanicola</i> sp. S124]
PE_2880	3-hydroxybutyryl-CoA dehydrogenase	paaH	EC:1.1.1.157	86.6	0	WP_068765301.1	3-hydroxybutyryl-CoA dehydrogenase [<i>Paenirhodobacter</i> sp. MME-103]
PE_0219	3-hydroxybutyryl-CoA dehydratase	croR	EC:4.2.1.55	84.7	1.92E-84	WP_071165728.1	(R)-hydratase [<i>Rhodobacter</i> sp. LPB0142] AOZ68795.1 (R)-hydratase [<i>Rhodobacter</i> sp. LPB0142]
PE_0062	enoyl-CoA hydratase	crt	EC:4.2.1.17	88.3	5.13E-136	WP_068768004.1	hypothetical protein [<i>Paenirhodobacter</i> sp. MME-103]
PE_0675	enoyl-CoA hydratase	crt	EC:4.2.1.17	82.2	1.01E-155	OOL18131.1	enoyl-CoA hydratase [<i>Ochrobactrum</i> sp. P6BS-III]
PE_0765	enoyl-CoA hydratase	crt	EC:4.2.1.17	85.1	1.54E-171	ACM04163.1	Enoyl-CoA hydratase/isomerase [<i>Rhodobacter sphaeroides</i> KD131]
PE_3213	enoyl-CoA hydratase	crt	EC:4.2.1.17	85.7	2.17E-163	SIS74030.1	short chain enoyl-CoA hydratase [<i>Rhodobacter aestuarii</i>]
PE_0499	butyryl-CoA dehydrogenase	bcd	EC:1.3.8.1	87.9	0	ETD84791.1	acyl-CoA dehydrogenase [<i>Rhodobacter capsulatus</i> B6]
PE_1054	acetate CoA/acetoacetate CoA-transferase alpha subunit	atoD	EC:2.8.3.8 2.8.3.9	78.2	8.72E-125	SFJ08131.1	acetate CoA/acetoacetate CoA-transferase alpha subunit [<i>Celeribacter neptunius</i>]
PE_3514	acetate CoA/acetoacetate CoA-transferase alpha subunit	atoD	EC:2.8.3.8 2.8.3.9	77.7	7.36E-119	WP_018633765.1	acetyl-CoA--acetoacetyl-CoA transferase subunit alpha [<i>Meganema perideroedes</i>]
PE_3515	acetate CoA/acetoacetate CoA-transferase beta subunit	atoA	EC:2.8.3.8 2.8.3.9	79.3	2.55E-118	OHC49010.1	succinyl-CoA--3-ketoacid-CoA transferase [<i>Rhodobacteraceae</i> bacterium GWF1_65_7]
S3_Bin008-Paenirhodobacter enshiensis-Ethanol production/oxidation							
PE_0265	aldehyde dehydrogenase (NAD+)	ALDH	EC:1.2.1.3	89.3	0	AOZ68323.1	aldehyde dehydrogenase family protein [<i>Rhodobacter</i> sp. LPB0142]

PE_0752	aldehyde dehydrogenase (NAD+)	ALDH	EC:1.2.1.3	83.2	0	KJZ21783.1	betaine-aldehyde dehydrogenase [<i>Ruegeria mobilis</i>]
PE_1339	aldehyde dehydrogenase (NAD+)	ALDH	EC:1.2.1.3	81.0	0	AOZ69140.1	aldehyde dehydrogenase family protein [<i>Rhodobacter</i> sp. LPB0142]
PE_1494	aldehyde dehydrogenase (NAD+)	ALDH	EC:1.2.1.3	87.9	0	AOZ68248.1	aldehyde dehydrogenase family protein [<i>Rhodobacter</i> sp. LPB0142]
PE_3251	aldehyde dehydrogenase (NAD+)	ALDH	EC:1.2.1.3	75.8	0	ETD90655.1	aldehyde dehydrogenase [<i>Rhodobacter capsulatus</i> YW2]
PE_3542	aldehyde dehydrogenase (NAD+)	ALDH	EC:1.2.1.3	51.2	0	WP_038076817.1	aldehyde dehydrogenase [<i>Thioclava pacifica</i>]
PE_0700	alcohol dehydrogenase	adh2	EC:1.1.1.-	88.1	0	WP_028095703.1	alcohol dehydrogenase [<i>Pseudodonghicola xiamenensis</i>]
PE_2370	alcohol dehydrogenase, propanol-preferring	adhP	EC:1.1.1.1	79.7	0	SDW45688.1	alcohol dehydrogenase, propanol-preferring [<i>Celeribacter indicus</i>]
S3_Bin008-Paenirhodobacter enshiensis-Membrane proteins involved in energy conservation-Fix system							
PE_3758	electron transfer flavoprotein beta subunit	fixA		93.6	1.94E-138	AOZ70298.1	electron transfer flavoprotein subunit beta [<i>Rhodobacter</i> sp. LPB0142]
PE_3757	electron transfer flavoprotein alpha subunit	fixB		89.7	9.76E-170	AOZ70299.1	electron transfer flavoprotein subunit alpha [<i>Rhodobacter</i> sp. LPB0142]
S3_Bin008-Paenirhodobacter enshiensis-ATPase							
PE_0226	F-type H ⁺ -transporting ATPase subunit epsilon			79.4	4.88E-67	AOZ68786.1	ATP synthase F1 subunit epsilon [<i>Rhodobacter</i> sp. LPB0142]
PE_0227	F-type H ⁺ -transporting ATPase subunit beta		EC:3.6.3.14	95.7	0	SIS87773.1	ATP synthase F1 subcomplex beta subunit [<i>Rhodobacter aestuarii</i>]
PE_0228	F-type H ⁺ -transporting ATPase subunit gamma			85.6	4.17E-180	AOZ68784.1	F0F1 ATP synthase subunit gamma [<i>Rhodobacter</i> sp. LPB0142]
PE_0229	F-type H ⁺ -transporting ATPase subunit alpha		EC:3.6.3.14	94.1	0	SIS87731.1	ATP synthase F1 subcomplex alpha subunit [<i>Rhodobacter aestuarii</i>]
PE_0230	F-type H ⁺ -transporting ATPase subunit delta			78.2	4.81E-96	ETD88720.1	F0F1 ATP synthase subunit delta [<i>Rhodobacter capsulatus</i> YW2]
PE_1195	ATP synthase			65.8	0	SFY39743.1	phospholipase/carboxylesterase [<i>Paracoccus pantotrophus</i>]
PE_2134	F-type H ⁺ -transporting ATPase subunit beta		EC:3.6.3.14	85.2	0	ALG89973.1	ATP F0F1 synthase subunit beta [<i>Confluentimicrobium</i> sp. EMB200-NS6]
PE_2135	F-type H ⁺ -transporting ATPase subunit epsilon			60.1	1.05E-51	KGB81292.1	ATP synthase F0F1 subunit epsilon [<i>Rhodovulum</i> sp. NI22]
PE_2136	ATP synthase protein I	atpI		69.1	5.94E-31	AKR55839.1	ATP synthase [<i>Devosia</i> sp. H5989]
PE_2138	F-type H ⁺ -transporting ATPase subunit a			75.0	1.74E-112	KGB81289.1	ATP synthase F0F1 subunit A [<i>Rhodovulum</i> sp. NI22]

PE_2139	F-type H ⁺ -transporting ATPase subunit c		87.5	5.41E-42	KIL04359.1	ATP F0F1 synthase subunit C [<i>Pseudomonas stutzeri</i>]	
PE_2140	F-type H ⁺ -transporting ATPase subunit b		55.9	3.12E-65	KGB81287.1	hypothetical protein JT55_14135 [<i>Rhodovulum</i> sp. NI22]	
PE_2141	F-type H ⁺ -transporting ATPase subunit alpha	EC:3.6.3.14	75.6	0	EIE49002.1	H ⁺ -transporting two-sector ATPase, alpha/beta subunit [<i>Citricella</i> sp. 357]	
PE_2142	F-type H ⁺ -transporting ATPase subunit gamma		61.8	3.60E-107	KGB81285.1	ATPase [<i>Rhodovulum</i> sp. NI22]	
S3_Bin009-Oscillibacter ruminantium-Glycerol oxidation 2							
OR_3173	glycerol kinase	glpK	EC:2.7.1.30	83.7	0	CDD40108.1	glycerol kinase 2 [<i>Clostridium</i> sp. CAG:299]
OR_3357	glycerol kinase	glpK	EC:2.7.1.30	100.0	0	WP_040659376.1	glycerol kinase [<i>Oscillibacter ruminantium</i>]
OR_0905	glycerol-3-phosphate dehydrogenase (NAD(P)+)	gpsA	EC:1.1.1.94	100.0	0	WP_040661836.1	glycerol-3-phosphate dehydrogenase [<i>Oscillibacter ruminantium</i>]
OR_3591	glycerol-3-phosphate dehydrogenase (NAD(P)+)	gpsA	EC:1.1.1.94	85.9	0	SCI69554.1	Glycerol-3-phosphate dehydrogenase [NAD(P)+] [uncultured <i>Clostridium</i> sp.]
S3_Bin009-Oscillibacter ruminantium-Central axis pathway							
OR_1769	triosephosphate isomerase (TIM)	TPI	EC:5.3.1.1	100.0	0	WP_040660011.1	triose-phosphate isomerase [<i>Oscillibacter ruminantium</i>]
OR_0104	glyceraldehyde 3-phosphate dehydrogenase	GAPDH	EC:1.2.1.12	100.0	0	WP_040660984.1	type I glyceraldehyde-3-phosphate dehydrogenase [<i>Oscillibacter ruminantium</i>]
OR_0650	glyceraldehyde 3-phosphate dehydrogenase	GAPDH	EC:1.2.1.12	93.2	0	WP_050619378.1	type I glyceraldehyde-3-phosphate dehydrogenase [<i>Intestinimonas massiliensis</i>]
OR_1884	glyceraldehyde 3-phosphate dehydrogenase	GAPDH	EC:1.2.1.12	100.0	0	WP_040658858.1	type I glyceraldehyde-3-phosphate dehydrogenase [<i>Oscillibacter ruminantium</i>]
OR_1770	phosphoglycerate kinase	PGK	EC:2.7.2.3	100.0	0	WP_040660014.1	phosphoglycerate kinase [<i>Oscillibacter ruminantium</i>]
OR_0492	probable phosphoglycerate mutase	gpmB	EC:5.4.2.12	100.0	0	WP_040659060.1	hypothetical protein [<i>Oscillibacter ruminantium</i>]
OR_1768	2,3-bisphosphoglycerate-independent phosphoglycerate mutase	gpmI	EC:5.4.2.12	100.0	0	WP_040660010.1	2,3-bisphosphoglycerate-independent phosphoglycerate mutase [<i>Oscillibacter ruminantium</i>]
OR_2875	enolase	ENO	EC:4.2.1.11	42.2	0.23	WP_057088306.1	hypothetical protein [<i>Bacteroides uniformis</i>]
OR_2630	pyruvate kinase	PK	EC:2.7.1.40	88.6	0	WP_052082408.1	pyruvate kinase [<i>Intestinimonas butyriciproducens</i>]

OR_2210	pyruvate dehydrogenase E1 component alpha subunit	PDHA	EC:1.2.4.1	100.0	0	WP_051131674.1	acetoin:2,6-dichlorophenolindophenol oxidoreductase subunit alpha [<i>Oscillibacter ruminantium</i>]
OR_2211	pyruvate dehydrogenase E1 component beta subunit	PDHB	EC:1.2.4.1	100.0	0	WP_040661190.1	alpha-ketoacid dehydrogenase subunit beta [<i>Oscillibacter ruminantium</i>]
OR_2217	pyruvate dehydrogenase E1 component alpha subunit	PDHA	EC:1.2.4.1	100.0	0	WP_040661196.1	acetoin:2,6-dichlorophenolindophenol oxidoreductase subunit alpha [<i>Oscillibacter ruminantium</i>]
OR_2218	pyruvate dehydrogenase E1 component beta subunit	PDHB	EC:1.2.4.1	100.0	0	WP_040661197.1	alpha-ketoacid dehydrogenase subunit beta [<i>Oscillibacter ruminantium</i>]
OR_2219	pyruvate dehydrogenase E2 component (dihydrolipoamide acetyltransferase)	DLAT	EC:2.3.1.12	100.0	0	WP_040661198.1	hypothetical protein [<i>Oscillibacter ruminantium</i>]
OR_0303	pyruvate-ferredoxin/flavodoxin oxidoreductase	por	EC:1.2.7.1 1.2.7.-	100.0	0	WP_040660745.1	pyruvate:ferredoxin (flavodoxin) oxidoreductase [<i>Oscillibacter ruminantium</i>]
OR_1623	pyruvate-ferredoxin/flavodoxin oxidoreductase	por	EC:1.2.7.1 1.2.7.-	85.9	0	WP_033118453.1	pyruvate:ferredoxin (flavodoxin) oxidoreductase [<i>Intestinimonas butyriciproducens</i>]
OR_3352	pyruvate ferredoxin oxidoreductase beta subunit	porB	EC:1.2.7.1	94.1	7.87E-155	BAK98548.1	pyruvate synthase subunit PorB [<i>Oscillibacter valericigenes</i> Sjm18-20]
S3_Bin009-Oscillibacter ruminantium-Acetate production							
OR_0108	phosphate acetyltransferase	pta	EC:2.3.1.8	99.7	0	WP_040660986.1	phosphate acetyltransferase [<i>Oscillibacter ruminantium</i>]
OR_2786	putative phosphotransacetylase	pta	EC:2.3.1.8	74.7	1.33E-112	WP_033116456.1	phosphate propanoyltransferase [<i>Intestinimonas butyriciproducens</i>]
OR_3028	phosphate acetyltransferase	pta	EC:2.3.1.8	88.3	0	WP_033118802.1	phosphate acetyltransferase [<i>Intestinimonas butyriciproducens</i>]
OR_0381	acetate kinase	ackA	EC:2.7.2.1	100.0	0	WP_040659222.1	acetate kinase [<i>Oscillibacter ruminantium</i>]
OR_1180	acetate kinase	ackA	EC:2.7.2.1	88.5	0	WP_033119262.1	acetate kinase [<i>Intestinimonas butyriciproducens</i>]
S3_Bin009-Oscillibacter ruminantium-Butyrate and caproate production							
OR_0079	acetyl-CoA C-acetyltransferase	atoB	EC:2.3.1.9	99.7	0	WP_040660251.1	acetyl-CoA acetyltransferase [<i>Oscillibacter ruminantium</i>]
OR_1778	acetyl-CoA C-acetyltransferase	atoB	EC:2.3.1.9	99.8	0	WP_040660027.1	acetyl-CoA acetyltransferase [<i>Oscillibacter ruminantium</i>]

OR_3143	acetyl-CoA C-acetyltransferase	atoB	EC:2.3.1.9	82.8	0	OLA37645.1	acetyl-CoA acetyltransferase [<i>Firmicutes</i> bacterium CAG:176_63_11]
OR_0080	3-hydroxybutyryl-CoA dehydrogenase	paaH	EC:1.1.1.157	99.7	0	WP_040660253.1	3-hydroxyacyl-CoA dehydrogenase [<i>Oscillibacter ruminantium</i>]
OR_0709	3-hydroxybutyryl-CoA dehydrogenase	paaH	EC:1.1.1.157	92.9	0	WP_050618924.1	3-hydroxybutyryl-CoA dehydrogenase [<i>Intestinimonas massiliensis</i>]
OR_1678	3-hydroxybutyryl-CoA dehydrogenase	paaH	EC:1.1.1.157	56.6	1.04E-119	WP_044567660.1	hypothetical protein [<i>Anaerococcus provenciensis</i>]
OR_3144	3-hydroxybutyryl-CoA dehydrogenase	paaH	EC:1.1.1.157	75.2	1.31E-152	WP_050618924.1	3-hydroxybutyryl-CoA dehydrogenase [<i>Intestinimonas massiliensis</i>]
OR_3441	3-hydroxybutyryl-CoA dehydrogenase	paaH	EC:1.1.1.157	87.0	0	WP_024723756.1	3-hydroxyacyl-CoA dehydrogenase [<i>Flavonifractor plautii</i>]
OR_0078	enoyl-CoA hydratase	crt	EC:4.2.1.17	99.6	0	WP_040660249.1	enoyl-CoA hydratase [<i>Oscillibacter ruminantium</i>]
OR_0615	enoyl-CoA hydratase	crt	EC:4.2.1.17	76.5	6.07E-149	WP_058117605.1	enoyl-CoA hydratase [<i>Intestinimonas butyriciproducens</i>]
OR_0708	enoyl-CoA hydratase	crt	EC:4.2.1.17	93.0	1.07E-172	WP_033118609.1	enoyl-CoA hydratase [<i>Intestinimonas butyriciproducens</i>]
OR_1669	enoyl-CoA hydratase	crt	EC:4.2.1.17	64.5	7.93E-121	WP_050618245.1	hypothetical protein [<i>Intestinimonas massiliensis</i>]
OR_1619	3-hydroxybutyryl-CoA dehydratase	croR	EC:4.2.1.55	71.0	1.07E-69	WP_016205959.1	dehydratase [<i>Clostridium sartagoforme</i>]
OR_1671	butyryl-CoA dehydrogenase	bcd	EC:1.3.8.1	73.6	0	WP_050618243.1	acyl-CoA dehydrogenase [<i>Intestinimonas massiliensis</i>]
OR_3620	butyryl-CoA dehydrogenase	bcd	EC:1.3.8.1	63.6	4.37E-169	WP_066240845.1	hypothetical protein [<i>Anaerospromusa subterranea</i>]
OR_1334	acetate CoA/acetoacetate CoA-transferase alpha subunit	atoD	EC:2.8.3.8 2.8.3.9	75.1	1.51E-124	WP_007288542.1	3-oxoadipate CoA-transferase subunit A [<i>Thermosinus carboxydivorans</i>]
OR_1533	propionate CoA-transferase	pct	EC:2.8.3.1	78.3	0	WP_044938912.1	3-oxoacid CoA-transferase [<i>Flavonifractor plautii</i>]
OR_1668	propionate CoA-transferase	pct	EC:2.8.3.1	79.5	0	WP_050618247.1	hypothetical protein [<i>Intestinimonas massiliensis</i>]
OR_1675	propionate CoA-transferase	pct	EC:2.8.3.1	70.5	0	WP_024723620.1	3-oxoacid CoA-transferase [<i>Flavonifractor plautii</i>]
OR_3499	propionate CoA-transferase	pct	EC:2.8.3.1	76.1	0	WP_054329786.1	3-oxoacid CoA-transferase [<i>Clostridia</i> bacterium UC5.1-1D10]
OR_3621	3-oxoacid CoA-transferase subunit B	scoB	EC:2.8.3.5	80.4	8.36E-129	WP_066240843.1	succinyl-CoA--3-ketoacid-CoA transferase [<i>Anaerospromusa subterranea</i>]
OR_3622	acetate CoA/acetoacetate CoA-transferase alpha subunit	atoD	EC:2.8.3.8 2.8.3.9	76.3	2.88E-138	WP_066240839.1	CoA-transferase [<i>Anaerospromusa subterranea</i>]

S3_Bin009-Oscillibacter ruminantium-Membrane proteins involved in

energy conservation-Rnf complex

OR_0160	electron transport complex protein RnfB	rnfB	100.0	0	WP_051131586.1	ferredoxin [<i>Oscillibacter ruminantium</i>]
OR_0161	electron transport complex protein RnfA	rnfA	99.5	4.32E-132	WP_040660478.1	electron transporter RnfA [<i>Oscillibacter ruminantium</i>]
OR_0162	electron transport complex protein RnfE	rnfE	100.0	2.89E-141	WP_040660480.1	electron transporter RnfE [<i>Oscillibacter ruminantium</i>]
OR_0163	electron transport complex protein RnfG	rnfG	100.0	8.78E-136	WP_040661009.1	electron transporter RnfG [<i>Oscillibacter ruminantium</i>]
OR_0164	electron transport complex protein RnfD	rnfD	100.0	0	WP_040660482.1	NADH:ubiquinone oxidoreductase [<i>Oscillibacter ruminantium</i>]
OR_0165	electron transport complex protein RnfC	rnfC	100.0	0	WP_040660484.1	electron transporter RnfC [<i>Oscillibacter ruminantium</i>]
OR_2484	electron transport complex protein RnfC	rnfC	88.1	0	WP_058117097.1	electron transporter RnfC [<i>Intestinimonas butyriciproducens</i>]
OR_2485	electron transport complex protein RnfD	rnfD	79.3	0	WP_033117458.1	NADH:ubiquinone oxidoreductase [<i>Intestinimonas butyriciproducens</i>]
OR_2486	electron transport complex protein RnfG	rnfG	64.7	1.75E-71	WP_052082630.1	electron transporter RnfG [<i>Intestinimonas butyriciproducens</i>]
OR_2487	electron transport complex protein RnfE	rnfE	71.4	5.53E-102	WP_007489469.1	MULTISPECIES: electron transporter RnfE [<i>Clostridiales</i>]
OR_2488	electron transport complex protein RnfA	rnfA	77.8	4.47E-105	WP_050617657.1	electron transport complex protein RnfA [<i>Intestinimonas massiliensis</i>]
OR_2489	electron transport complex protein RnfB	rnfB	73.3	1.64E-148	WP_070103821.1	ferredoxin, partial [<i>Flavonifractor plautii</i>]
OR_2965	electron transfer flavoprotein alpha subunit	fixB	89.3	0	WP_033119152.1	electron transfer flavoprotein subunit alpha [<i>Intestinimonas butyriciproducens</i>]
OR_2966	electron transfer flavoprotein beta subunit	fixA	95.1	0	WP_033119151.1	electron transfer flavoprotein subunit beta [<i>Intestinimonas butyriciproducens</i>]

S3_Bin009-Oscillibacter ruminantium-ATPase

OR_3409	F-type H ⁺ -transporting ATPase subunit epsilon	atpC	100.0	3.28E-92	WP_040664116.1	ATP synthase F1 subunit epsilon [<i>Oscillibacter ruminantium</i>]	
OR_3410	F-type H ⁺ -transporting ATPase subunit beta	atpD	EC:3.6.3.14	100.0	0	WP_040664113.1	ATP synthase subunit beta [<i>Oscillibacter ruminantium</i>]
OR_3411	F-type H ⁺ -transporting ATPase subunit gamma	atpG	100.0	0	WP_040664110.1	ATP synthase F0F1 subunit gamma [<i>Oscillibacter ruminantium</i>]	
OR_3412	F-type H ⁺ -transporting ATPase subunit alpha	atpA	EC:3.6.3.14	99.8	0	WP_040664107.1	ATP synthase subunit alpha [<i>Oscillibacter ruminantium</i>]
OR_3413	F-type H ⁺ -transporting ATPase subunit delta	atpH	97.7	2.50E-119	WP_040664104.1	hypothetical protein [<i>Oscillibacter ruminantium</i>]	
OR_3414	F-type H ⁺ -transporting ATPase subunit b	atpF	100.0	4.23E-112	WP_040664101.1	ATP synthase F0 subunit B [<i>Oscillibacter ruminantium</i>]	

OR_3415	F-type H ⁺ -transporting ATPase subunit c	atpE	100.0	2.72E-38	WP_040664098.1	ATP synthase F0 subunit C [<i>Oscillibacter ruminantium</i>]	
OR_3416	F-type H ⁺ -transporting ATPase subunit a	atpB	98.7	1.07E-156	WP_040664316.1	F0F1 ATP synthase subunit A [<i>Oscillibacter ruminantium</i>]	
OR_0025	flagellum-specific ATP synthase	fliI	EC:3.6.3.14	100.0	0	WP_040660167.1	ATP synthase [<i>Oscillibacter ruminantium</i>]
OR_1423	flagellum-specific ATP synthase	fliI	EC:3.6.3.14	82.9	0	WP_023345954.1	flagellar protein export ATPase FliI [<i>Firmicutes</i> bacterium ASF500]
S3_Bin011-Clostridiales bacterium DRI-13-Glycerol oxidation 1							
CB_3449	Glycerol dehydrogenase	gldA	EC:1.1.1.6	73.4	0	WP_042682775.1	glycerol dehydrogenase [<i>Anaerosalibacter massiliensis</i>]
CB_0712	dihydroxyacetone kinase, C-terminal domain	dhaL	EC:2.7.1.-	63.4	5.28E-84	KYH29213.1	PTS-dependent dihydroxyacetone kinase, ADP-binding subunit DhaL [<i>Clostridium colicanis</i> DSM 13634]
CB_0713	dihydroxyacetone kinase, N-terminal domain	dhaK	EC:2.7.1.-	78.2	0	KYO65477.1	PTS-dependent dihydroxyacetone kinase, dihydroxyacetone-binding subunit DhaK [<i>Thermovenabulum gondwanense</i>]
CB_0785	dihydroxyacetone kinase, N-terminal domain	dhaK	EC:2.7.1.-	80.1	0	OFL91225.1	glycerol kinase [<i>Fusobacterium</i> sp. HMSC073F01]
CB_0786	dihydroxyacetone kinase, C-terminal domain	dhaL	EC:2.7.1.-	45.9	3.04E-63	OFL91226.1	Dak phosphatase [<i>Fusobacterium</i> sp. HMSC073F01]
S3_Bin011-Clostridiales bacterium DRI-13-Glycerol oxidation 2							
CB_0718	glycerol kinase	glpK	EC:2.7.1.30	87.1	0	KXG76970.1	Glycerol kinase [<i>Fervidicola ferrireducens</i>]
CB_0717	glycerol-3-phosphate dehydrogenase	glpA	EC:1.1.5.3	68.3	0	AEE90760.1	FAD dependent oxidoreductase [<i>Tepidanaerobacter acetatoxydans</i> Re1]
CB_2035	glycerol-3-phosphate dehydrogenase	glpA	EC:1.1.5.3	75.8	0	SHK15780.1	glycerol-3-phosphate dehydrogenase [<i>Caminicella sporogenes</i> DSM 14501]
CB_1563	glycerol-3-phosphate dehydrogenase (NAD(P) ⁺)	gpsA	EC:1.1.1.94	71.3	8.66E-173	WP_034423582.1	glycerol-3-phosphate dehydrogenase [<i>Clostridiales</i> bacterium DRI-13]
S3_Bin011-Clostridiales bacterium DRI-13-Central axis pathway							
CB_0868	triosephosphate isomerase (TIM)	TPI	EC:5.3.1.1	61.6	2.91E-116	WP_034420300.1	triose-phosphate isomerase [<i>Clostridiales</i> bacterium DRI-13]
CB_0870	glyceraldehyde 3-phosphate dehydrogenase	GAPDH	EC:1.2.1.12	79.3	0	WP_034420302.1	type I glyceraldehyde-3-phosphate dehydrogenase [<i>Clostridiales</i> bacterium DRI-13]
CB_0869	phosphoglycerate kinase	PGK	EC:2.7.2.3	74.8	0	WP_034420301.1	phosphoglycerate kinase [<i>Clostridiales</i> bacterium DRI-13]

CB_0867	2,3-bisphosphoglycerate-independent phosphoglycerate mutase	gpmI	EC:5.4.2.12	70.2	0	WP_034420299.1	2,3-bisphosphoglycerate-independent phosphoglycerate mutase [<i>Clostridiales</i> bacterium DRI-13]
CB_0866	Enolase	ENO	EC:4.2.1.11	82.4	0	WP_034420297.1	phosphopyruvate hydratase [<i>Clostridiales</i> bacterium DRI-13]
CB_2450	Enolase	ENO	EC:4.2.1.11	74.5	0	OHD71009.1	phosphopyruvate hydratase [<i>Spirochaetes</i> bacterium RBG_16_49_21]
CB_0710	Pyruvate kinase	PK	EC:2.7.1.40	77.5	3.71E-93	GAU75712.1	ATP synthase F0 sector subunit c [<i>Fusibacter</i> sp. 3D3]
CB_1412	Pyruvate kinase	PK	EC:2.7.1.40	70.0	0	WP_034424334.1	pyruvate kinase [<i>Clostridiales</i> bacterium DRI-13]
CB_0990	pyruvate dehydrogenase E2 component (dihydropolipoamide acetyltransferase)	DLAT	EC:2.3.1.12	59.8	8.44E-167	WP_034421312.1	dihydropolypoLlysine acetyltransferase [<i>Clostridiales</i> bacterium DRI-13]
CB_0992	pyruvate dehydrogenase E1 component beta subunit	PDHB	EC:1.2.4.1	78.0	0	GAK59197.1	acetoin:2,6-dichlorophenolindophenol oxidoreductase subunit beta [<i>Candidatus Vecturithrix granuli</i>]
CB_0993	pyruvate dehydrogenase E1 component alpha subunit	PDHA	EC:1.2.4.1	80.9	0	WP_034421314.1	acetoin:2,6-dichlorophenolindophenol oxidoreductase subunit alpha [<i>Clostridiales</i> bacterium DRI-13]
CB_1064	pyruvate dehydrogenase E1 component beta subunit	PDHB	EC:1.2.4.1	100.0	0	NP_009780.1	pyruvate dehydrogenase (acetyl-transferring) subunit E1 beta [<i>Saccharomyces cerevisiae</i> S288c]
CB_2223	pyruvate dehydrogenase E2 component (dihydropolipoamide acetyltransferase)	DLAT	EC:2.3.1.12	40.0	2.73E-67	KUO41294.1	hypothetical protein APZ16_00235 [<i>Hadesarchaea archaeon</i> YNP_45]
CB_2224	pyruvate dehydrogenase E1 component alpha subunit	PDHA	EC:1.2.4.1	43.3	2.45E-84	OIP38758.1	pyruvate dehydrogenase (acetyl-transferring) E1 component subunit alpha [<i>Desulfobacteraceae</i> bacterium CG2_30_51_40]
CB_2225	pyruvate dehydrogenase E1 component beta subunit	PDHB	EC:1.2.4.1	58.0	5.31E-129	WP_026499684.1	alpha-ketoacid dehydrogenase subunit beta [<i>Caldibacillus debilis</i>]
CB_1687	pyruvate-ferredoxin/ferredoxin oxidoreductase	por	EC:1.2.7.1 1.2.7.-	75.9	0	ACL70827.1	pyruvate flavodoxin/ferredoxin oxidoreductase domain protein [<i>Halothermothrix orenii</i> H 168]
CB_1733	pyruvate ferredoxin oxidoreductase gamma subunit	porG	EC:1.2.7.1	48.1	3.68E-54	WP_053965824.1	hypothetical protein [<i>Clostridiales</i> bacterium mt11]
CB_1734	pyruvate ferredoxin oxidoreductase delta subunit	porD	EC:1.2.7.1	51.9	1.59E-21	SCJ87391.1	Pyruvic-ferredoxin oxidoreductase subunit delta [uncultured <i>Clostridium</i> sp.]
CB_1735	pyruvate ferredoxin oxidoreductase alpha subunit	porA	EC:1.2.7.1	56.4	2.50E-159	CEO89423.1	Pyruvate synthase subunit porA (Pyruvate:ferredoxin

CB_1736	pyruvate ferredoxin oxidoreductase beta subunit	porB	EC:1.2.7.1	61.8	4.02E-128	WP_053965821.1	oxidoreductase, alpha subunit) [<i>Syntrophaceticus schinkii</i> 2-ketoisovalerate ferredoxin oxidoreductase [<i>Clostridiales</i> bacterium mt11]
S3_Bin011-Clostridiales bacterium DRI-13-Acetate production							
CB_0525	putative phosphotransacetylase	pta	EC:2.3.1.8	75.0	5.96E-121	WP_042678834.1	phosphate propanoyltransferase [<i>Anaerosalibacter massiliensis</i>]
CB_1020	phosphate acetyltransferase	pta	EC:2.3.1.8	79.1	0	WP_034422861.1	phosphate acetyltransferase [<i>Clostridiales</i> bacterium DRI-13]
CB_1457	putative phosphotransacetylase	pta	EC:2.3.1.8	70.0	2.33E-101	KYO64150.1	Phosphate propanoyltransferase [<i>Thermovenabulum gondwanense</i>]
CB_1832	putative phosphotransacetylase	pta	EC:2.3.1.8	63.6	1.85E-88	WP_034420556.1	propanediol utilization protein [<i>Clostridiales</i> bacterium DRI-13]
S3_Bin011-Clostridiales bacterium DRI-13-Butyrate and caproate production							
CB_1930	acetyl-CoA C-acetyltransferase	atoB	EC:2.3.1.9	77.3	0	AGL03899.1	acetyl-CoA acetyltransferase [<i>Desulfotomaculum gibsoniae</i> DSM 7213]
CB_2031	acetyl-CoA C-acetyltransferase	atoB	EC:2.3.1.9	66.6	0	OIQ00517.1	acetyl-CoA acetyltransferase [Candidatus <i>Wirthbacteria</i> bacterium CG2_30_54_11]
CB_2048	acetyl-CoA C-acetyltransferase	atoB	EC:2.3.1.9	75.0	2.08E-50	OAJ35251.1	Acetyl-CoA acetyltransferase [<i>Piscirickettsiaceae</i> bacterium NZ-RLO]
CB_2236	acetyl-CoA C-acetyltransferase	atoB	EC:2.3.1.9	78.0	0	WP_034420106.1	acetyl-CoA acetyltransferase [<i>Clostridiales</i> bacterium DRI-13]
CB_2668	acetyl-CoA C-acetyltransferase	atoB	EC:2.3.1.9	77.8	0	AGL03899.1	acetyl-CoA acetyltransferase [<i>Desulfotomaculum gibsoniae</i> DSM 7213]
CB_2670	acetyl-CoA C-acetyltransferase	atoB	EC:2.3.1.9	78.3	0	WP_034420106.1	acetyl-CoA acetyltransferase [<i>Clostridiales</i> bacterium DRI-13]
CB_3152	acetyl-CoA C-acetyltransferase	atoB	EC:2.3.1.9	84.4	0	WP_042678749.1	acetyl-CoA acetyltransferase [<i>Anaerosalibacter massiliensis</i>]
CB_1931	3-hydroxybutyryl-CoA dehydrogenase	paaH	EC:1.1.1.157	70.4	5.63E-147	KKM10416.1	3-hydroxybutyryl-CoA dehydrogenase [<i>Clostridiales</i> bacterium PH28_bin88]
CB_2235	3-hydroxybutyryl-CoA dehydrogenase	paaH	EC:1.1.1.157	71.3	6.51E-152	KJS22912.1	3-hydroxybutyryl-CoA dehydrogenase [<i>Clostridiaceae</i> bacterium BRH_c20a]

CB_2671	3-hydroxybutyryl-CoA dehydrogenase	paaH	EC:1.1.1.157	69.5	9.14E-143	WP_034423482.1	3-hydroxybutyryl-CoA dehydrogenase [<i>Clostridiales</i> bacterium DRI-13]
CB_1929	enoyl-CoA hydratase	crt	EC:4.2.1.17	73.7	2.90E-138	EOD00318.1	3-hydroxybutyryl-CoA dehydratase [<i>Caldisalibacter kiritimatiensis</i>]
CB_2234	enoyl-CoA hydratase	crt	EC:4.2.1.17	77.0	2.66E-145	KJS83836.1	crotonase [<i>Peptococcaceae</i> bacterium BICA1-8]
CB_3100	enoyl-CoA hydratase	crt	EC:4.2.1.17	70.1	1.73E-125	WP_011878111.1	enoyl-CoA hydratase [<i>Desulfotomaculum reducens</i>]
CB_1263	acyl-CoA dehydrogenase	bcd	EC:1.3.8.1	86.4	1.12E-41	CUH92999.1	hypothetical protein SD1D_1453 [<i>Herbinix luporum</i>]
CB_1926	4-hydroxybutyrate CoA-transferase	cat2	EC:2.8.3.-	68.7	0	WP_011641322.1	4-hydroxybutyrate CoA-transferase [<i>Syntrophomonas wolfei</i>]
CB_2231	4-hydroxybutyrate CoA-transferase	cat2	EC:2.8.3.-	70.9	0	CUQ33858.1	4-hydroxybutyrate CoA-transferase [<i>Flavonifractor plautii</i>]
CB_2029	acetate CoA/acetoacetate CoA-transferase beta subunit	atoA	EC:2.8.3.8 2.8.3.9	66.8	2.98E-102	ABK17973.1	butyryl-CoA:acetate CoA transferase [<i>Syntrophobacter fumaroxidans</i> MPOB]
CB_2468	acetate CoA/acetoacetate CoA-transferase beta subunit	atoA	EC:2.8.3.8 2.8.3.9	70.5	1.32E-108	SDY67414.1	butyryl-CoA:acetoacetate CoA-transferase beta subunit [<i>Proteiniborus ethanolicus</i>]
CB_2469	acetate CoA/acetoacetate CoA-transferase alpha subunit	atoD	EC:2.8.3.8 2.8.3.9	67.1	3.61E-98	EOC99457.1	Butyrate-acetoacetate CoA-transferase subunit A [<i>Caldisalibacter kiritimatiensis</i>]
CB_3150	acetate CoA/acetoacetate CoA-transferase beta subunit	atoA	EC:2.8.3.8 2.8.3.9	87.2	7.99E-137	KYH34211.1	butyrate--acetoacetate CoA-transferase subunit B [<i>Clostridium tepidiprofundum</i> DSM 19306]
CB_3151	acetate CoA/acetoacetate CoA-transferase alpha subunit	atoD	EC:2.8.3.8 2.8.3.9	75.7	1.87E-116	AOT70096.1	branched-chain amino acid dehydrogenase [<i>Geosporobacter ferrireducens</i>]
CB_2672	propionate CoA-transferase	pct	EC:2.8.3.1	78.6	0	WP_034421685.1	hypothetical protein [<i>Clostridiales</i> bacterium DRI-13]
CB_2323	phosphate butyryltransferase	ptb	EC:2.3.1.19	65.4	8.43E-138	WP_034420080.1	phosphate butyryltransferase [<i>Clostridiales</i> bacterium DRI-13]
CB_3421	phosphate butyryltransferase	ptb	EC:2.3.1.19	78.4	2.09E-166	SHH49166.1	phosphate butyryltransferase [<i>Caloranaerobacter azorensis</i> DSM 13643]
CB_2227	butyrate kinase	buk	EC:2.7.2.7	63.9	3.21E-170	SET81966.1	butyrate kinase [<i>Natronincola peptidivorans</i>]
CB_2322	butyrate kinase	buk	EC:2.7.2.7	63.8	4.89E-170	SET81966.1	butyrate kinase [<i>Natronincola peptidivorans</i>]

S3_Bin011-Clostridiales bacterium DRI-13-Ethanol production/oxidation

CB_0133	acetaldehyde dehydrogenase / alcohol dehydrogenase	adhE	EC:1.2.1.10 1.1.1.1	76.4	0	SDD67225.1	acetaldehyde dehydrogenase /alcohol dehydrogenase AdhE [<i>Sporomusa acidovorans</i>]
CB_0526	acetaldehyde dehydrogenase (acetylating)		EC:1.2.1.10	74.9	0	CRK81810.1	acetaldehyde dehydrogenase [<i>Bacillus</i> sp. LF1]
CB_0539	acetaldehyde dehydrogenase (acetylating)		EC:1.2.1.10	77.4	0	OAA92437.1	Aldehyde-alcohol dehydrogenase [<i>Clostridium ljungdahlii</i>]
CB_1454	acetaldehyde dehydrogenase (acetylating)		EC:1.2.1.10	66.5	0	GAQ24101.1	acetaldehyde dehydrogenase [<i>Tepidanaerobacter syntrophicus</i>]
CB_1860	alcohol dehydrogenase	adh2	EC:1.1.1.-	63.7	7.71E-168	CDC25113.1	putative uncharacterized protein [<i>Firmicutes</i> bacterium CAG:466]
CB_2625	acetaldehyde dehydrogenase / alcohol dehydrogenase	adhE	EC:1.2.1.10 1.1.1.1	63.6	1.61E-173	KUO68657.1	alcohol dehydrogenase [<i>Clostridia</i> bacterium BRH_c25]
CB_3444	alcohol dehydrogenase	adh	EC:1.1.1.1	76.9	0	KJF27414.1	alcohol dehydrogenase [<i>Clostridium aceticum</i>]

S3_Bin011-Clostridiales bacterium DRI-13-Glycerol reduction to 1,3-PDO

CB_1825	propanediol dehydratase large subunit	pduC	EC:4.2.1.28	86.7	0	WP_034420514.1	propanediol dehydratase [<i>Clostridiales</i> bacterium DRI-13]
CB_1826	propanediol dehydratase medium subunit	pduD	EC:4.2.1.28	74.2	7.14E-109	WP_034420513.1	propanediol dehydratase [<i>Clostridiales</i> bacterium DRI-13]
CB_1827	propanediol dehydratase small subunit	pduE	EC:4.2.1.28	63.1	6.02E-75	WP_034420512.1	propanediol dehydratase [<i>Clostridiales</i> bacterium DRI-13]
CB_1829	propanediol dehydratase medium subunit	pduD	EC:4.2.1.28	45.4	1.65E-33	WP_051965455.1	hypothetical protein [<i>Clostridiales</i> bacterium DRI-13]

S3_Bin011-Clostridiales bacterium DRI-13-Membrane proteins involved in energy conservation-Rnf complex

CB_1310	electron transport complex protein RnfC	rnfC		56.5	9.75E-175	WP_053957529.1	electron transporter RnfC [<i>Clostridiaceae</i> bacterium mt12]
CB_1311	electron transport complex protein RnfD	rnfD		56.9	6.60E-118	WP_061325102.1	NADH:ubiquinone oxidoreductase [<i>Clostridium botulinum</i>] FMN-binding domain-containing protein [<i>Oxobacter pfennigii</i>]
CB_1312	electron transport complex protein RnfG	rnfG		42.9	5.31E-41	WP_054875717.1	KPU43836.1 electron transport complex subunit RnfG [<i>Oxobacter pfennigii</i>]
CB_1313	electron transport complex protein RnfE	rnfE		61.4	4.67E-83	ABY91404.1	electron transport complex, RnfABCDGE type, E subunit [<i>Thermoanaerobacter</i> sp. X514]
CB_1314	electron transport complex protein RnfA	rnfA		71.2	1.99E-91	SHE67843.1	electron transport complex protein RnfA [<i>Alkalibacter</i>]

							<i>saccharofermentans</i> DSM 14828]
CB_1315	electron transport complex protein RnfB	rnfB	54.2	2.20E-89	ADL07472.1		electron transport complex, RnfABCDGE type, B subunit [<i>Thermosediminibacter oceani</i> DSM 16646]
CB_3044	electron transport complex protein RnfC	rnfC	80.3	0	WP_069649212.1		electron transporter RnfC [<i>Caloranaerobacter ferrireducens</i>]
CB_3045	electron transport complex protein RnfD	rnfD	84.1	0	WP_069649213.1		NADH:ubiquinone oxidoreductase [<i>Caloranaerobacter ferrireducens</i>]
CB_3046	electron transport complex protein RnfG	rnfG	57.5	9.42E-75	SCL81994.1		Nitrogen fixation protein RnfG [<i>Sporanaerobacter</i> sp. PP17-6a]
CB_3047	electron transport complex protein RnfE	rnfE	82.3	3.22E-109	SDZ32054.1		electron transport complex protein RnfE [<i>Proteiniborus ethanoligenes</i>]
CB_3048	electron transport complex protein RnfA	rnfA	88.3	2.38E-111	KPU27845.1		electron transporter RnfA [<i>Caloranaerobacter</i> sp. TR13]
CB_3049	electron transport complex protein RnfB	rnfB	77.2	2.04E-179	WP_026893757.1		electron transporter RnfB [<i>Clostridiisalibacter paucivorans</i>]
S3_Bin011-Clostridiales bacterium DRI-13-ATPase							
CB_2546	F-type H+-transporting ATPase subunit a	atpB	79.5	5.94E-131	WP_051965468.1		ATP synthase F0 subunit A [<i>Clostridiales</i> bacterium DRI-13]
CB_2547	F-type H+-transporting ATPase subunit c	atpE	71.4	7.10E-28	KJS20239.1		ATP synthase F0 subunit C [<i>Clostridiaceae</i> bacterium BRH_c20a]
CB_2548	F-type H+-transporting ATPase subunit b	atpF	60.2	2.60E-61	WP_034420587.1		ATP synthase F0 subunit B [<i>Clostridiales</i> bacterium DRI-13]
CB_2549	F-type H+-transporting ATPase subunit delta	atpH	48.4	1.52E-57	WP_034420588.1		hypothetical protein [<i>Clostridiales</i> bacterium DRI-13]
CB_2550	F-type H+-transporting ATPase subunit alpha	atpA	EC:3.6.3.14	84.2	0	WP_034420589.1	ATP synthase subunit alpha [<i>Clostridiales</i> bacterium DRI-13]
CB_2551	F-type H+-transporting ATPase subunit gamma	atpG	60.8	3.19E-123	WP_034420590.1		ATP synthase F1 subunit gamma [<i>Clostridiales</i> bacterium DRI-13]
CB_2552	F-type H+-transporting ATPase subunit beta	atpD	EC:3.6.3.14	86.0	0	WP_034420592.1	ATP synthase subunit beta [<i>Clostridiales</i> bacterium DRI-13]
CB_2553	F-type H+-transporting ATPase subunit epsilon	atpC	54.6	8.43E-43	KKM10784.1		ATP synthase F0F1 subunit epsilon [<i>Clostridiales</i> bacterium PH28_bin88]
CB_2703	F-type H+-transporting ATPase subunit epsilon	atpC	71.4	8.78E-63	SHH82272.1		ATP synthase F1 subcomplex epsilon subunit [<i>Caloranaerobacter azorensis</i> DSM 13643]
CB_2704	F-type H+-transporting ATPase subunit beta	atpD	EC:3.6.3.14	85.1	0	WP_069650578.1	F0F1 ATP synthase subunit beta [<i>Caloranaerobacter ferrireducens</i>]
CB_2705	F-type H+-transporting ATPase subunit gamma	atpG	68.3	3.83E-146	EOC99447.1		ATP synthase gamma chain [<i>Caldisaliniibacter kiritimatiensis</i>]

CB_2706	F-type H ⁺ -transporting ATPase subunit alpha	atpA	EC:3.6.3.14	86.8	0	SCG81862.1	F-type H ⁺ -transporting ATPase subunit alpha [<i>Proteiniborus</i> sp. DW1]
CB_2707	F-type H ⁺ -transporting ATPase subunit delta	atpH		63.2	2.49E-74	EOC99449.1	ATP synthase delta chain [<i>Caldisalibacter kiritimatiensis</i>]
CB_2708	F-type H ⁺ -transporting ATPase subunit b	atpF		63.5	1.75E-69	EOC99450.1	ATP synthase B chain [<i>Caldisalibacter kiritimatiensis</i>]
CB_2709	F-type H ⁺ -transporting ATPase subunit c	atpE		92.9	2.04E-42	KPU27398.1	ATP synthase F0F1 subunit C [<i>Caloranaerobacter</i> sp. TR13]
CB_2711	F-type H ⁺ -transporting ATPase subunit a	atpB		80.4	3.51E-124	KPU27543.1	ATP synthase F0 subunit A [<i>Caloranaerobacter</i> sp. TR13]
CB_0087	flagellum-specific ATP synthase	fliI	EC:3.6.3.14	75.5	0	WP_051965358.1	flagellar protein export ATPase FliI [<i>Clostridiales</i> bacterium DRI-13]
S3_Bin011-Clostridiales bacterium DRI-13-Hydrogenases and coupling enzymes							
CB_1861	hydrogenase expression/formation protein HypE	hypE		65.3	4.22E-156	WP_034420072.1	hydrogenase expression/formation protein HypE [<i>Clostridiales</i> bacterium DRI-13]
CB_1862	hydrogenase expression/formation protein HypD	hypD		60.1	1.13E-151	WP_034420071.1	hydrogenase formation protein HypD [<i>Clostridiales</i> bacterium DRI-13]
CB_1863	hydrogenase expression/formation protein HypC	hypC		60.8	2.51E-27	WP_034420070.1	hypothetical protein [<i>Clostridiales</i> bacterium DRI-13]
CB_1864	hydrogenase maturation protein HypF	hypF		59.2	0	WP_051965397.1	carbamoyltransferase HypF [<i>Clostridiales</i> bacterium DRI-13]
CB_1865	hydrogenase nickel incorporation protein HypB	hypB		72.6	2.52E-108	WP_034420236.1	hydrogenase accessory protein HypB [<i>Clostridiales</i> bacterium DRI-13]
CB_1866	hydrogenase nickel incorporation protein HypA/HybF	hypA		59.3	1.77E-44	WP_034420069.1	hypothetical protein [<i>Clostridiales</i> bacterium DRI-13]
CB_1867	hydrogenase maturation protease	hyaD	EC:3.4.23.-	38.8	3.29E-35	SFH25243.1	hydrogenase maturation protease [<i>Desulfotomaculum arcticum</i>]
CB_1868	hydrogenase small subunit	hyaA	EC:1.12.99.6	75.5	2.40E-167	KJS76055.1	Ni/Fe hydrogenase [<i>Desulfotomaculum</i> sp. BICA1-6]
CB_1869	hydrogenase large subunit	hyaB	EC:1.12.99.6	68.3	0	OAT79946.1	nickel-dependent hydrogenase large subunit [<i>Desulfotomaculum copahuensis</i>]
S3_Bin013-Proteiniphilum acetatigenes-Pyruvate to acetyl-CoA							
PA_1106	pyruvate-ferredoxin/ferredoxin oxidoreductase	por	EC:1.2.7.1	99.9	0	SCD19401.1	Pyruvate dehydrogenase (NADP(+)) [<i>Proteiniphilum</i>

							1.2.7.-	<i>saccharofermentans</i>
PA_1341	pyruvate dehydrogenase E1 component alpha subunit	PDHA	EC:1.2.4.1	99.7	0	WP_019541063.1	pyruvate dehydrogenase (acetyl-transferring) E1 component subunit alpha [<i>Proteiniphilum acetatigenes</i>]	
PA_1342	pyruvate dehydrogenase E1 component beta subunit	PDHB	EC:1.2.4.1	98.2	0	WP_019541064.1	alpha-ketoacid dehydrogenase subunit beta [<i>Proteiniphilum acetatigenes</i>]	
PA_1343	pyruvate dehydrogenase E2 component (dihydrolipoamide acetyltransferase)	DLAT	EC:2.3.1.12	99.1	0	SCD19867.1	branched-chain alpha-keto acid dehydrogenase subunit E2 [<i>Proteiniphilum saccharofermentans</i>]	
PA_2140	pyruvate dehydrogenase E1 component alpha subunit	PDHA	EC:1.2.4.1	100.0	0	SCD21251.1	TPP-dependent acetoin dehydrogenase complex, E1 component, alpha subunit [<i>Proteiniphilum saccharofermentans</i>]	
PA_2141	pyruvate dehydrogenase E1 component beta subunit	PDHB	EC:1.2.4.1	100.0	0	SCD21250.1	Pyruvate dehydrogenase (acetyl-transferring) [<i>Proteiniphilum saccharofermentans</i>]	
PA_2142	pyruvate dehydrogenase E2 component (dihydrolipoamide acetyltransferase)	DLAT	EC:2.3.1.12	100.0	0	SCD21249.1	dihydrolipoamide acetyltransferase [<i>Proteiniphilum saccharofermentans</i>]	
PA_3150	pyruvate dehydrogenase E1 component alpha subunit	PDHA	EC:1.2.4.1	100.0	0	EIW10975.1	Pda1p [<i>Saccharomyces cerevisiae</i> CEN.PK113-7D]	
S3_Bin013-Proteiniphilum acetatigenes-Acetate production								
PA_1749	phosphate acetyltransferase	pta	EC:2.3.1.8	100.0	0	SCD21544.1	Phosphate acetyltransferase [<i>Proteiniphilum saccharofermentans</i>]	
PA_1751	acetate kinase	ackA	EC:2.7.2.1	100.0	0	SFK27731.1	acetate kinase [<i>Porphyromonadaceae</i> bacterium KH3CP3RA]	
PA_3123	acetate kinase	ackA	EC:2.7.2.1	90.7	4.84E-69	OFX54921.1	acetate kinase [<i>Bacteroidetes</i> bacterium GWC2_46_850]	
S3_Bin013-Proteiniphilum acetatigenes-Butyrate production								
PA_2097	acetyl-CoA acetyltransferase	atoB	EC:2.3.1.9	95.9	0	SCD22188.1	hypothetical protein PSM36_3404 [<i>Proteiniphilum saccharofermentans</i>]	
PA_1750	3-hydroxybutyryl-CoA dehydrogenase	paaH	EC:1.1.1.157	100.0	0	SFT08001.1	3-hydroxybutyryl-CoA dehydrogenase [<i>Porphyromonadaceae</i> bacterium NLAE-zl-C104]	
PA_2878	enoyl-CoA hydratase	crt	EC:4.2.1.17	75.5	1.06E-143	WP_019228234.1	hypothetical protein [<i>Sedimentibacter</i> sp. B4]	
PA_1153	butyryl-CoA dehydrogenase	bcd	EC:1.3.8.1	100.0	0	WP_076930396.1	acyl-CoA dehydrogenase [<i>Proteiniphilum saccharofermentans</i>]	

PA_1154	electron transfer flavoprotein alpha subunit	etfA	100.0	0	SCD20374.1	electron transfer flavoprotein subunit alpha [<i>Proteiniphilum saccharofermentans</i>]	
PA_1155	electron transfer flavoprotein beta subunit	etfB	100.0	0	SCD20373.1	putative electron transfer flavoprotein beta-subunit [<i>Proteiniphilum saccharofermentans</i>]	
PA_2164	phosphate butyryltransferase	ptb	EC:2.3.1.19	91.9	0	SFL27465.1	phosphate butyryltransferase [<i>Porphyromonadaceae</i> bacterium KH3CP3RA]
PA_2165	butyrate kinase	buk	EC:2.7.2.7	99.2	0	SCD21990.1	Butyrate kinase [<i>Proteiniphilum saccharofermentans</i>]
S3_Bin013-Proteiniphilum acetatigenes-Membrane proteins involved in energy conservation-Rnf complex							
PA_0178	electron transport complex protein RnfB	RnfB	100.0	0	SDZ86045.1	Na ⁺ -translocating ferredoxin:NAD ⁺ oxidoreductase RNF, RnfB subunit [<i>Porphyromonadaceae</i> bacterium KH3R12]	
PA_0179	electron transport complex protein RnfC	RnfC	99.8	0	CD19710.1	electron transport complex protein RnfC [<i>Proteiniphilum saccharofermentans</i>]	
PA_0180	electron transport complex protein RnfD	RnfD	99.4	0	SFS96080.1	electron transport complex protein RnfD [<i>Porphyromonadaceae</i> bacterium NLAE-zl-C104]	
PA_0181	electron transport complex protein RnfG	RnfG	100.0	1.88E-174	SDZ86001.1	electron transport complex protein RnfG [<i>Porphyromonadaceae</i> bacterium KH3R12]	
PA_0182	electron transport complex protein RnfE	RnfE	100.0	5.00E-135	SDZ85990.1	electron transport complex protein RnfE [<i>Porphyromonadaceae</i> bacterium KH3R12]	
PA_0183	electron transport complex protein RnfA	RnfA	100.0	1.12E-129	SCD19706.1	Electron transport complex protein RnfA [<i>Proteiniphilum saccharofermentans</i>]	
S3_Bin013-Proteiniphilum acetatigenes-ATPase							
PA_1194	V/A-type H ⁺ /Na ⁺ -transporting ATPase subunit E	ATPVE	99.5	1.84E-136	SFS76148.1	V/A-type H ⁺ -transporting ATPase subunit E [<i>Porphyromonadaceae</i> bacterium NLAE-zl-C104]	
PA_1195	V/A-type H ⁺ /Na ⁺ -transporting ATPase subunit C	ATPVC	95.8	0	SFS76135.1	Protein of unknown function [<i>Porphyromonadaceae</i> bacterium NLAE-zl-C104]	

PA_1196	V/A-type H ⁺ /Na ⁺ -transporting ATPase subunit A	ATPVA	EC:3.6.3.14 3.6.3.15	98.5	0	SDZ91858.1	V/A-type H ⁺ -transporting ATPase subunit A [<i>Porphyromonadaceae</i> bacterium KH3R12]
PA_1197	V/A-type H ⁺ /Na ⁺ -transporting ATPase subunit B	ATPVB		100.0	0	SCD21060.1	V-type ATP synthase beta chain [<i>Proteiniphilum saccharofermentans</i>]
PA_1198	V/A-type H ⁺ /Na ⁺ -transporting ATPase subunit D	ATPVD		99.5	1.41E-145	SCD21061.1	V-type ATP synthase subunit D [<i>Proteiniphilum saccharofermentans</i>]
PA_1199	V/A-type H ⁺ /Na ⁺ -transporting ATPase subunit I	ATPVI		86.4	0	WP_019537732.1	V-type ATP synthase subunit I [<i>Proteiniphilum acetatigenes</i>]
PA_1200	V/A-type H ⁺ /Na ⁺ -transporting ATPase subunit K	ATPVK		95.4	5.21E-96	WP_019537733.1	V-type ATP synthase subunit K [<i>Proteiniphilum acetatigenes</i>]
S3_Bin013-<i>Proteiniphilum acetatigenes</i>-Hydrogenase (putative electron-bifurcating hydrogenase)							
PA_2833	ferredoxin--NADP ⁺ reductase	fpr	EC:1.18.1.2	100.0	0	SCD20716.1	ferredoxin-NADP(+) reductase subunit alpha [<i>Proteiniphilum saccharofermentans</i>]
S6_Bin001-<i>Actinomyces provencensis</i>-Glycerol oxidation 2							
AP_0992	glycerol kinase	glpK	EC:2.7.1.30	96.7	0	WP_043535862.1	glycerol kinase [<i>Actinomyces polynesiensis</i>]
AP_1608	glycerol-3-phosphate dehydrogenase (NAD(P) ⁺)	gpsA	EC:1.1.1.94	97.6	0	WP_075890310.1	glycerol-3-phosphate acyltransferase [<i>Actinomyces provencensis</i>]
AP_0891	glycerol-3-phosphate dehydrogenase subunit B	glpB	EC:1.1.5.3	99.3	0	WP_075888552.1	anaerobic glycerol-3-phosphate dehydrogenase subunit B [<i>Actinomyces provencensis</i>]
AP_0892	glycerol-3-phosphate dehydrogenase	glpA	EC:1.1.5.3	99.1	0	WP_075888554.1	sn-glycerol-3-phosphate dehydrogenase subunit A [<i>Actinomyces provencensis</i>]
AP_2148	glycerol-3-phosphate dehydrogenase	glpA	EC:1.1.5.3	98.1	0	WP_075890934.1	glycerol-3-phosphate dehydrogenase [<i>Actinomyces provencensis</i>]
AP_2149	glycerol uptake facilitator protein	GLPF		97.8	0	WP_043535861.1	glycerol transporter [<i>Actinomyces polynesiensis</i>]
S6_Bin001-<i>Actinomyces provencensis</i>-Central axis pathway							
AP_0354	triosephosphate isomerase (TIM)	TPI	EC:5.3.1.1	45.4	1.47E-61	WP_025733286.1	triose-phosphate isomerase [<i>Carnimonas nigrificans</i>]
AP_0713	triosephosphate isomerase (TIM)	TPI	EC:5.3.1.1	98.8	0	WP_075889582.1	triose-phosphate isomerase [<i>Actinomyces provencensis</i>]

AP_0580	glyceraldehyde 3-phosphate dehydrogenase	GAPDH	EC:1.2.1.12	98.8	0	WP_075889586.1	type I glyceraldehyde-3-phosphate dehydrogenase [<i>Actinomyces provencensis</i>]
AP_1899	glyceraldehyde 3-phosphate dehydrogenase	GAPDH	EC:1.2.1.12	92.1	0	WP_043535446.1	type I glyceraldehyde-3-phosphate dehydrogenase [<i>Actinomyces polynesiensis</i>]
AP_0714	phosphoglycerate kinase	PGK	EC:2.7.2.3	97.9	0	WP_075889584.1	phosphoglycerate kinase [<i>Actinomyces provencensis</i>]
AP_0097	probable phosphoglycerate mutase	gpmB	EC:5.4.2.12	99.6	7.27E-164	WP_075889274.1	hypothetical protein [<i>Actinomyces provencensis</i>]
AP_1518	2,3-bisphosphoglycerate-dependent phosphoglycerate mutase	PGAM	EC:5.4.2.11	100.0	4.81E-180	WP_075892264.1	phosphoglyceromutase [<i>Actinomyces provencensis</i>]
AP_0922	enolase	ENO	EC:4.2.1.11	100.0	0	WP_078062515.1	phosphopyruvate hydratase [<i>Actinomyces provencensis</i>]
AP_0308	pyruvate, orthophosphate dikinase	ppdK	EC:2.7.9.1	99.6	0	WP_075892335.1	pyruvate, phosphate dikinase [<i>Actinomyces provencensis</i>]
AP_2376	pyruvate dehydrogenase E1 component beta subunit	PDHB	EC:1.2.4.1	100.0	2.30E-174	WP_075891946.1	alpha-ketoacid dehydrogenase subunit beta [<i>Actinomyces provencensis</i>]
AP_2377	pyruvate dehydrogenase E2 component (dihydrolipoamide acetyltransferase)	DLAT	EC:2.3.1.12	97.4	0	WP_075891948.1	diaminohydroxyphosphoribosylaminopyrimidine deaminase [<i>Actinomyces provencensis</i>]
S6_Bin001-Actinomyces provencensis-Acetate production							
AP_1455	phosphate acetyltransferase	pta	EC:2.3.1.8	71.9	0	ENO18742.1	phosphate acetyltransferase [<i>Actinomyces cardiffensis</i> F0333]
AP_1456	acetate kinase	ackA	EC:2.7.2.1	99.7	0	WP_078062518.1	acetate kinase [<i>Actinomyces provencensis</i>]
S6_Bin001-Actinomyces provencensis-Ethanol production/oxidation							
AP_0139	acetaldehyde dehydrogenase / alcohol dehydrogenase	adhE	EC:1.2.1.10 1.1.1.1	98.7	0	WP_078062118.1	hypothetical protein [<i>Actinomyces provencensis</i>]
S6_Bin001-Actinomyces provencensis-Membrane proteins involved in energy conservation-Fix system							
AP_1459	electron transfer flavoprotein beta subunit	fixA		100.0	0	WP_075888696.1	electron transfer flavoprotein subunit beta [<i>Actinomyces provencensis</i>]
AP_1460	electron transfer flavoprotein alpha subunit	fixB		100.0	0	WP_075888694.1	electron transporter [<i>Actinomyces provencensis</i>]
S6_Bin003-Eubacterium limosum-Wood Ljungdahl pathway							

EL_0894	formate dehydrogenase major subunit	fdoG	EC:1.2.1.2	99.9	0	WP_038352620.1	molybdopterin oxidoreductase [<i>Eubacterium limosum</i>]
EL_4218	formate dehydrogenase alpha subunit	fdhA	EC:1.2.1.43	99.6	0	WP_038354071.1	formate dehydrogenase subunit alpha [<i>Eubacterium limosum</i>]
EL_1980	formate-tetrahydrofolate ligase	fhs	EC:6.3.4.3	100.0	0	WP_038351869.1	formate--tetrahydrofolate ligase [<i>Eubacterium limosum</i>]
EL_1979	methenyl-THF cyclohydrolase	fchA		100.0	6.34E-150	WP_038351868.1	sugar ABC transporter substrate-binding protein [<i>Eubacterium limosum</i>]
EL_1978	methylenetetrahydrofolate dehydrogenase (NADP+) / methenyltetrahydrofolate cyclohydrolase	foID	EC:1.5.1.5; 3.5.4.9	100.0	0	WP_038351867.1	methylenetetrahydrofolate dehydrogenase [<i>Eubacterium limosum</i>]
EL_1353	methylenetetrahydrofolate reductase (NADPH)	metF	EC:1.5.1.20	99.6	0	WP_038351520.1	5,10-methylenetetrahydrofolate reductase [<i>Eubacterium limosum</i>]
EL_1496	5-methyltetrahydrofolate corrinoid/iron sulfur protein methyltransferase	acsE	EC:2.1.1.258	100.0	0	ADO38562.1	putative methyltetrahydrofolate:corrinoid/iron-sulfur protein methyltransferase [<i>Eubacterium limosum</i> KIST612]
EL_1495	carbon-monoxide dehydrogenase catalytic subunit	cooS	EC:1.2.7.4	100.0	0	WP_038352890.1	carbon-monoxide dehydrogenase catalytic subunit [<i>Eubacterium limosum</i>]
EL_1494	CO dehydrogenase maturation factor	cooC		100.0	0	WP_038352889.1	carbon monoxide dehydrogenase [<i>Eubacterium limosum</i>]
EL_1501	CO dehydrogenase maturation factor	cooC		100.0	0	WP_038352894.1	carbon monoxide dehydrogenase [<i>Eubacterium limosum</i>]
EL_1493	acetyl-CoA synthase	acsB	EC:2.3.1.169	100.0	0	SHK89002.1	CO-methylating acetyl-CoA synthase precursor /acetyl-CoA decarbonylase/synthase beta subunit [<i>Eubacterium callanderi</i>]
EL_1497	acetyl-CoA decarbonylase/synthase complex subunit gamma	cdhE	EC:2.1.1.245	100.0	0	WP_038352891.1	acetyl-CoA synthase subunit gamma [<i>Eubacterium limosum</i>]
EL_1498	acetyl-CoA decarbonylase/synthase complex subunit delta	cdhD	EC:2.1.1.245	100.0	0	WP_038352892.1	acetyl-CoA synthase subunit delta [<i>Eubacterium limosum</i>]
S6_Bin003-Eubacterium limosum-Glycerol oxidation 1							
EL_0118	glycerol dehydrogenase	gldA	EC:1.1.1.6	99.2	0	WP_038353946.1	glycerol dehydrogenase [<i>Eubacterium limosum</i>]
EL_1094	glycerol dehydrogenase	gldA	EC:1.1.1.6	100.0	0	ADO38429.1	glycerol dehydrogenase [<i>Eubacterium limosum</i> KIST612]
EL_1695	dihydroxyacetone kinase, C-terminal domain	dhaL	EC:2.7.1.-	99.5	4.23E-149	WP_038352007.1	DAK2 domain-containing protein [<i>Eubacterium limosum</i>]
EL_1697	dihydroxyacetone kinase, N-terminal domain	dhaK	EC:2.7.1.-	100.0	0	SFO97100.1	dihydroxyacetone kinase, N-terminal domain [<i>Eubacterium callanderi</i>]
EL_2829	dihydroxyacetone kinase, C-terminal domain	dhaL	EC:2.7.1.-	100.0	1.31E-154	WP_038351073.1	dihydroxyacetone kinase subunit L [<i>Eubacterium limosum</i>]

EL_2830	dihydroxyacetone kinase, N-terminal domain	dhaK	EC:2.7.1.-	99.7	0	SFO23221.1	dihydroxyacetone kinase DhaK subunit [<i>Eubacterium callanderi</i>]
EL_3471	dihydroxyacetone kinase, C-terminal domain	dhaL	EC:2.7.1.-	100.0	0	WP_038350668.1	dihydroxyacetone kinase subunit DhaK [<i>Eubacterium limosum</i>]
EL_3472	dihydroxyacetone kinase, N-terminal domain	dhaK	EC:2.7.1.-	99.5	8.06E-151	ADO38052.1	hypothetical protein ELI_3083 [<i>Eubacterium limosum</i> KIST612]
S6_Bin003-Eubacterium limosum-Glycerol oxidation 2							
EL_0111	glycerol kinase	glpK	EC:2.7.1.30	99.8	0	WP_038353941.1	glycerol kinase [<i>Eubacterium limosum</i>]
EL_0505	glycerol kinase	glpK	EC:2.7.1.30	100.0	0	SFO34581.1	glycerol kinase [<i>Eubacterium callanderi</i>]
EL_1301	glycerol kinase	glpK	EC:2.7.1.30	99.4	0	WP_038351560.1	glycerol kinase [<i>Eubacterium limosum</i>]
EL_1871	glycerol kinase	glpK	EC:2.7.1.30	100.0	0	WP_038351422.1	glycerol kinase [<i>Eubacterium limosum</i>]
EL_3010	glycerol kinase	glpK	EC:2.7.1.30	99.2	0	WP_058695680.1	hypothetical protein [<i>Eubacterium limosum</i>]
EL_3470	glycerol kinase	glpK	EC:2.7.1.30	99.8	0	WP_038350669.1	glycerol kinase [<i>Eubacterium limosum</i>]
EL_3923	glycerol kinase	glpK	EC:2.7.1.30	100.0	0	WP_038351202.1	glycerol kinase [<i>Eubacterium limosum</i>]
EL_0350	glycerol-3-phosphate dehydrogenase (NAD(P)+)	gpsA	EC:1.1.1.94	100.0	0	SHL05067.1	glycerol-3-phosphate dehydrogenase (NAD(P)+) [<i>Eubacterium callanderi</i>]
EL_3860	glycerol-3-phosphate dehydrogenase (NAD(P)+)	gpsA	EC:1.1.1.94	100.0	0	WP_038350631.1	glycerol-3-phosphate dehydrogenase [<i>Eubacterium limosum</i>]
EL_0110	glycerol-3-phosphate dehydrogenase	glpA	EC:1.1.5.3	99.8	0	WP_052237462.1	FAD-dependent oxidoreductase [<i>Eubacterium limosum</i>]
EL_1063	glycerol-3-phosphate dehydrogenase	glpA	EC:1.1.5.3	98.6	0	SFP62776.1	glycerol-3-phosphate dehydrogenase [<i>Eubacterium callanderi</i>]
EL_1304	glycerol-3-phosphate dehydrogenase	glpA	EC:1.1.5.3	99.1	0	WP_052237143.1	hypothetical protein [<i>Eubacterium limosum</i>]
EL_2196	glycerol-3-phosphate dehydrogenase	glpA	EC:1.1.5.3	99.0	0	WP_038353326.1	FAD/NAD(P)-binding oxidoreductase [<i>Eubacterium limosum</i>]
EL_2221	glycerol-3-phosphate dehydrogenase	glpA	EC:1.1.5.3	99.2	0	WP_038353344.1	FAD/NAD(P)-binding oxidoreductase [<i>Eubacterium limosum</i>]
EL_2672	glycerol-3-phosphate dehydrogenase	glpA	EC:1.1.5.3	99.6	0	WP_038351204.1	FAD/NAD(P)-binding oxidoreductase [<i>Eubacterium limosum</i>]
EL_2812	glycerol-3-phosphate dehydrogenase	glpA	EC:1.1.5.3	99.8	0	WP_038351061.1	FAD/NAD(P)-binding oxidoreductase [<i>Eubacterium limosum</i>]
EL_3009	glycerol-3-phosphate dehydrogenase	glpA	EC:1.1.5.3	98.5	0	ALU15927.1	FAD-dependent oxidoreductase [<i>Eubacterium limosum</i>]
EL_3468	glycerol-3-phosphate dehydrogenase	glpA	EC:1.1.5.3	100.0	0	WP_038350670.1	FAD/NAD(P)-binding oxidoreductase [<i>Eubacterium limosum</i>]
S6_Bin003-Eubacterium limosum-Central axis pathway							
EL_0677	triosephosphate isomerase	TPI	EC:5.3.1.1	98.8	1.40E-175	WP_038350858.1	triose-phosphate isomerase [<i>Eubacterium limosum</i>]

EL_1848	triosephosphate isomerase	TPI	EC:5.3.1.1	97.9	1.28E-168	WP_038351440.1	triose-phosphate isomerase [<i>Eubacterium limosum</i>]
EL_2644	triosephosphate isomerase	TPI	EC:5.3.1.1	99.6	2.02E-167	WP_038353251.1	triose-phosphate isomerase [<i>Eubacterium limosum</i>]
EL_2834	triosephosphate isomerase	TPI	EC:5.3.1.1	100.0	0	WP_038351075.1	triose-phosphate isomerase [<i>Eubacterium limosum</i>]
EL_0252	glyceraldehyde-3-phosphate dehydrogenase (NADP+)	gapN	EC:1.2.1.9	99.0	0	WP_052237499.1	NADP-dependent glyceraldehyde-3-phosphate dehydrogenase [<i>Eubacterium limosum</i>]
EL_0679	glyceraldehyde 3-phosphate dehydrogenase	GAPDH	EC:1.2.1.12	100.0	0	WP_038350860.1	type I glyceraldehyde-3-phosphate dehydrogenase [<i>Eubacterium limosum</i>]
EL_0678	phosphoglycerate kinase	PGK	EC:2.7.2.3	99.5	0	SFO29749.1	phosphoglycerate kinase [<i>Eubacterium callanderi</i>]
EL_0676	2,3-bisphosphoglycerate-independent phosphoglycerate mutase	gpmI	EC:5.4.2.12	99.2	0	SFO29794.1	phosphoglycerate mutase [<i>Eubacterium callanderi</i>]
EL_2723	2,3-bisphosphoglycerate-dependent phosphoglycerate mutase	PGAM	EC:5.4.2.11	99.6	0	WP_038351252.1	phosphoglyceromutase [<i>Eubacterium limosum</i>]
EL_3185	probable phosphoglycerate mutase	gpmB	EC:5.4.2.12	99.6	6.77E-165	WP_038350984.1	histidine phosphatase family protein [<i>Eubacterium limosum</i>]
EL_2548	enolase	ENO	EC:4.2.1.11	99.8	0	WP_038353181.1	phosphopyruvate hydratase [<i>Eubacterium limosum</i>]
EL_3483	pyruvate kinase	pyk	EC:2.7.1.40	99.3	0	ADO38040.1	pyruvate kinase [<i>Eubacterium limosum</i> KIST612]
EL_1654	pyruvate dehydrogenase E2 component (dihydrolipoamide acetyltransferase)	DLAT/p dhc	EC:2.3.1.12	99.8	0	ADO36112.1	catalytic domain of components of various dehydrogenase complexes [<i>Eubacterium limosum</i> KIST612]
EL_1655	pyruvate dehydrogenase E1 component beta subunit	PDHB	EC:1.2.4.1	100.0	0	WP_038351975.1	alpha-ketoacid dehydrogenase subunit beta [<i>Eubacterium limosum</i>]
EL_1656	pyruvate dehydrogenase E1 component alpha subunit	PDHA	EC:1.2.4.1	100.0	0	SHL32931.1	pyruvate dehydrogenase E1 component alpha subunit [<i>Eubacterium callanderi</i>]
EL_0253	pyruvate-ferredoxin/flavodoxin oxidoreductase	por	EC:1.2.7.1 1.2.7.-	100.0	0	WP_038354167.1	pyruvate:ferredoxin (flavodoxin) oxidoreductase [<i>Eubacterium limosum</i>]
EL_2073	pyruvate ferredoxin oxidoreductase beta subunit	porB	EC:1.2.7.1	99.7	0	WP_038351931.1	2-ketoisovalerate ferredoxin oxidoreductase [<i>Eubacterium limosum</i>]
EL_2074	pyruvate ferredoxin oxidoreductase alpha subunit	porA	EC:1.2.7.1	99.7	0	WP_038351932.1	pyruvate ferredoxin oxidoreductase [<i>Eubacterium limosum</i>]
EL_2075	pyruvate ferredoxin oxidoreductase delta subunit	porD	EC:1.2.7.1	99.0	5.47E-67	WP_038351933.1	pyruvate ferredoxin oxidoreductase [<i>Eubacterium limosum</i>]
EL_2076	pyruvate ferredoxin oxidoreductase gamma subunit	porG	EC:1.2.7.1	100.0	2.88E-128	ALU13014.1	2-ketoisovalerate ferredoxin oxidoreductase gamma subunit [<i>Eubacterium limosum</i>]

EL_2254	pyruvate ferredoxin oxidoreductase gamma subunit	porG	EC:1.2.7.1	100.0	2.61E-138	WP_038353370.1	pyruvate synthase [<i>Eubacterium limosum</i>]
EL_2255	pyruvate ferredoxin oxidoreductase delta subunit	porD	EC:1.2.7.1	100.0	1.07E-67	WP_038353371.1	ferredoxin [<i>Eubacterium limosum</i>]
EL_2256	pyruvate ferredoxin oxidoreductase alpha subunit	porA	EC:1.2.7.1	99.5	0	WP_038353372.1	pyruvate ferredoxin oxidoreductase [<i>Eubacterium limosum</i>]
EL_2257	pyruvate ferredoxin oxidoreductase beta subunit	porB	EC:1.2.7.1	99.7	0	WP_038353373.1	pyruvate ferredoxin oxidoreductase [<i>Eubacterium limosum</i>]
S6_Bin003-Eubacterium limosum-Acetate production							
EL_0991	putative phosphotransacetylase	Pta	EC:2.3.1.8	100.0	2.34E-156	SDP49526.1	putative phosphotransacetylase [<i>Eubacterium limosum</i>]
EL_2377	putative phosphotransacetylase	Pta	EC:2.3.1.8	98.6	1.01E-156	SDP60926.1	putative phosphotransacetylase [<i>Eubacterium limosum</i>]
EL_3888	acetate kinase	ackA	EC:2.7.2.1	100.0	0	WP_038354231.1	acetate kinase [<i>Eubacterium limosum</i>]
S6_Bin003-Eubacterium limosum-Butyrate production							
EL_3224	acetyl-CoA C-acetyltransferase	atoB	EC:2.3.1.9	100.0	0	WP_038350953.1	acetyl-CoA acetyltransferase [<i>Eubacterium limosum</i>]
EL_3226	3-hydroxybutyryl-CoA dehydrogenase	paaH	EC:1.1.1.157	100.0	0	SFO26749.1	3-hydroxybutyryl-CoA dehydrogenase [<i>Eubacterium callanderi</i>]
EL_0831	enoyl-CoA hydratase	crt	EC:4.2.1.17	99.6	0	WP_038353019.1	enoyl-CoA hydratase [<i>Eubacterium limosum</i>]
EL_3225	enoyl-CoA hydratase	crt	EC:4.2.1.17	100.0	0	WP_038350952.1	enoyl-CoA hydratase [<i>Eubacterium limosum</i>]
EL_0829	butyryl-CoA dehydrogenase	bcd	EC:1.3.8.1	99.2	0	SFO81465.1	butyryl-CoA dehydrogenase [<i>Eubacterium callanderi</i>]
EL_3227	butyryl-CoA dehydrogenase	bcd	EC:1.3.8.1	100.0	0	SFO26775.1	butyryl-CoA dehydrogenase [<i>Eubacterium callanderi</i>]
EL_3228	electron transfer flavoprotein beta subunit	etfB		100.0	0	WP_038350951.1	electron transfer flavoprotein subunit beta [<i>Eubacterium limosum</i>]
EL_3229	electron transfer flavoprotein alpha subunit	etfA		100.0	0	ALU16220.1	electron transfer flavoprotein alpha subunit [<i>Eubacterium limosum</i>]
EL_0830	propionate CoA-transferase	pct	EC:2.8.3.1	99.4	0	WP_038353018.1	3-oxoacid CoA-transferase [<i>Eubacterium limosum</i>]
EL_0498	phosphate butyryltransferase	ptb	EC:2.3.1.19	99.3	0	WP_038352195.1	phosphate butyryltransferase [<i>Eubacterium limosum</i>]
EL_3573	phosphate butyryltransferase	ptb	EC:2.3.1.19	100.0	0	WP_052237430.1	phosphate butyryltransferase [<i>Eubacterium limosum</i>]
S6_Bin003-Eubacterium limosum-Ethanol production/oxidation							
EL_2556	acetaldehyde dehydrogenase	adhE	EC:1.2.1.10	99.7	0	WP_038353188.1	butanol dehydrogenase [<i>Eubacterium limosum</i>]
EL_2935	acetaldehyde dehydrogenase	adhE	EC:1.2.1.10	99.7	0	SFO36846.1	hypothetical protein SAMN04487888_101644 [<i>Eubacterium callanderi</i>]
EL_1014	alcohol dehydrogenase	adh2	EC:1.1.1.-	100.0	0	SFP64208.1	alcohol dehydrogenase [<i>Eubacterium callanderi</i>]

S6_Bin003-Eubacterium limosum-Glycerol reduction to 1,3-PDO

EL_2378	propanediol utilization protein	pduK	99.3	3.19E-103	ADO39020.1	BMC domain protein [<i>Eubacterium limosum</i> KIST612]	
EL_2379	propanediol dehydratase reactivation protein, small subunit	pduH	100.0	8.90E-82	WP_038352521.1	glycerol dehydratase [<i>Eubacterium limosum</i>]	
EL_2380	propanediol dehydratase reactivation protein, large subunit	pduG	100.0	0	ADO39022.1	Diol/glycerol dehydratase reactivating factor large subunit [<i>Eubacterium limosum</i> KIST612]	
EL_2381	propanediol dehydratase small subunit	pduE	EC:4.2.1.28	100.0	1.50E-118	WP_038352519.1	propanediol dehydratase [<i>Eubacterium limosum</i>]
EL_2382	propanediol dehydratase medium subunit	pduD	EC:4.2.1.28	100.0	2.87E-159	SDP61038.1	propanediol dehydratase medium subunit [<i>Eubacterium limosum</i>]
EL_2383	propanediol dehydratase large subunit	pduC	EC:4.2.1.28	100.0	0	SFP43929.1	propanediol dehydratase large subunit [<i>Eubacterium callanderi</i>]
EL_2384	Propanediol utilization protein	pduB	100.0	0	ALU13306.1	microcompartment protein PduB [<i>Eubacterium limosum</i>]	
EL_2385	Propanediol utilization polyhedral body protein	PduA	100.0	1.14E-57	ALU13305.1	microcompartment protein PduA [<i>Eubacterium limosum</i>]	
EL_0104	1,3-propanediol dehydrogenase	dhaT	EC:1.1.1.202	99.8	0	OEZ04839.1	1,3-propanediol dehydrogenase [[<i>Butyrbacterium</i> <i>methylophilicum</i>]

S6_Bin003-Eubacterium limosum-Membrane proteins involved in energy**conservation-Rnf complex**

EL_3628	electron transport complex protein RnfC	rnfC	100.0	0	WP_038351329.1	electron transporter RnfC [<i>Eubacterium limosum</i>]
EL_3629	electron transport complex protein RnfD	rnfD	99.7	0	ADO37623.1	RnfD [<i>Eubacterium limosum</i> KIST612]
EL_3630	electron transport complex protein RnfG	rnfG	99.5	8.40E-146	WP_052237107.1	electron transporter [<i>Eubacterium limosum</i>]
EL_3631	electron transport complex protein RnfE	rnfE	100.0	4.05E-142	WP_038351331.1	electron transport complex subunit RsxE [<i>Eubacterium limosum</i>]
EL_3632	electron transport complex protein RnfA	rnfA	100.0	9.36E-129	ADO37620.1	RnfA [<i>Eubacterium limosum</i> KIST612]
EL_3633	electron transport complex protein RnfB	rnfB	100.0	0	WP_052237108.1	electron transporter RnfB [<i>Eubacterium limosum</i>]

S6_Bin003-Eubacterium limosum-Membrane proteins involved in energy**conservation-FAD (or Fe-S) reductase linked to ETF**

EL_3001	Acryloyl-CoA reductase electron transfer subunit beta	etfA	91.8	0	SHL94193.1	electron transfer flavoprotein alpha subunit apoprotein [<i>Eubacterium callanderi</i>]
EL_3002	Acryloyl-CoA reductase electron transfer subunit gamma	etfB	98.5	0	WP_038352172.1	hypothetical protein [<i>Eubacterium limosum</i>]

EL_3003	putative FAD-linked oxidoreductase			96.7	0	WP_038352173.1	FAD-binding oxidoreductase [<i>Eubacterium limosum</i>]
EL_3004	Electron transfer flavoprotein subunit alpha	etfA		97.8	0	WP_052237223.1	hypothetical protein [<i>Eubacterium limosum</i>]
EL_3005	Electron transfer flavoprotein subunit beta	etfB		98.9	0	WP_038352174.1	hypothetical protein [<i>Eubacterium limosum</i>]
EL_3006	putative FAD-linked oxidoreductase			98.7	0	ALU15924.1	FAD-linked oxidase [<i>Eubacterium limosum</i>]
EL_3048	putative FAD-linked oxidoreductase			99.6	0	ADO36936.1	FAD/FMN-containing dehydrogenase [<i>Eubacterium limosum</i> KIST612]
EL_3049	Acryloyl-CoA reductase electron transfer subunit beta	etfA		99.3	0	ADO36935.1	electron transfer flavoprotein [<i>Eubacterium limosum</i> KIST612]
EL_3050	Acryloyl-CoA reductase electron transfer subunit gamma	etfB		100.0	0	WP_038352354.1	electron transfer flavoprotein subunit beta [<i>Eubacterium limosum</i>]
S6_Bin003-Eubacterium limosum-Hydrogenases and coupling enzymes							
EL_0486	NADP-reducing hydrogenase subunit HndD	hndD	EC:1.12.1.3	99.3	0	WP_038352187.1	ferredoxin [<i>Eubacterium limosum</i>]
EL_0487	NADP-reducing hydrogenase subunit HndC	HndC	EC:1.12.1.3	100.0	0	ADO35860.1	NADH dehydrogenase (quinone) [<i>Eubacterium limosum</i> KIST612]
EL_0488	NADP-reducing hydrogenase subunit HndB	HndB	EC:1.12.1.3	100.0	5.63E-88	ALU15940.1	iron-dependent hydrogenase subunit D HydD [<i>Eubacterium limosum</i>]
EL_0490	NADP-reducing hydrogenase subunit HndA	hndA	EC:1.12.1.3	100.0	4.02E-109	SHL93496.1	NADP-reducing hydrogenase subunit HndA [<i>Eubacterium callanderi</i>]
EL_3084	NADH-quinone oxidoreductase subunit G	nuoG	EC:1.6.5.3	100.0	2.65E-179	WP_050814047.1	MULTISPECIES: ferredoxin [<i>Clostridiales</i>]
EL_3085	NADH-quinone oxidoreductase subunit F	nuoF	EC:1.6.5.3	99.7	0	WP_038353796.1	NADH dehydrogenase [<i>Eubacterium limosum</i>]
EL_3086	NADH-quinone oxidoreductase subunit E	nuoE	EC:1.6.5.3	98.8	8.12E-116	WP_038353797.1	hydrogenase [<i>Eubacterium limosum</i>]
EL_3677	Iron hydrogenase 1			99.6	0	WP_038350720.1	hydrogenase assembly protein HupF [<i>Eubacterium limosum</i>]
EL_3678	Ferredoxin, 2Fe-2S			100.0	1.94E-54	ADO36201.1	NADH dehydrogenase subunit E [<i>Eubacterium limosum</i> KIST612]
EL_1912	NAD-reducing hydrogenase subunit HoxE	nuoE	EC:1.6.5.3	100.0	1.13E-53	WP_038351390.1	hypothetical protein [<i>Eubacterium limosum</i>]
EL_1913	Iron hydrogenase 1			100.0	0	WP_038351389.1	iron hydrogenase [<i>Eubacterium limosum</i>]
EL_0895	NADH-quinone oxidoreductase subunit F	nuoF	EC:1.6.5.3	99.8	0	WP_038352621.1	NADH dehydrogenase [<i>Eubacterium limosum</i>]
EL_0896	NADH-quinone oxidoreductase subunit E	nuoE	EC:1.6.5.3	99.4	5.16E-124	WP_038352622.1	NADH dehydrogenase [<i>Eubacterium limosum</i>]
S6_Bin003-Eubacterium limosum-ATPase							

EL_1175	V/A-type H ⁺ /Na ⁺ -transporting ATPase subunit G/H	ATPVG	100.0	3.89E-61	SFO68675.1	V/A-type H ⁺ -transporting ATPase subunit G/H [<i>Eubacterium callanderi</i>]	
EL_1176	V/A-type H ⁺ /Na ⁺ -transporting ATPase subunit I	ATPVI	99.7	0	ADO37168.1	V-type ATPase 116 kDa subunit [<i>Eubacterium limosum</i> KIST612]	
EL_1177	V/A-type H ⁺ /Na ⁺ -transporting ATPase subunit K	ATPVK	100.0	1.18E-99	SDO86232.1	V/A-type H ⁺ -transporting ATPase subunit K [<i>Eubacterium limosum</i>]	
EL_1178	V/A-type H ⁺ /Na ⁺ -transporting ATPase subunit E	ATPVE	100.0	1.47E-139	WP_038351650.1	hypothetical protein [<i>Eubacterium limosum</i>]	
EL_1179	V/A-type H ⁺ /Na ⁺ -transporting ATPase subunit C	ATPVC	99.7	0	WP_038351649.1	hypothetical protein [<i>Eubacterium limosum</i>]	
EL_1180	V/A-type H ⁺ /Na ⁺ -transporting ATPase subunit F	ATPVF	100.0	8.02E-69	ADO37172.1	ATP synthase F subunit [<i>Eubacterium limosum</i> KIST612]	
EL_1181	V/A-type H ⁺ /Na ⁺ -transporting ATPase subunit A	ATPVA	EC:3.6.3.14 3.6.3.15	99.8	0	ADO37173.1	ATP synthase [<i>Eubacterium limosum</i> KIST612]
EL_1182	V/A-type H ⁺ /Na ⁺ -transporting ATPase subunit B	ATPVB	100.0	0	ADO37174.1	sodium-transporting two-sector ATPase [<i>Eubacterium limosum</i> KIST612]	
EL_1183	V/A-type H ⁺ /Na ⁺ -transporting ATPase subunit D	ATPVD	100.0	4.51E-150	ADO37175.1	hypothetical protein ELI_2192 [<i>Eubacterium limosum</i> KIST612]	
EL_1792	V/A-type H ⁺ /Na ⁺ -transporting ATPase subunit D	ATPVD	99.5	7.03E-147	SDP23599.1	V/A-type H ⁺ -transporting ATPase subunit D [<i>Eubacterium limosum</i>]	
EL_1793	V/A-type H ⁺ /Na ⁺ -transporting ATPase subunit B	ATPVB	100.0	0	SFO73027.1	V/A-type H ⁺ -transporting ATPase subunit B [<i>Eubacterium callanderi</i>]	
EL_1794	V/A-type H ⁺ /Na ⁺ -transporting ATPase subunit A	ATPVA	EC:3.6.3.14 3.6.3.15	99.2	0	ADO37400.1	V-type ATP synthase subunit A [<i>Eubacterium limosum</i> KIST612]
EL_1795	V/A-type H ⁺ /Na ⁺ -transporting ATPase subunit E	ATPVE	100.0	7.67E-148	WP_038351485.1	V-ATPase E-subunit VatE [<i>Eubacterium limosum</i>]	
EL_1796	V/A-type H ⁺ /Na ⁺ -transporting ATPase subunit F	ATPVF	100.0	5.33E-65	SDP23471.1	V/A-type H ⁺ -transporting ATPase subunit F [<i>Eubacterium limosum</i>]	
EL_1797	V/A-type H ⁺ /Na ⁺ -transporting ATPase subunit K	ATPVK	100.0	1.12E-92	ADO37403.1	V-type sodium ATP synthase subunit K [<i>Eubacterium limosum</i> KIST612]	
EL_1798	V/A-type H ⁺ /Na ⁺ -transporting ATPase subunit I	ATPVI	99.8	0	WP_038351484.1	ATPase [<i>Eubacterium limosum</i>]	

EL_1799	V/A-type H ⁺ /Na ⁺ -transporting ATPase subunit C	ATPVC	99.7	0	ADO37405.1	H(+)-transporting two-sector ATPase [<i>Eubacterium limosum</i> KIST612]
S6_Bin004-Massilibacterium senegalense strain mt8-Glycerol oxidation 2						
MS_1884	glycerol kinase	glpK	EC:2.7.1.30	96.6	0	WP_062197477.1 glycerol kinase [<i>Massilibacterium senegalense</i>]
MS_0086	glycerol-3-phosphate dehydrogenase (NAD(P) ⁺)	gpsA	EC:1.1.1.94	96.8	0	WP_062198284.1 glycerol-3-phosphate dehydrogenase [<i>Massilibacterium senegalense</i>]
MS_1883	glycerol-3-phosphate dehydrogenase	glpA	EC:1.1.5.3	91.9	0	WP_062197478.1 glycerol-3-phosphate dehydrogenase [<i>Massilibacterium senegalense</i>]
S6_Bin004-Massilibacterium senegalense strain mt8-Central axis pathway						
MS_1396	triosephosphate isomerase	TPI	EC:5.3.1.1	96.0	0	WP_062199675.1 triose-phosphate isomerase [<i>Massilibacterium senegalense</i>]
MS_0395	glyceraldehyde 3-phosphate dehydrogenase	GAPDH	EC:1.2.1.12	97.9	0	WP_062199123.1 glyceraldehyde-3-phosphate dehydrogenase [<i>Massilibacterium senegalense</i>]
MS_1398	glyceraldehyde 3-phosphate dehydrogenase	GAPDH	EC:1.2.1.12	94.3	0	WP_062199679.1 type I glyceraldehyde-3-phosphate dehydrogenase [<i>Massilibacterium senegalense</i>]
MS_1397	phosphoglycerate kinase	PGK	EC:2.7.2.3	99.0	0	WP_062199677.1 phosphoglycerate kinase [<i>Massilibacterium senegalense</i>]
MS_1395	2,3-bisphosphoglycerate-independent phosphoglycerate mutase	gpmI	EC:5.4.2.12	98.2	0	WP_062199673.1 phosphoglycerate mutase (2,3-diphosphoglycerate-independent) [<i>Massilibacterium senegalense</i>]
MS_2085	probable phosphoglycerate mutase	gpmB	EC:5.4.2.12	100.0	4.88E-143	WP_062198149.1 histidine phosphatase family protein [<i>Massilibacterium senegalense</i>]
MS_1394	enolase	ENO	EC:4.2.1.11	99.5	0	WP_062199671.1 phosphopyruvate hydratase [<i>Massilibacterium senegalense</i>]
MS_0410	pyruvate kinase	pyk	EC:2.7.1.40	96.8	0	WP_062199156.1 pyruvate kinase [<i>Massilibacterium senegalense</i>]
MS_1726	pyruvate dehydrogenase E2 component (dihydrolipoamide acetyltransferase)	DLAT	EC:2.3.1.12	90.3	0	WP_062197722.1 branched-chain alpha-keto acid dehydrogenase subunit E2 [<i>Massilibacterium senegalense</i>]
MS_1727	pyruvate dehydrogenase E1 component beta subunit	PDHB	EC:1.2.4.1	98.5	0	WP_062197721.1 alpha-ketoacid dehydrogenase subunit beta [<i>Massilibacterium senegalense</i>]
MS_1728	pyruvate dehydrogenase E1 component alpha subunit	PDHA	EC:1.2.4.1	95.6	0	WP_062197720.1 pyruvate dehydrogenase (acetyl-transferring) E1 component subunit

							alpha [<i>Massilibacterium senegalense</i>]
S6_Bin004-Massilibacterium senegalense strain mt8-Acetate production							
MS_1179	phosphate acetyltransferase	Pta	EC:2.3.1.8	96.0	0	WP_062200212.1	phosphate acetyltransferase [<i>Massilibacterium senegalense</i>]
MS_0436	acetate kinase	ackA	EC:2.7.2.1	98.8	0	WP_062199195.1	acetate kinase [<i>Massilibacterium senegalense</i>]
S6_Bin004-Massilibacterium senegalense strain mt8-Butyrate and caproate production							
MS_1621	acetyl-CoA C-acetyltransferase	atoB	EC:2.3.1.9	99.5	0	WP_062200168.1	acetyl-CoA acetyltransferase [<i>Massilibacterium senegalense</i>]
MS_1622	3-hydroxybutyryl-CoA dehydrogenase	paaH	EC:1.1.1.157	99.7	0	WP_062200165.1	3-hydroxybutyryl-CoA dehydrogenase [<i>Massilibacterium senegalense</i>]
MS_2108	3-hydroxybutyryl-CoA dehydrogenase	paaH	EC:1.1.1.157	98.2	0	WP_062197210.1	3-hydroxybutyryl-CoA dehydrogenase [<i>Massilibacterium senegalense</i>]
MS_2453	3-hydroxybutyryl-CoA dehydrogenase	paaH	EC:1.1.1.157	95.5	0	WP_062199605.1	3-hydroxybutyryl-CoA dehydrogenase [<i>Massilibacterium senegalense</i>]
MS_0368	enoyl-CoA hydratase	fadB	EC:4.2.1.17	98.5	0	WP_062199071.1	enoyl-CoA hydratase [<i>Massilibacterium senegalense</i>]
MS_2107	enoyl-CoA hydratase	crt	EC:4.2.1.17	97.7	0	WP_062197209.1	enoyl-CoA hydratase [<i>Massilibacterium senegalense</i>]
MS_2450	enoyl-CoA hydratase	paaF	EC:4.2.1.17	95.0	0	WP_062199608.1	enoyl-CoA hydratase [<i>Massilibacterium senegalense</i>]
MS_0014	3-hydroxybutyryl-CoA dehydratase	croR	EC:4.2.1.55	99.3	5.15E-101	WP_062198196.1	3-hydroxybutyryl-CoA dehydratase [<i>Massilibacterium senegalense</i>]
MS_2109	butyryl-CoA dehydrogenase	bcd	EC:1.3.8.1	98.1	0	WP_062197211.1	acyl-CoA dehydrogenase [<i>Massilibacterium senegalense</i>]
MS_0266	butyryl-CoA dehydrogenase	bcd	EC:1.3.8.1	98.7	0	WP_062198984.1	acyl-CoA dehydrogenase [<i>Massilibacterium senegalense</i>]
MS_1623	butyryl-CoA dehydrogenase	bcd	EC:1.3.8.1	99.7	0	WP_062200164.1	acyl-CoA dehydrogenase [<i>Massilibacterium senegalense</i>]
MS_1624	Acyl-CoA dehydrogenase	acd	EC:1.3.8.7	99.7	0	WP_062200161.1	acyl-CoA dehydrogenase [<i>Massilibacterium senegalense</i>]
MS_2421	Acyl-CoA dehydrogenase	acd	EC:1.3.8.7	93.7	0	WP_062196993.1	acyl-CoA dehydrogenase [<i>Massilibacterium senegalense</i>]
MS_2666	butyryl-CoA dehydrogenase	bcd	EC:1.3.8.1	97.1	0	WP_062199581.1	acyl-CoA dehydrogenase [<i>Massilibacterium senegalense</i>]
MS_0366	electron transfer flavoprotein alpha subunit	etfA		96.9	0	WP_062199067.1	electron transfer flavoprotein subunit alpha [<i>Massilibacterium senegalense</i>]
MS_0367	electron transfer flavoprotein beta subunit	etfB		99.2	1.36E-178	WP_062199069.1	electron transfer flavoprotein subunit beta [<i>Massilibacterium</i>

							<i>senegalense</i>]
MS_0258	3-oxoacid CoA-transferase subunit B		EC:2.8.3.5	100.0	2.76E-156	WP_062198969.1	succinyl-CoA--3-ketoacid-CoA transferase [<i>Massilibacterium senegalense</i>]
MS_0259	3-oxoacid CoA-transferase subunit A		EC:2.8.3.5	97.8	1.31E-164	WP_062198971.1	succinyl-CoA--3-ketoacid-CoA transferase [<i>Massilibacterium senegalense</i>]
S6_Bin004-Massilibacterium senegalense strain mt8-Ethanol production/oxidation							
MS_2149	aldehyde dehydrogenase (NAD ⁺)	ALDH	EC:1.2.1.3	99.8	0	WP_062198102.1	betaine-aldehyde dehydrogenase [<i>Massilibacterium senegalense</i>]
MS_2265	aldehyde dehydrogenase (NAD ⁺)	ALDH	EC:1.2.1.3	96.0	0	WP_062198142.1	aldehyde dehydrogenase [<i>Massilibacterium senegalense</i>]
MS_2419	aldehyde dehydrogenase	aldB	EC:1.2.1.-	82.4	0	KGR79783.1	aldehyde dehydrogenase [<i>Lysinibacillus manganicus</i> DSM 26584]
MS_2452	aldehyde dehydrogenase (NAD ⁺)	ALDH	EC:1.2.1.3	98.8	0	WP_062199606.1	aldehyde dehydrogenase [<i>Massilibacterium senegalense</i>]
MS_1568	alcohol dehydrogenase	adh2	EC:1.1.1.-	98.2	0	WP_062197043.1	NADH-dependent alcohol dehydrogenase [<i>Massilibacterium senegalense</i>]
MS_2418	alcohol dehydrogenase	yaY	EC:1.1.1.1	98.4	0	WP_062196988.1	L-threonine dehydrogenase [<i>Massilibacterium senegalense</i>]
S6_Bin004-Massilibacterium senegalense strain mt8-Hydrogenases and coupling enzymes							
MS_1148	[NiFe] hydrogenase small subunit	hyaA	EC:1.12.99.6	99.2	0	WP_062200288.1	[NiFe] hydrogenase small subunit HydA [<i>Massilibacterium senegalense</i>]
MS_1149	hydrogenase large subunit	hyaB	EC:1.12.99.6	99.7	0	WP_062200285.1	hydrogenase [<i>Massilibacterium senegalense</i>]
MS_1150	Ni/Fe-hydrogenase, b-type cytochrome subunit	hyaC		98.4	0	WP_062200282.1	Ni/Fe-hydrogenase, b-type cytochrome subunit [<i>Massilibacterium senegalense</i>]
MS_1151	hydrogenase maturation protease	hyaD	EC:3.4.23.-	98.1	2.91E-106	WP_062201373.1	hydrogenase maturation protease [<i>Massilibacterium senegalense</i>]
MS_1153	hydrogenase nickel incorporation protein	hypA		98.3	9.60E-79	WP_062200276.1	hydrogenase nickel incorporation protein HypA [<i>Massilibacterium senegalense</i>]
MS_1154	hydrogenase nickel incorporation protein	hypB		99.5	9.32E-163	WP_062200274.1	hydrogenase accessory protein HypB [<i>Massilibacterium</i>

							<i>senegalense</i>]
MS_1155	hydrogenase maturation protein	hypF	94.7	0	WP_062200271.1		carbamoyltransferase HypF [<i>Massilibacterium senegalense</i>]
MS_1156	hydrogenase expression/formation protein	hypC	98.7	1.88E-47	WP_062200267.1		hydrogenase assembly protein HypC [<i>Massilibacterium senegalense</i>]
MS_1157	hydrogenase expression/formation protein	hypD	99.2	0	WP_062201371.1		hydrogenase formation protein HypD [<i>Massilibacterium senegalense</i>]
MS_1158	hydrogenase expression/formation protein	hypE	97.9	0	WP_062200266.1		hydrogenase expression/formation protein HypE [<i>Massilibacterium senegalense</i>]
MS_2018	NADH dehydrogenase	ndh	EC:1.6.99.3	97.5	0	WP_062199499.1	NADH dehydrogenase [<i>Massilibacterium senegalense</i>]
MS_2517	thioredoxin reductase (NADPH)	trxB	EC:1.8.1.9	95.5	0	WP_062199484.1	ferredoxin--NADP(+) reductase [<i>Massilibacterium senegalense</i>]
MS_2518	NADH dehydrogenase	ndh	EC:1.6.99.3	99.0	0	WP_062201308.1	NADH dehydrogenase [<i>Massilibacterium senegalense</i>]
MS_113	ferredoxin	fer	100.0	3.65E-51	WP_062198330.1		ferredoxin [<i>Massilibacterium senegalense</i>]
S6_Bin006-Mesotoga infera-Glycerol oxidation 2							
ML_0319	glycerol kinase	glpK	EC:2.7.1.30	99.8	0	CCU86017.1	Glycerol kinase 2 [<i>Mesotoga infera</i>]
ML_0653	glycerol-3-phosphate dehydrogenase	glpA	EC:1.1.5.3	100.0	0	CCU85716.1	FAD dependent oxidoreductase [<i>Mesotoga infera</i>]
S6_Bin006-Mesotoga infera-Central axis pathway							
ML_0460	triosephosphate isomerase	TPI	EC:5.3.1.1	100.0	0	CCU84081.1	Bifunctional PGK/TIM (Includes: Phosphoglycerate kinase ; Triosephosphate isomerase) [<i>Mesotoga infera</i>]
ML_0460	phosphoglycerate kinase	PGK	EC:2.7.2.3	100.0	0	CCU84081.1	Bifunctional PGK/TIM (Includes: Phosphoglycerate kinase ; Triosephosphate isomerase) [<i>Mesotoga infera</i>]
ML_0461	glyceraldehyde 3-phosphate dehydrogenase	GAPDH	EC:1.2.1.12	99.7	0	CCU84080.1	Glyceraldehyde-3-phosphate dehydrogenase [<i>Mesotoga infera</i>]
ML_0203	probable phosphoglycerate mutase	gpmB	EC:5.4.2.12	100.0	8.26E-149	CCU85905.1	Phosphoglycerate mutase [<i>Mesotoga infera</i>]
ML_2026	probable phosphoglycerate mutase	gpmB	EC:5.4.2.12	100.0	2.16E-166	WP_014731744.1	fructose 2,6-bisphosphatase [<i>Mesotoga prima</i>]
ML_1425	enolase	ENO	EC:4.2.1.11	100.0	0	CCU85457.1	Enolase [<i>Mesotoga infera</i>]
ML_0598	pyruvate kinase	pyk	EC:2.7.1.40	100.0	0	CCU84234.1	Pyruvate kinase [<i>Mesotoga infera</i>]

MI_2016	pyruvate kinase	pyk	EC:2.7.1.40	99.7	0	CCU84646.1	Pyruvate kinase [<i>Mesotoga infera</i>]
MI_1541	pyruvate-ferredoxin/ flavodoxin oxidoreductase	por	EC:1.2.7.1 1.2.7.-	95.3	0	WP_006488153.1	pyruvate:ferredoxin (flavodoxin) oxidoreductase [<i>Mesotoga prima</i>]
MI_1871	pyruvate-ferredoxin/ flavodoxin oxidoreductase	por	EC:1.2.7.1 1.2.7.-	98.9	0	CCU84521.1	Pyruvate-flavodoxin oxidoreductase [<i>Mesotoga infera</i>]
S6_Bin006-Mesotoga infera-Acetate production							
MI_0299	phosphate acetyltransferase	Pta	EC:2.3.1.8	100.0	3.38E-140	CCU86038.1	Phosphate propanoyltransferase [<i>Mesotoga infera</i>]
MI_0391	acetate kinase	ackA	EC:2.7.2.1	100.0	0	CCU85692.1	Acetate kinase [<i>Mesotoga infera</i>]
S6_Bin010-Bacteroidia bacterium 43-41-Pyruvate to acetyl-CoA							
BB_1709	pyruvate-ferredoxin/ flavodoxin oxidoreductase	por	EC:1.2.7.1 1.2.7.-	94.9	0	OJV35651.1	pyruvate:ferredoxin (flavodoxin) oxidoreductase [<i>Bacteroidia bacterium 43-41</i>]
BB_0722	pyruvate dehydrogenase E1 component alpha subunit	PDHA	EC:1.2.4.1	93.9	0	OJV36229.1	pyruvate dehydrogenase (acetyl-transferring) E1 component subunit alpha [<i>Bacteroidia bacterium 43-41</i>]
BB_0723	pyruvate dehydrogenase E1 component beta subunit	PDHB	EC:1.2.4.1	95.4	0	OJV36230.1	alpha-ketoacid dehydrogenase subunit beta [<i>Bacteroidia bacterium 43-41</i>]
BB_0724	pyruvate dehydrogenase E2 component (dihydrolipoamide acetyltransferase)	DLAT	EC:2.3.1.12	83.5	0	OJV36231.1	hypothetical protein BGO33_05085 [<i>Bacteroidia bacterium 43-41</i>]
BB_2030	pyruvate dehydrogenase E1 component alpha subunit	PDHA	EC:1.2.4.1	94.0	0	OJV37110.1	pyruvate dehydrogenase [<i>Bacteroidia bacterium 43-41</i>]
BB_2031	pyruvate dehydrogenase E1 component beta subunit	PDHB	EC:1.2.4.1	99.1	0	OJV37109.1	alpha-ketoacid dehydrogenase subunit beta [<i>Bacteroidia bacterium 43-41</i>]
BB_2032	pyruvate dehydrogenase E2 component (dihydrolipoamide acetyltransferase)	DLAT	EC:2.3.1.12	90.9	0	OJV37108.1	dihydrolipoamide acetyltransferase [<i>Bacteroidia bacterium 43-41</i>]
S6_Bin010-Bacteroidia bacterium 43-41-Acetate production							
BB_2256	phosphate acetyltransferase	pta	EC:2.3.1.8	92.3	0	OJV37359.1	phosphate acetyltransferase [<i>Bacteroidia bacterium 43-41</i>]
BB_2258	acetate kinase	ackA	EC:2.7.2.1	94.7	0	OJV37468.1	acetate kinase [<i>Bacteroidia bacterium 43-41</i>]

S6_Bin010-Bacteroidia bacterium 43-41-Butyrate and caproate production

BB_0687	acetyl-CoA C-acetyltransferase	atoB	EC:2.3.1.9	88.5	0	OJV36545.1	acetyl-CoA acetyltransferase [<i>Bacteroidia</i> bacterium 43-41]
BB_0685	3-hydroxybutyryl-CoA dehydrogenase	paaH	EC:1.1.1.157	92.1	0	OJV36511.1	3-hydroxybutyryl-CoA dehydrogenase [<i>Bacteroidia</i> bacterium 43-41]
BB_0686	enoyl-CoA hydratase	crt	EC:4.2.1.17	85.7	3.82E-161	OJV36546.1	hypothetical protein BGO33_12475 [<i>Bacteroidia</i> bacterium 43-41]
BB_0688	acetate CoA/acetoacetate CoA-transferase beta subunit	atoA	EC:2.8.3.8 2.8.3.9	95.0	2.07E-149	OJV36510.1	succinyl-CoA--3-ketoacid-CoA transferase [<i>Bacteroidia</i> bacterium 43-41]
BB_2152	butyryl-CoA dehydrogenase	bcd	EC:1.3.8.1	98.1	0	OJV35776.1	acyl-CoA dehydrogenase [<i>Bacteroidia</i> bacterium 43-41]
BB_2153	electron transfer flavoprotein alpha subunit	etfA		93.8	0	SFU32761.1	electron transfer flavoprotein alpha subunit apoprotein [<i>Porphyromonadaceae</i> bacterium KHP3R9]
BB_2154	electron transfer flavoprotein beta subunit	etfB		94.1	0	OJV35778.1	electron transfer flavoprotein subunit beta [<i>Bacteroidia</i> bacterium 43-41]
BB_1016	phosphate butyryltransferase	ptb	EC:2.3.1.19	84.2	0	OJV32515.1	phosphate butyryltransferase [<i>Bacteroidia</i> bacterium 43-41]
BB_1015	butyrate kinase	buk	EC:2.7.2.7	97.5	0	SFU39491.1	butyrate kinase [<i>Porphyromonadaceae</i> bacterium KHP3R9]

S6_Bin010-Bacteroidia bacterium 43-41-Membrane proteins involved in energy conservation-Rnf complex

BB_0085	electron transport complex protein RnfA	RnfA		97.9	8.76E-128	OJV38119.1	electron transport complex subunit RxsA [<i>Bacteroidia</i> bacterium 43-41]
BB_0086	electron transport complex protein RnfE	RnfE		95.9	5.53E-126	OJV38118.1	electron transport complex subunit RxsE [<i>Bacteroidia</i> bacterium 43-41]
BB_0087	electron transport complex protein RnfG	RnfG		85.1	8.39E-131	SFU38380.1	electron transport complex protein RnfG [<i>Porphyromonadaceae</i> bacterium KHP3R9]
BB_0088	electron transport complex protein RnfD	RnfD		92.2	0	OJV38116.1	Na ⁺ -transporting NADH:ubiquinone oxidoreductase subunit D [<i>Bacteroidia</i> bacterium 43-41]
BB_0089	electron transport complex protein RnfC	RnfC		92.3	0	OJV38115.1	electron transporter RnfC [<i>Bacteroidia</i> bacterium 43-41]

BB_0090	electron transport complex protein RnfB	RnfB	94.4	0	OJV38114.1	ferredoxin [<i>Bacteroidia</i> bacterium 43-41]
S6_Bin010-Bacteroidia bacterium 43-41-Membrane proteins involved in energy conservation-Fix system						
BB_2153	electron transfer flavoprotein alpha subunit	fixB	93.8	0	SFU32761.1	electron transfer flavoprotein alpha subunit apoprotein [<i>Porphyromonadaceae</i> bacterium KHP3R9]
BB_2154	electron transfer flavoprotein beta subunit	fixA	94.1	0	OJV35778.1	electron transfer flavoprotein subunit beta [<i>Bacteroidia</i> bacterium 43-41]
S6_Bin010-Bacteroidia bacterium 43-41-ATPase						
BB_0941	F-type H ⁺ -transporting ATPase subunit gamma		82.7	1.23E-167	OJV33098.1	ATP synthase F1 subunit gamma [<i>Bacteroidia</i> bacterium 43-41]
BB_0942	F-type H ⁺ -transporting ATPase subunit alpha	EC:3.6.3.14	91.5	0	OJV33097.1	F0F1 ATP synthase subunit alpha [<i>Bacteroidia</i> bacterium 43-41]
BB_0943	F-type H ⁺ -transporting ATPase subunit delta		85.4	1.72E-108	OJV33096.1	ATP synthase F1 subunit delta [<i>Bacteroidia</i> bacterium 43-41]
BB_0944	F-type H ⁺ -transporting ATPase subunit b		82.5	3.70E-94	OJV33095.1	ATP synthase F0 subunit B [<i>Bacteroidia</i> bacterium 43-41]
BB_0945	F-type H ⁺ -transporting ATPase subunit c		93.9	4.24E-44	OJV33094.1	ATP synthase F0 subunit C [<i>Bacteroidia</i> bacterium 43-41]
BB_0946	F-type H ⁺ -transporting ATPase subunit a		83.0	0	OJV33107.1	ATP synthase F0 subunit A [<i>Bacteroidia</i> bacterium 43-41]
BB_0947	ATP synthase protein I2		77.1	5.22E-60	OJV33093.1	hypothetical protein BGO33_13645 [<i>Bacteroidia</i> bacterium 43-41]
BB_0948	F-type H ⁺ -transporting ATPase subunit epsilon		84.5	1.95E-41	OJV33092.1	ATP synthase F1 subunit epsilon [<i>Bacteroidia</i> bacterium 43-41]
BB_0949	F-type H ⁺ -transporting ATPase subunit beta	EC:3.6.3.14	95.0	0	OJV33091.1	F0F1 ATP synthase subunit beta [<i>Bacteroidia</i> bacterium 43-41]
BB_1339	V/A-type H ⁺ /Na ⁺ -transporting ATPase subunit E	ATPVE	89.7	1.01E-119	OJV39048.1	hypothetical protein BGO33_13835 [<i>Bacteroidia</i> bacterium 43-41]
BB_1340	V/A-type H ⁺ /Na ⁺ -transporting ATPase subunit C	ATPVC	92.2	0	OJV39049.1	hypothetical protein BGO33_13840 [<i>Bacteroidia</i> bacterium 43-41]
BB_1341	V/A-type H ⁺ /Na ⁺ -transporting ATPase subunit A	ATPVA EC:3.6.3.14 3.6.3.15	95.7	0	OJV39050.1	V-type ATP synthase subunit A [<i>Bacteroidia</i> bacterium 43-41]
BB_1342	V/A-type H ⁺ /Na ⁺ -transporting ATPase subunit B	ATPVB	98.9	0	OJV39051.1	V-type ATP synthase subunit B [<i>Bacteroidia</i> bacterium 43-41]
BB_1343	V/A-type H ⁺ /Na ⁺ -transporting ATPase subunit D	ATPVD	95.6	1.40E-134	OJV39052.1	V-type ATP synthase subunit D [<i>Bacteroidia</i> bacterium 43-41]
BB_1344	V/A-type H ⁺ /Na ⁺ -transporting ATPase subunit I	ATPVI	87.1	0	OJV39053.1	V-type ATP synthase subunit I [<i>Bacteroidia</i> bacterium 43-41]
BB_1345	V/A-type H ⁺ /Na ⁺ -transporting ATPase subunit K	ATPVK	98.0	9.98E-99	SFU52137.1	V/A-type H ⁺ -transporting ATPase subunit K [<i>Porphyromonadaceae</i> bacterium KHP3R9]

S6_Bin010-*Bacteroidia bacterium* 43-41-Hydrogenase (putative electron-bifurcating hydrogenase)

BB_1168	NADH-quinone oxidoreductase subunit E	nuoE	EC:1.6.5.3	85.4	4.61E-102	OJV38404.1	hypothetical protein BGO33_06290 [<i>Bacteroidia bacterium</i> 43-41]
BB_1169	NADH-quinone oxidoreductase subunit F	nuoF	EC:1.6.5.3	88.3	0	OJV38405.1	NADH dehydrogenase [<i>Bacteroidia bacterium</i> 43-41]
BB_1170	NADH-quinone oxidoreductase subunit G	nuoG	EC:1.6.5.3	90.8	0	OJV38406.1	ferredoxin [<i>Bacteroidia bacterium</i> 43-41]
BB_2775	ferredoxin--NADP+ reductase	fpr	EC:1.18.1.2	96.9	0	OJV36298.1	ferredoxin-NADP reductase [<i>Bacteroidia bacterium</i> 43-41]

S6_Bin012-*Clostridium kluyveri*-Ethanol oxidation

CK_1079	alcohol dehydrogenase	yiaY	EC:1.1.1.1	99.7	0	APM41305.1	L-threonine dehydrogenase [<i>Clostridium kluyveri</i>]
CK_1814	alcohol dehydrogenase	adh2	EC:1.1.1.-	100.0	0	APM38446.1	NADH-dependent alcohol dehydrogenase [<i>Clostridium kluyveri</i>]
CK_1816	alcohol dehydrogenase	yiaY	EC:1.1.1.1	99.7	0	APM38444.1	L-threonine dehydrogenase [<i>Clostridium kluyveri</i>]
CK_2119	alcohol dehydrogenase	yiaY	EC:1.1.1.1	100.0	0	APM40732.1	L-threonine dehydrogenase [<i>Clostridium kluyveri</i>]
CK_2520	alcohol dehydrogenase	yiaY	EC:1.1.1.1	100.0	0	APM39276.1	ethanolamine utilization protein EutG [<i>Clostridium kluyveri</i>]
CK_1679	acetaldehyde dehydrogenase / alcohol dehydrogenase	adhE	EC:1.2.1.10; 1.1.1.1	100.0	0	APM37882.1	butanol dehydrogenase [<i>Clostridium kluyveri</i>]
CK_2949	aldehyde dehydrogenase (NAD+)	ALDH	EC:1.2.1.3	100.0	0	APM39462.1	aldehyde dehydrogenase family protein [<i>Clostridium kluyveri</i>]
CK_1809	acetaldehyde dehydrogenase (acetylating)		EC:1.2.1.10	100.0	0	APM38451.1	acetaldehyde dehydrogenase (acetylating) [<i>Clostridium kluyveri</i>]
CK_2925	acetaldehyde dehydrogenase / alcohol dehydrogenase	adhE	EC:1.2.1.10; 1.1.1.1	100.0	0	APM38120.1	alcohol dehydrogenase [<i>Clostridium kluyveri</i>]
CK_3473	acetaldehyde dehydrogenase / alcohol dehydrogenase	adhE	EC:1.2.1.10; 1.1.1.1	98.8	0	APM38455.1	alcohol dehydrogenase [<i>Clostridium kluyveri</i>]

S6_Bin012-*Clostridium kluyveri*-Reverse β -oxidation for butyrate and caproate production

CK_0235	acetyl-CoA C-acetyltransferase		EC:2.3.1.9	100.0	0	APM41005.1	acetyl-CoA acetyltransferase [<i>Clostridium kluyveri</i>]
CK_0236	acetyl-CoA C-acetyltransferase		EC:2.3.1.9	100.0	0	APM41004.1	acetyl-CoA acetyltransferase [<i>Clostridium kluyveri</i>]
CK_0237	acetyl-CoA C-acetyltransferase		EC:2.3.1.9	100.0	0	APM41003.1	acetyl-CoA acetyltransferase [<i>Clostridium kluyveri</i>]

CK_0295	3-hydroxybutyryl-CoA dehydrogenase	paaH	EC:1.1.1.157	100.0	0	APM40071.1	3-hydroxybutyryl-CoA dehydrogenase [<i>Clostridium kluyveri</i>]
CK_3075	3-hydroxybutyryl-CoA dehydrogenase	paaH	EC:1.1.1.157	99.4	3.08E-101	APM38896.1	hypothetical protein BS101_09100 [<i>Clostridium kluyveri</i>]
CK_1050	3-hydroxybutyryl-CoA dehydratase	croR	EC:4.2.1.55	100.0	4.02E-96	APM40240.1	enoyl-CoA hydratase [<i>Clostridium kluyveri</i>]
CK_1240	butyryl-CoA dehydrogenase	bcd	EC:1.3.8.1	100.0	0	WP_073537711.1	acyl-CoA dehydrogenase [<i>Clostridium kluyveri</i>]
CK_0704	4-hydroxybutyrate CoA-transferase	cat2	EC:2.8.3.-	100.0	0	APM40939.1	4-hydroxybutyrate CoA-transferase [<i>Clostridium kluyveri</i>]
CK_1054	4-hydroxybutyrate CoA-transferase	cat2	EC:2.8.3.-	100.0	0	APM41307.1	4-hydroxybutyrate CoA-transferase [<i>Clostridium kluyveri</i>]
CK_2573	ferredoxin--NADP+ reductase	fpr	EC:1.18.1.2	99.7	0	APM37777.1	NAD-binding oxidoreductase [<i>Clostridium kluyveri</i>]
CK_2574	3-hydroxybutyryl-CoA dehydrogenase	paaH	EC:1.1.1.157	99.6	0	APM41175.1	3-hydroxybutyryl-CoA dehydrogenase [<i>Clostridium kluyveri</i>]
CK_2575	electron transfer flavoprotein subunit alpha	etfA		100.0	0	APM37776.1	electron transfer flavoprotein subunit alpha [<i>Clostridium kluyveri</i>]
CK_2576	electron transfer flavoprotein subunit beta	etfB		100.0	0	APM37775.1	electron transfer flavoprotein subunit beta [<i>Clostridium kluyveri</i>]
CK_2577	butyryl-CoA dehydrogenase	bcd	EC:1.3.8.1	100.0	0	APM37774.1	acyl-CoA dehydrogenase [<i>Clostridium kluyveri</i>]
CK_2578	enoyl-CoA hydratase	crt	EC:4.2.1.17	100.0	0	APM37773.1	crotonase [<i>Clostridium kluyveri</i>]
S6_Bin012-Clostridium kluyveri-Membrane proteins involved in energy conservation-Rnf complex							
CK_0795	electron transport complex protein RnfB	rnfB		100.0	0	APM38647.1	RnfABCDGE type electron transport complex subunit B [<i>Clostridium kluyveri</i>]
CK_0796	electron transport complex protein RnfA	rnfA		100.0	2.15E-129	APM38646.1	electron transport complex subunit R _{sxA} [<i>Clostridium kluyveri</i>]
CK_0797	electron transport complex protein RnfE	rnfE		100.0	3.71E-149	APM38645.1	electron transport complex subunit R _{sxE} [<i>Clostridium kluyveri</i>]
CK_0798	electron transport complex protein RnfG	rnfG		100.0	4.92E-129	APM38644.1	RnfABCDGE type electron transport complex subunit G [<i>Clostridium kluyveri</i>]
CK_0799	electron transport complex protein RnfD	rnfD		100.0	0	APM38643.1	electron transporter RnfD [<i>Clostridium kluyveri</i>]
CK_0800	electron transport complex protein RnfC	rnfC		99.8	0	APM38642.1	electron transporter RnfC [<i>Clostridium kluyveri</i>]
S6_Bin012-Clostridium kluyveri-Membrane proteins involved in energy conservation-FAD (or Fe-S) reductase lined to ETF							
CK_2896	Acryloyl-CoA reductase electron transfer subunit gamma			100.0	0	APM40840.1	electron transfer flavoprotein, beta subunit [<i>Clostridium kluyveri</i>]

CK_2897	Acryloyl-CoA reductase electron transfer subunit beta		100.0	0	APM40839.1	electron transfer flavoprotein, alpha subunit [<i>Clostridium kluyveri</i>]	
CK_2898	putative FAD-linked oxidoreductase		100.0	0	APM41340.1	FAD-binding protein [<i>Clostridium kluyveri</i>]	
S6_Bin012-Clostridium kluyveri-Membrane proteins involved in energy conservation-Fix system							
CK_3270	ferredoxin like protein	fixX	98.9	1.44E-60	APM41235.1	4Fe-4S ferredoxin [<i>Clostridium kluyveri</i>]	
CK_3271	electron transfer flavoprotein-quinone oxidoreductase	fixC	EC:1.5.5.-	98.6	0	APM38882.1	nitrogen fixation protein FixC [<i>Clostridium kluyveri</i>]
CK_3272	electron transfer flavoprotein alpha subunit	fixB		99.5	0	APM38881.1	electron transfer flavoprotein subunit alpha [<i>Clostridium kluyveri</i>]
CK_3273	electron transfer flavoprotein beta subunit	fixA		99.6	0	APM38880.1	electron transfer flavoprotein subunit beta [<i>Clostridium kluyveri</i>]
S6_Bin012-Clostridium kluyveri-ATPase							
CK_0238	ATP synthase I chain		100.0	9.89E-78	APM41002.1	ATP synthase subunit I [<i>Clostridium kluyveri</i>]	
CK_0239	F-type H+-transporting ATPase subunit a	atpB		100.0	1.54E-159	APM41001.1	F0F1 ATP synthase subunit A [<i>Clostridium kluyveri</i>]
CK_0240	F-type H+-transporting ATPase subunit c	atpE		100.0	5.00E-47	APM41000.1	ATP synthase F0 subunit C [<i>Clostridium kluyveri</i>]
CK_0241	F-type H+-transporting ATPase subunit b	atpF		99.4	7.34E-108	APM40999.1	ATP synthase F0 subunit B [<i>Clostridium kluyveri</i>]
CK_0242	F-type H+-transporting ATPase subunit delta	atpH		100.0	2.36E-123	APM40998.1	F0F1 ATP synthase subunit delta [<i>Clostridium kluyveri</i>]
CK_0243	F-type H+-transporting ATPase subunit alpha	atpA	EC:3.6.3.14	99.8	0	APM40997.1	F0F1 ATP synthase subunit alpha [<i>Clostridium kluyveri</i>]
CK_0244	F-type H+-transporting ATPase subunit gamma	atpG		99.6	0	APM40996.1	F0F1 ATP synthase subunit gamma [<i>Clostridium kluyveri</i>]
CK_0245	F-type H+-transporting ATPase subunit beta	atpD	EC:3.6.3.14	100.0	0	APM40995.1	F0F1 ATP synthase subunit beta [<i>Clostridium kluyveri</i>]
CK_0246	F-type H+-transporting ATPase subunit epsilon	atpC		100.0	1.43E-90	APM40994.1	ATP synthase F1 subunit epsilon [<i>Clostridium kluyveri</i>]
CK_1829	flagellum-specific ATP synthase	fliI	EC:3.6.3.14	100.0	4.60E-95	APM38542.1	flagellar protein export ATPase FliI [<i>Clostridium kluyveri</i>]
S6_Bin012-Clostridium kluyveri-Hydrngenases-Periplasmic [NiFeSe] hydrogenase complex							
CK_3054	hydrogenase expression/formation protein HypE	hypE		100.0	0	APM38845.1	hydrogenase expression/formation protein HypE [<i>Clostridium kluyveri</i>]
CK_3055	hydrogenase expression/formation protein HypD	hypD		100.0	0	APM38844.1	hydrogenase formation protein HypD [<i>Clostridium kluyveri</i>]
CK_3056	hydrogenase expression/formation protein HypC	hypC		100.0	4.21E-43	APM38843.1	hydrogenase assembly protein HypC [<i>Clostridium kluyveri</i>]

CK_3057	hydrogenase maturation protein HypF	hypF	99.7	0	APM41229.1	carbamoyltransferase HypF [<i>Clostridium kluyveri</i>]
CK_3058	hydrogenase nickel incorporation protein	HypA	100.0	1.68E-52	APM38842.1	hypothetical protein BS101_08785 [<i>Clostridium kluyveri</i>]
CK_3059	cytochrome b-like heme/steroid binding domain containing protein		100.0	3.96E-97	APM38841.1	steroid-binding protein [<i>Clostridium kluyveri</i>]
CK_3060	hydrogenase maturation protease	hyaD	EC:3.4.23.-	100.0	1.22E-101	hydrogenase maturation protease [<i>Clostridium kluyveri</i>]
CK_3061	hydrogenase large subunit	hyaB	EC:1.12.99.6	100.0	0	Ni/Fe hydrogenase [<i>Clostridium kluyveri</i>]
CK_3062	hydrogenase small subunit	hyaA	EC:1.12.99.6	100.0	0	Ni/Fe hydrogenase [<i>Clostridium kluyveri</i>]
S6_Bin012-Clostridium kluyveri-Glycerol reduction to 1,3-PDO production						
CK_2795	Propanediol utilization polyhedral body protein	PduA		100.0	1.55E-56	ethanolamine utilization protein EutM [<i>Clostridium kluyveri</i>]
CK_2796	propanediol dehydratase large subunit	pduC	EC:4.2.1.28	100.0	0	propanediol dehydratase [<i>Clostridium kluyveri</i>]
CK_2797	propanediol dehydratase small subunit	pduE	EC:4.2.1.28	96.7	1.87E-123	hypothetical protein CKR_0757 [<i>Clostridium kluyveri</i> NBRC 12016]
CK_2798	Propanediol utilization polyhedral body protein	PduA		84.8	3.89E-73	Predicted microcompartment shellprotein [<i>Clostridium kluyveri</i> DSM 555]
CK_1349	1,3-propanediol dehydrogenase	dhaT	EC:1.1.1.202	100.0	0	alcohol dehydrogenase [<i>Clostridium kluyveri</i>]
S6_Bin013-Anaerostipes caccae-Glycerol oxidation 1						
AC_1531	Glycerol dehydrogenase	gldA	EC:1.1.1.6	100.0	0	MULTISPECIES: glycerol dehydrogenase [<i>Anaerostipes</i>]
AC_3149	Glycerol dehydrogenase	gldA	EC:1.1.1.6	100.0	0	MULTISPECIES: glycerol dehydrogenase [<i>Anaerostipes</i>]
AC_1311	dihydroxyacetone kinase, C-terminal domain	dhaL	EC:2.7.1.-	100.0	1.75E-151	DAK2 domain-containing protein [<i>Anaerostipes</i> sp. 3_2_56FAA]
AC_1313	dihydroxyacetone kinase, N-terminal domain	dhaK	EC:2.7.1.-	100.0	0	Dak1 domain-containing protein [<i>Anaerostipes</i> sp. 3_2_56FAA]
AC_1474	dihydroxyacetone kinase, C-terminal domain	dhaL	EC:2.7.1.-	100.0	3.54E-145	DAK2 domain-containing protein [<i>Anaerostipes</i> sp. 3_2_56FAA]
AC_1475	dihydroxyacetone kinase, N-terminal domain	dhaK	EC:2.7.1.-	100.0	0	Dak1 domain-containing protein [<i>Anaerostipes</i> sp. 3_2_56FAA]
AC_1478	dihydroxyacetone kinase, N-terminal domain	dhaK	EC:2.7.1.-	100.0	0	Dak1 domain-containing protein [<i>Anaerostipes</i> sp. 3_2_56FAA]
AC_2399	dihydroxyacetone kinase, C-terminal domain	dhaL	EC:2.7.1.-	100.0	1.22E-169	dAK2 domain-containing protein [<i>Anaerostipes</i> sp. CAG:276]
AC_2400	dihydroxyacetone kinase, N-terminal domain	dhaK	EC:2.7.1.-	100.0	0	Dak1 domain-containing protein [<i>Anaerostipes</i> sp. 3_2_56FAA]
AC_2545	dihydroxyacetone kinase, C-terminal domain	dhaL	EC:2.7.1.-	100.0	2.78E-151	DAK2 domain-containing protein [<i>Anaerostipes</i> sp. 3_2_56FAA]

AC_2546	dihydroxyacetone kinase, N-terminal domain	dhaK	EC:2.7.1.-	99.4	0	EDR98779.1	DAK1 domain protein [<i>Anaerostipes caccae</i> DSM 14662]
S6_Bin013-Anaerostipes caccae-Glycerol oxidation 2							
AC_0688	Glycerol kinase	glpK	C:2.7.1.30	100.0	0	EFV23466.1	glycerol kinase [<i>Anaerostipes</i> sp. 3_2_56FAA]
AC_1969	glycerol-3-phosphate dehydrogenase (NAD(P)+)	gpsA	EC:1.1.1.94	100.0	0	EDR98278.1	putative glycerol-3-phosphate dehydrogenase [NAD(P)+] [<i>Anaerostipes caccae</i> DSM 14662]
AC_2893	glycerol-3-phosphate dehydrogenase (NAD(P)+)	gpsA	EC:1.1.1.94	100.0	0	EDR96703.1	NAD-dependent glycerol-3-phosphate dehydrogenase C-terminal domain protein [<i>Anaerostipes caccae</i> DSM 14662]
AC_2913	Glycerol-3-phosphate dehydrogenase [NAD(P)+]	gpsA	EC:1.1.1.94	99.7	0	EFV20853.1	NAD-dependent glycerol-3-phosphate dehydrogenase [<i>Anaerostipes</i> sp. 3_2_56FAA]
S6_Bin013-Anaerostipes caccae-Central axis pathway							
AC_1431	triosephosphate isomerase (TIM)	TPI	EC:5.3.1.1	99.6	8.81E-166	EFV22551.1	triose-phosphate isomerase [<i>Anaerostipes</i> sp. 3_2_56FAA]
AC_1935	triosephosphate isomerase (TIM)	TPI	EC:5.3.1.1	100.0	0	WP_039930792.1	MULTISPECIES: triose-phosphate isomerase [<i>Anaerostipes</i>]
AC_2621	triosephosphate isomerase (TIM)	TPI	EC:5.3.1.1	100.0	8.82E-167	EDR98634.1	triose-phosphate isomerase [<i>Anaerostipes caccae</i> DSM 14662]
AC_1933	glyceraldehyde 3-phosphate dehydrogenase	GAPDH	EC:1.2.1.12	100.0	0	EFV20889.1	glyceraldehyde-3-phosphate dehydrogenase [<i>Anaerostipes</i> sp. 3_2_56FAA]
AC_1934	phosphoglycerate kinase	PGK	EC:2.7.2.3	100.0	0	EDR96773.1	phosphoglycerate kinase [<i>Anaerostipes caccae</i> DSM 14662]
AC_1644	probable phosphoglycerate mutase	gpmB	EC:5.4.2.12	100.0	1.08E-147	EFV23711.1	phosphoglycerate mutase [<i>Anaerostipes</i> sp. 3_2_56FAA]
AC_1813	probable phosphoglycerate mutase	gpmB	EC:5.4.2.12	100.0	0	CDC34743.1	phosphoglycerate mutase family protein [<i>Anaerostipes</i> sp. CAG:276]
AC_1938	2,3-bisphosphoglycerate-independent phosphoglycerate mutase	gpmI	EC:5.4.2.12	100.0	0	EDR96770.1	2,3-bisphosphoglycerate-independent phosphoglycerate mutase [<i>Anaerostipes caccae</i> DSM 14662]
AC_2330	2,3-bisphosphoglycerate-independent phosphoglycerate mutase	apgM	EC:5.4.2.12	99.7	0	WP_009289914.1	cofactor-independent phosphoglycerate mutase [<i>Anaerostipes</i> sp. 3_2_56FAA]
AC_0883	phosphoglucomutase	pgm	EC:5.4.2.2	100.0	0	EFV22143.1	phosphoglucomutase/phosphomannomutase [<i>Anaerostipes</i> sp. 3_2_56FAA]

AC_0286	enolase	ENO	EC:4.2.1.11	100.0	0	WP_006566048.1	MULTISPECIES: phosphopyruvate hydratase [<i>Anaerostipes</i>]
AC_1939	enolase	ENO	EC:4.2.1.11	100.0	0	EFV20895.1	phosphopyruvate hydratase [<i>Anaerostipes</i> sp. 3_2_56FAA]
AC_1033	pyruvate kinase	PK	EC:2.7.1.40	100.0	0	CDC35279.1	pyruvate kinase [<i>Anaerostipes</i> sp. CAG:276]
AC_2508	pyruvate-ferredoxin/flavodoxin oxidoreductase	por	EC:1.2.7.1 1.2.7.-	100.0	0	EFV21168.1	ferredoxin oxidoreductase [<i>Anaerostipes</i> sp. 3_2_56FAA]
S6_Bin013-<i>Anaerostipes caccae</i>-Acetate production							
AC_1048	phosphate acetyltransferase	pta	EC:2.3.1.8	100.0	0	EDR99093.1	phosphate acetyltransferase [<i>Anaerostipes caccae</i> DSM 14662]
AC_1049	acetate kinase	ackA	EC:2.7.2.1	100.0	0	EFV21773.1	acetokinase [<i>Anaerostipes</i> sp. 3_2_56FAA]
S6_Bin013-<i>Anaerostipes caccae</i>-Butyrate and caproate production							
AC_3165	acetyl-CoA C-acetyltransferase	atoB	EC:2.3.1.9	100.0	0	WP_039930536.1	acetyl-CoA acetyltransferase [<i>Anaerostipes</i> sp. 3_2_56FAA]
AC_3167	3-hydroxybutyryl-CoA dehydrogenase	paaH	EC:1.1.1.157	100.0	0	EFV21686.1	3-hydroxyacyl-CoA dehydrogenase [<i>Anaerostipes</i> sp. 3_2_56FAA]
AC_0348	3-hydroxybutyryl-CoA dehydratase	croR	EC:4.2.1.55	100.0	7.77E-94	WP_009290664.1	enoyl-CoA hydratase [<i>Anaerostipes</i> sp. 3_2_56FAA]
AC_2342	3-hydroxybutyryl-CoA dehydratase	croR	EC:4.2.1.55	100.0	4.26E-103	WP_006568567.1	MULTISPECIES: enoyl-CoA hydratase [<i>Anaerostipes</i>]
AC_0163	enoyl-CoA hydratase	crt	EC:4.2.1.17	100.0	0	EFV23880.1	enoyl-CoA hydratase/isomerase [<i>Anaerostipes</i> sp. 3_2_56FAA]
AC_3166	enoyl-CoA hydratase	crt	EC:4.2.1.17	100.0	0	EDR99005.1	3-hydroxybutyryl-CoA dehydratase [<i>Anaerostipes caccae</i> DSM 14662]
AC_0539	butyryl-CoA dehydrogenase	bcd	EC:1.3.8.1	100.0	0	EDR97724.1	acyl-CoA dehydrogenase, C-terminal domain protein [<i>Anaerostipes caccae</i> DSM 14662]
AC_3168	butyryl-CoA dehydrogenase	bcd	EC:1.3.8.1	100.0	0	EFV21687.1	acyl-CoA dehydrogenase domain-containing protein [<i>Anaerostipes</i> sp. 3_2_56FAA]
AC_0164	propionate CoA-transferase	pct	EC:2.8.3.1	100.0	0	CDC38503.1	acetate CoA-transferase YdiF [<i>Anaerostipes</i> sp. CAG:276]
AC_0350	4-hydroxybutyrate CoA-transferase	cat2	EC:2.8.3.-	100.0	0	CDC37756.1	acetyl-CoA hydrolase/transferase domain-containing protein [<i>Anaerostipes</i> sp. CAG:276]
AC_0665	acetate CoA/acetoacetate CoA-transferase alpha subunit	atoD	EC:2.8.3.8 2.8.3.9	100.0	5.51E-174	WP_009289219.1	MULTISPECIES: acetoacetate--butyrate CoA transferase [<i>Anaerostipes</i>]

AC_0666	acetate CoA/acetoacetate CoA-transferase beta subunit	atoA	EC:2.8.3.8 2.8.3.9	100.0	3.51E-157	EDR96145.1	3-oxoacid CoA-transferase, B subunit [<i>Anaerostipes caccae</i> DSM 14662]
AC_1864	acetate CoA-transferase	ydiF	EC:2.8.3.8	99.8	0	CDC36559.1	acetate CoA-transferase YdiF [<i>Anaerostipes</i> sp. CAG:276]
AC_2343	propionate CoA-transferase	pct	EC:2.8.3.1	100.0	0	CDC36734.1	acetate CoA-transferase YdiF [<i>Anaerostipes</i> sp. CAG:276]
AC_3169	electron transfer flavoprotein beta subunit	etfB		100.0	0	EDR99002.1	electron transfer flavoprotein domain protein [<i>Anaerostipes caccae</i> DSM 14662]
AC_3170	electron transfer flavoprotein alpha subunit	etfA		100.0	0	EFV21689.1	electron transfer flavoprotein FAD-binding domain-containing protein [<i>Anaerostipes</i> sp. 3_2_56FAA]
S6_Bin013-<i>Anaerostipes caccae</i>-Ethanol production/oxidation							
AC_1208	aldehyde dehydrogenase (NAD ⁺)	ALDH	EC:1.2.1.3	100.0	0	CDC37217.1	aldehyde dehydrogenase [<i>Anaerostipes</i> sp. CAG:276]
AC_0138	alcohol dehydrogenase	adh2	EC:1.1.1.-	99.7	0	CDC38414.1	alcohol dehydrogenase iron-dependent [<i>Anaerostipes</i> sp. CAG:276]
AC_0386	alcohol dehydrogenase	adh2	EC:1.1.1.-	100.0	0	EFV23191.1	iron-containing alcohol dehydrogenase [<i>Anaerostipes</i> sp. 3_2_56FAA]
AC_0659	alcohol dehydrogenase	adh2	EC:1.1.1.-	100.0	0	EDR96137.1	alcohol dehydrogenase, iron-dependent [<i>Anaerostipes caccae</i> DSM 14662]
AC_1877	alcohol dehydrogenase	adh2	EC:1.1.1.-	100.0	0	CDC36582.1	iron-containing alcohol dehydrogenase [<i>Anaerostipes</i> sp. CAG:276]
AC_2049	alcohol dehydrogenase	yiaY	EC:1.1.1.1	100.0	0	EFV21981.1	iron-containing alcohol dehydrogenase [<i>Anaerostipes</i> sp. 3_2_56FAA]
AC_2456	alcohol dehydrogenase	adh2	EC:1.1.1.-	100.0	0	EDR97981.1	alcohol dehydrogenase, iron-dependent [<i>Anaerostipes caccae</i> DSM 14662]
AC_2479	alcohol dehydrogenase	adh2	EC:1.1.1.-	100.0	0	EFV22801.1	iron-containing alcohol dehydrogenase [<i>Anaerostipes</i> sp. 3_2_56FAA]
AC_2659	alcohol dehydrogenase	adh2	EC:1.1.1.-	100.0	0	CDC36055.1	iron-containing alcohol dehydrogenase [<i>Anaerostipes</i> sp. CAG:276]
S6_Bin013-<i>Anaerostipes caccae</i>-Membrane proteins involved in energy conservation-Rnf complex							

AC_2708	electron transport complex protein RnfC	rnfC	100.0	0	EFV22726.1	electron transport complex [<i>Anaerostipes</i> sp. 3_2_56FAA]
AC_2709	electron transport complex protein RnfD	rnfD	100.0	0	EFV22725.1	electron transport complex [<i>Anaerostipes</i> sp. 3_2_56FAA]
AC_2710	electron transport complex protein RnfG	rnfG	100.0	4.20E-141	EDR98049.1	electron transport complex, RnfABCDGE type, G subunit [<i>Anaerostipes caccae</i> DSM 14662]
AC_2711	electron transport complex protein RnfE	rnfE	100.0	1.60E-164	EDR98048.1	electron transport complex, RnfABCDGE type, E subunit [<i>Anaerostipes caccae</i> DSM 14662]
AC_2712	electron transport complex protein RnfA	rnfA	100.0	3.37E-129	EDR98047.1	electron transport complex, RnfABCDGE type, A subunit [<i>Anaerostipes caccae</i> DSM 14662]
AC_2713	electron transport complex protein RnfB	rnfB	100.0	0	EDR98046.1	electron transport complex, RnfABCDGE type, B subunit [<i>Anaerostipes caccae</i> DSM 14662]
S6_Bin013-<i>Anaerostipes caccae</i>-Membrane proteins involved in energy conservation-FAD (or Fe-S) reductase lined to ETF						
AC_0540	Acryloyl-CoA reductase electron transfer subunit gamma		100.0	0	EDR97725.1	electron transfer flavoprotein subunit beta [<i>Anaerostipes caccae</i> DSM 14662]
AC_0541	Acryloyl-CoA reductase electron transfer subunit beta		100.0	0	EFV23041.1	electron transfer flavoprotein FAD-binding domain-containing protein [<i>Anaerostipes</i> sp. 3_2_56FAA]
AC_0543	Acryloyl-CoA reductase electron transfer subunit gamma		100.0	0	EFV23044.1	electron transfer flavoprotein domain-containing protein [<i>Anaerostipes</i> sp. 3_2_56FAA]
AC_0544	Acryloyl-CoA reductase electron transfer subunit beta		100.0	0	EFV23045.1	electron transfer flavoprotein FAD-binding domain-containing protein [<i>Anaerostipes</i> sp. 3_2_56FAA]
AC_0545	putative FAD-linked oxidoreductase		100.0	0	CDC38868.1	putative glycolate oxidase subunit GlcD [<i>Anaerostipes</i> sp. CAG:276]
S6_Bin013-<i>Anaerostipes caccae</i>-ATPase						
AC_0979	F-type H ⁺ -transporting ATPase subunit a		100.0	1.28E-157	EDR95665.1	ATP synthase F0, A subunit [<i>Anaerostipes caccae</i> DSM 14662]
AC_0980	F-type H ⁺ -transporting ATPase subunit c		100.0	2.73E-39	EDR95664.1	ATP synthase F0, C subunit [<i>Anaerostipes caccae</i> DSM 14662]
AC_0981	F-type H ⁺ -transporting ATPase subunit b		100.0	9.39E-110	EDR95663.1	ATP synthase F0, B subunit [<i>Anaerostipes caccae</i> DSM 14662]

AC_0982	F-type H ⁺ -transporting ATPase subunit delta		100.0	1.02E-118	EFV21852.1	ATP synthase F1 [<i>Anaerostipes</i> sp. 3_2_56FAA]
AC_0983	F-type H ⁺ -transporting ATPase subunit alpha	EC:3.6.3.14	100.0	0	EFV21853.1	ATP synthase F1 [<i>Anaerostipes</i> sp. 3_2_56FAA]
AC_0984	F-type H ⁺ -transporting ATPase subunit gamma		100.0	0	EDR95660.1	ATP synthase F1, gamma subunit [<i>Anaerostipes caccae</i> DSM 14662]
AC_0985	F-type H ⁺ -transporting ATPase subunit beta	EC:3.6.3.14	100.0	0	EDR95659.1	ATP synthase F1, beta subunit [<i>Anaerostipes caccae</i> DSM 14662]
AC_0986	F-type H ⁺ -transporting ATPase subunit epsilon		100.0	2.78E-96	EDR95658.1	ATP synthase F1, epsilon subunit [<i>Anaerostipes caccae</i> DSM 14662]
AC_0987	Ca ²⁺ -transporting ATPase	EC:3.6.3.8	100.0	0	EFV21858.1	ATPase [<i>Anaerostipes</i> sp. 3_2_56FAA]
AC_1210	V/A-type H ⁺ /Na ⁺ -transporting ATPase subunit D	ATPVD	100.0	6.28E-149	EFV22893.1	ATP synthase subunit D protein [<i>Anaerostipes</i> sp. 3_2_56FAA]
AC_1211	V/A-type H ⁺ /Na ⁺ -transporting ATPase subunit B	ATPVB	99.8	0	EDR97894.1	ATP synthase ab domain protein [<i>Anaerostipes caccae</i> DSM 14662]
AC_1212	V/A-type H ⁺ /Na ⁺ -transporting ATPase subunit A	ATPVA	99.5	0	EDR97895.1	ATP synthase ab domain protein [<i>Anaerostipes caccae</i> DSM 14662]
AC_1213	V/A-type H ⁺ /Na ⁺ -transporting ATPase subunit E	ATPVE	100.0	2.82E-136	EDR97896.1	hypothetical protein ANACAC_01519 [<i>Anaerostipes caccae</i> DSM 14662]
AC_1214	V/A-type H ⁺ /Na ⁺ -transporting ATPase subunit F	ATPVF	100.0	1.66E-65	EFV22897.1	ATP synthase subunit protein [<i>Anaerostipes</i> sp. 3_2_56FAA]
AC_1215	V/A-type H ⁺ /Na ⁺ -transporting ATPase subunit K	ATPVK	99.3	1.56E-89	EFV22898.1	ATP synthase subunit C protein [<i>Anaerostipes</i> sp. 3_2_56FAA]
AC_1216	V/A-type H ⁺ /Na ⁺ -transporting ATPase subunit I	ATPVI	100.0	0	EFV22899.1	V-type ATPase 116kDa subunit protein [<i>Anaerostipes</i> sp. 3_2_56FAA]
AC_1217	V/A-type H ⁺ /Na ⁺ -transporting ATPase subunit C	ATPVC	99.4	0	CDC37134.1	aTP synthase subunit C [<i>Anaerostipes</i> sp. CAG:276]
AC_1455	F-type H ⁺ -transporting ATPase subunit epsilon		100.0	1.27E-93	EDR96894.1	ATP synthase F1, epsilon subunit [<i>Anaerostipes caccae</i> DSM 14662]
AC_1456	F-type H ⁺ -transporting ATPase subunit beta	EC:3.6.3.14	100.0	0	EDR96895.1	ATP synthase F1, beta subunit [<i>Anaerostipes caccae</i> DSM 14662]
AC_1457	F-type H ⁺ -transporting ATPase subunit gamma		100.0	0	EFV23294.1	ATP synthase F1 [<i>Anaerostipes</i> sp. 3_2_56FAA]
AC_1458	F-type H ⁺ -transporting ATPase subunit alpha	EC:3.6.3.14	100.0	0	EDR96897.1	ATP synthase F1, alpha subunit [<i>Anaerostipes caccae</i> DSM 14662]
AC_1459	F-type H ⁺ -transporting ATPase subunit delta		100.0	4.81E-124	EFV23296.1	ATP synthase delta subunit protein [<i>Anaerostipes</i> sp. 3_2_56FAA]

AC_1460	F-type H ⁺ -transporting ATPase subunit b			100.0	6.26E-116	EFV23297.1	ATP synthase F0 [<i>Anaerostipes</i> sp. 3_2_56FAA]
AC_1461	F-type H ⁺ -transporting ATPase subunit c			100.0	1.70E-51	EDR96900.1	ATP synthase F0, C subunit [<i>Anaerostipes caccae</i> DSM 14662]
AC_1462	F-type H ⁺ -transporting ATPase subunit a			100.0	7.93E-174	EFV23299.1	ATP synthase subunit A protein [<i>Anaerostipes</i> sp. 3_2_56FAA]
AC_1463	ATP synthase protein I	atpI		100.0	3.57E-97	EDR96902.1	hypothetical protein ANACAC_02131 [<i>Anaerostipes caccae</i> DSM 14662]
AC_2235	ferredoxin--NADP ⁺ reductase	fpr	EC:1.18.1.2	99.6	0	EFV22008.1	oxidoreductase NAD-binding domain-containing protein [<i>Anaerostipes</i> sp. 3_2_56FAA]

Appendix VI Table

Gene name	Predicted function	Enzyme commission number	CDS	Identity (%)	e-value	Closely related protein
<i>atoB/phaA</i>	acetyl-CoA acetyltransferase	EC:2.3.1.9	MS_2106	97.2	0	WP_062197208.1 beta-ketoadipyl CoA thiolase [<i>Massilibacterium senegalense</i>]
<i>crt</i>	enoyl-CoA hydratase	EC:4.2.1.17	MS_2107	97.7	0	WP_062197209.1 enoyl-CoA hydratase [<i>Massilibacterium senegalense</i>]
<i>paaH</i>	3-hydroxybutyryl-CoA dehydrogenase	EC:1.1.1.157	MS_2108	98.2	0	WP_062197210.1 3-hydroxybutyryl-CoA dehydrogenase [<i>Massilibacterium senegalense</i>]
<i>bcd</i>	butyryl-CoA dehydrogenase	EC:1.3.8.1	MS_2109	98.1	0	WP_062197211.1 acyl-CoA dehydrogenase [<i>Massilibacterium senegalense</i>]
<i>phbC</i>	polyhydroxyalkanoate synthase	EC:2.3.1.-	MS_0009	96.4	0	WP_074018155.1 class III poly(R)-hydroxyalkanoic acid synthase subunit PhaC [<i>Massilibacterium senegalense</i>]
<i>phbB</i>	acetoacetyl-CoA reductase	EC:1.1.1.36	MS_0010	98.8	2.86E-176	WP_062198192.1 beta-ketoacyl-ACP reductase [<i>Massilibacterium senegalense</i>]

References

- Abbad-Andaloussi, S., Guedon, E., Spiesser, E., & Petitdemange, H. (1996). Glycerol dehydratase activity: The limiting step for 1,3-propanediol production by *Clostridium butyricum* DSM 5431. *Letters in Applied Microbiology*, 22(4), 311-314.
- Agler, M. T., Spirito, C. M., Usack, J. G., Werner, J. J., & Angenent, L. T. (2012). Chain elongation with reactor microbiomes: upgrading dilute ethanol to medium-chain carboxylates. *Energy & Environmental Science*, 5(8), 8189-8192.
- Agler, M. T., Wrenn, B. A., Zinder, S. H., & Angenent, L. T. (2011). Waste to bioproduct conversion with undefined mixed cultures: the carboxylate platform. *Trends in Biotechnology*, 29(2), 70-78.
- Albertsen, M., Karst, S. M., Ziegler, A. S., Kirkegaard, R. H., & Nielsen, P. H. (2015). Back to Basics - The Influence of DNA Extraction and Primer Choice on Phylogenetic Analysis of Activated Sludge Communities. *Plos One*, 10(7).
- Alberty, R. A. (2001). Effect of temperature on standard transformed Gibbs energies of formation of reactants at specified pH and ionic strength and apparent equilibrium constants of biochemical reactions. *Journal of Physical Chemistry B*, 105(32), 7865-7870.
- Alberty, R. A. (2005). *Thermodynamics of biochemical reactions*: John Wiley & Sons.
- Amos, D. A., & Mcinerney, M. J. (1989). Poly-Beta-Hydroxyalkanoate in *Syntrophomonas Wolfei*. *Archives of Microbiology*, 152(2), 172-177.
- Angenent, L. T., Richter, H., Buckel, W., Spirito, C. M., Steinbusch, K. J. J., Plugge, C. M., . . . Hamelers, H. V. M. (2016). Chain Elongation with Reactor Microbiomes: Open-Culture Biotechnology To Produce Biochemicals. *Environmental Science & Technology*, 50(6), 2796-2810.
- Balasubramanian, S., & Tyagi, R. D. (2017a). 2 - Value-Added Bio-products From Sewage Sludge. *Current Developments in Biotechnology and Bioengineering* (pp. 27-42): Elsevier.
- Balasubramanian, S., & Tyagi, R. D. (2017b). 3 - Biopesticide Production From Solid Wastes. *Current Developments in Biotechnology and Bioengineering* (pp. 43-58): Elsevier.
- Bankevich, A., Nurk, S., Antipov, D., Gurevich, A. A., Dvorkin, M., Kulikov, A. S., . . . Pevzner, P. A. (2012). SPAdes: A New Genome Assembly Algorithm and Its Applications to Single-Cell Sequencing. *Journal of Computational Biology*, 19(5), 455-477.
- Barbirato, F., Himmi, E. H., Conte, T., & Bories, A. (1998). 1,3-propanediol production by fermentation: An interesting way to valorize glycerin from the ester and ethanol industries. *Industrial Crops and Products*, 7(2-3), 281-289.
- Barker, H., Kamen, M., & Bornstein, B. (1945). The synthesis of butyric and caproic acids from ethanol and acetic acid by *Clostridium kluveri*. *Proceedings of the National Academy of Sciences*, 31(12), 373-381.
- Barker, H. A. (1937). The production of caproic and butyric acids by the methane

- fermentation of ethyl alcohol. *Archives of Microbiology*, 8(1-4), 415-421.
- Barker, H. A., Kamen, M. D., & Bornstein, B. T. (1945). The Synthesis of Butyric and Caproic Acids from Ethanol and Acetic Acid by *Clostridium Kluyveri*. *Proceedings of the National Academy of Sciences of the United States of America*, 31(12), 373-381.
- Ben Hania, W., Fadhlaoui, K., Brochier-Armanet, C., Persillon, C., Postec, A., Hamdi, M., . . . Erauso, G. (2015). Draft genome sequence of *Mesotoga* strain PhosAC3, a mesophilic member of the bacterial order *Thermotogales*, isolated from a digester treating phosphogypsum in Tunisia. *Standards in Genomic Sciences*, 10.
- Ben Hania, W., Postec, A., Aullo, T., Ranchou-Peyruse, A., Erauso, G., Brochier-Armanet, C., . . . Fardeau, M. L. (2013). *Mesotoga infera* sp nov., a mesophilic member of the order *Thermotogales*, isolated from an underground gas storage aquifer. *International Journal of Systematic and Evolutionary Microbiology*, 63, 3003-3008.
- Biddle, A. S., Leschine, S., Huntemann, M., Han, J., Chen, A., Kyrpides, N., . . . Blanchard, J. L. (2014). The complete genome sequence of *Clostridium indolis* DSM 755(T). *Standards in Genomic Sciences*, 9(3).
- Biebl, H. (2001). Fermentation of glycerol by *Clostridium pasteurianum* - batch and continuous culture studies. *Journal of Industrial Microbiology & Biotechnology*, 27(1), 18-26.
- Boenigk, R., Bowien, S., & Gottschalk, G. (1993). Fermentation of Glycerol to 1,3-Propanediol in Continuous Cultures of *Citrobacter Freundii*. *Applied Microbiology and Biotechnology*, 38(4), 453-457.
- Bolger, A. M., Lohse, M., & Usadel, B. (2014). Trimmomatic: a flexible trimmer for Illumina sequence data. *Bioinformatics*, 30(15), 2114-2120.
- Bornstein, B., & Barker, H. (1948). The nutrition of *Clostridium kluyveri*. *Journal of Bacteriology*, 55(2), 223.
- Boss, B., Hazlett, R., & Shepard, R. (1973). Analysis of normal paraffin oxidation products in the presence of hydroperoxides. *Analytical Chemistry*, 45(14), 2388-2392.
- Breitenstein, A., Wiegel, J., Haertig, C., Weiss, N., Andreesen, J. R., & Lechner, U. (2002). Reclassification of *Clostridium hydroxybenzoicum* as *Sedimentibacter hydroxybenzoicus* gen. nov., comb. nov., and description of *Sedimentibacter saalensis* sp nov. *International Journal of Systematic and Evolutionary Microbiology*, 52, 801-807.
- Bryant, M. P., Campbell, L. L., Reddy, C. A., & Crabill, M. R. (1977). Growth of *Desulfovibrio* in Lactate or Ethanol Media Low in Sulfate in Association with H₂-Utilizing Methanogenic Bacteria. *Applied and Environmental Microbiology*, 33(5), 1162-1169.
- Buckel, W., & Thauer, R. K. (2013). Energy conservation via electron bifurcating ferredoxin reduction and proton/Na⁺ translocating ferredoxin oxidation. *Biochimica et Biophysica Acta (BBA)-Bioenergetics*, 1827(2), 94-113.
- Caporaso, J. G., Kuczynski, J., Stombaugh, J., Bittinger, K., Bushman, F. D., Costello, E. K., . . . Knight, R. (2010). QIIME allows analysis of

- high-throughput community sequencing data. *Nature Methods*, 7(5), 335-336.
- Chantoom, K., Vikromvarasiri, N., & Pisutpaisal, N. (2014). Kinetics of Bioethanol Production from Glycerol by *Enterobacter Aerogenes*. *Energy Procedia*, 61, 2244-2248.
- Chen, P., Xie, Q. L., Addy, M., Zhou, W. G., Liu, Y. H., Wang, Y. P., . . . Ruan, R. (2016). Utilization of municipal solid and liquid wastes for bioenergy and bioproducts production. *Bioresource Technology*, 215, 163-172.
- Chen, S. Y., & Dong, X. Z. (2005). *Proteiniphilum acetatigenes* gen. nov., sp nov., from a UASB reactor treating brewery wastewater. *International Journal of Systematic and Evolutionary Microbiology*, 55, 2257-2261.
- Chen, W. S., Strik, D. P. B. T. B., Buisman, C. J. N., & Kroeze, C. (2017). Production of Caproic Acid from Mixed Organic Waste: An Environmental Life Cycle Perspective. *Environmental Science & Technology*, 51(12), 7159-7168.
- Chen, Y., Wang, T., Shen, N., Zhang, F., & Zeng, R. J. (2016). High-purity propionate production from glycerol in mixed culture fermentation. *Bioresource Technology*, 219, 659-667.
- Cheon, Y., Kim, J. S., Park, J. B., Heo, P., Lim, J. H., Jung, G. Y., . . . Kweon, D. H. (2014). A biosynthetic pathway for hexanoic acid production in *Kluyveromyces marxianus*. *Journal of Biotechnology*, 182, 30-36.
- Choi, K., Jeon, B. S., Kim, B. C., Oh, M. K., Um, Y., & Sang, B. I. (2013). In situ biphasic extractive fermentation for hexanoic acid production from sucrose by *Megasphaera elsdenii* NCIMB 702410. *Appl Biochemistry and Biotechnology*, 171(5), 1094-1107.
- Clark, M. E., He, Z. L., Redding, A. M., Joachimiak, M. P., Keasling, J. D., Zhou, J. Z. Z., . . . Fields, M. W. (2012). Transcriptomic and proteomic analyses of *Desulfovibrio vulgaris* biofilms: Carbon and energy flow contribute to the distinct biofilm growth state. *BMC Genomics*, 13.
- Clavel, T., Lepage, P., & Charrier, C. (2014). The Family *Coriobacteriaceae*. In E. Rosenberg, E. F. DeLong, S. Lory, E. Stackebrandt, & F. Thompson (Eds.), *The Prokaryotes: Actinobacteria* (pp. 201-238). Berlin, Heidelberg: Springer Berlin Heidelberg.
- Colin, T., Bories, A., Lavigne, C., & Moulin, G. (2001). Effects of acetate and butyrate during glycerol fermentation by *Clostridium butyricum*. *Current Microbiology*, 43(4), 238-243.
- Collins, M. D., Lawson, P. A., Willems, A., Cordoba, J. J., Fernandez-Garayzabal, J., Garcia, P., . . . Farrow, J. A. (1994). The phylogeny of the genus *Clostridium*: proposal of five new genera and eleven new species combinations. *International Journal of Systematic Bacteriology*, 44(4), 812-826.
- da Silva, G. P., Mack, M., & Contiero, J. (2009). Glycerol: a promising and abundant carbon source for industrial microbiology. *Biotechnology Advances*, 27(1), 30-39.
- Devereux, R., Willis, S. G., & Hines, M. E. (1997). Genome sizes of *Desulfovibrio desulfuricans*, *Desulfovibrio vulgaris*, and *Desulfohalobium propionicum* estimated by pulsed-field gel electrophoresis of linearized chromosomal DNA. *Current Microbiology*, 34(6), 337-339.

- Dietz, D., & Zeng, A. P. (2014). Efficient production of 1,3-propanediol from fermentation of crude glycerol with mixed cultures in a simple medium. *Bioprocess and Biosystems Engineering*, 37(2), 225-233.
- Ding, H. B., Tan, G. Y. A., & Wang, J. Y. (2010). Caproate formation in mixed-culture fermentative hydrogen production. *Bioresource Technology*, 101(24), 9550-9559.
- Eggerth, A. H., & Gagnon, B. H. (1933). The *bacteroides* of human feces. *Journal of Bacteriology*, 25(4), 389-413.
- Ezaki, T., Kawamura, Y., Li, N., Li, Z. Y., Zhao, L. C., & Shu, S. E. (2001). Proposal of the genera *Anaerococcus* gen. nov., *Peptoniphilus* gen. nov and *Gallicola* gen. nov for members of the genus *Peptostreptococcus*. *International Journal of Systematic and Evolutionary Microbiology*, 51, 1521-1528.
- Facklam, R. R., & Collins, M. D. (1989). Identification of *Enterococcus* Species Isolated from Human Infections by a Conventional Test Scheme. *Journal of Clinical Microbiology*, 27(4), 731-734.
- Fonknechten, N., Chaussonnerie, S., Tricot, S., Lajus, A., Andreesen, J. R., Perchat, N., . . . Kreimeyer, A. (2010). *Clostridium sticklandii*, a specialist in amino acid degradation: revisiting its metabolism through its genome sequence. *BMC Genomics*, 11.
- Forage, R. G., & Foster, M. A. (1982). Glycerol Fermentation in *Klebsiella Pneumoniae* - Functions of the Coenzyme-B12-Dependent Glycerol and Diol Dehydratases. *Journal of Bacteriology*, 149(2), 413-419.
- Forage, R. G., & Lin, E. C. C. (1982). Dha System Mediating Aerobic and Anaerobic Dissimilation of Glycerol in *Klebsiella Pneumoniae* Ncib-418. *Journal of Bacteriology*, 151(2), 591-599.
- Galperin, M. Y., Brover, V., Tolstoy, I., & Yutin, N. (2016). Phylogenomic analysis of the family *Peptostreptococcaceae* (*Clostridium* cluster XI) and proposal for reclassification of *Clostridium litorale* (Fendrich et al. 1991) and *Eubacterium acidaminophilum* (Zindel et al. 1989) as *Peptoclostridium litorale* gen. nov comb. nov and *Peptoclostridium acidaminophilum* comb. nov. *International Journal of Systematic and Evolutionary Microbiology*, 66, 5506-5513.
- Gao, Z. M., Xu, X., & Ruan, L. W. (2014). Enrichment and characterization of an anaerobic cellulolytic microbial consortium SQD-1.1 from mangrove soil. *Applied Microbiology and Biotechnology*, 98(1), 465-474.
- Genthner, B. R. S., Davis, C. L., & Bryant, M. P. (1981). Features of Rumen and Sewage-Sludge Strains of *Eubacterium limosum*, a Methanol-Utilizing and H₂-CO₂-Utilizing Species. *Applied and Environmental Microbiology*, 42(1), 12-19.
- Ghaffar, T., Irshad, M., Anwar, Z., Aqil, T., Zulifqar, Z., Tariq, A., . . . Mehmood, S. (2014). Recent trends in lactic acid biotechnology: A brief review on production to purification. *Journal of Radiation Research and Applied Sciences*, 7(2), 222-229.
- Gonzalez-Pajuelo, M., Meynial-Salles, I., Mendes, F., Soucaille, P., & Vasconcelos, I. (2006). Microbial conversion of glycerol to 1,3-propanediol: Physiological

- comparison of a natural producer, *Clostridium butyricum* VPI 3266, and an engineered strain, *Clostridium acetobutylicum* DG1(pSPD5). *Applied and Environmental Microbiology*, 72(1), 96-101.
- Gossner, A. S., Kusel, K., Schulz, D., Trenz, S., Acker, G., Lovell, C. R., & Drake, H. L. (2006). Trophic interaction of the aerotolerant anaerobe *Clostridium intestinale* and the acetogen *Sporomusa rhizae* sp. nov. isolated from roots of the black needlerush *Juncus roemerianus*. *Microbiology*, 152(4), 1209-1219.
- Granda, C. B., Zhu, L., & Holtzapfle, M. T. (2007). Sustainable liquid biofuels and their environmental impact. *Environmental Progress*, 26(3), 233-250.
- Gray, C. T., Wimpenny, J. W., Hughes, D. E., & Mossman, M. R. (1966). Regulation of metabolism in facultative bacteria. I. Structural and functional changes in *Escherichia coli* associated with shifts between the aerobic and anaerobic states. *Biochimica et Biophysica Acta (BBA)*, 117(1), 22-32.
- Groom, M. J., Gray, E. M., & Townsend, P. A. (2008). Biofuels and biodiversity: Principles for creating better policies for biofuel production. *Conservation Biology*, 22(3), 602-609.
- Grootscholten, T. I. M., Steinbusch, K. J. J., Hamelers, H. V. M., & Buisman, C. J. N. (2013). Chain elongation of acetate and ethanol in an upflow anaerobic filter for high rate MCFA production. *Bioresource Technology*, 135, 440-445.
- Gungormusler, M., Gonen, C., & Azbar, N. (2011). Continuous production of 1,3-propanediol using raw glycerol with immobilized *Clostridium beijerinckii* NRRL B-593 in comparison to suspended culture. *Bioprocess and Biosystems Engineering*, 34(6), 727-733.
- Gurevich, A., Saveliev, V., Vyahhi, N., & Tesler, G. (2013). QUASt: quality assessment tool for genome assemblies. *Bioinformatics*, 29(8), 1072-1075.
- Haas, B. J., Gevers, D., Earl, A. M., Feldgarden, M., Ward, D. V., Giannoukos, G., . . . Consortium, H. M. (2011). Chimeric 16S rRNA sequence formation and detection in Sanger and 454-pyrosequenced PCR amplicons. *Genome Research*, 21(3), 494-504.
- Harding, K. C., Lee, P. K. H., Bill, M., Buscheck, T. E., Conrad, M. E., & Alvarez-Cohen, L. (2013). Effects of Varying Growth Conditions on Stable Carbon Isotope Fractionation of Trichloroethene (TCE) by tceA-containing *Dehalococcoides mccartyi* strains. *Environmental Science & Technology*, 47(21), 12342-12350.
- Harper, W. J. (1957). Lipase Systems Used in the Manufacture of Italian Cheese. II. Selective Hydrolysis. *Journal of Dairy Science*, 40(5), 556-563.
- Heidelberg, J. F., Seshadri, R., Haveman, S. A., Hemme, C. L., Paulsen, I. T., Kolonay, J. F., . . . Fraser, C. M. (2004). The genome sequence of the anaerobic, sulfate-reducing bacterium *Desulfovibrio vulgaris* Hildenborough. *Nature Biotechnology*, 22(5), 554-559.
- Hendriks, A. T. W. M., & Zeeman, G. (2009). Pretreatments to enhance the digestibility of lignocellulosic biomass. *Bioresource Technology*, 100(1), 10-18.
- Herrmann, G., Jayamani, E., Mai, G., & Buckel, W. (2008). Energy conservation via electron-transferring flavoprotein in anaerobic bacteria. *Journal of*

- Bacteriology*, 190(3), 784-791.
- Ho, D. P., Ngo, H. H., & Guo, W. (2014). A mini review on renewable sources for biofuel. *Bioresource Technology*, 169, 742-749.
- Hoover, R., Laurentius, S. F., & Gunetileke, K. G. (1973). Spoilage of Coconut Oil Purification and Properties of a Fungal Lipase That Attacks Coconut Oil. *Journal of the American Oil Chemists Society*, 50(3), 64-67.
- Hu, P., Bowen, S. H., & Lewis, R. S. (2011). A thermodynamic analysis of electron production during syngas fermentation. *Bioresource Technology*, 102(17), 8071-8076.
- Ito, T., Nakashimada, Y., Senba, K., Matsui, T., & Nishio, N. (2005). Hydrogen and ethanol production from glycerol-containing wastes discharged after biodiesel manufacturing process. *Journal of Bioscience and Bioengineering*, 100(3), 260-265.
- Jabari, L., Gannoun, H., Cayol, J. L., Hedi, A., Sakamoto, M., Falsen, E., . . . Fardeau, M. L. (2012). *Macellibacteroides fermentans* gen. nov., sp nov., a member of the family *Porphyromonadaceae* isolated from an upflow anaerobic filter treating abattoir wastewaters. *International Journal of Systematic and Evolutionary Microbiology*, 62, 2522-2527.
- Jackson, B. E., & McInerney, M. J. (2002). Anaerobic microbial metabolism can proceed close to thermodynamic limits. *Nature*, 415(6870), 454-456.
- Jacobs, N. J., & VanDemark, P. (1960). Comparison of the mechanism of glycerol oxidation in aerobically and anaerobically grown *Streptococcus faecalis*. *Journal of Bacteriology*, 79(4), 532.
- Jarvis, G. N., Moore, E. R. B., & Thiele, J. H. (1997). Formate and ethanol are the major products of glycerol fermentation produced by a *Klebsiella planticola* strain isolated from red deer. *Journal of Applied Microbiology*, 83(2), 166-174.
- Jeon, B. S., Choi, O., Um, Y., & Sang, B. I. (2016). Production of medium-chain carboxylic acids by *Megasphaera* sp. MH with supplemental electron acceptors. *Biotechnology for Biofuels*, 9, 129.
- Jeon, B. S., Kim, B. C., Um, Y., & Sang, B. I. (2010). Production of hexanoic acid from D-galactitol by a newly isolated *Clostridium* sp. BS-1. *Applied Microbiology and Biotechnology*, 88(5), 1161-1167.
- Jin, R. Z., Forage, R. G., & Lin, E. C. C. (1982). Glycerol Kinase as a Substitute for Dihydroxyacetone Kinase in a Mutant of *Klebsiella Pneumoniae*. *Journal of Bacteriology*, 152(3), 1303-1307.
- Johnson, D. T., & Taconi, K. A. (2007). The glycerin glut: Options for the value-added conversion of crude glycerol resulting from biodiesel production. *Environmental Progress*, 26(4), 338-348.
- Jung, S., & Regan, J. M. (2007). Comparison of anode bacterial communities and performance in microbial fuel cells with different electron donors. *Applied Microbiology and Biotechnology*, 77(2), 393-402.
- Jungermann, K., Thauer, R. K., & Decker, K. (1968). The synthesis of one-carbon units from CO₂ in *Clostridium kluyveri*. *European Journal of Biochemistry*, 3(3), 351-359.

- Kalia, V. C. (2016). *Microbial Factories: Biofuels, Waste Treatment* (Vol. 1): Springer.
- Kamagata, Y. (2015). *Oscillospira Bergey's Manual of Systematics of Archaea and Bacteria*: John Wiley & Sons, Ltd.
- Kanehisa, M., Sato, Y., & Morishima, K. (2016). BlastKOALA and GhostKOALA: KEGG Tools for Functional Characterization of Genome and Metagenome Sequences. *Journal of Molecular Biology*, 428(4), 726-731.
- Kelly, W. J., Henderson, G., Pacheco, D. M., Li, D., Reilly, K., Naylor, G. E., . . . Leahy, S. C. (2016). The complete genome sequence of *Eubacterium limosum* SA11, a metabolically versatile rumen acetogen. *Standards in Genomic Sciences*, 11.
- Kenealy, W. R., Cao, Y., & Weimer, P. J. (1995). Production of caproic acid by cocultures of ruminal cellulolytic bacteria and *Clostridium kluyveri* grown on cellulose and ethanol. *Applied Microbiology and Biotechnology*, 44(3-4), 507-513.
- Kenealy, W. R., & Waselefsky, D. M. (1985). Studies on the Substrate Range of *Clostridium Kluyveri* - the Use of Propanol and Succinate. *Archives of Microbiology*, 141(3), 187-194.
- Khanal, S. K. (2009). Microbiology and biochemistry of anaerobic biotechnology. *Anaerobic Biotechnology for Bioenergy Production: Principles and Applications*, 29-41.
- Kleerebezem, R., & van Loosdrecht, M. C. M. (2007). Mixed culture biotechnology for bioenergy production. *Current Opinion in Biotechnology*, 18(3), 207-212.
- Kouzuma, A., Kato, S., & Watanabe, K. (2015). Microbial interspecies interactions: recent findings in syntrophic consortia. *Frontiers in Microbiology*, 6, 477.
- Kozich, J. J., Westcott, S. L., Baxter, N. T., Highlander, S. K., & Schloss, P. D. (2013). Development of a Dual-Index Sequencing Strategy and Curation Pipeline for Analyzing Amplicon Sequence Data on the MiSeq Illumina Sequencing Platform. *Applied and Environmental Microbiology*, 79(17), 5112-5120.
- Kremer, D. R., & Hansen, T. A. (1987). Glycerol and Dihydroxyacetone Dissimilation in *Desulfovibrio* Strains. *Archives of Microbiology*, 147(3), 249-256.
- Lan, T. Q., Gleisner, R., Zhu, J. Y., Dien, B. S., & Hector, R. E. (2013). High titer ethanol production from SPORL-pretreated lodgepole pine by simultaneous enzymatic saccharification and combined fermentation. *Bioresource Technology*, 127, 291-297.
- Laue, H., Denger, K., & Cook, A. M. (1997). Taurine reduction in anaerobic respiration of *Bilophila wadsworthia* RZATAU. *Applied and Environmental Microbiology*, 63(5), 2016-2021.
- Lee, C. S., Aroua, M. K., Daud, W. M. A. W., Cognet, P., Peres-Lucchese, Y., Fabre, P. L., . . . Latapie, L. (2015). A review: Conversion of bioglycerol into 1,3-propanediol via biological and chemical method. *Renewable & Sustainable Energy Reviews*, 42, 963-972.
- Lee, G. H., Kumar, S., Lee, J. H., Chang, D. H., Kim, D. S., Choi, S. H., . . . Kim, B.

- C. (2012). Genome Sequence of *Oscillibacter ruminantium* Strain GH1, Isolated from Rumen of Korean Native Cattle. *Journal of Bacteriology*, *194*(22), 6362-6362.
- Lee, G. H., Rhee, M. S., Chang, D. H., Lee, J., Kim, S., Yoon, M. H., & Kim, B. C. (2013). *Oscillibacter ruminantium* sp nov., isolated from the rumen of Korean native cattle. *International Journal of Systematic and Evolutionary Microbiology*, *63*, 1942-1946.
- Leng, L., Yang, P. X., Mao, Y. P., Wu, Z. Y., Zhang, T., & Lee, P. H. (2017). Thermodynamic and physiological study of caproate and 1,3-propanediol co-production through glycerol fermentation and fatty acids chain elongation. *Water Research*, *114*, 200-209.
- Li, A., Antizar-Ladislao, B., & Khraisheh, M. (2007). Bioconversion of municipal solid waste to glucose for bio-ethanol production. *Bioprocess and Biosystems Engineering*, *30*(3), 189-196.
- Li, A., Chu, Y. N., Wang, X. M., Ren, L. F., Yu, J., Liu, X. L., . . . Li, S. Z. (2013). A pyrosequencing-based metagenomic study of methane-producing microbial community in solid-state biogas reactor. *Biotechnology for Biofuels*, *6*.
- Li, F., Hinderberger, J., Seedorf, H., Zhang, J., Buckel, W., & Thauer, R. K. (2008). Coupled ferredoxin and crotonyl coenzyme a (CoA) reduction with NADH catalyzed by the butyryl-CoA dehydrogenase/Etf complex from *Clostridium kluyveri*. *Journal of Bacteriology*, *190*(3), 843-850.
- Li, H., Tao, Y. S., Wang, H., & Zhang, L. (2008). Impact odorants of Chardonnay dry white wine from Changli County (China). *European Food Research and Technology*, *227*(1), 287-292.
- Liew, F., Martin, M. E., Tappel, R. C., Heijstra, B. D., Mihalcea, C., & Kopke, M. (2016). Gas Fermentation A Flexible Platform for Commercial Scale Production of Low-Carbon-Fuels and Chemicals from Waste and Renewable Feedstocks. *Frontiers in Microbiology*, *7*.
- Lin, E. C. C. (1976). Glycerol Dissimilation and Its Regulation in Bacteria. *Annual Review of Microbiology*, *30*, 535-578.
- Lindley, N. D., Loubiere, P., Pacaud, S., Mariotto, C., & Goma, G. (1987). Novel Products of the Acidogenic Fermentation of Methanol during Growth of *Eubacterium limosum* in the Presence of High-Concentrations of Organic-Acids. *Journal of General Microbiology*, *133*, 3557-3563.
- Liu, B. C., Christiansen, K., Parnas, R., Xu, Z. H., & Li, B. K. (2013). Optimizing the production of hydrogen and 1,3-propanediol in anaerobic fermentation of biodiesel glycerol. *International Journal of Hydrogen Energy*, *38*(8), 3196-3205.
- Liu, C. X., Finegold, S. M., Song, Y. J., & Lawson, P. A. (2008). Reclassification of *Clostridium coccoides*, *Ruminococcus hansenii*, *Ruminococcus hydrogenotrophicus*, *Ruminococcus luti*, *Ruminococcus productus* and *Ruminococcus schinkii* as *Blautia coccoides* gen. nov., comb. nov., *Blautia hansenii* comb. nov., *Blautia hydrogenotrophica* comb. nov., *Blautia luti* comb. nov., *Blautia producta* comb. nov., *Blautia schinkii* comb. nov and description of *Blautia wexlerae* sp nov., isolated from human faeces.

- International Journal of Systematic and Evolutionary Microbiology*, 58, 1896-1902.
- Liu, H., Hu, H., Chignell, J., & Fan, Y. (2010). Microbial electrolysis: novel technology for hydrogen production from biomass. *Biofuels*, 1(1), 129-142.
- Liu, W. T., Marsh, T. L., Cheng, H., & Forney, L. J. (1997). Characterization of microbial diversity by determining terminal restriction fragment length polymorphisms of genes encoding 16S rRNA. *Applied and Environmental Microbiology*, 63(11), 4516-4522.
- Louis, P., & Flint, H. J. (2009). Diversity, metabolism and microbial ecology of butyrate-producing bacteria from the human large intestine. *Fems Microbiology Letters*, 294(1), 1-8.
- Ludwig, W., Strunk, O., Westram, R., Richter, L., Meier, H., Yadhukumar, . . . Schleifer, K. H. (2004). ARB: a software environment for sequence data. *Nucleic Acids Research*, 32(4), 1363-1371.
- Mackie, R. I., Aminov, R. I., Hu, W., Klieve, A. V., Ouwkerk, D., Sundset, M. A., & Kamagata, Y. (2003). Ecology of Uncultivated *Oscillospira* Species in the Rumen of Cattle, Sheep, and Reindeer as Assessed by Microscopy and Molecular Approaches. *Applied and Environmental Microbiology*, 69(11), 6808-6815.
- Mandegari, M. A., Farzad, S., & Görgens, J. F. (2016). Process Design, Flowsheeting, and Simulation of Bioethanol Production from Lignocelluloses. *Biofuels: Production and Future Perspectives*, 255.
- Marounek, M., Fliegrova, K., & Bartos, S. (1989). Metabolism and Some Characteristics of Ruminal Strains of *Megasphaera Elsdenii*. *Applied and Environmental Microbiology*, 55(6), 1570-1573.
- Marx, H., Graf, A. B., Totto, N. E., Thallinger, G. G., Mattanovich, D., & Sauer, M. (2011). Genome sequence of the ruminal bacterium *Megasphaera elsdenii*. *Journal of Bacteriology*, 193(19), 5578-5579.
- McCarty, P. L., & Bae, J. (2011). Model to Couple Anaerobic Process Kinetics with Biological Growth Equilibrium Thermodynamics. *Environmental Science & Technology*, 45(16), 6838-6844.
- McDonald, D., Price, M. N., Goodrich, J., Nawrocki, E. P., DeSantis, T. Z., Probst, A., . . . Hugenholtz, P. (2012). An improved Greengenes taxonomy with explicit ranks for ecological and evolutionary analyses of bacteria and archaea. *ISME Journal*, 6(3), 610-618.
- McGuire, A. M., Cochrane, K., Griggs, A. D., Haas, B. J., Abeel, T., Zeng, Q. D., . . . Earl, A. M. (2014). Evolution of Invasion in a Diverse Set of *Fusobacterium* Species. *mBio*, 5(6).
- McInerney, M. J., Amos, D. A., Kealy, K. S., & Palmer, J. A. (1992). Synthesis and Function of Polyhydroxyalkanoates in Anaerobic Syntrophic Bacteria. *Fems Microbiology Letters*, 103(2-4), 195-205.
- McInerney, M. J., Sieber, J. R., & Gunsalus, R. P. (2009). Syntrophy in anaerobic global carbon cycles. *Current Opinion in Biotechnology*, 20(6), 623-632.
- McKendry, P. (2002). Energy production from biomass (part 2): conversion technologies. *Bioresource Technology*, 83(1), 47-54.

- Men, Y. J., Feil, H., VerBerkmoes, N. C., Shah, M. B., Johnson, D. R., Lee, P. K. H., . . . Alvarez-Cohen, L. (2012). Sustainable syntrophic growth of *Dehalococcoides ethenogenes* strain 195 with *Desulfovibrio vulgaris* Hildenborough and *Methanobacterium congolense*: global transcriptomic and proteomic analyses. *ISME Journal*, 6(2), 410-421.
- Menzel, K., Ahrens, K., Zeng, A. P., & Deckwer, W. D. (1998). Kinetic, dynamic, and pathway studies of glycerol metabolism by *Klebsiella pneumoniae* in anaerobic continuous culture: IV. Enzymes and fluxes of pyruvate metabolism. *Biotechnology and Bioengineering*, 60(5), 617-626.
- Menzel, K., Zeng, A. P., & Deckwer, W. D. (1997). High concentration and productivity of 1,3-propanediol from continuous fermentation of glycerol by *Klebsiella pneumoniae*. *Enzyme and Microbial Technology*, 20(2), 82-86.
- Miller, T. L. (1978). The pathway of formation of acetate and succinate from pyruvate by *Bacteroides succinogenes*. *Archives of Microbiology*, 117(2), 145-152.
- Miyazaki, K., Hino, T., & Itabashi, H. (1991). Effects of Extracellular Ph on the Intracellular Ph, Membrane-Potential, and Growth-Yield of *Megasphaera Elsdenii* in Relation to the Influence of Monensin, Ethanol, and Acetate. *Journal of General and Applied Microbiology*, 37(5), 415-422.
- Mohapatra, P. K. (2008). *Textbook of environmental microbiology*: IK International Publishing House.
- Moscoviz, R., Trably, E., & Bernet, N. (2016). Consistent 1,3-propanediol production from glycerol in mixed culture fermentation over a wide range of pH. *Biotechnology for Biofuels*, 9.
- Munasinghe, P. C., & Khanal, S. K. (2010). Biomass-derived syngas fermentation into biofuels: Opportunities and challenges. *Bioresource Technology*, 101(13), 5013-5022.
- Murarka, A., Dharmadi, Y., Yazdani, S. S., & Gonzalez, R. (2008). Fermentative utilization of glycerol by *Escherichia coli* and its implications for the production of fuels and chemicals. *Applied and Environmental Microbiology*, 74(4), 1124-1135.
- Narihiro, T., Nobu, M. K., Tamaki, H., Kamagata, Y., Sekiguchi, Y., & Liu, W. T. (2016). Comparative genomics of syntrophic branched-chain fatty acid degrading bacteria. *Microbes and Environments*, 31(3), 288-292.
- Ndongo, S., Andrieu, C., Fournier, P. E., Lagier, J. C., & Raoult, D. (2017). '*Actinomyces provencensis*' sp. nov., '*Corynebacterium bouchesdurhonense*' sp. nov., '*Corynebacterium provencense*' sp. nov. and '*Xanthomonas massiliensis*' sp. nov., 4 new species isolated from fresh stools of obese French patients. *New Microbes and New Infections*, 18, 24-27.
- Nesbo, C. L., Bradnan, D. M., Adebuseyi, A., Dlutek, M., Petrus, A. K., Foght, J., . . . Noll, K. M. (2012). *Mesotoga prima* gen. nov., sp nov., the first described mesophilic species of the *Thermotogales*. *Extremophiles*, 16(3), 387-393.
- Nurk, S., Bankevich, A., Antipov, D., Gurevich, A., Korobeynikov, A., Lapidus, A., . . . Pevzner, P. A. (2013). Assembling Genomes and Mini-metagenomes from Highly Chimeric Reads. In M. Deng, R. Jiang, F. Sun, & X. Zhang

- (Eds.), *Research in Computational Molecular Biology: 17th Annual International Conference, RECOMB 2013, Beijing, China, April 7-10, 2013. Proceedings* (pp. 158-170). Berlin, Heidelberg: Springer Berlin Heidelberg.
- Oh, B. R., Seo, J. W., Heo, S. Y., Hong, W. K., Luo, L. H., Joe, M. H., . . . Kim, C. H. (2011). Efficient production of ethanol from crude glycerol by a *Klebsiella pneumoniae* mutant strain. *Bioresource Technology*, *102*(4), 3918-3922.
- Oh, S. E., Van Ginkel, S., & Logan, B. E. (2003). The relative effectiveness of pH control and heat treatment for enhancing biohydrogen gas production. *Environmental Science & Technology*, *37*(22), 5186-5190.
- Oliveros, J. C. (2007-2015). An interactive tool for comparing lists with Venn's diagrams. *Venny*, Retrieved from <http://bioinfogp.cnb.csic.es/tools/venny/index.html>
- Panke, S., Held, M., & Wubbolts, M. (2004). Trends and innovations in industrial biocatalysis for the production of fine chemicals. *Current Opinion in Biotechnology*, *15*(4), 272-279.
- Parks, D. H., Imelfort, M., Skennerton, C. T., Hugenholtz, P., & Tyson, G. W. (2015). CheckM: assessing the quality of microbial genomes recovered from isolates, single cells, and metagenomes. *Genome Research*, *25*(7), 1043-1055.
- Parry, M. L., & Intergovernmental Panel on Climate Change. Working Group II. (2007). *Climate Change 2007 : impacts, adaptation and vulnerability : contribution of Working Group II to the fourth assessment report of the Intergovernmental Panel on Climate Change*. New York: Cambridge University Press,.
- Patel, S. (2014). IEA's World Energy Outlook 2013: Renewables and Natural Gas to Surge Through 2035. Retrieved from <http://www.powermag.com/ieas-world-energy-outlook-2013-renewables-and-natural-gas-to-surge-through-2035/>
- Pommet, M., Redl, A., Morel, M. H., & Guilbert, S. (2003). Study of wheat gluten plasticization with fatty acids. *Polymer*, *44*(1), 115-122.
- Potrykus, J., White, R. L., & Bearne, S. L. (2008). Proteomic investigation of amino acid catabolism in the indigenous gut anaerobe *Fusobacterium varium*. *Proteomics*, *8*(13), 2691-2703.
- Prabhu, R., Altman, E., & Eiteman, M. A. (2012). Lactate and Acrylate Metabolism by *Megasphaera elsdenii* under Batch and Steady-State Conditions. *Applied and Environmental Microbiology*, *78*(24), 8564-8570.
- Pryde, S. E., Duncan, S. H., Hold, G. L., Stewart, C. S., & Flint, H. J. (2002). The microbiology of butyrate formation in the human colon. *Fems Microbiology Letters*, *217*(2), 133-139.
- Quispe, C. A.G., Coronado, C. J.R., Carvalho Jr. J. A. (2013). Glycerol: Production, consumption, prices, characterization and new trends in combustion. *Renewable and Sustainable Energy Reviews*, *27*(2013), 475-493
- Ragsdale, S. W., & Pierce, E. (2008). Acetogenesis and the Wood-Ljungdahl pathway of CO₂ fixation. *Biochimica Et Biophysica Acta-Proteins and Proteomics*, *1784*(12), 1873-1898.
- Rajeev, L., Hillesland, K. L., Zane, G. M., Zhou, A. F., Joachimiak, M. P., He, Z.

- L., . . . Stahl, D. A. (2012). Deletion of the *Desulfovibrio vulgaris* Carbon Monoxide Sensor Invokes Global Changes in Transcription. *Journal of Bacteriology*, 194(21), 5783-5793.
- Rautio, M., Eerola, E., Vaisanen-Tunkelrott, M. L., Molitoris, D., Lawson, P., Collins, M. D., & Jousimies-Somer, H. (2003). Reclassification of *Bacteroides putredinis* (Weinberg et al., 1937) in a New Genus *Alistipes* gen. nov., as *Alistipes putredinis* comb. nov., and description of *Alistipes finegoldii* sp nov., from human sources. *Systematic and Applied Microbiology*, 26(2), 182-188.
- Raynaud, C., Lee, J., Sarcabal, P., Croux, C., Meynial-Salles, I., & Soucaille, P. (2011). Molecular characterization of the glycerol-oxidative pathway of *Clostridium butyricum* VPI 1718. *Journal of Bacteriology*, 193(12), 3127-3134.
- Raynaud, C., Sarcabal, P., Meynial-Salles, I., Croux, C., & Soucaille, P. (2003). Molecular characterization of the 1,3-propanediol (1,3-PD) operon of *Clostridium butyricum*. *Proceedings of the National Academy of Sciences of the United States of America*, 100(9), 5010-5015.
- Richey, D. P., & Lin, E. C. (1972). Importance of facilitated diffusion for effective utilization of glycerol by *Escherichia coli*. *Journal of Bacteriology*, 112(2), 784-790.
- Rittmann, B. E., & McCarty, P. L. (2012). *Environmental biotechnology: principles and applications*: Tata McGraw-Hill Education.
- Roh, H., Ko, H. J., Kim, D., Choi, D. G., Park, S., Kim, S., . . . Choi, I. G. (2011). Complete genome sequence of a carbon monoxide-utilizing acetogen, *Eubacterium limosum* KIST612. *Journal of Bacteriology*, 193(1), 307-308.
- Saintamans, S., Perlot, P., Goma, G., & Soucaille, P. (1994). High Production of 1,3-Propanediol from Glycerol by *Clostridium Butyricum* Vpi-3266 in a Simply Controlled Fed-Batch System. *Biotechnology Letters*, 16(8), 831-836.
- Sakai, S., Nakashimada, Y., Yoshimoto, H., Watanabe, S., Okada, H., & Nishio, N. (2004). Ethanol production from H₂ and CO₂ by a newly isolated thermophilic bacterium, *Moorella* sp. HUC22-1. *Biotechnology Letters*, 26(20), 1607-1612.
- Sato, K., Nishina, Y., Setoyama, C., Miura, R., & Shiga, K. (1999). Unusually high standard redox potential of acrylyl-CoA/propionyl-CoA couple among enoyl-CoA/acyl-CoA couples: A reason for the distinct metabolic pathway ay of propionyl-CoA from longer acyl-CoAs. *Journal of Biochemistry*, 126(4), 668-675.
- Schink, B. (1997). Energetics of syntrophic cooperation in methanogenic degradation. *Microbiology and Molecular Biology Reviews*, 61(2), 262-80.
- Schink, B., & Stams, A. J. (2013). *Syntrophism among prokaryotes*: Springer.
- Schlegel, H. G. n. (1993). *General microbiology*: Cambridge university press.
- Schloss, P. D., Westcott, S. L., Ryabin, T., Hall, J. R., Hartmann, M., Hollister, E. B., . . . Weber, C. F. (2009). Introducing mothur: Open-Source, Platform-Independent, Community-Supported Software for Describing and Comparing Microbial Communities. *Applied and Environmental Microbiology*, 75(23), 7537-7541.

- Schuchmann, K., & Muller, V. (2014). Autotrophy at the thermodynamic limit of life: a model for energy conservation in acetogenic bacteria. *Nature Reviews Microbiology*, *12*(12), 809-821.
- Schwartz, A., Hold, G. L., Duncan, S. H., Gruhl, B., Collins, M. D., Lawson, P. A., . . . Blaut, M. (2002). *Anaerostipes caccae* gen. nov., sp. nov., a new saccharolytic, acetate-utilising, butyrate-producing bacterium from human faeces. *Systematic and Applied Microbiology*, *25*(1), 46-51.
- Seedorf, H., Fricke, W. F., Veith, B., Bruggemann, H., Liesegang, H., Strittmatter, A., . . . Gottschalk, G. (2008). The genome of *Clostridium kluyveri*, a strict anaerobe with unique metabolic features. *Proceedings of the National Academy of Sciences of the United States of America*, *105*(6), 2128-2133.
- Seemann, T. (2014). Prokka: rapid prokaryotic genome annotation. *Bioinformatics*, *30*(14), 2068-2069.
- Segata, N., Bornigen, D., Morgan, X. C., & Huttenhower, C. (2013). PhyloPhlAn is a new method for improved phylogenetic and taxonomic placement of microbes. *Nature Communications*, *4*.
- Selemba, P. A., Perez, J. M., Lloyd, W. A., & Logan, B. E. (2009). Enhanced Hydrogen and 1,3-Propanediol Production From Glycerol by Fermentation Using Mixed Cultures. *Biotechnology and Bioengineering*, *104*(6), 1098-1106.
- Shoaie, S., Karlsson, F., Mardinoglu, A., Nookaew, I., Bordel, S., & Nielsen, J. (2013). Understanding the interactions between bacteria in the human gut through metabolic modeling. *Scientific Reports*, *3*.
- Sieber, J. R., Crable, B. R., Sheik, C. S., Hurst, G. B., Rohlin, L., Gunsalus, R. P., & McInerney, M. J. (2015). Proteomic analysis reveals metabolic and regulatory systems involved in the syntrophic and axenic lifestyle of *Syntrophomonas wolfei*. *Frontiers in Microbiology*, *6*.
- Smith, D. P., & Mccarty, P. L. (1989). Energetic and Rate Effects on Methanogenesis of Ethanol and Propionate in Perturbed Cstrs. *Biotechnology and Bioengineering*, *34*(1), 39-54.
- Smith, G. M., Kim, B. W., Franke, A. A., & Roberts, J. D. (1985). ¹³C NMR studies of butyric fermentation in *Clostridium kluyveri*. *Journal of Biological Chemistry*, *260*(25), 13509-13512.
- Speers, A. M., Young, J. M., & Reguera, G. (2014). Fermentation of Glycerol into Ethanol in a Microbial Electrolysis Cell Driven by a Customized Consortium. *Environmental Science & Technology*, *48*(11), 6350-6358.
- Spirito, C. M., Richter, H., Rabaey, K., Stams, A. J. M., & Angenent, L. T. (2014). Chain elongation in anaerobic reactor microbiomes to recover resources from waste. *Current Opinion in Biotechnology*, *27*, 115-122.
- Stackebrandt, E., & Osawa, R. (2015). Phascolarctobacterium *Bergey's Manual of Systematics of Archaea and Bacteria*: John Wiley & Sons, Ltd.
- Stams, A. J. M., & Plugge, C. M. (2009). Electron transfer in syntrophic communities of anaerobic bacteria and archaea. *Nature Reviews Microbiology*, *7*(8), 568-577.
- Steinbusch, K. J. J., Arvaniti, E., Hamelers, H. V. M., & Buisman, C. J. N. (2009).

- Selective inhibition of methanogenesis to enhance ethanol and n-butyrate production through acetate reduction in mixed culture fermentation. *Bioresource Technology*, 100(13), 3261-3267.
- Steinbusch, K. J. J., Hamelers, H. V. M., Plugge, C. M., & Buisman, C. J. N. (2011). Biological formation of caproate and caprylate from acetate: fuel and chemical production from low grade biomass. *Energy & Environmental Science*, 4(1), 216-224.
- Szymanowska-Powaowska, D., & Kubiak, P. (2015). Effect of 1,3-propanediol, organic acids, and ethanol on growth and metabolism of *Clostridium butyricum* DSP1. *Applied Microbiology and Biotechnology*, 99(7), 3179-3189.
- Tao, X. Y., Li, Y. B., Huang, H. Y., Chen, Y., Liu, P., & Li, X. K. (2014). *Desulfovibrio vulgaris* Hildenborough prefers lactate over hydrogen as electron donor. *Annals of Microbiology*, 64(2), 451-457.
- Temudo, M. F., Muyzer, G., Kleerebezem, R., & van Loosdrecht, M. C. M. (2008). Diversity of microbial communities in open mixed culture fermentations: impact of the pH and carbon source. *Applied Microbiology and Biotechnology*, 80(6), 1121-1130.
- Temudo, M. F., Poldermans, R., Kleerebezem, R., & van Loosdrecht, M. C. M. (2008). Glycerol fermentation by (open) mixed cultures: A chemostat study. *Biotechnology and Bioengineering*, 100(6), 1088-1098.
- Thauer, R. K., Jungermann, K., & Decker, K. (1977). Energy conservation in chemotrophic anaerobic bacteria. *Bacteriological Reviews*, 41(1), 100-180.
- Tidjani Alou, M., Rathored, J., Lagier, J. C., Khelaifia, S., Labas, N., Sokhna, C., . . . Dubourg, G. (2016). *Massilibacterium senegalense* gen. nov., sp. nov., a new bacterial genus isolated from the human gut. *New Microbes and New Infections*, 10, 101-111.
- Tilman, D., Socolow, R., Foley, J. A., Hill, J., Larson, E., Lynd, L., . . . Williams, R. (2009). Beneficial Biofuels-The Food, Energy, and Environment Trilemma. *Science*, 325(5938), 270-271.
- Tremblay, P. L., Zhang, T., Dar, S. A., Leang, C., & Lovley, D. R. (2013). The Rnf Complex of *Clostridium ljungdahlii* is a Proton-Translocating Ferredoxin:NAD(+) Oxidoreductase Essential for Autotrophic Growth. *mBio*, 4(1).
- U.S. Energy Information Administration, E. (2016). *INTERNATIONAL ENERGY OUTLOOK 2016* (DOE/EIA-0484(2016)). Retrieved from <https://www.eia.gov/outlooks/ieo/>
- Varrone, C., Giussani, B., Izzo, G., Massini, G., Marone, A., Signorini, A., & Wang, A. J. (2012). Statistical optimization of biohydrogen and ethanol production from crude glycerol by microbial mixed culture. *International Journal of Hydrogen Energy*, 37(21), 16479-16488.
- Vasudevan, D., Richter, H., & Angenent, L. T. (2014). Upgrading dilute ethanol from syngas fermentation to n-caproate with reactor microbiomes. *Bioresource Technology*, 151, 378-382.
- Vasudevan, P., Sharma, S., & Kumar, A. (2005). Liquid fuel from biomass: An

- overview. *Journal of Scientific & Industrial Research*, 64(11), 822-831.
- Viana, Q. M., Viana, M. B., Vasconcelos, E. A., Santaella, S. T., & Leitao, R. C. (2014). Fermentative H₂ production from residual glycerol: a review. *Biotechnology Letters*, 36(7), 1381-1390.
- Vikromvarasiri, N., Laothanachareon, T., Champreda, V., & Pisutpaisal, N. (2014). Bioethanol Production from Glycerol by Mixed Culture System. *Energy Procedia*, 61, 1213-1218.
- Voegelé, R. T., Sweet, G. D., & Boos, W. (1993). Glycerol Kinase of *Escherichia Coli* Is Activated by Interaction with the Glycerol Facilitator. *Journal of Bacteriology*, 175(4), 1087-1094.
- Wallace, R. J., Chaudhary, L. C., Miyagawa, E., McKain, N., & Walker, N. D. (2004). Metabolic properties of *Eubacterium pyruvativorans*, a ruminal 'hyper-ammonia-producing' anaerobe with metabolic properties analogous to those of *Clostridium kluyveri*. *Microbiology*, 150, 2921-2930.
- Wallace, R. J., McKain, N., McEwan, N. R., Miyagawa, E., Chaudhary, L. C., King, T. P., . . . Newbold, C. J. (2003). *Eubacterium pyruvativorans* sp nov., a novel non-saccharolytic anaerobe from the rumen that ferments pyruvate and amino acids, forms caproate and utilizes acetate and propionate. *International Journal of Systematic and Evolutionary Microbiology*, 53, 965-970.
- Wang, D., Liu, H. L., Zheng, S. X., & Wang, G. J. (2014). *Paenirhodobacter enshiensis* gen. nov., sp nov., a non-photosynthetic bacterium isolated from soil, and emended descriptions of the genera *Rhodobacter* and *Haematobacter*. *International Journal of Systematic and Evolutionary Microbiology*, 64, 551-558.
- Watanabe, Y., Nagai, F., & Morotomi, M. (2012). Characterization of *Phascolarctobacterium succinatutens* sp. nov., an asaccharolytic, succinate-utilizing bacterium isolated from human feces. *Applied and Environmental Microbiology*, 78(2), 511-518. doi:10.1128/AEM.06035-11
- Wu, Y. W., Tang, Y. H., Tringe, S. G., Simmons, B. A., & Singer, S. W. (2014). MaxBin: an automated binning method to recover individual genomes from metagenomes using an expectation-maximization algorithm. *Microbiome*, 2.
- Xu, G. R., Xu, S. H., & Tao, J. (1990). New technology of producing caproic acid by 2-octanol and/or 2-octanone: Google Patents.
- Yang, Y., Li, B., Ju, F., & Zhang, T. (2013). Exploring Variation of Antibiotic Resistance Genes in Activated Sludge over a Four-Year Period through a Metagenomic Approach. *Environmental Science & Technology*, 47(18), 10197-10205.
- Yazdani, S. S., & Gonzalez, R. (2007). Anaerobic fermentation of glycerol: a path to economic viability for the biofuels industry. *Current Opinion in Biotechnology*, 18(3), 213-219.
- Yuksel, F., & Yuksel, B. (2004). The use of ethanol-gasoline blend as a fuel in an SI engine. *Renewable Energy*, 29(7), 1181-1191.
- Zhang, K. G., Song, L., & Dong, X. Z. (2010). *Proteiniclasticum ruminis* gen. nov., sp. nov., a strictly anaerobic proteolytic bacterium isolated from yak rumen. *International Journal of Systematic and Evolutionary Microbiology*, 60,

2221-2225.

- Zhaxybayeva, O., Swithers, K. S., Foght, J., Green, A. G., Bruce, D., Detter, C., . . . Nesbo, C. L. (2012). Genome Sequence of the Mesophilic *Thermotogales* Bacterium *Mesotoga prima* MesG1.Ag.4.2 Reveals the Largest *Thermotogales* Genome To Date. *Genome Biology and Evolution*, 4(8), 812-820.
- Zhu, X. Y., Zhou, Y., Wang, Y., Wu, T. T., Li, X. Z., Li, D. P., & Tao, Y. (2017). Production of high-concentration n-caproic acid from lactate through fermentation using a newly isolated *Ruminococcaceae* bacterium CPB6. *Biotechnology for Biofuels*, 10(1), 102.